Georgia Tech Institute of Paper Science and Technology

FINAL TECHNICAL REPORT

Contactless Real-Time Monitoring of Paper Mechanical Behavior During Papermaking

Prepared by: Institute of Paper Science & Technology at Georgia Institute of Technology

FINAL TECHNICAL REPORT

Project Title: Contactless Real-Time Monitoring of Paper Mechanical Behavior During Papermaking

Covering Period: October 1, 1997 to March 31, 2004

Date of Report: August 30, 2005

Recipients: Institute of Paper Science and Technology at Georgia Tech, Atlanta, GA
And Lawrence Berkeley National Laboratory, Berkeley, CA

Award Number: DE-FC07-97ID13578

Disclaimer: Any opinions, findings, and conclusions or recommendations expressed in this material are those of the authors and do not necessarily reflect the views of the Department of Energy

Subcontractors: Georgia Institute of Technology, Department of Mechanical Engineering, Professor Yves Berthelot

Other Partners: ABB Industrial systems (Industrial partner)

Contact(s): E. Lafond 404-894-3707, emmanuel.lafond@ipst.gatech.edu
Rick Russo 510-486-4258, rerusso@lbl.gov

Project Team: DOE Program Managers: Dickson Ozokwelu, Joseph Springer; Research Team: IPST@GT: Ted Jackson, Emmanuel Lafond, Xinya Zhang, Gary Baum; LBNL: Paul Ridgway, Rick Russo; INL: Ken Telschow, Vance Deason;
Georgia Tech/Mechanical Engineering: Yves Berthelot, David Griggs

Project Objective: The objective is to provide a sensor that uses non-contact, laser ultrasonics to inspect the mechanical state of paper on-line. Tasks include optimization of ultrasound generation on moving paper, development of interferometric detection schemes for on-line operation, construction of a prototype for application on a paper machine, and development of an on-line sensor suitable for industrial environments.

Background: Laser ultrasonic methods have the potential to succeed in the on-line environment of the mill where traditional contacting technologies have not. A critical consideration for papermakers before implementing a new sensor is the risk of web breaks. As such, they have traditionally been hesitant to embrace technologies that contact the sheet. Also, previous contacting ultrasonic measurement schemes have been difficult to apply to moving paper applications at a reasonable cost and effectiveness. By contrast, the LUS technology is a single-sided measurement that requires no contact with the sheet at all.

Laser ultrasonic methods are also able to determine flexural rigidity and thereby bending stiffness directly, which earlier on-line ultrasonic methods for determining planar modulus of elasticity, could only infer indirectly. Flexural rigidity is the property that determines end-product rigidity and is of great importance to a wide variety of paper grades. Laser ultrasonics could also provide single-sensor in-plane and out-of-plane characterization and give the first on-line gauge of stiffness orientation, being easily reconfigurable while in operation to measure along any planar orientation.

This project represents the combined efforts of two organizations with complementary experiences in paper physics and laser ultrasonics. LNBL is expert in the art of laser acoustic wave generation and has made good progress in developing instrumentation and techniques for inducing optimally large ultrasonic excitations in paper while avoiding damage to the sheet. They developed a scanning-mirror, Mach-Zehnder interferometer that works well at high speeds on a web-simulator. IPST at GeorgiaTech contributes paper physics expertise and close relations with the paper industry, has provided working experience in the construction of unique laboratory ultrasonic systems for paper, and experience with the design and implementation upon a host ABB Smart Platform scanning system. The two organizations continue to work together to improve these technologies for web measurements. Our industrial partner is ABB and they are contributing web stabilization technology, advice for design of on-line instrument, environmental specifications for on-line instruments, and various software for interfacing our sensor with the existing sensors on their scanning platform.

CONTENTS

Historical summary of the project

The early precursors of laser ultrasonics on paper were Prof. Y. Berthelot from the Georgia Institute of Technology/ Mechanical Engineering department, and Prof. P. Brodeur from the Institute of Paper Science and Technology, both located in Atlanta, Georgia. The first Ph.D. thesis that shed quite some light on the topic, but also left some questions unanswered, was completed by Mont A. Johnson in 1996. Mont Johnson was Prof. Berthelot's student at Georgia Tech. In 1997 P. Brodeur proposed a project involving himself, Y. Berthelot, Dr. Ken Telschow and Mr. Vance Deason from INL, Honeywell-Measurex and Dr. Rick Russo from LBNL. The first time the proposal was not accepted and P. Brodeur decided to re-propose it without the involvement from LBNL. Rick Russo proposed a separate project on the same topic on his side. Both proposals were finally accepted and work started in the fall of 1997 on the two projects. Early on, the biggest challenge was to find an optical detection method which could detect laser-induced displacements of the web surface that are of the order of .1 micron in the ultrasonic range. This was to be done while the web was having an out-of-plane amplitude of motion in the mm range due to web flutter; while moving at 10 m/s to 30 m/s in the plane of the web, on the paper machine. Both teams grappled with the same problems and tried similar methods in some cases, but came up with two similar but different solutions one year later. The IPST, GT, INL team found that an interferometer made by Lasson Technologies Inc. using the photo-induced electro-motive force in Gallium Arsenide was able to detect ultrasonic waves up to 12-15 m/s. It also developed in house an interferometer using the Two-Wave Mixing effect in photorefractive crystals that showed good promises for on-line applications, and experimented with a scanning mirror to reduce motion-induced texture noise from the web and improve signal to noise ratio. On its side, LBNL had the idea to combine a commercial Mach-Zehnder interferometer to a spinning mirror synchronized to the web speed, in order to make almost stationary measurements. The method was demonstrated at up to 10 m/s. Both teams developed their own version of a web simulator that was driving a web of paper at 10 m/s or higher.

The Department of Energy and members of the Agenda 2020 started to make a push for merging the two projects. This made sense because their topics were really identical but this was not well received by Prof. Brodeur. Finally IPST decided to reassign the direction of the IPST-INL-GT project in the spring of 1999 to Prof. Chuck Habeger so that the two teams could work together. Also at this time, Honeywell-Measurex dropped as a member of the team. It was replaced by ABB Industrial Systems whose engineers had extensive previous experience of working with ultrasonic sensors on paperboard. INL also finished its work on the project as its competencies were partly redundant with LBNL. From the summer of 1999, the IPST-GT and LBNL teams were working together and helped each other often by collaborating and visiting either laboratory when was necessary. Around the beginning of 2000, began an effort at IPST to create an off-line laser-ultrasonics instrument that could perform automated measurements of paper and paperboard's bending stiffness. It was widely known that the mechanical bending tests of paper used for years by the paper industry were very inaccurate and exhibited poor reproducibility; therefore the team needed a new instrument of reference to validate its future on-line results. In 1999-2000, the focus of the on-line instrument was on a pre-industrial demonstration on a pilot coater while reducing the damage to the web caused by the generation laser, below the threshold where it could be visible by the naked eye. During the spring of 2000 Paul Ridgway traveled to IPST and brought with him a redesigned system still using the same Mach-Zehnder interferometer as before, but this time employing an electric motor-driven

spinning mirror instead of the previously belt-driven mechanical spinning mirror. For testing we chose to use a 1 foot-wide paper loop running on IPST's large scale web handler which could reach a web speed of 2,000 feet/min (10.16 m/s). This was more representative of the conditions encountered of a pilot coater, than on a table-top scale web simulator. The Mach-Zehnder + spinning mirror and the Two-Wave Mixing in Gallium Arsenide photorefractive crystal interferometer were compared side to side for different paper grades ranging from light weight (publishing paper) to heavy weight (linerboard 42 Lb). It was found that the signal to noise ratio of the two-wave mixing interferometer was dropping very rapidly as the web speed increased and most of the ultrasonic wave signal had disappeared by 5 m/s and higher, even when using a spinning mirror. The addition of the spinning mirror didn't seem to help much as the interference grating created inside the crystal was wiped out by the apparent motion of the web along the direction of the beam when the optical path of the signal beam was decreased and then increased by the rotation of the beam.

Therefore the Mach-Zehnder + spinning mirror was chosen as the preferred method for an on-line system and the teams worked together in that direction. Emmanuel Lafond went to LBNL help Paul Ridgway carry several laser ultrasonics experiments during a few weeks in the summer of 2000 and went back again in July 2001 to help speed up the pilot coater demonstration. Most of the 2000-2001 period was dedicated on LBNL side to build the hardware for a pilot coater demonstration, while IPST was developing a software capable to acquire the data in real time and to manipulate it in order to extract the flexural rigidity (bending stiffness), and working on improving the two-wave mixing interferometer for off-line measurements for an off-line laboratory instrument.

The pilot coater demonstration occurred during 1 week in August 2001 at the Mead Research Center in Chillicothe, Ohio, in difficult environmental conditions (very high heat and high humidity). Nevertheless the support of the pilot coater's operators and Mead research personnel was outstanding and the results went beyond our hopes. We went up to 5000 feet/min (25 m/s) (the maximum speed of the pilot coater) and still observed good signal to noise ratio. The waveforms acquired during the trial, were processed later at IPST to extract the stiffness information. We investigated 7 grades and got marginal results on only one of them; a multiply linerboard. A representative from ABB also attended part of the trial. LBNL (Paul Ridgway) deserved most of the credit for the trial as he prepared and built almost all the hardware while IPST contributed a fiber optic launch, software and management of the tests.

The demonstration that the sensor could work and work very well, in an unprotected environment outside of the laboratory, gave us much confidence for the future. In 2002 the Phase II (development) of this project started under a new award, while remaining funds from Phase I were used to contribute to Phase II. The main goal in phase II was to make a full scale mill demonstration directly on a commercial paper machine while it was producing paper. It was planned that the sensor would be using very much the same architecture as the Chillicothe pilot coater sensor, but would be hardened for industrial use and that the software would be greatly improved and automated so that automatic real-time determination of elastic constants would be possible. Also the development of the laser ultrasonics laboratory instrument was to be pursued until it would be completely automated. The instrument would be used in order to compare the laser ultrasonics test results to the traditional mechanical bending tests on multiple paper grades to establish laser ultrasonics in paper laboratories.

The Chillicothe sensor installed above the web was roughly 1 foot by 1 foot by 3 feet in size. The team quickly realized that it would be impossible to install a sensor this bulky on a commercial paper machine where empty spaces between rolls are by design kept as small as possible. So we focused on dramatically reducing the sensor's size especially along the machine direction (MD) where the space is traditionally the most restricted on the paper machine. Paul Ridgway tested a miniaturized Mach-Zehnder interferometer manufactured by the same provider as the interferometer of the pilot coater trial, that worked well. He also redesigned the spinning mirror spindle and motor ensemble so as to reduce its footprint. Ted Jackson was our software specialist on the project. To build a running software, he started from a basic phase unwrapping software that needed considerable operator input for signal processing, and that he had developed previously with input from Chuck Habeger for the laboratory instrument. Ted Jackson connected it to a data acquisition software and he increased the automation of the software little by little after much experimentation, replacing the operator input by software intelligence. This was made possible in part by an initial zeroing of the fit parameters using a "best guess" estimate based on the basis weight (weight per unit area) of the paper. The software was built with LabVIEW, which is nowadays widely used in industrial environments and research labs for running instruments, robots, doing signal processing, etc.

In the winter of 2002-2003, we were partnering with MeadWestvaco, the same company that we did the pilot coater trial with, to find a trial site for the full scale demonstration. MeadWestvaco suggested the paper machine #1 in the coated paper mill of Escanaba, MI, for the full scale mill demonstration. Emmanuel and Paul visited the mill in April 2003, made contact with the persons in charge there and found out that it was doable to install the sensor on this machine. The machine was about 3 m wide and it was a rather slow (3,200 feet per minute) and old machine. But it was suitable for our purpose as it had a recent ABB scanner similar to the one the sensor was hooked up to, at IPST. To spread the burden of the full scale mill demonstration, the tasks were divided between LBNL and IPST by having LBNL in charge of designing and engineering the detection system, sensor enclosure module, cable transport system, and auxiliary system for cooling the sensor enclosure and controlling various axes of translation. IPST was in charge of the generation laser system, fiber optic delivery to the sensor enclosure, software for data acquisition and processing and software for interface the sensor with the other sensors of the ABB platform. IPST and LBNL shared the general organization and communication tasks with the mill.

During our communications and talks with mill's engineers, it appeared that measuring the web's stiffness properties at a single CD position was not nearly as interesting for process control as compared to obtaining a whole profile by scanning along the cross direction as the sensors of the ABB scanning head does. CD is the cross direction, along the width of the web, and is at 90 degrees from the machine direction in which the web is moving, called MD. Therefore, after consultation with DOE, we readjusted our aim, to produce a sensor closer to a commercial unit, that would have more capabilities and scan along the CD. The sensor would scan by being attached to the scanning head package of an ABB platform. To accommodate this, Paul devised a special cable transport system with a swinging boom to carry various cables between the auxiliary system and the sensor enclosure.

Our target date for the trial was sometime during the winter of 2003-2004. During the summer of 2003, it appeared that this would have to be postponed to the spring of 2004 in order for us to be sufficiently prepared and to test the sensor prior to the installation. IPST was working on obtaining the basis weight, moisture, CD (cross direction at 90 degrees from the machine direction) from the ABB platform. The moisture was especially difficult to obtain as it is a combination of several measurements that had to be processed to extract the moisture content in a given point.

In December 2003, the Escanaba mill went through reorganization and downsizing of the mill personnel and it become increasingly difficult to communicate back and forth with the mill personnel. We readied the sensor for the mill trial in March, only to be told by the mill that due to personnel shortage they couldn't host the mill trial at Escanaba. We then reiterated with MeadWestvaco to find another mill where to host the trial. Work on this project continued under award 02ID14344 and finally a full scale mill demonstration occurred in a mill from a company different from MeadWestvaco in February 2005. As award 97ID13578 ended on March 31, 2004, this subsequent work isn't described in the report presented here.

ECONOMIC BENEFITS OF AN ON-LINE STIFFNESS SENSOR FOR A PAPER MILL
(Estimate of August 20, 2003)

The benefits to the industry of an on-line stiffness sensor follow from the availability of a real-time, on-line monitoring of paper mechanical properties.

This will reduce the quantity of off-specification production. The energy required to recycle substandard product will thereby decrease and machine throughput will increase. A mechanical quality control monitor will provide feedback to meet performance standards with minimum material and energy expenditure.

The sensor will avoid the over-engineering of the paper web which can occur in some paper mills in order to reach a targeted stiffness value.

BENEFITS:

Based on a 2.13 % projected reduction in basis weight needed while still reaching stiffness targets on a machine producing 175,000 Metric Ton per year of uncoated free sheet, savings of approximately $1,070,000 per year are expected due to reduced fiber, chemicals and energy use.

Additionally, an estimated reduction in off-standard product from 6.2% to 5.2% (1% absolute increase in first grade production) is expected to lead to a corresponding savings of about $376,000 per year.

The total is therefore an estimated savings of $1.446 million per year.

The calculation was made using the Jaako Poyry model of IPST, by David White, Technology Transfer Director at IPST (tel: 404 894-1080).

The model can be run for 3 different types of grades: Newsprint, UnCoated Free Sheet, and Linerboard. UnCoated Free Sheet was chosen because it has the most similarities with the Base paper of a Coated Free Sheet, on which the laser ultrasonic sensor could be used.

Input Parameters:

- production of Escanaba paper machine #1 estimated to 175,000 Metric Ton/ year;
- average machine speed 2600 fpm;
- grammage of base paper (before coating): 75 g/m^2;
- Fiber and Chemicals costs: $140 /ton (fiber) and $103/ton (chemicals) apply for the South East U.S. – might be higher for North Midwest
- Energy costs: 5 cents / kW hour , $20 / barrel of oil

In table A on page 3, the reduced capital investments (in maintenance, recovery boiler replacement, etc…) that would be coming from running the machine with less fibers, chemicals and using less energy, are not included. That is because this would vary too much from mill to mill. Also not included is the avoidance of buying commercial pulp from outside, when the wood yard cannot supply enough fiber (maybe not applicable to Escanaba mill). Those two items could lead to significant additional savings though.

In table B on page 3 the cost, to the mill, of recycling the off-standard product is not comprised in the savings, and would add to them. It is believed it will contribute much less to profits than a higher percentage of saleable efficiency. That is why it was not included.

Also in table B, we deliberately didn't include the reduction of paper breaks that could be coming from a paper produced with higher out-of-plane stiffness. Usually out-of-plane stiffness and tensile strength correlate rather well; hence an increase in out-of-plane stiffness would make the paper less likely to break. This is however much too risky to predict before having the experimental and statistical results of a mill trial in hand.

The benefits need to be compared to:

COSTS

+ Anticipated costs of the fabrication of the sensor: $76 k to $101 k (see breakdown of the costs below)

- Cost of the parts $54 k + assembly $5 k
- Maintenance of sensor $7 k /year (done by ABB personnel)*
- Installing into empty head package slot: $10-15k (installation, wiring, software)

or

- Installing with head package rebuilt to add additional space for sensor: $25-35k

+ Mark-up charged by the company selling the sensor: est. + 100 % → $76 k to $101 k

Total Cost of sensor to a paper machine: $152 to $202 k

The duration it takes for the sensor to break even compared to its cost, is therefore less than 2 months. That is providing we can reduce the basis weight by 2%, and decrease the percentage of off-standard product by 1%. If we would reach only half of the total objective above, the payback duration would become about 3.5 months.

If one uses the current cost of oil, (which is now significantly higher than $20 per barrel) and the current cost of natural gas, the energy savings would be even higher; thereby, reducing the payback duration further.

*change flash lamp of generation laser once per month during a machine shutdown (about $3k a year); + labor for inspection, cleaning, and change of minor parts.

TABLE A
EFFECT OF LOWERING BASIS WEIGHT (FOR UCFS)

		Base Case	Lower Basis Weight Cases (Equivalent strength)							
Basis weight	**(g/m^2)**	**75.2**	**74.4**	**73.6**	**72.7**	**71.9**	**71.1**	**70.3**	**69.5**	**68.7**
(lb/3M sq. f		**46**	**45.5**	**45**	**44.5**	**44**	**43.5**	**43**	**42.5**	**42**
Machine production rate *	(FMT/y)	175,000	173,098	171,196	169,293	167,391	165,489	163,587	161,685	159,783
Savings										
- Fiber (@ $139/t)	($000/y)	-	264	527	791	1,055	1,318	1,582	1,845	2,109
- Chemicals (@ $103/t)	($000/y)	-	195	391	586	781	977	1,172	1,367	1,563
- Energy ** (@ $40/t)	($000/y)	-	76	152	228	304	379	455	531	607
- Total, fiber + chemicals + energy	**($000/y)**	**-**	**535**	**1,070**	**1,605**	**2,140**	**2,674**	**3,209**	**3,743**	**4,279**

* Constant machine speed

** Purchased electricity @ $0.05/kWh; fuel oil @ $20/ barrel

TABLE B
EFFECT OF INCREASING PM EFFICIENCY: LESS OFF-STANDARD (FOR UCFS)

		Base Case	Lower Off-Standard			
Basis weight	(g/m^2)	75.2	75.2	75.2	75.2	75.2
Basis weight (lb/3M sq. ft.)		46	46	46	46	46
Machine production rate *	(FMT/y)	175,000	176,810	178,675	180,540	182,405
Machine Losses						
Shut-downs	(%)	3	3	3	3	3
Breaks	(%)	3	3	3	3	3
Total up-time	(%)	94	94	94	94	94
Off-standard	**(%)**	**6.2**	**5.2**	**4.2**	**3.2**	**2.2**
PM saleable efficiency	(%)	93.8	94.8	95.8	96.8	97.8
PM efficiency	**(%)**	**88.2**	**89.1**	**90.1**	**91.0**	**91.9**
Increase in net profit **	**($000/y)**	**-**	**376**	**763**	**1,150**	**1,537**

* Constant machine speed

** @ UCFS selling price = $630/short ton; Base paper for Coated Free Sheet would be slightly higher.

October 1, 1997 through September 30, 1998 Report Status:

This project is a multi-phase project with the final goal of demonstrating a single-point, non-contact monitoring system which can be mounted to a scanning platform. Ultimately, this monitoring system will be used to control the papermaking process. Phase I of the project, was concerned with evaluating available technologies for the monitoring system, including stiffness and fiber orientation measurement methods. Phase II will demonstrate an integrated system in a laboratory setting. Phase II will also begin to look at the process control issues, in particular, what to do with the information available from the monitoring system. Phase III will take the integrated system from Phase II to several mills for field trials. At the end of Phase I, we are proud to announce that all goals for the first year have been met or exceeded.

On the instrumentation side of the project, a pair of web simulators were constructed which can take strips of machine made papers and move them at speeds in excess of 25 m/s, plus apply a simulated “flutter”. These instruments have allowed the evaluation of 5 different types of laser based ultrasound detection systems (for determination of stiffness properties) on moving paper in a laboratory setting. These detectors included:

+ Fabry-Pérot
+ Frequency domain photorefractive interferometers
+ Time domain photorefractive interferometers
+ Self-mixing vibrometer
+ Photoinduced-EMF

All five detectors were capable of measuring ultrasound waves on stationary paper, and three (Fabry-Pérot, self-mixing vibrometer, and photoinduced-EMF) were able to make measurements on various grades of paper at production speeds (up to 25 m/s) completely non-contact.

Fiber orientation distribution (FOD) is another area of investigation during Phase I of the project. Two fiber-orientation measuring instruments were built and successfully tested. The first is based upon the measuring of dyed fibers in a sample, and is intended as a reference instrument. The second is based upon non-contact light transmission/scattering through the sample. Both were found to agree well with each other.

Also beginning earlier than originally planned, the equipment to evaluate the effect of moisture content and temperature on ultrasonic velocities has begun to be assembled.

Phase II of the project will involve the integration of these technologies into an instrument that will be used to probe the fundamentals of the papermaking process, with the intent to control the paper machine for optimal product properties.

October 1, 1998 through September 30, 1999 Report Status

Early-on, the idea that on-line textural noise could be eliminated by the use of a synchronized scanning mirror was independently conceived at LBNL and IPST. From the IPST perspective the idea was validated by experiments at INL on a Fabry-Perot interferometer. Nonetheless, at the beginning of this year the IPST contingent felt that the Lasson Technologies Photo-induced EMF interferometer provided the simplest, likely-successful on-line method for detection of paper ultrasonic signals. Extensive trials were performed with the photo-emf system on the IPST web simulator. The ability of this interferometer was impressive, but it was deemed insufficient, and we returned to the scanning mirror approach. A scanning mirror patent application was submitted and an invention disclosure for the “peanut shell” technique was written. Experiments were conducted with an axicon lens for excitation.

In the third quarter LNBL generated and detected ultrasonic waves in paper moving at 20 and 30 m/sec. Ao and So waves were detected easily at 30 m/sec. So wave velocity measurements appeared to be unaffected by paper speed, within experimental error. There was still evidence of ablation with the laser energy used in this work.

Improvement of the Mach-Zehnder/scanning mirror detection system proceeded with evaluation and purchase of data acquisition and system control hardware. Another improvement was an increase in the bandwith of the signal level indicator.

Also in the third quarter, IPST continued to develop the gallium arsenide (GaAs), two-wave mixing interferometer. On static paper this technique gave the best results yet seen at IPST. For the first time, we had a system that functioned well with fully thermo-elastic excitations. It was deemed suitable for incorporation into a “master” laboratory instrument and perhaps tried on-line.

The photo-emf interferometer rented from Lasson Technologies was further evaluated for on-line operation. This detection system was of interest because it held the promise of functioning on moving webs without implementation of a scanning mirror. After considerable adjustment, the photo-emf detector was made to detect ultrasonic signals at up to 30 m/s web speeds. However, all good results were achieved while abating the web. We continued to improve the system, but feared that, in the end, it would not function well enough in the thermo-elastic regime. Anticipating this outcome, we plan to incorporate a scanning mirror into our GaAs, two-wave mixing interferometer since it functions best on static paper and has the most to gain from addition of a scanning mirror.

In July LBNL personnel visited IPST and the two parties agreed to terms of collaboration. One outcome was that IPST agreed to send one of their paper moving systems to LBNL so that the different detection systems being developed in the two locations can be more readily compared.

During the final quarter, LBNL worked to enhance sensitivity of the So wave, the detection beam was set to an angle of incidence to the paper surface of 45 degrees. The results were compared with data taken at an incidence angle of 90 degrees. As predicted, So wave signal amplitudes were larger at 45 degrees, and the amplitudes of the Ao waves were slightly diminished. No significant increase in the noise level in the Mach-Zehnder interferometer signal was encountered at 45 degrees. Apparently the efficiency of light collection was not significantly diminished. The paper-moving machine was fitted with a scanning mirror

which applied the detection beam to the paper at 45 degrees. With the enhanced sensitivity to the So wave obtained at this detection angle, the generation laser pulse energy was decreased to less than the damage threshold of the paper, and with the paper moving at 20 m/sec and 30 m/sec good quality signals showing both So and Ao waves were collected. At these lower generation energies, the scope traces averaged well.

Preliminary data was gathered for ZD measurements. There were many issues that need to be addressed for continuing such work and determining its significance. However, the preliminary data were encouraging. 1064nm YAG and 10.6 □m CO2 lasers were used in stationary measurements to generate and detect ultrasonic waves in the thickness direction on paper, and cardboard of varying thickness. In all these materials, it appeared that there was a minimum thickness below which time of flight of the ultrasonic wave did not change with thickness. Using the CO2 laser, the time of flight of the wave fronts varied linearly with thickness from .050" (1270 microns) down to .008" (200 microns). Paper samples included boxboard, 69-pound and #22-pound linerboard. With the 1.06 um YAG laser generation, the time of flight of the wave fronts varied linearly with thickness down to .018" (460 microns). The ability of the 10.6 □m CO2 laser generated signals to distinguish between thinner papers may be due to higher absorption of that wavelength at the surface of the sheet.

A comparison was made between signals excited with a 1.06 □m, 5ns YAG and a 10.6 □m 125 ns CO2 generation laser. The frequency spectra of signals generated with the CO2 laser differed markedly from signals generated with the YAG laser. The much larger amplitudes in the YAG-generated Ao signals are concentrated in the higher frequency components (>250KHz). On the other hand, these spectra also showed that the lower frequency components (< 25Khz) are greatly enhanced in CO2 laser-generated signals. (The low frequency components are important for obtaining bending stiffness. The high frequency components are needed to obtain in-plane extensional stiffnesses.)

At IPST development continued with the gallium arsenide (GaAs), two-wave mixing interferometer. Generation and detection hardware was improved and signals on a range of paper grades were amassed. Progress was made in deciphering stiffnesses coefficient from laser ultrasonic signals. Well-formed and rational Ao dispersion curves were reproduced and a technique was discovered for easily deducing out of plane shear stiffness for these dispersion curves. We made axicon lens experiments to assess the potential of the "peanut shell" excitation approach. The axicon lens allowed us to form the excitation line pulse into a circle. On an isotropic handsheet sample, we detected at the center of the circle and compared results with line sources of the same energy, length, and intensity. The signal strength using the circular excitation was from four to nine times greater than that using the linear excitation source. Although not as dramatic as we had hoped, this is an encouraging result. We will consider the peanut shell approach after we achieve proper signal to noise ratios on moving webs by standard excitation means.

Experiments with direct out-of-plane laser-ultrasonic measurements were also conducted at IPST. The laser excitation is on one surface of the sheet and detection is directly opposite on the other side. We have recorded some very interesting signals at excitation wavelengths of 355 nm, 532 nm, and 1064nm. Further analysis is necessary before we can confidently decode stiffness properties.

The second web simulator built at IPST was refurbished and shipped to LBNL.

October 1, 1999 through September 30, 2000 Report Status:

In the first quarter, we developed a signal analysis technique for robust determination of bending stiffness and out-of-plane shear rigidity using Ao laser ultrasonic signals from two separations. We upgraded the optics for the gallium arsenide two-wave-mixing interferometer and made progress on integrating the scanning mirror into the GaAs interferometer. We established ABB as our industrial sponsor.

During the second quarter, a pulsed carbon dioxide laser was compared with a pulsed YAG laser for excitation of ultrasound. Damage threshold pulse energies on five paper types were determined using the CO2 and YAG lasers. Above the damage threshold, YAG-generated signals had much greater amplitudes. Below the damage threshold, larger amplitudes were obtained by YAG or CO2 excitation depending on the type of paper studied. With the YAG laser, the effect of generation line-width on the damage threshold energy was measured. Even though the damage threshold energy increased with spot size, no difference in signal amplitude at the damage threshold was observed. Signals were recorded at a variety of generation and detection point separations at energy levels ranging through the damage threshold on the five paper types with the YAG and CO2 lasers. We evaluated signal quality with respect to elastic property information by generating experimental dispersion curves and comparing with those predicted by theory.

We adapted our homemade Gallium Arsenide (GaAs), two-wave mixing interferometer for on-line application. We modified the optical design for greater depth of focus. We evaluated the interferometer by artificially imposing an ultrasonic signal on the reference beam with a piezoelectric element sending ultrasonic vibrations into a mirror. The signal beam was reflected off a moving paper web and mixed with the reference beam in a photorefractive GaAs crystal. The ultrasonic signal to noise ratio was monitored as a function of machine speed. The first experiments were conducted without using a scanning mirror in the signal beam path for the reduction of textural noise. The signal to noise ratio decreased significantly with web speed; however, by averaging we achieved acceptable signals to 25 m/s on several paper grades. High speed results were deemed to be at least as good as we observed with the photo-emf interferometer without a scanning mirror. Next we applied a scanning mirror to the signal beam so that the detection spot tracked the moving web. After considerable tinkering, we achieved a factor of three improvement of signal to noise. However, due the limited focal length of the optics and the curved surface of the web simulator, an out-of-plane Doppler effect limited the time period for which the scanning mirror reduced the textural noise. With our setup, the scanning was effective for only about 12 □sec. This was sufficient for analysis of the So signal, but not the Ao signal which lasts for over 100 microseconds. We are considering methods to extend the length of the scanning sweet spot. We evaluated the GaAs TWM interferometer on moving paper with laser excitation and no scanning mirror.

Considerable progress was made at IPST and GIT (see below) in the decoding of elastic properties from laser ultrasonic signals. At IPST, we developed methods for determining the bending stiffness and the out-of-plane shear rigidity by phase velocity calculations from signals at two different source-receiver separations. We compared phase velocity results with the single-spacing wavelet technique pioneered at GIT. The wavelet method has considerable practical advantage especially for on-line application since only one excitation-reception spacing is required. We prepared to evaluate a Short Time Fourier Transform method that also requires only one separation that is computationally simpler than the wavelet approach.

We started preparations for open web trials on the IPST/DOE web transport system. This already had an installed ABB scanner and provided a convenient means for experimentation in an on-line environment. ABB kindly provided a Bernoulli plate web stabilization assembly for the laser platform.

Thanks to the addition of Ted Jackson to our team, we began design of the automated laboratory laser ultrasonic instrument. We were debating as to the nature of the proper sample and transducer transport, the fiber optic delivery system, and the sample hold-down method.

In the third quarter, IPST continued the Ao signal analysis development for application to the laboratory instrument using the GaAs TWM interferometer. In order to establish appropriate operating conditions for the laboratory instrument, we experimented with different combinations of signal excitation, ultrasound travel distance, and elastic parameter decoding. We compared (on board and paper samples) line source to point source excitation, ablation to thermoelastic energy levels, results for 5, 10, and 20 millimeter travel distances, and phase velocity, d□d□, and wavelet dispersion curve fit techniques. More energy can be imparted to the sheet without damage by the use of line sources. However, in this particular case, the improvement in signal to noise ratio over point source excitation is minimal. Excitation from finite line sources requires difficult diffraction corrections to the velocity measurements. Calculations show that these can be significant in some applications; therefore, we conclude that (for laboratory applications with already-acceptable signal to noise ratios) any signal strength improvements from line source generation are unlikely to be worth their confusion. At a five millimeter and below transmitter-receiver separations on board samples there are near-field distortions in the Ao signal; therefore, we can accept 5 and 10 mm travel distances for paper samples but recommend 10, 15, and 20 mm travel distances for board samples. Our results demonstrate that the two-separation phase velocity technique is much more repeatable and robust than the d□/d□ or the wavelet techniques. For the laboratory unit the implementation of a two-point measurement will merely be an instrument inconvenience and a time drain. Therefore, for the sake of good measurement, we intended to outfit the laboratory unit as a two-separation, thermo-elastic point-source apparatus. The software implementation of the phase velocity technique into the laboratory instrument is straightforward with one exception; the frequency range for dispersion curve fitting is now selected by-eye. We intended to objectify this subjective process and capture it in code.

Carlos Rivera-Carpio of LBNL developed and implemented a new dispersion analysis approach (Group Fourier approach). He supplied the algorithm available to IPST for inclusion in their signal analysis evaluation study. Carlos also conceived and developed an “Ao waveform simulation tool” for evaluation of accuracy and sensitivity of signal analysis and interpretation tools.

There was good progress toward the construction of the laser-ultrasonic laboratory instrument. A tensioning sample holder was designed and constructed. All of the motion stages necessary for sample translation and rotation and for fiber optic manipulation were in-house. Programming the control of the mechanical devices was underway, as was the conversion of signal analysis software to the Lab-View platform to be used for the instrument. The fiber optics hook-ups were being developed.

Contrary to our previous pronouncements, we discovered that on-line web tension will have an influence on Ao wave propagation in lightweight sheets. Experimental investigations for comparison with our calculations began. We decided to determine whether this is a bane or

a boon. Would we be precluded from on-line analysis of newsprint weight papers or would we be able to measure web tension as well as bending stiffness and shear rigidity?

Emmanuel Lafond, from IPST and Paul Ridgway from LBNL, spent a productive month in California collaborating and working with LBNL's LUS system. A joint invention disclosure was filed. Their work included stabilization of the web with ABB's Bernoulli plate, evaluation of various optical modifications to the Mach-Zehnder detection system, and multiple-point laser generation using diffractive optics. The effect of tension in the MD on Ao phase velocities in the MD was studied on newsprint (49g/m^2), uncoated publishing grade (92g/m^2) and 42-lb linerboard. Ultrasonic velocities were clearly affected in the newsprint but not in the heavier samples.

We decided that the next set of trials should be conducted on the web handler at IPST. LBNL and IPST began the design and construction of equipment for tests on the IPST pilot web. At the reception end, we planned to make a heads-up comparison of the IPST developed GaAs two-wave-mixing interferometer and the heterodyning Mach-Zehnder from LBNL. Both methods would use LBNL's scanning mirror/timing system for textural noise reduction. We planned to implement a common solution integrating technology developed at IPST and LBNL. Emmanuel devised a simple optical method (not the parabolic mirror scheme proposed earlier) to scan normally and extend the scanning sweet-time. For excitation, an Nd:YAG laser from LBNL was to be used exclusively. Since it can be triggered externally, it was easier to synchronize with a scanning mirror. Preparations for mounting the necessary lasers, optics, and web stabilizing equipment on the web handler were underway.

Signal analysis work for determination of paper bending stiffness and out-of-plane shear rigidity from laser ultrasonic Ao wave measurements continued. Studies of the influence of near field and diffraction artifact demonstrated that point source excitation is preferred to line source excitation and that excitation to reception distances should be at least 5 mm. Analysis of the influence of web tension on lightweight papers began. Programming of the signal analysis and the elastic stiffness decoding processes has progressed for the phase velocity, d□/d□, group-Fourier, and wavelet methods. We were converting the off-line Math Lab software to the Lab View language that could be used for the imbedded calculations in the laboratory and on-line instruments. At that time stiffness determinations required operator intervention at critical decision points. This process was codified in software. Some fundamental limitations of our implementation of the wavelet technique were being investigated by Yves Berthelot at GIT.

The hardware for the paper and fiber optic transport portions of the laboratory instrument had been assembled. The software for manipulation of sample and transducer heads had been written, installed, and debugged. The next critical step was to construct the fiber optic link between the lasers and the transducer head.

Most of the effort during the last quarter was in preparation for the October 2000 on-line trial on the IPST web handler. LBNL's scanning mirror, excitation timing system and excitation beam delivery system were adapted to and installed on IPST's web handler. The LBNL Nd:YAG laser was chosen (largely because of its ease of use with a scanning mirror) as the excitation source. Mounting hardware for this laser was constructed. A Mach-Zehnder interferometer from LBNL and Ga As TWM from IPST were both outfitted for trial on the web handler. The web handler was modified for the trial to handle the lasers and interferometers. A Bernoulli plate web stabilizer was installed. A first set of data has been collected with the Mach-Zehnder interferometer. Excellent signal to noise ratios have been obtained without visible paper damage. The Ga As TWM interferometer has been installed on the web handler and the trial will resume shortly.

October 1, 2000 through September 30, 2001 Report Status:

During late October and early November 2000, we conducted simulated on-line trials of laser ultrasonic equipment on the IPST web handler. Five paper types were examined: copy paper, postal wrap, bleached board, a coated board, and linerboard. The results were extremely encouraging. With the LBNL Mach-Zehnder interferometer and scanning mirror, we detected signals whose quality at 2,000 ft/min (top web handler speed) that was nearly equivalent to that of static signals. Ability to achieve sufficient signal-to-noise ratios at machine speeds has been the biggest concern for the paper-application of on-line laser ultrasonics. We have every reason to expect to continued success at speeds well above 2,000 ft/min. Thus, we are confident that the scanning mirror trick will vault us over the highest hurdles.

This did not mean that we are out of issues. Experimental dispersion curves derived from the LBNL Mach-Zehnder and IPST TWM interferometers taken at the trial did not provide stable elastic constant determinations. We are working hard to overcome this problem. To further develop and test the validity of our experimental techniques, we gathered and analyzed LUS data for three different metal test specimens. In contrast to paper samples, metal test specimens are homogeneous, elastic, and of uniform thickness and therefore both their bending stiffness and ultrasonic plate wave dispersion characteristics can be reliably estimated from known physical and elastic properties. Initial experiments on metal samples have helped improve both data collection and data processing, which have lead in turn to significant improvements in both experimental dispersion curves and bending stiffness determinations. Preliminary results for bending stiffness derived from our LUS technique were found to be within 20% of their estimated values. This result is very significant and encouraging since it is the first demonstration of the applicability of our LUS method for reliable bending stiffness determination on metals and indicates its real potential for paper samples. For paper samples, the high variability in elastic constant determination comes from the limited frequency composition of the signals, the low signal-to-noise ratios of the critical lower-frequency components, and from some peculiarities of our Fourier analysis routine. We made improvements in bandwidth and have some ideas to improve the elastic constant determination algorithms. It's imperative (for laboratory as well as on line operation) that we overcome here.

Development of the TWM-based laboratory instrument continued. A laser-safety housing with interlocks was completed. Signal analysis and elastic constant determination software progressed, as did software for mechanical manipulation.

Work on the fiber optic delivery systems went on. These were for incorporation into the laboratory systems and perhaps the on-line system as well. We were concentrating on the development of generation-side fiber optics. Only one fiber is required for generation whereas two different fibers are required for detection. Thus the generation side provided a simpler first-time challenge. Multi-mode fibers were employed to reduce the power density. In preliminary testing, we achieved over 10 mJ per pulse through-transmission from 12 mJ incident pulses both in single shot and in continuous mode operation at 10 Hz. Over 12,000 shots were transmitted continuously through the fiber without noticeable decrease of transmission efficiency both at 1064 nm and 532 nm. The lens used to focus the free space beam to the entrance of the fiber has a long focal length in order to avoid plasma creation in the air near the focal point. Nonetheless, plasma discharges were sometimes observed. These were most probably initiated from dust particle traversing the focal region. Plasma discharges are rare in the laboratory, but they could cause a serious problem on-line. Therefore, we constructed a custom, sealed fiber-launch chamber. We experimented with smaller diameter fibers to obtain increased flexibility for

limited-space application. At exit-end of excitation fiber optic cable, we employed miniature aspheric lenses to replace the standard spherical optics of bulky microscope objectives. This reduced the bulk of our laboratory end-effector and facilitated experimentation in the tight confines of an on-line sensor.

Most of our effort in the second quarter was in preparation for the August 2001 trial, which was conducted on the pilot coater at Mead Central Research in Chillicothe OH. In February LBNL and IPST personnel visited the Mead Research Center. Plans were made for a July trial on the coater. We hope to demonstrate applicability on grades with basis weights ranging from copy paper to paperboard basis, with bleached and unbleached furnishes, and with coated and uncoated surfaces. For the first time, we will be able to test our techniques at high machine speeds under near-production conditions.

To facilitate same-side signal excitation and detection in the August 2001 trial, the detection system's spinning mirror was reduced from 1 inch to ¼ inch in diameter. No loss of signal quality was observed. Rick Goodlin of Mead Corporation visited LBNL to discuss details of the trial location on the pilot web machine, and the structural modifications to the machine to be made by Mead. We have evaluated a compact version of our on-line Mach-Zehnder interferometer. The Polytec CLV 700 vibrometer is small enough to be housed in an ABB scanner. Use of this device would eliminate the need for reception fiber optics and reduce the overall complexity of the on-line instrument. We concluded that we can use this vibrometer on-line if an ultra compact sensor is required.

Development of the TWM-based laboratory instrument continued. By taking advantage of unique characteristics of the time-domain Ao signal, we automated and improved our elastic constant evaluation process. The time-domain Ao signal is a burst with the high frequency components up-front. Therefore, a signal averaging technique that implements progressively longer averaging intervals in the later portions of the recorded signal can improve signal quality. Also, the Ao signal must be time-windowed before Fourier analysis to eliminate the So signal and exclude signal-poor, noise-rich intervals. By analyzing preliminary, representative signal, we automated the time-windowing and the progressive signal averaging. This has greatly improved the fidelity and repeatability of our elastic constant determinations. The process was to be utilized in the on-line as well as the laboratory system. Probe and paper manipulation software was complete, whereas user-interface and elastic constant determination software development was ongoing.

We ran experiments on copy paper grade and board samples with the TWM interferometer to assess the repeatability of the laser-ultrasonic measurements and the spatial variability of the 5-mm-span bending stiffness and shear rigidity of paper. We found that same-spot repeatability was the order of a few percent for bending stiffness on both grades and shear rigidity of on paperboard. The bending stiffness spatial variability from one location to another was about 10%. Given the rough formation of machine-made paper and the high dependence of bending stiffness on caliper, we decided that this was a reasonable expectation for 5-mm span measurements.

The Georgia Tech. contingent made preliminary measurements of copy paper bending stiffnesses over a moisture content range of 3.5 to 9.0 % and a temperature range from 25 to 75 ^{o}C. Results are in-line with expectations extrapolated from contact ultrasonic literature values. Good results with a single-separation wavelet approach have been demonstrated. The plan is to investigate a computationally simpler single-point d□/d□ Fourier technique. If success

continues along these lines, we will gladly consider adapting one of them for the laboratory and/or on-line instruments.

In the third quarter, preparation for the laser ultrasonic demonstration on the pilot coater at Mead Central Research in Chillicothe Ohio continued to be our principal activity. We implemented means for mounting the instrument to the pilot machine, installed an x-y motorized translation stage to control detected ultrasonic wave travel distance and direction, and developed a fiber optic laser beam delivery system. We improved our scanning mirror design and deployment and added software features in anticipation of special on-line needs and to compensate for shortcomings in the commercial interferometer. The trial was scheduled for the week on August 13, 2001. A total of 3 people from IPST and LBNL were assigned to carry out the trials and both LBNL and IPST principal investigators are scheduled to attend. ABB was also represented.

Development of the TWM-based laboratory instrument continued. We made important progress on the last major technological challenge. The fiber optic delivery and return optics for the interferometer was greatly improved, and collection efficiency was approaching that of free-space optics. Signal analysis software development continued and we were ready for full implementation. The first checkout was planned right after the mill trial.

We expected that the potential of the laser ultrasonic methods to measure MD and CD web tension on lightweight sheets might be an extra boon for our technology. On-machine profiles of CD web tension could provide a valuable papermaking tool. A calibrated sheet tensioning apparatus has been constructed in order to assess the feasibility of this idea and quantify the influence of tension on the Ao wave propagation.

Our main goal for final quarter was to make a successful sensor demonstration on the pilot coater at Mead Central Research in Chillicothe, Ohio. The trials transpired during the week of August 13. Four researchers from IPST and LBNL (along with a representative of ABB, our industrial partner) attended the trial. The support from Mead staff was outstanding, and we are indebted to Rick Goodlin and his associates.

We are pleased to report that the demonstration was extremely successful. We examined six different paper grades with basis weights ranging from 38 g/m^2 to 280 g/m^2. With only one exception, we obtained excellent signals at all machine speeds including the 5,000 ft/min maximum. The exception was the 280 g/m^2 multi-layer paperboard. At first this outcome was puzzling since we have had good results on paperboards in the past. In the end, we attributed the puzzling A_0 wave propagation in this sample to the reflection of ultrasonic waves at the interface between the heterogeneous layers of the paperboard. Laser excitation does slightly mark the sheets. However, without location foreknowledge, these marks are difficult to find, and all were amazed at the lack of damage. Waveform analyses and elastic constant determinations were preformed on-site and later-on more deliberately in the laboratory. Results were in-line with laser ultrasonic laboratory results and were in expected agreement with estimations from contact ultrasonic measurements. When moisture was purposefully applied to the web on the coater, the decrease in calculated elastic properties was in accord with expectations. The measured effects on changing web tension agreed, to the uncertainty in the measurements, with theoretical expectations. We experimented successfully with fiber optic delivery of the laser excitation beam.

Back in Atlanta, a laboratory web-tensioning device was constructed in order investigate the role of tension on A_0 wave propagation in paper. Results are forthcoming, and we will soon know whether the tension effect follows our theory, if elastic constants determined on lightweight grades need to be corrected for web tension, and whether it is possible to also measure web tension on with laser ultrasonics.

Progress on waveform analysis continued, and more work is outstanding. Except for frequency bounding, the elastic constant determination was automated. Poor on-line signals due to Mach-Zehnder automatic gain control kick-in during signal recording were culled out. Evaluation of wavelet utility for on-line and laboratory determinations started. Full automation will proceed when the automatic laboratory instrument is functional and routine evaluation is feasible.

We have scaled down the research proposal for the continuation of the project in accordance with the requests from the D.O.E. Sensors and Control committee. We resubmitted a stripped down proposal in December 2001.

October 1, 2001 through September 30, 2002 Report Status:

We spent quite some time on the first quarter (mid- September till December 2001) covered by this report, analyzing the considerable amount of data obtained from the pilot coater trial at Mead Central Research in Chillicothe, Ohio conducted in August 2001. The parameters we analyzed were: influence of web speed on the analysis of the elastic constants, influence of web tension, influence of moisture content. The influence of those parameters was as we expected similar to their influence on off-line ultrasonic testing which was comforting.

Preliminary data from the laboratory web-tensioning device was analyzed. We tested 4 different grades ranging from Newsprint to 42-lb Linerboard and compared the dispersion curves for different tensions applied to the web. As we suspected, it appeared that laser ultrasonic dispersion curves on lightweight can and must be corrected for the influence of web tension. It didn't appear, however, that the dispersion curves are sufficiently sensitive to tension to allow accurate, independent tension measurements.

We made plans for the mill trial scheduled in 2003. We have made a list of the issues to address for hardening the laser ultrasonic sensor and making a full test on a production line as successful as the trial in August 2001.

Paul Ridgway has completed a first draft of publication concerning our August 2001 trial at Mead Research in Chillicothe, OH. An article submitted by Emmanuel Lafond to *Ultrasonics* a while ago was accepted by reviewers, to be published towards the end of 2002. It deals with ultrasonic measurements of Lamb waves in paper by photorefractive interferometers.

We made progress on the development of fiber optic delivery systems. Nonetheless, this remained the major technological hurdle in the construction of an automated laboratory laser ultrasonic instrument. Fiber optic couplers for both laser excitation and reception have been mated to the end effector of the apparatus that manipulates the sample. For the first time, we recorded and analyzed many waveforms with a complete lab instrument. However, results (especially the extent of the bandwidth of over which the mechanical constant are derived) were disappointing when compared to the standard performance of our free-space optics. After examination and rumination, we thought that the problem came mainly from the generation side. Because of same-side generation and detection implemented from the end effector, the generation spot is too large.

We made experiments with different configurations, and we think we have come up with a design that will give consistently good results. Also, electro-mechanical operation of the end effector and sample manipulation system caused new noise problems in our detection electronics. Fiber optics development continues, as does troubleshooting of the new noise problems caused by the robot.

Progress has been made in the automation of the online sensor's mechanical operations. Control of the scanning mirror rotation speed can now be linked to an encoder signal indicating web speed. The generation laser timing system is now computer-based and shows improved stability.

We reevaluated our industry support agreements. We sent letters to the on-line equipment manufacturers requesting more technical involvement. This hopefully will lead to greater

participation and commitment on their parts. We feel industry advice and support will be determinant for making a commercially viable sensor for the industry.

Also, a no-cost extension for completion of ongoing tasks was approved by DOE in the Jan-March quarter of 2002.

In the April-June quarter of 2002, LBNL and IPST project members finally completed the publication concerning our August 2001 trial at Mead Research in Chillicothe, OH that was submitted to JPPS.

IPST worked mainly on the laboratory instrument that quarter. We implemented a new design for the generation end-effector with a smaller diameter fiber for generation that gives good signal to noise ratios and a wide bandwidth comparable to the one obtained for free space optics. We think we solved the noise problems we had last quarter due to the robot moving the paper. To do so we had to use an optical/electrical one way system (no adverse feedback) to measure the amount of light coming back to the interferometer. We built the software part for this feedback that will be integrated to the main software in the future. Ted Jackson also developed a RS232 software interface to drive the generation laser by computer.

On the 2nd quarter of 2002 we were in the process of searching for a generation laser dedicated entirely to the lab instrument with more stringent requirement on a maintenance-free operation and long lifetime + much smaller footprint than the current laser. We reviewed different generation lasers and expected to test at least one of them next quarter before purchase.

Progress was also made in the automation of the online sensor's mechanical operations. Control of the scanning mirror rotation speed can be linked to an encoder signal indicating web speed. The generation laser timing system is now computer-based and shows improved stability.
Signal analysis software developed at IPST in conjunction with the lab instrument was sent to LBNL, where it will be integrated with the online sensor.

To expand our capability to analyze heavier grades on-line we needed to enhance low frequency signal amplitude or detector sensitivity. We evaluated ways to increase the excitation laser pulse width and testing detector modifications.
A digital decoder was tested with the existing Mach Zehnder interferometer, and found not to give increased sensitivity to low-frequency signals. A variable pulse width YAG laser has been located in Livermore National laboratory, and arrangements were made to test the effect of longer pulse widths on low-frequency signal amplitude.

A much smaller sensor head, tested last year, has been ordered to replace the Polytec-PI OFV 353 head used in the August 2001 trial of the on-line sensor. This will facilitate construction of a more compact system for the Summer 2003 full-scale mill test.

ABB has answered our letter that was asking for more industry involvement with some interesting suggestions and some questions. We wrote back a letter trying to answer their questions & suggestions step by step. We also contacted Honeywell (HMX) by telephone to get their feedback about our first letter. Ross MacHattie (HMX) told us the company wasn't currently favorable to long-term projects, although he is convinced of the potential of our sensor. Hence he will keep trying to persuade his superiors and asked us to be given more time.

Chuck Habeger retired from IPST on June 30th but continued to work on the project during 6 months as a part-time consultant. He will continue to help us with his paper physics knowledge and signal processing development after September 2002. With Rick's agreement Emmanuel Lafond replaced him as the principal investigator at IPST. Change of P.I. has been submitted to DOE for approval.

For the last quarter (July –September 2002) covered by this report, IPST continued to work mostly on the laboratory instrument. We tested then purchased a generation laser to be dedicated and integrated to the laboratory instrument. Its advantages are a much smaller footprint for the laser head than the current laser, a much longer time interval between any maintenance operation, for a slightly smaller price. Meanwhile we continued the testing and software writing of the probe manipulation of the lab instrument with the existing generation laser. The robot has been programmed to do polar plots determination and standard MD-CD testing. We have automated a process to optimize the elevation of the laser optics above the paper sample for each measurement.

Ted Jackson and Chuck Habeger did several studies for optimizing the displacement of the probe on two grades: white raw stock (87 g/m^2) and 42-Lb brown linerboard (205 g/m^2). They concluded that for both papers grades (and any grade) at least 10 signals should be averaged before any analysis, and that the sample should be translated 0.1 mm between laser firing to avoid signal washout from the generation beam repeatedly impinging the paper. They are currently studying the effect of the reflections at the edge (to avoid miscalculating elastic constants).

LBNL has been studying double signal generation, and though results are promising, the technique is not as accurate or reliable as single generation. A digital filtering scheme was proposed to improve discrimination between near and far signal components but we have no conclusion on that topic yet.
The compact interferometer head was received and tests have begun. The advantage of the smaller size is offset partially by more signal dropouts. The analysis software can reduce or eliminate this problem, at the cost of longer data acquisition times. Reduction of the optical path length is expected to reduce this problem as well.
Ted Jackson and Paul Ridgway have been making good progress adapting the software for automated data acquisition developed at IPST to the online instrument. Scheduling issues with the owners of the variable pulse width laser have delayed experiments with longer pulse widths. We hope to be able to do these experiments next quarter.

For the full-scale trial next summer we have requested installation on a paper machine that uses a sensor scanner with at least one (preferably two) unused instrument slots available for installation of the LUS sensor. We are thankful for Paul Ridgway and Rick Goodlin to lead the effort to find a host mill for the full-scale mill trial. They are trying first with a mill at MeadWestvaco but other alternatives could be envisioned as well.

Following Gideon Varga's suggestion, Paul, Emmanuel and Gideon visited the Timken steel mill in Ohio where a laser-ultrasonic sensor has been installed (DOE/OIT-funded project). It was quite impressive to see how well the sensor operated in this harsh industrial environment. The possibility of partnering with Tecnar was discussed. We recommend that paper industry representatives and sensor suppliers also visit the Timken mill.

October 1, 2002 through September 30, 2003 Report Status:

In the Fall of 2002, IPST tested then purchased a detection laser for integration to the laboratory instrument. One of its advantages is a significantly smaller footprint than the current laser, but mostly, a much smaller price tag compared to the current laser which is an older model. However free lunches don't exist in the technical world. Hence we had to purchase and add an optical isolator to this new laser because it was too sensitive to the back-scattered light compared to the previous laser, if it were to be used as is. We calculated that the cost reduction achieved was well worth adding a little complexity to the instrument. Using this new detection laser and the new generation laser we purchased last quarter decreases considerably the cost of a potential LUS lab instrument measuring Flexural and Shear Rigidities. A more accurate near/far translation stage for the generation probe was also implemented to the instrument.

We also continued the testing and software writing of the probe manipulation of the lab instrument. We have automated further the signal processing and it can now determine automatically the best frequency range over which the mechanical constants are calculated. Moreover, both the previous or newer generation lasers (interlock open, laser firing, etc…) are now controlled by the software through the computer. An article about the Two Wave Mixing method we use for ultrasonic detection was published in December 2002 in the journal *Ultrasonics.* Chuck Habeger who retired from IPST in June, continued to consult for the project till December 2002 and is now working at the Weyerhaeuser Technology Center in Tacoma, WA.

In an effort to expand the range of sheet basis weights that can be analyzed with the online instrument from 130 g/m2 to heavier grades, experiments were carried out at two longer excitation laser pulse widths, 125 nanoseconds and 5 microseconds. The pulse width we have been using up to now has been 5 nanoseconds. Re-determining the maximum basis weight we can analyze at 5 nanoseconds, we found it to be 165 g/m2, by analyzing signals obtained at 5 mm longer separation distances than are optimum for lighter grades. We found that the two longer pulse widths gave similar amplifications of the low frequency portions of the signals, and that these signals allow correct measurements to be obtained on sheets of basis weights up to 210 g/m2. Further experiments are planned for higher basis weight materials.

Experiments showed that Flexural Rigidity (FR) is proportional to the cube of the caliper. FR is proportional to the first order to sheet density, tensile elasticity, and Poisson's ratio also. However, it is likely that our sensor provides a valuable noncontact sensor of caliper variation because 1) these other properties change less than caliper, 2) FR is so much more sensitive to changes in caliper than to these other properties.

For the production mill trial, we have requested installation on a paper machine that uses a sensor scanner with at least one (preferably two) unused instrument slots available for installation of the LUS sensor.

Preparation for a full-scale mill demonstration is proceeding. A search is under way at MeadWestvaco for a mill site. We have narrowed the search to one of two machines at one mill site, a paper making machine and a coater. The two machines produce coated grades with basis weights ranging from 100-160 g/m^2.

Recent experiments have shown that using our standard generation laser (with 5 nanoseconds pulse width) with modified generation-detection distance spacing, we can get good signal to

noise ratio A_0 waves producing the bending stiffness values we expect. This is obtained with the online instrument on paper with basis weights up to at least 165 g/m^2, but not on basis weights of 205 g/m^2 or more. This is a considerable improvement over our previous basis weight upper limit of 100 g/m^2.

IPST has provided LBNL with the latest version of the software for acquisition and analysis of the A_0 waves for the on-line software.

We are running the laser ultrasonic (LU) laboratory instrument with the new low cost detection laser purchased earlier. The instrument gives good results on lightweight grades.

The automated signals analysis software routine is giving good results on lightweight paper and light linerboard. We still have some difficulties with the quality of the A0 waves obtained on heavy linerboard and are working to improve the signal to noise ratio.

We are comparing both the Two-Wave Mixing and Mach-Zehnder LUS results to measurements more commonly used by the industry (Tabor test; resonance method, and contact ultrasonic testing) so as to establish a correlation. Measurements of bending stiffness by already existing methods are inherently less accurate than by laser ultrasonics due to the inaccuracy on the caliper measurement. We expect that once confidence in the laser ultrasonic measurement has been established, this correlation will reveal the inherent uncertainty that plagues the conventional mechanical measurements.

Preparation for the full-scale mill demonstration is moving forward. On April 28 and 29, Paul Ridgway and Emmanuel Lafond visited the paper mill site of Escanaba, MI (a MeadWestvaco mill). They met the process control Senior Engineer (Mark Ryan) of one of the paper machines and checked the other paper machines and coaters, for an installation of the sensor. Following this visit we have narrowed the search to a paper making machine and a coater. We expect the mill to allow us to install the sensor on one of these two. The advantage of these machines is that they have scanning sensor heads made by ABB, our industrial partner. Therefore we have support for the installation and interfacing of our sensor with the other sensors on the scanning head. The prototype sensor is being designed to mount onto the side of ABB scanning head. This mounting technique, which is routinely used by ABB for testing their prototype sensors online, will allow a relatively easy installation for the mill trial. No disassembly of the ABB scanning head or Smart Platform frame will be required.

We have back-engineered and tested with success a Bernoulli web stabilization plate with a wider aperture (for the laser beams) for the mill trial. This will enable us to test at wider separation distances between the generation and reception spots, if needed.

Construction of the sensor system has begun and the system will probably be finished and may be tested, within a few months.

Flexural Rigidity results must be corrected for the moisture content in the paper. Thus, we are working with Ake Hellstrom (ABB Senior Engineer) to incorporate an ABB LabView code and a circuit into the interface of the sensor so that it can decipher the moisture content information coming from the moisture sensor on the ABB scanning head. Ake has also contributed considerable time and valuable assistance with the design of the prototype sensor.

Before installation in the mill, we will thoroughly test the completed sensor unit at IPST on a pilot scale web handler equipped with an ABB Smart Platform scanner. Our prototype sensor will be installed and operated in the manner planned for the mill trial. MeadWestvaco representatives will be encouraged to witness the operation of the sensor on the IPST web handler, and give their comments and suggestions for the mill trial.

We calculated the savings of energy, fibers, chemicals that will be resulting from the use of the sensor information for improving the process control of the paper machine. This was done using a Jaakko Poyry Consultants model available at IPST. The savings are more substantial than we thought:

Based on a 2.13 % projected reduction in basis weight needed while still reaching stiffness targets on a machine producing 175,000 Metric Ton per year of uncoated free sheet, savings of approximately $1,070,000 per year are expected due to reduced fiber, chemicals and energy use. Additionally, an estimated reduction in off-standard product from 6.2% to 5.2% (1% absolute increase in first grade production) is expected to lead to a corresponding savings of about $376,000 per year. The total is therefore an estimated savings of $1.446 million per year. This needs to be compared to the total estimated cost of a sensor to a paper mill comprised between $152 and $202 k. The duration it takes for the sensor to break even compared to its cost is therefore less than 2 months. Those numbers encourage us to proceed with the mill trial and to demonstrate the sensor on a paper machine as soon as possible.

Since the decision was made to implement the LUS technology as an add-on prototype module to the ABB Smart Platform scanning head package, enabling web-width profiling (as opposed to single point) and easing potential integration into the head package as a standard production module later, it was a natural decision to make use of some existing platform instrumentation and sensors, including the platform's basis weight and moisture sensors, which are necessary for accurate LUS calculations. Tapping the basis weight sensor entails the development of calibration methods for accurate translation of raw electrometer voltages corresponding to mass absorption into actual basis weight numbers. Tapping the moisture sensor has entailed building electronic circuitry and developing software to emulate the platform's internal translation of raw sensor integration pulses into actual moisture numbers and for controlling moisture signal gain. Interfacing to the platform's gliding caliper sensor was a simple and straightforward additional element.

Lastly, the head package's scan position encoder was tapped, including the construction of electronics, which will allow direct measures of scanning head position for accurate scan-to-scan alignment. In the past few months, we have completed all of that work. Additionally, we implemented controls for scanning and standardizing of the position of the head package of our pilot-scale scanner. The main benefit of this work is that installing the LUS sensor in the mill should be a very quick and painless operation that will involve an absolute minimum of time during which the platform is not able to perform its regular duties.

Also, it will be possible to operate the sensor in the laboratory under conditions that will be nearly identical to those that will be present at the mill, increasing our confidence that the actual mill trial will go smoothly and as planned with few hidden variables. Pass-through interface connectors were designed and constructed so that no part of the Smart Platform electronics will need to be modified or hard-wired to in any way, which should be attractive to mill personnel. Removal of the sensor and interfacing in the mill should take only five to ten minutes.

We have tested the output of the generation laser for the mill trial with the fiber optics running continuously at the maximum repetition rate and observed no drop in energy per pulse. The laser pulse duration has been increased so as to allow the fiber tip to withstand without deterioration the thousands of laser shots it will be submitted to in the mill trial.

The drawings of the prototype sensor have gone through several iterations between LBNL and IPST and Ake Hellstrom (ABB Senior Engineer) participated to the iterations (reword). He gave us extremely valuable insights to the design of the sensor with many suggestions and drawings.

We plan to test the completed prototype sensor unit at IPST on our pilot scale web handler equipped with an ABB Smart Platform scanner in between November 2003 and February 2004. Then, after discussion with the mill and the acceptance of the drawings for installation on their machine, we will proceed with the mill trial. We foresee the full scale mill demonstration occurring in Spring 2004.

IPST integrated into the Georgia Institute of Technology on July 1st, 2003 to become the newest department of Georgia Tech as IPST @ Georgia Tech. This slowed the project somewhat on IPST side because of administrative complications but did not stop us in moving forward. Transfer of the allocated DOE funds from IPST to IPST @ GT should be done before the end of the year.

October 1, 2003 through March 31, 2004 Report Status:

During the Fall of 2003 Paul Ridgway finalized the on-line sensor design with the input of Ted Jackson and Ake Hellstrom (ABB Senior Engineer). This implied making many drawings of the parts for machining them at LBNL. The design of the auxiliary system (cooling circuit regulation, clean air supply, electrical, detection laser, etc…) was also completed by Paul in the Fall of 2003.

To spread the workload and speed up the delivery of the system it was decided jointly that IPST would be in charge of assembling and testing the auxiliary system. IPST tested a vortex tube to cool down the sensor housing using air at 80 psi and 40 cubic feet/min air and it seems the cooling will be more than sufficient for the mill environment. The preliminary set up of the auxiliary system has been done and it worked as expected.

Ted Jackson has pursued the development of the automated acquisition and analysis software. We are targeting the maximum repetition rate of the generation laser for the acquisition and processing of a signal (10 Hz). But due to the extensive calculations needed we do not know yet if we will be able to achieve this rate. Other strategies may be needed to shorten the computing time, such as rewriting part of the code, keeping the frequency window analysis constant, etc…

Mark Ryan (Process Control Engineer from Escanaba) will ship to IPST some paper stripes so that the shake down of the sensor is performed on several grades typical of those produced at Escanaba.

In prevision for a shake down of the sensor at IPST preliminary to its installation at Escanaba, Ted Jackson and Emmanuel Lafond have also put back into running condition the IPST pilot scale web handler, ABB scanning platform and laser interlock system.

In January 2004, Ted Jackson with the help of another engineer of IPST, tested the auxiliary system for the on-line sensor successfully. The auxiliary system harbors the controller for the translation stages which position the generation end-effector, also hosts the detection laser, and various air supplies to cool down the sensor, feed the web stabilization device, etc…
At the same time but on the west coast, Paul Ridgway finished the design, construction and assembly of the sensor housing and most of the sensor hardware at LBNL and did some preliminary testing. This equipment was then shipped to Atlanta for the final assembly of the complete system and hardware shakedown tests.

The system assembly and the hardware shake down of the sensor took place from February 2 to February 13, 2004 at IPST with Paul Ridgway traveling to Atlanta for the occasion. We assembled the sensor system, fed the wires and cable to the sensor through a flexible hose so that it doesn't require the installation of any new cables inside the ABB frame. We attached the sensor to the ABB head package on the Smart platform the same way it will be in the mill. The sensor is noticeably easy and quick to install on an ABB head package.

We ran the sensor on a 77 g/m^2 offset paper moving with a speed ranging from 500 feet/min to 2500 feet/min (maximum speed of the web handler) and obtained MD and CD flexural rigidities conform to those obtained with our laser ultrasonic laboratory instrument (those results are reported in our TAPPI spring conference paper, to be published at Papersummit 2004).

In February and March, Ted Jackson assembled the different components of the software that were not previously integrated (MD and CD motion control for generation system; spinning mirror control) and did much troubleshooting. Now, the software processes signals faster than the maximum repetition rate of the generation laser (10 Hz); which was our objective. He also linked the acquisition panel to a signal processing panel so that we can either do real-time processing of the data, or “re-play” the flexural rigidity and shear rigidity history through recorded ultrasonic signals.

We had planned to visit the MeadWestvaco Escanaba mill again shortly after the IPST shakedown and discuss the drawings of our system so as to sort out installation requirements and plan the full-scale trial with the mill. In mid-March 2004 we heard back from MeadWestvaco, with the word that due to severe personnel shortage and downsizing, the Escanaba mill can no longer welcome us for the mill demonstration of our sensor. The mill personnel is spread too thin already and won’t be able to supervise the installation of a new sensor and exploit its results. We then proposed that IPST at Georgia Tech hires back temporarily one of the process control engineer that the mill had let go, to which the mill objected that there were not comfortable doing that.

This is obviously a setback as we were ready for an immediate mill demonstration. But we are pursuing talks with MeadWestvaco for a test in another of their mills (a board mill) and with another paper company that very recently expressed interest. At this stage, the technical and software hurdles having been solved and the sensor having been built, we feel our focus needs to be on finding a new host mill quickly so that we can do our full-scale demonstration as planned.

Our paper entitled “Laser Ultrasonic System for Online Measurement of Elastic Properties of Paper”, which was published in the September 2003 issue of the Journal of Pulp and Paper Science, was chosen as the recipient of the TAPPI Journal Editorial Board’s 2003 Outstanding Research Paper Award. Honorary plaques will be awarded to the authors on May 4 at the TAPPI Spring Technical Conference.

The beginning: Experiments for determining laser ultrasonics methods suitable for on-line measurements of stiffness on paper

This part of the report shows the essential elements from a previous report written in 1998. Some chapters have been omitted to keep the length of the final project report within reasonable limits.

1 INTRODUCTION

1.1 Motivation for Present Work

Baum stated in a landmark paper published in 1987 the following (Baum, 1987):

> "The elastic properties of paper form a basic set of parameters which are useful for monitoring the effects caused by changes in process variables, capable of predicting end use performance, and overall, help to provide a better understanding of the fibrous network we call paper. Elastic parameters also are important in product design and modeling, e.g., in the construction of tubes, boxes, food containers, etc. Eventually their use will help to control the paper machine automatically. Because most of the elastic parameters needed to describe paper can now be determined easily and non-destructively using wave propagation methods, the opportunity exists to move forward in each of these areas."

In the context of real-time control of the papermaking process, which is the long-term motivation behind the present project, Table 1.1.1 summarizes in a very simple way the effect of machine variables on different elastic stiffness properties (Baum, 1987; Ishisaki, 1997). It can be seen that the inverse problem of predicting the behavior of individual sub-processes from elastic stiffness measurements is complex because some of the processes can produce similar trends on stiffnesses (e.g., refining and wet pressing). This implies that additional information is needed such as the geometrical fiber orientation distribution (FOD) and the stiffness orientation distribution (SOD). Differences between FOD and SOD can be appreciated in Figures 1.1.1 and 1.1.2. In Figure 1.1.1, one can see that the FOD for laboratory machine-made paper samples manufactured under different wet straining and restrained conditions is unaffected by these processes. This is not the case for the SOD in Figure 1.1.2, which is sensitive to wet straining and/or restrained drying. Contrary to FOD, SOD depends upon built-in stresses.

Table 1.1.1 Effect of machine variables on elastic stiffness properties.

Elastic Stiffness Constants	Refining Level	Anisotropy Ratio	Wet Pressing Level	MD Wet Straining Level	Restrained Drying
	From Low to High	*From Low to High*	*From Low to High*	*From Low to High*	*From Full Restraints to CD Only*
MD: C_{11}	↑	↑	↑	↑	0
CD: C_{22}	↑	↓	↑	↓	↑
ZD: C_{33}	↑	0	↑	↓	0
MD-CD: C_{66}		↓	↑	0	
MD-ZD: C_{55}		↑	↑	↓	
CD-ZD: C_{44}		↓	↑	↓	

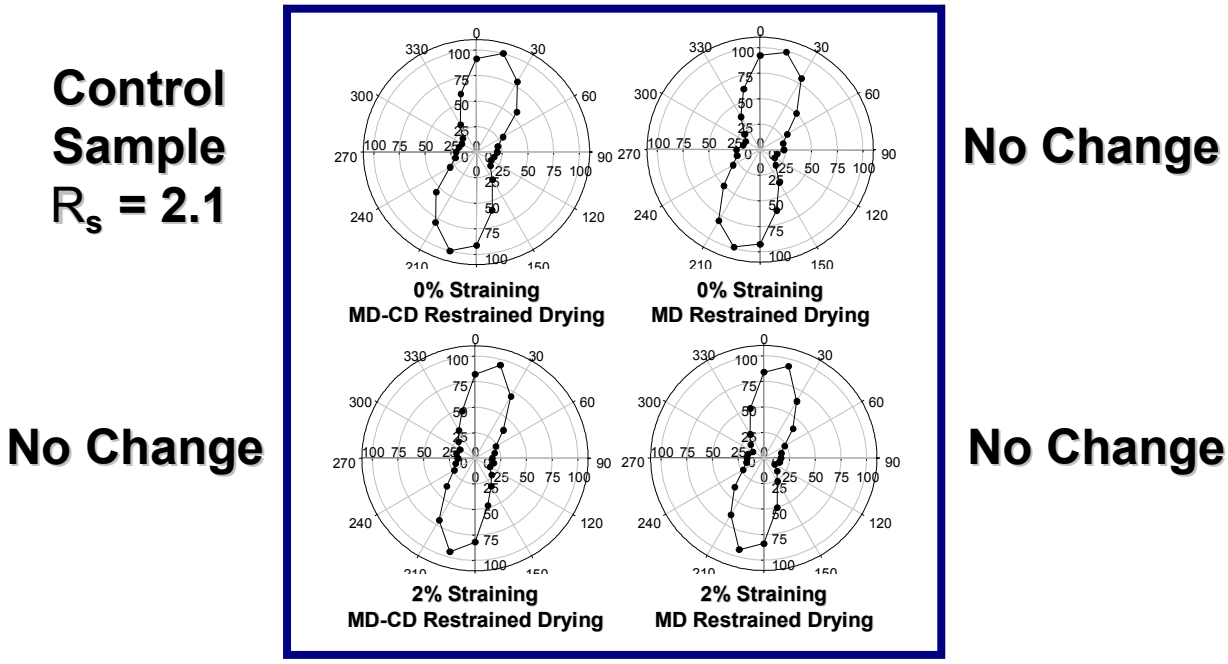

Figure 1.1.1 Geometrical Fiber Orientation Distribution (FOD) for different paper samples manufactured under different wet straining and restrained drying conditions. Control sample (MD/CD ratio = 2.8) is in upper left corner. Straining and restraint drying do no appreciably affect the FOD.

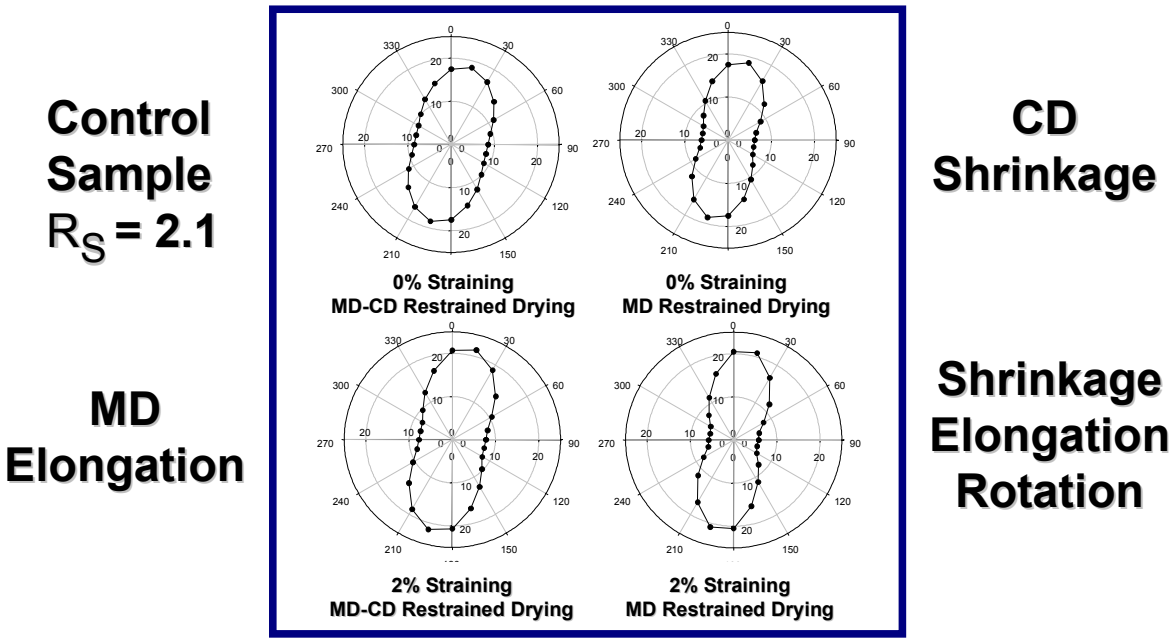

Figure 1.1.2 Stiffness Orientation Distribution (SOD) obtained for different paper samples manufactured under different wet straining and restrained drying conditions. Control sample is in the upper left corner. Restraint drying and wet straining affect SOD.

To this day, nobody has attempted to tackle the inverse problem presented by Baum, experimentally, numerically, or theoretically. Because it is so difficult, it is believed that an experimental approach must first be investigated to gather hard evidence. Also, it is postulated that existing information obtained on a paper machine (grammage, thickness, moisture content, web temperature) and currently unavailable information such as stiffness properties, FOD and SOD, can be used in a meaningful manner to provide a preliminary layout of a model to control the papermaking process.

1.2 Introduction to the Project

The task of achieving real-time control of the papermaking process is a long-term goal. First it is necessary to develop appropriate instrumentation to determine stiffness properties, FOD, and SOD, and demonstrate the functioning of this instrumentation first in the laboratory, then in a mill environment. Since measurements would be of limited interest without an attempt to interpret them and predict the impact of machine variables on paper mechanical properties, it is important to begin as early as possible an investigation of the relationships between machine variables and mechanical properties. This is the essence of this project. Commercialization of technology, development of process control strategies, actuators, and development of a monitoring system considering full sheet inspection rather than a scanner-based approach are beyond the scope of the project.

The purpose of the project is two-fold:

1) To develop and demonstrate from the laboratory to the mill a new technology aimed at determining stiffness properties, FOD and SOD on a moving paper web;

2) To begin an investigation of the inverse problem of relating paper mechanical properties to paper machine variables.

There have been several research and development efforts associated with the development of test methods to monitor paper stiffness properties on a moving web. However, all of them have focused on the use of contact methods to probe paperboard. It is believed that the availability of a non-contact method is largely preferable for several reasons: no potential damage to the web, rich information content, extended grade monitoring. There are two possible approaches: air-coupled transduction and laser-based ultrasound. The use of air-coupled transducers is a priori attractive because it offers simplicity and is cost-effective. However, it suffers from one major problem: measurements are sensitive to air path parameters (temperature, humidity level, turbulence level). Also, the available information may be inadequate. The second approach, laser ultrasonics, is more complex, but can provide the desirable information (stiffness properties, FOD, and SOD). This approach was chosen for the following reasons:

- Extensive scientific support;
- Rich and reliable information content;
- Simultaneous detection of FOD and SOD;
- Unlikely to damage to the web;
- Test method suitable for fine papers and paperboards (universal method);
- Potential for 100% web inspection implementation.

As a first step aimed at demonstrating the concept of laser ultrasonics on non-moving paper, The Institute of Paper Science and Technology requested the assistance of the Georgia Institute of Technology (GIT) in 1994 to initiate research work on the use of lasers to excite and detect Lamb waves in paper. Exploratory internal funding for a one-year project was awarded by both institutions in September 1994. Results were obtained very early in the project (see Figure 1.2.1) and showed that the technique was very promising. Since then, results have been reported on different paper and paperboard grades (Brodeur et al., 1997).

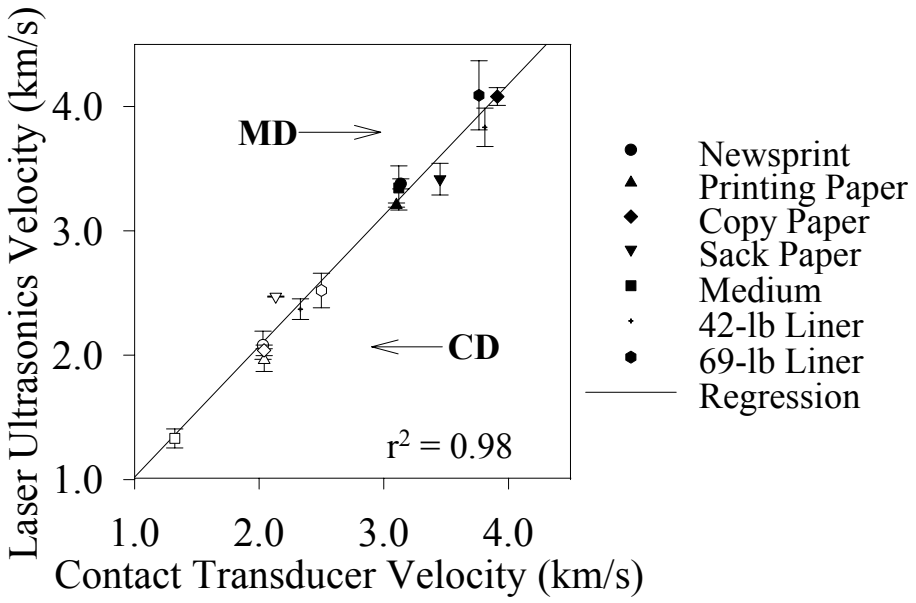

Figure 1.2.1 Laser ultrasonics validation results as obtained using different non-moving paper and paperboard samples. One can see that machine direction (MD) and cross-machine direction (CD) velocity results gathered using contact transducers and laser ultrasonics are in very good agreement (Brodeur et al., 1997).

The next step in this endeavor was to address the more challenging task of performing laser ultrasonics measurements on moving paper, first in the laboratory, then on a paper machine. A research proposal was submitted to the Department of Energy, Office of Industrial Technologies Agenda 2020 Program in 1996. The following organizations were invited to collaborate with IPST: Idaho National Engineering and Environmental Laboratory, Georgia Institute of Technology, and Honeywell-Measurex Corporation.

The proposal was reviewed and recommended for funding by the Sensors and Controls Task Group of the American Forest and Paper Association. The Department of Energy awarded a three-year contract to IPST in September 1997 and funding was granted for the first two phases of the project. It was agreed that additional funding would be provided for Phase III on the basis of successful completion of Phase II.

As soon as the project was authorized, the research team met for the first time at IPST. Following an intensive brainstorming session on the latest scientific and technical developments in the field of laser ultrasonics, a research plan for Phase I was devised. This plan was continuously reviewed and updated to optimize resources and fully meet or exceed project

objectives. Also, two extensive review meetings were held in March and May. The actual Statement of Work for Phase I can be seen in Appendix B. Also, anticipated Tasks for Phases II and III, and an updated Time Schedule for the full project are displayed in Appendix B.

Now, one year later, we are very pleased to report that we were able to fully meet or exceed project objectives for Phase I, especially the laboratory demonstration of laser ultrasonics on moving paper. The experimental methodology and the results are reported in the following sections.

2. Experimental methodology

2.1 Introduction

One of the major unknown variables in the strategy to understand and control the papermaking process is the stiffness properties of the web. Ultrasonics has long been used to determine, non-destructively, the stiffness of materials. This section details the use of non-contact, laser-based ultrasound generation and detection on a moving web.

This section starts off with a review of laser ultrasound generation and detection. Five different laser ultrasound detectors are then described and evaluated. In order to determine how well they work on moving paper, a laboratory web simulator was constructed. Finally, an optical scanning technique is described which reduces surface noise, and the effect of laser wavelength on generation is investigated

2.4 Moving web simulator

A web simulator system was developed to provide a controlled environment for simulating the behavior of a paper web in an open draw. Factors considered during design of the system included: maintaining machine direction orientation of the paper sample, providing an unsupported area of paper for testing, variable speed capability, accurate positioning for flutter simulation, and an adjustable base for aligning the motion of the paper perpendicular to the laser. Two web simulators were built, one for use by IPST and another for INL. The INL system was installed in April 1998. After some minor changes to the design of the drive system, the IPST system was installed in June 1998.

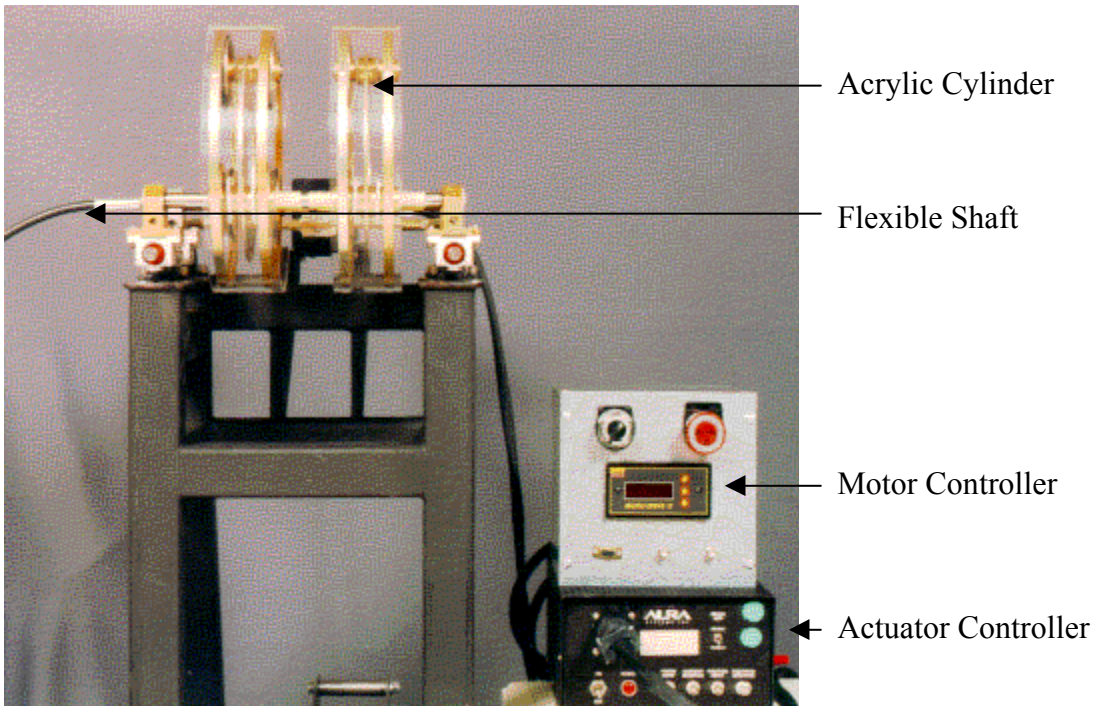

Figure 2.4.1 Web simulator cylinder detail.

Paper samples of the size 84 cm machine direction by 20 cm cross-machine direction are attached to two acrylic drums that are separated by 5 cm (see Figure 2.4.1). In addition to the separation gap, one configuration of the system utilizes drums that have 10.0 cm diameter access holes (see Figure 2.4.2). This configuration allows the transducers to be mounted behind the paper during sheet flutter simulation as well as during smooth operation (no flutter). Another configuration utilizes solid disks mounted to the drive shaft and the acrylic drums (see Figure 2.4.3). In this arrangement, the vibration of the surface of the drums is minimized while the maximum speed of the system is substantially increased.

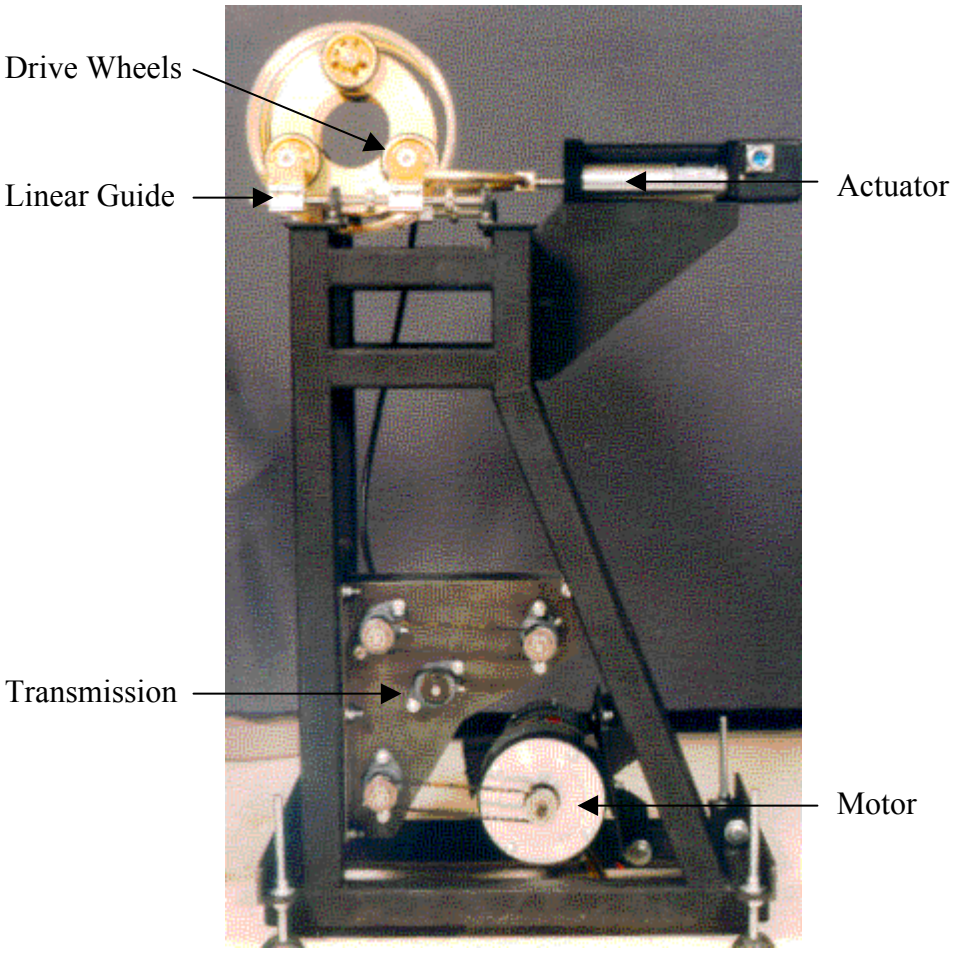

Figure 2.4.2 Wire side access configuration.

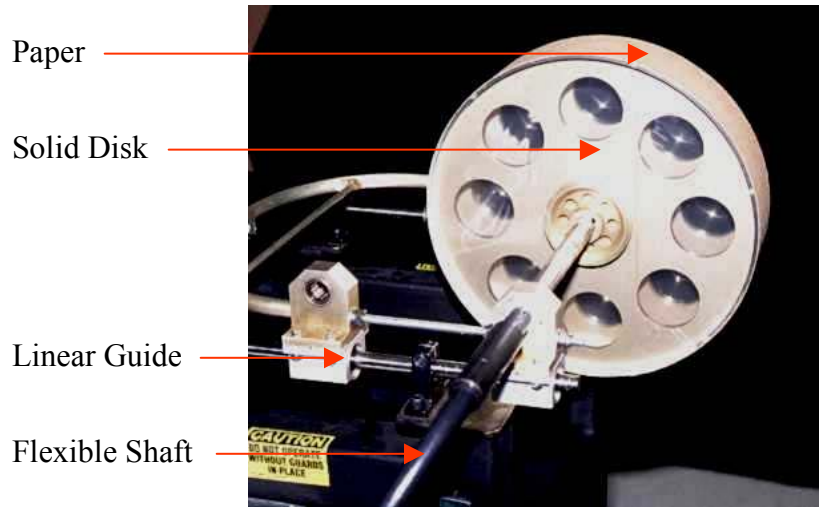

Figure 2.4.3 Solid Disk Configuration.

The system utilizes a variable speed DC drive that currently provides a speed range from 0.4 to 13.5 m/s (25 to 810 m/min or 82 to 2660 fpm) in the configuration with the access holes (configuration #1). In the configuration utilizing solid disks mounted to the drive shaft (configuration #2), the speed range is from 2 to 47.5 m/s (120 to 2850 m/min or 394 to 9350 fpm). A linear electromagnetic actuator with integral position feedback is utilized for simulation of sheet flutter. This arrangement provides 2 cm peak to peak displacement at frequencies up to 10 Hz with a reduction in displacement to 0.25 mm at 100 Hz. The actuator also has the capability of producing complex wave shapes in addition to basic sine waves. Accurate speed control of the cylinder during flutter trials is accomplished through the use of a flexible drive shaft. Surface speed is monitored by a fiber optic trigger that senses reflective tape attached to the cylinder.

All hardware is controlled by a custom LabVIEW program utilizing a National Instruments data acquisition card. The software allows the user to control surface speed via RS-232 cabling to the motor controller. Timing signals from the motor tachometer and cylinder trigger are used to determine cylinder speed and rotation position at the time of lasing. Similarly, LVDT feedback from the linear actuator is used to determine distance from the paper sample to the optics, linear velocity, and direction of travel. The program also allows the user to control the frequency and amplitude of the linear displacement as well as step and hold to a given linear position.

Several safety features were added to the design to prevent operator injury or damage to the laser and optics in the event of a failure. These features include: a completely enclosed drive system; a detachable hood covering top, sides, and back of the acrylic cylinder; a fail-safe brake on the motor; an emergency switch to disable power to all system components; locking collars on the linear slides; and a cylinder design that includes aluminum backing rings for strength and prevents the cylinder from being thrown from the machine in the event of a failure. In addition, all rotating elements were specified to operate at approximately 75% of their recommended continuous speed.

2.5 Laser Ultrasonics

2.5.1 Introduction

The reception of ultrasonic signals propagating along moving paper webs is a challenging assignment. The webs travel at high speed in mechanically noisy environments. Progress has been made using piezoelectric techniques, nonetheless laser detection promises significant advantages. The ability to receive ultrasonic signals without contacting the web is the foremost attraction of the laser approach. Laser interferometry can recover a trace of the ultrasonic disturbance by mixing a reference beam with another coherent laser beam reflected from the surface. There is no need to struggle with direct piezoelectric connections to the paper. The papermakers' reservations about instrument damage to the product fall away. Also, laser interferometry is a more broadband detection method; pulse transmissions are not distorted and elongated as they are when using the more resonant piezoelectric techniques. Measurements can be made at higher frequencies allowing application to shorter ultrasonic paths. The laser detectors are much more sensitive to antisymmetric mode propagation than are piezoelectric instruments.

The experimental investigation of laser-based methods to generate and detect Lamb waves in paper constituted the bulk of the research work during Phase I. Since the main goal was to demonstrate that laser ultrasonics can indeed be successfully used to detect Lamb waves in moving paper, our first task was to analyze all existing approaches and determine which ones would most likely work on moving paper before proceeding to experimental work.

2.5.2 Principles of Laser Ultrasonics generation

On paper products, like many other materials, there are basically four ways to generate ultrasound with a laser beam. The means of generation depend on the power density of the spot (power/area of the spot) at the surface of the material (Scruby et al., 1990; Castagnede et al., 1992; Edwards et al., 1989).

At low power density, the generation occurs in the so-called thermoelastic regime. In this regime, the surface of the material is heated very quickly by the laser beam. The sudden thermal expansion and subsequent contraction caused by heating generate stresses inside the material in a very short time, which become ultrasonic waves. In this regime, the ultrasonic waves are generated in the plane of the material. In the case of paper, this regime is expected to generate mainly in-plane S_0 waves (see Figure 2.5.1).

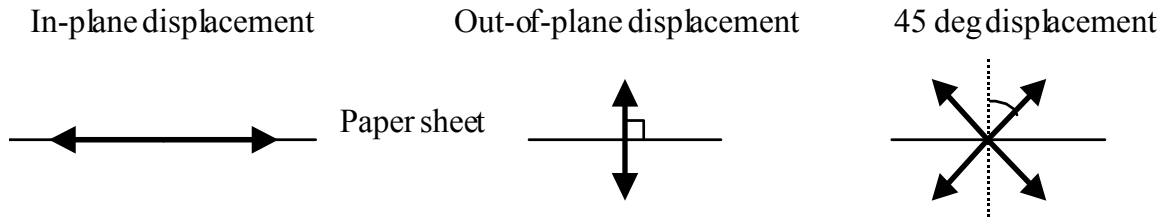

Figure 2.5.1 Definitions of displacement directions.

At higher power densities, the laser spot can be intense enough to vaporize the material surface to a depth of a few nanometers or micrometers. The sudden vaporization of the material creates a reaction over the surface that in turn generates stress mainly in the out-of plane direction. Waves generated using this ablation regime are essentially A_0 waves due to the out-of-plane stresses.

At an intensity in between those of the thermoelastic and ablation regimes occurs the so-called intermediate regime, which utilizes a combination of slight ablation and thermoelastic expansion. This regime generates both in-plane and out-of-plane waves and thus is appropriate when we need to generate both S_0 and A_0 waves.

The fourth way to generate ultrasonic waves is in the high energy plasma regime where vaporized and ionized particles from the material surface can start a laser-generated plasma at the laser spot. The plasma can also be ignited in the air by focusing the laser beam tight enough that the intensity exceeds the breakdown level of the air. This plasma creates a shock wave that propagates in the air and the incoming wavefront generates out-of plane stresses and displacements when it hits the material. The amount of energy required is much higher than for the other generation regimes and the spectrum of waves generated usually consists of lower frequencies. Therefore, this method of generating ultrasound was not investigated.

2.5.2.1 Generation of ultrasound

Table 2.5.1 FWHM and maximum pulse power for Continuum Surelite I-20 Nd:YAG pulse laser.

Wavelength:	1064 nm (infrared)	532 nm (green)	355 nm (ultraviolet)
Pulse FWHM	5-7 ns	4-6 ns	4-6 ns
Maximum energy per pulse	420mJ (theor.) 413mJ (meas.)	160mJ (theor.) 168mJ (meas.)	55mJ (theor.) 57mJ (meas.)
Repetition rate	20 Hz	20 Hz	20 Hz

The generation system used at IPST is a pulsed Nd:YAG laser capable of generating a 1064 nm fundamental wavelength (near infrared), plus harmonics at 532 nm (green) and 355 nm (ultraviolet) with the use of nonlinear optical crystals. The laser is a Continuum Surelite I-20 with doubling and tripling crystals, and wavelength separators. The FWHM (Full Width at Half Maximum) of the laser pulse and the maximum energy are displayed in Table 2.5.1.

The diameter of the beam at the output of the laser is 6 mm at $1/e^2$ intensity. This beam needs to be focused, typically into a spot of 1 mm or less on the paper so that it can generate high frequency acoustic waves.

INL also uses a pulsed Nd:YAG for laser generation of ultrasound. This laser operates at 1064 or 532 nm, with a pulse length of 15 ns and up to 400 mJ of energy per pulse.

The maximum energy available from the pulsed lasers is far too high for paper and would damage its surface when the spot is focused, so the beams are attenuated using an optical attenuator placed after the output of the laser beam.

Contact piezoelectric transducers specially designed for sending S_0 or A_0 waves into the paper can also be used for ultrasound generation.

The set up of the laser based ultrasound system used at IPST is a relatively standard one. The pulsed generation laser is the master of the system and triggers the data acquisition. The detection system detects displacements continuously since the laser used for the detection system is CW (Continuous Wave). The setup at INL is very similar.

2.5.2.2 Data acquisition system

Traditional time based signals are recorded in a straightforward manner. At the output of the interferometer, the signal may be sent directly to the data acquisition system, or an ultrasonic preamplifier may be used to boost the signal before recording. The preamplifier used at IPST has a gain of 39.2 dB with a bandwidth of 16 kHz to 6 MHz at -3 dB. Figure 2.5.2 shows a picture of the data acquisition system used at IPST.

Figure 2.5.2 Data acquisition system, IPST setup. Computer with A/D is on the left, and digital oscilloscope is on the right. Panametrics preamplifier is the small blue box between the computer monitor and the oscilloscope.

The A/D board used with the IPST laser-based ultrasound setup allows a sampling rate of 130 MSamples/sec on one channel or 65 MSamples/sec on 2 channels. It is an 8 bit (256

levels) A/D board which allows collection of pre- and post-trigger data for recording times ranging from a few μs up to a few ms on 5 different voltage scales. The A/D board is driven with custom software written in LabVIEW and the data files are saved in an ASCII format.

An alternate method is to use a digital oscilloscope with storage capabilities. This was done at INL. Frequency based data storage techniques are more complicated and are described later in Section 2.6.4.

2.5.2.3 Ultrasonic detection systems used at INL

Two different ultrasonic detection systems were evaluated at INL during Phase I:

- Fabry-Pérot system already in place from other research.
- Time domain PRC method already in place from other research.

Both of these systems were optimized for use on paper. The two detectors were completely self-sufficient (they did not share parts) and were both able to be run through the entire year. In addition, INL provided valuable help in establishing the BSO time based interferometer at IPST.

2.5.2.4 Ultrasonic detection systems used at IPST

Three different detection systems have been investigated at IPST on paper products during the first year.

- An in-house built Photorefractive interferometer with a BSO crystal for measurements on static paper only.
- A photoinduced-EMF interferometer with a custom optical design for paper, on loan from Lasson Technologies, Inc., both on static and moving paper.
- A vibrometer using the self-mixing method, on loan from Metrolaser, Inc.

The first two systems used an Innova 308, 1.9 Watt single line argon:ion laser from Coherent. The vibrometer used a built in 5 mW diode laser at 780 nm.

In Phase II of the project, an in-house built Photorefractive interferometer with a GaAs or CdTe:V crystal for detection will be used on static and moving paper. This interferometer will use a Compass Nd:YVO_4 laser from Coherent with fundamental output of 600 mW at 1064 nm.

2.5.3 Comparative analysis of interferometric methods

This section is focused on the choice of a laser-based ultrasonic detection device. The comparative analysis of interferometric methods is valid for paper products only. For other products, the results of the analysis could be quite different.

Paper is a very interesting material to inspect in the sense that its properties make it more difficult to do non-contact ultrasound detection than most of the usual industrial materials. The problems that need to be addressed are the following:

- Detection on a moving surface.
- Surface moving with a very high speed.
- Paper surface is highly scattering (diffuse reflection of light).

- Optically absorbing surface in some cases (unbleached grades) or partially transparent (low basis weight grades), therefore only a small portion of the incident light is retro-reflected.
- Paper surface is easily damaged by too much power.

The objective is to detect ultrasonic displacements as low as 1 nm (S_0 wave) with a bandwidth of 50 kHz to 4 MHz over a duration of about 200 □s on a surface moving at a speed between 10 m/s and 25 m/s.

All available “interferometric” optical methods can be separated into different groups and subcategories:

- Non-interferometric method: knife-edge detection.
- Mach-Zehnder and Michelson interferometers.
- Fabry-Pérot interferometer.
- Self-mixing laser interferometer.
- Photorefractive adaptive interferometers:
  - °Self pumped phase-conjugate mirror and Double phase conjugate mirror techniques.
  - °Two wave mixing using BSO or infrared photorefractive crystals, time domain detection.
  - ° Two and four wave mixing for imaging techniques, frequency domain detection.
  - °Photoinduced electromagnetic force interferometer.

The main criteria when dealing with these interferometers are their response time, their étendue, and their sensitivity to displacement. The speckle pattern of the paper changes extremely quickly and can prevent the interferometer from working and thus prevent the ultrasonic signal from being detected. The different techniques for ultrasound detection are reviewed in the following sections.

2.5.3.1 Knife-edge detection

In the case of the knife edge detection, this type of detector only works well with a specular reflection, and the sensitivity to displacement is significantly reduced on scattering surfaces. Also any fluttering of the paper will induce huge artificial signals totally unrelated to ultrasonic displacements, thus masking the signals of interest. Figure 2.5.3 shows a schematic diagram of the knife-edge detection system.

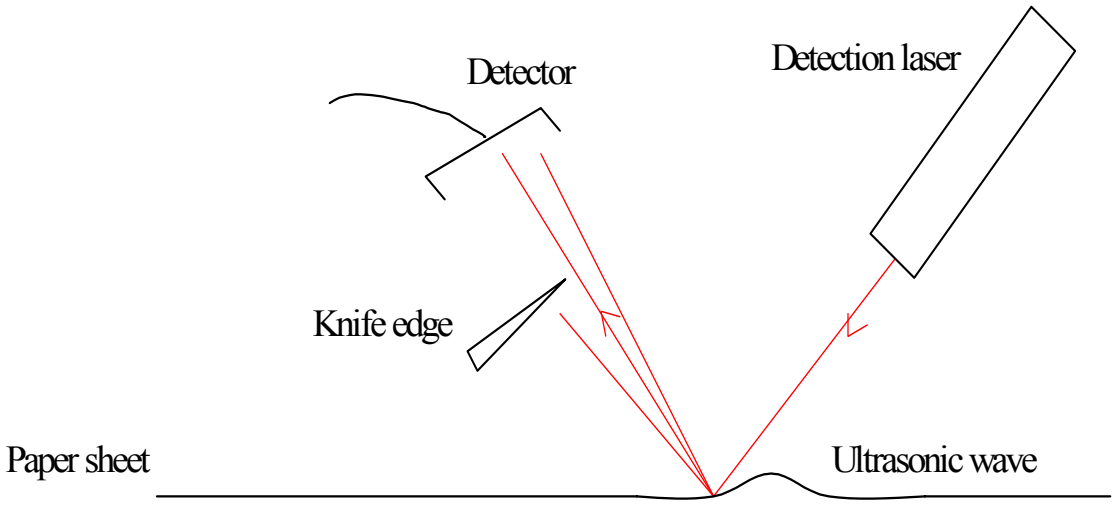

Figure 2.5.3Knife-edge detection system.

2.5.3.2 Mach-Zehnder and Michelson interferometers

In the case of the Mach-Zehnder and Michelson interferometers (see Figure 2.5.4), another problem occurs caused by the changing speckle pattern of the paper. The Mach-Zehnder and Michelson interferometers work correctly only when they detect a single speckle of light. In order to detect a single coherent speckle, the detection laser beam needs to be focused close to the diffraction limit onto the surface of the sample. This makes these detectors very sensitive to small displacements but also leads to the disadvantage of a very small étendue (product of the solid angle of scattered light collected by the detection optics and the area of illuminated surface). The étendue parameter characterizes the ability for an optical system to collect light efficiently. Hence, these two interferometers have to be aligned very accurately to pick up a good speckle pattern.

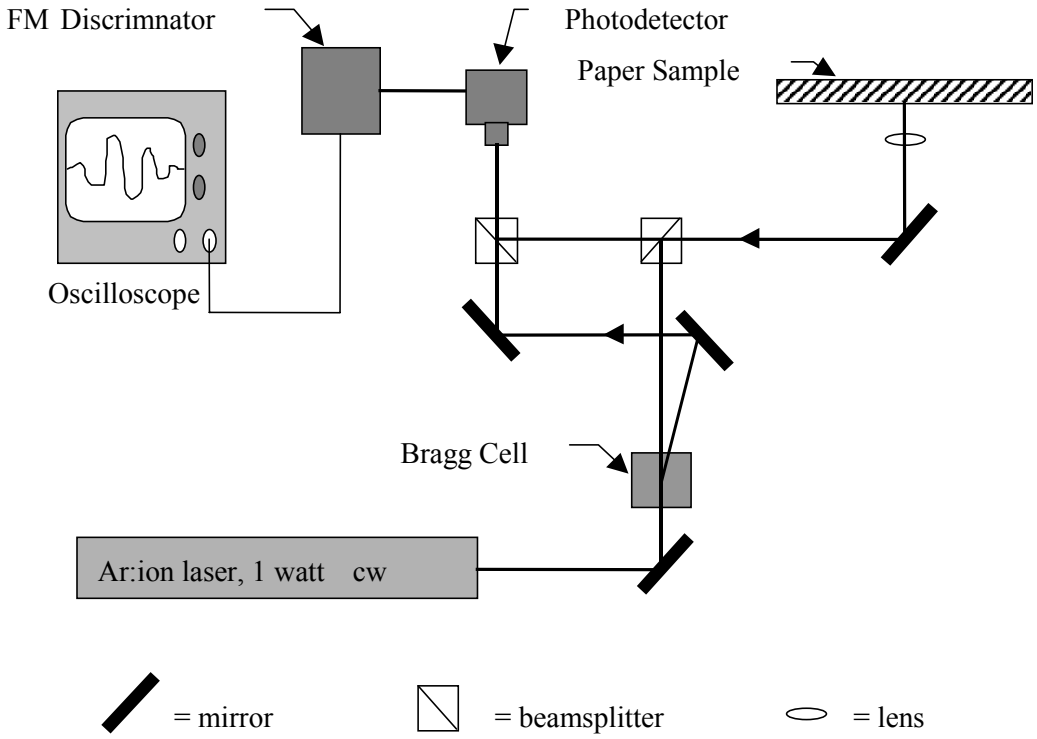

Figure 2.5.4 Mach-Zehnder heterodyne interferometer (from Johnson 1996).

Since the speckle pattern is dependent on the sample surface roughness, as soon as the surface changes under the beam, the speckle pattern changes and the interferometer is no longer properly aligned, resulting in the loss of the ultrasonic signal. For a moving surface, the signal appears and disappears randomly and the higher the speed the greater the amount of time spent without a signal. Sagnac and/or polarimatric interferometers (which are not described here) have the same problem as the Mach-Zehnder and the stabilized Michelson do: they only work with a single speckle. Note that it is possible in some cases to use those interferometers with the simultaneous detection of multiple speckles outside of their diffraction limit, but in that case the signal to noise decreases significantly.

2.5.3.3 Fabry-Pérot interferometer

The Fabry-Pérot interferometer, as schematically shown in Figure 2.5.5, is a much better alternative than the previously described interferometers for measurements on moving products since the interferometry is done between the same optical wavefront delayed by a very short time. This eliminates the single speckle requirement, so it does not matter if the light coming back from the surface is speckled or not. Also, the Fabry-Pérot is the fastest of the interferometers able to work on rough surface (typical response time: 0.1□s). A confocal Fabry-Pérot has a very large étendue so it collects light very efficiently and provides a good signal to noise ratio.

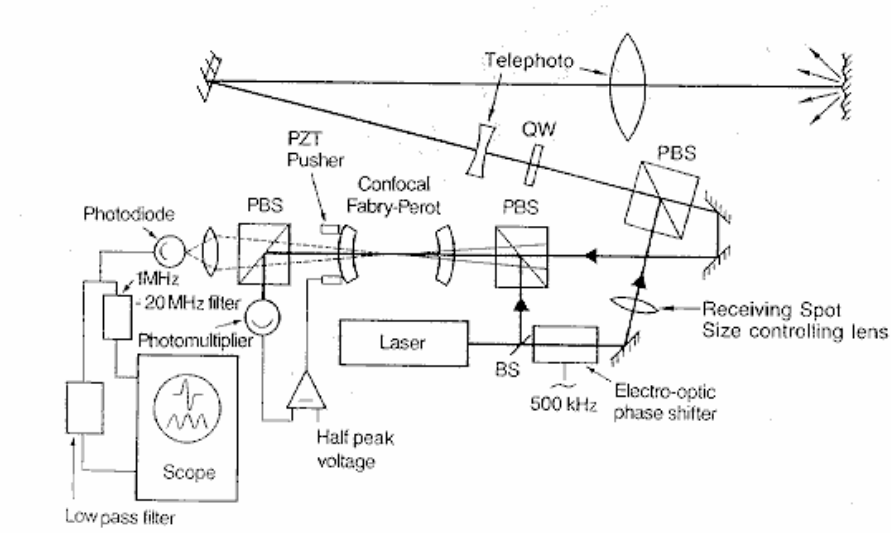

Figure 2.5.5 Fabry-Pérot interferometer (Monchalin and Héon 1986).

Up to now, the Fabry-Pérot is the only optical interferometer that has been successfully used in an industrial application for ultrasonic detection. J.P. Monchalin (1986) from Industrial Materials Institute in Canada has used the Fabry-Pérot for ultrasound detection on hot steel pipes moving over 4 m/s.

The two disadvantages of the Fabry-Pérot are as follows: first, the interferometer is quite large (typically 1 m long and 0.5 m wide), second, the frequency response of the device is not flat, and the sensitivity falls off rapidly outside its typical bandwidth of 1 to 100 MHz. The second disadvantage makes this device not optimal for detection of Lamb waves in paper, which are mainly below 1 MHz. Bandwidth can be lowered into the region for paper by increasing the cavity length. However, this increases the size of the interferometer as well as making it more sensitive to alignment.

2.5.3.4 Self-mixing interferometer

For self-mixing interferometers, as shown in Figure 2.5.6, the weakness is the same as the one pointed out in the Mach-Zehnder interferometer; that is, it can only work with a single speckle. Nevertheless, an advantage exists in that it can work with much less light than the Mach-Zehnder interferometer.

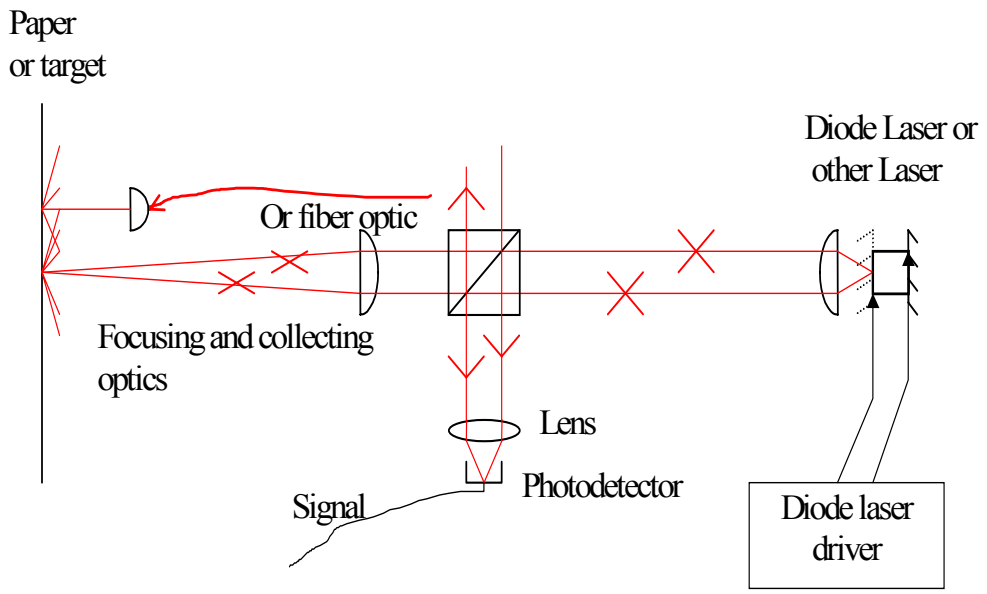

Figure 2.5.6 Self-mixing laser interferometer.

The self-mixing interferometer will likely have a decent signal to noise ratio (SNR) on both highly reflective and very absorbing surfaces (such as kraft linerboard) even with a low power laser. There is still the same problem of losing the signal with the change of speckle pattern caused by the moving paper. It is likely that the noise caused by the changing speckle pattern will be added to the signal coming from the ultrasonic displacements and will be of much higher amplitude than the signal (hence masking the signal).

2.5.3.5 Photorefractive adaptive interferometers

Photorefractive interferometers are the newest type of interferometer and have a high potential of further improvement as advances in material science (to produce quality optical crystals) are taking place very fast in this area. This type of interferometer uses photorefractive crystals to adapt a planar reference wavefront to a speckled signal wavefront (light back scattered from the paper). This can produce significantly more efficient interferometry than the Mach-Zehnder interferometers can on rough surfaces. Photorefractive interferometers can come in two beams designs like the Mach-Zehnder, as well as 4 beams designs. However, the theoretical sensitivity limit of such interferometers is smaller than that of a Mach-Zehnder heterodyne interferometer on mirror-like surfaces. Of course this theoretical sensitivity limit is irrelevant to paper products which have a very scattering surface. In this latter case, a higher sensitivity is achieved using the photorefractive interferometer even on static targets.

2.5.3.5.1 Self pumped phase-conjugate mirror and Double phase conjugate mirror techniques

These techniques, as shown in Figure 2.5.7, were not investigated experimentally because despite the fact that they can collect and use much more light than the Mach-Zehnder interferometer, they are extremely slow to achieve the effect they rely on (typically a few seconds).

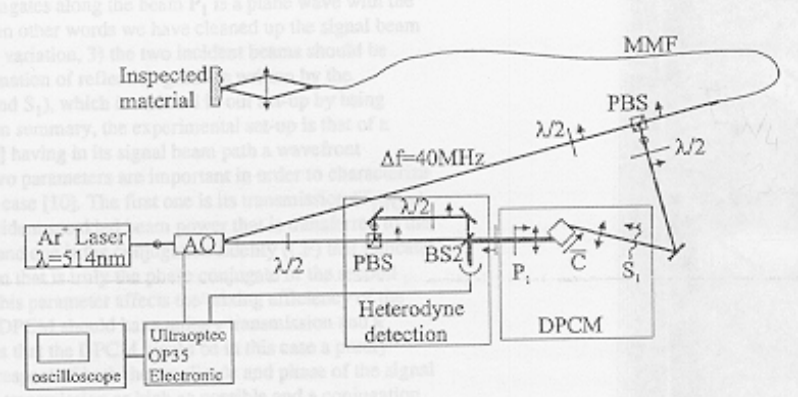

Figure 2.5.7 Double phase conjugate mirror (Delaye et al. 1996).

This slow response time makes them unsuitable for on-line detection in a mill and will prevent them from being used on moving paper.

2.5.3.5.2 Two-wave mixing using BSO or infrared photorefractive crystals, time domain detection

Two-wave mixing is the second fastest of the photorefractive techniques and has been used for ultrasound detection since 1991 (Ing et al., 1991). The response time of a two-wave mixing interferometer depends mainly on the type of photorefractive crystal employed. It can be used for detection in the frequency domain or in the time domain. The sensitivity to displacements (related to the gain of the crystal) and response time (related to laser power density) depends on many different factors such as the material constants, the wavelength used, and whether a DC or AC voltage is applied to the crystal.

There is a big difference both in sensitivity and response time between the two classes of photorefractive crystals: the Sillenite type, such as $Bi_{12}SiO_{20}$ (BSO), $Bi_{12}GeO_{20}$ (BGO), $Bi_{12}TiO_{20}$(BTO), working in the visible range, and the semiconductor photorefractive crystals which work in the infrared range, such as undoped GaAs, InP:Fe and CdTe:V.

The Sillenite type crystals are very sensitive to displacements and have a slow response time (> 10 ms), whereas the semiconductor photorefractive crystals have the opposite properties. However, the sensitivity of semiconductors can be greatly increased by applying a DC or AC voltage to the sides of the crystal. By opposition, the response time cannot be dramatically reduced for crystals of the Sillenite type by any means.

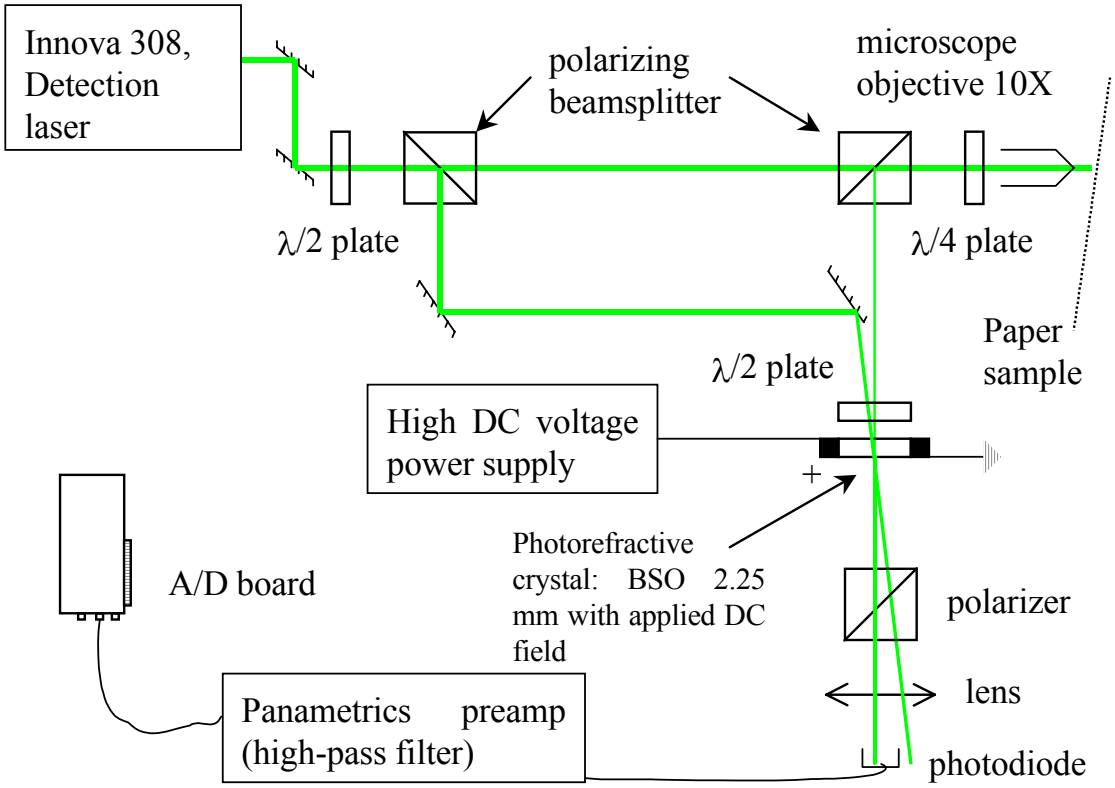

Figure 2.5.8 Two wave mixing photorefractive interferometer version 1.5, IPST setup.

IPST currently uses a BSO crystal in its photorefractive interferometer for measurements on static paper, as shown in Figure 2.5.8. It has been found that a crystal with a very fast response (typically a semiconductor crystal) should be used with moving paper instead of the BSO because the speckle pattern changes so rapidly. A typical response time of a GaAs or CdTe:V crystal is between 1 and 10 □s, and this is probably the maximum acceptable for paper moving at high speeds.

A Canadian company, UltraOptec Inc. has recently been marketing a laser-ultrasonic receiver using an InP:Fe crystal, but it appears that the sensitivity of this detector decreases quickly with increasing speed. Its sensitivity goes down to 20% of its maximum value at speeds of 1-2 m/s. It is unlikely that this receiver would work without a device such as a scanning mirror (see Section 2.6.7.2) to reduce the differential speed between the detection beam and the web. However, an interferometer using a GaAs or CdTe:V crystal could be fast enough for paper and will be investigated in the future.

2.5.3.5.3 Four wave mixing and two wave mixing for imaging techniques (frequency domain detection)

This technique, as shown in Figure 2.5.9, uses four wave mixing or two wave mixing optical lock-in methods to display the ultrasonic displacement field of the paper's surface onto a CCD camera through the photorefractive crystal.

The crystals that can be used for this method are the same as the ones for two-wave mixing with the same advantages and drawbacks. The big advantage of this method on static paper is that it can obtain the complete information about wave velocity in all directions all at once, at one fixed frequency. The drawback is that instead of being focused, the beam of the detection laser is spread over a large surface and thus the quantity of light coming back onto the crystal (and hence on the detector) from any one speckle is very small. This method works well for static paper samples. However, when it becomes necessary to detect waves on a moving web, it seems unlikely that both the signal to noise ratio and the response time will have adequate values.

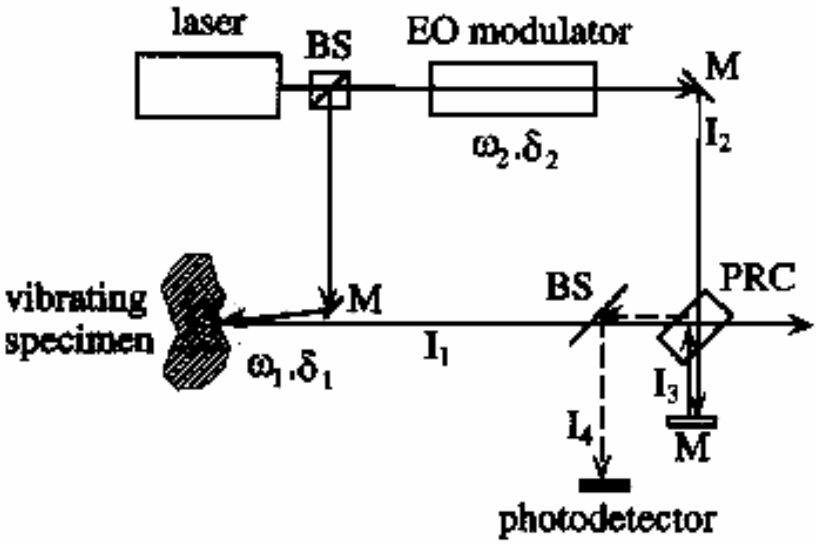

Figure 2.5.9 Four wave mixing imaging technique. PRC = photorefractive crystal; EOM = electro-optic modulator; BS = beam splitter; M = mirror; □1 and □2 = phase modulated signal and reference beams, respectively (reproduced from Hale and Telschow 1997).

Until there is a great improvement in the sensitivity of photorefractive crystals, the four wave mixing and two wave mixing imaging techniques in the frequency domain do not seem to be suitable for moving paper. But it is definitely a method that should be watched in the future when the sensitivity improves with better photorefractive materials (polymers for example) because of its capacity to do full field ultrasonic imaging.

2.5.3.5.4 Photoinduced electromagnetic force interferometer

This interferometer, as shown in Figure 2.5.10, relies on a phenomenon that makes it the fastest of all photorefractive interferometers because some of the usual steps required for a photorefractive interferometer to work properly are skipped. Due to the photoconductivity property of a photorefractive crystal, a very small current is created on the surface of the crystal by the slight phase shift of the speckles caused by the ultrasonic motion of the paper surface. The current generated by photoconductivity is representative of the ultrasonic motion and can be measured between two electrodes on the sides of the crystal.

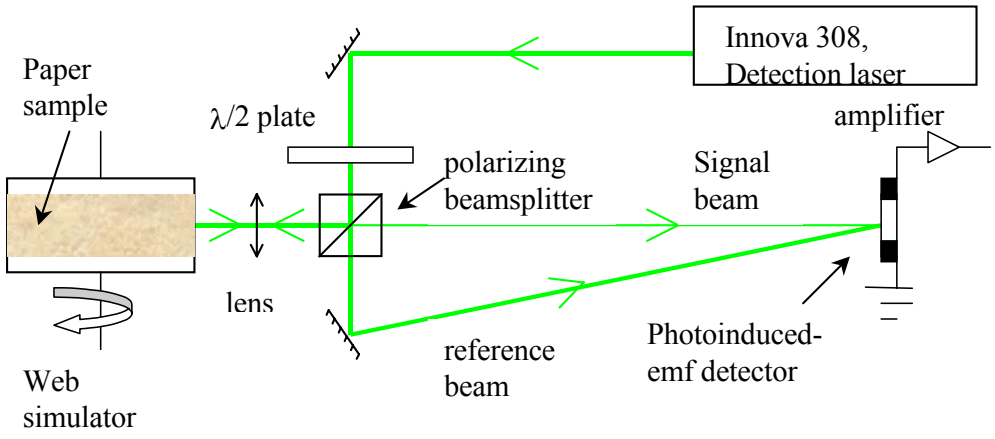

Figure 2.5.10 Photoinduced-EMF interferometer.

The detection spot can be either a point or a line, as with a two wave mixing-time domain interferometer. All photorefractive crystals create a photoinduced-EMF current, hence any crystals can be used. The device on loan from Lasson Technologies that was tested at IPST on the web simulator relies on a Chromium doped GaAs crystal (GaAs:Cr).

As in the case of two-wave mixing time domain interferometers, the frequency response of this interferometer is flat and very well adapted to the purpose of Lamb waves detection. It cuts off the low frequencies that are typically present in a mill (below 1 kHz) and the upper limit can be set at any value by the electronic bandwidth of the amplifier.

On 42-lb linerboard and bleachboard, the photoinduced-EMF detector was able to detect signals at speeds up to 14.5 m/s (maximum speed of the web simulator at that time).

2.5.3.6 Improvement of an interferometric method by using a scanner

Some of the interferometric methods cited above are likely to be improved when a scanning mirror is used. The scanning mirror should reduce the differential of speed between the laser detection beam and the web surface. Indeed, theoretical and experimental observations show that when the web speed increases, the signal to noise ratio drops sharply. This is caused by an increase of the noise with the speed and a decrease of the signal (not enough time for the speckle pattern to build up the diffracted beam).

2.6 Laser Ultrasonics measurements

2.6.1 Analysis of Paper Using Orthotropic Plate Theory

This section provides an overview of how to investigate stiffness properties of paper samples using a non-contact laser ultrasonic technique. Assuming that paper can be modeled as an orthotropic material, that is, a material that has three mutually orthogonal symmetry planes, then there exists an empirical relationship between the properties of paper stiffness and the elastic constants [Baum, 1987]. For a thin paper, two fundamental Lamb wave modes, the S_0 and A_0, are present (Figure 2.6.1). The S_0 mode is also called the fundamental dilatational mode and is used to predict longitudinal stiffness properties. The A_0 mode is the fundamental

bending mode and is used to determine shear stiffness properties. As the signal propagates in the paper, the two modes are detected and analyzed in relation to the stiffness properties.

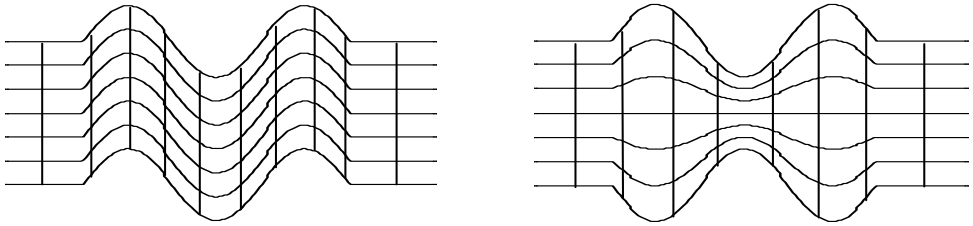

Figure 2.6.11 A_0 antisymmetric (left) and S_0 symmetric (right) mode shapes as viewed from the edge of a sheet of paper.

The symmetric S_0 mode is nondispersive in the low frequency limit, and a time-of-flight measurement can evaluate the longitudinal stiffness properties by measuring the velocity of ultrasound along MD and CD. On the other hand, the antisymmetric A_0 mode is dispersive and the asymptotic A_0 velocity in the high frequency region can be used to determine the shear stiffness properties in the out-of-plane directions. It is also possible to determine the stiffness properties using the characteristics of the A_0 velocity in the low frequency region by way of non-linear curve fitting.

The velocity of the S_0 mode is analyzed for selected samples using a cross-correlation technique and compared with the one obtained using contact transducers by Brodeur et al. (1997). The analysis of the A_0 mode is an important tool because the A_0 mode is readily detectable in the signal due to its large amplitude.

Nevertheless, the interpretation of the A_0 mode is not straightforward because the phase velocity disperses as a function of frequency. A data analysis technique is developed to interpret the dispersive A_0 signal using a similar approach taken by Schumacher et al. (1993). The technique contains a method of extracting phase velocities from Fast Fourier Transformation and unwrapped phase angle spectrum. Furthermore, phase angle corrections are required to compensate for the phase shift in the low frequency region. The analysis technique is compared with the one described by Johnson (1996) on copy paper.

The theory of Lamb waves typically used in paper has been studied by Habeger et al. (1979), Cheng and Berthelot (1996) and Johnson (1996). They all have described an important relationship between frequency and wave velocity that must be satisfied for a Lamb wave to exist. It is known as the dispersion equation in the following form:

$$\frac{\tan(k_{z+} \cdot h)}{\tan(k_{z-} \cdot h)} = \left[\frac{H_- \cdot G_+}{H_+ \cdot G_-} \right]^{\pm 1} \qquad (1)$$

where h is the half thickness of paper, $k_{z\pm}$, $H_\pm$ and $G_\pm$ are functions of frequency f, wave velocity c and the elastic constants of paper. The wave motion of a particular mode can be predicted by choosing f and c that can satisfy the dispersion equation. The symmetric modes correspond to the solutions of the dispersion equation with a positive exponent, while the antisymmetric modes correspond to those with a negative exponent.

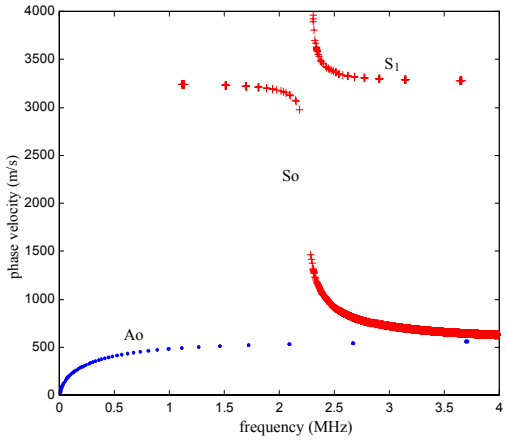

(a) Solutions for copy paper in MD

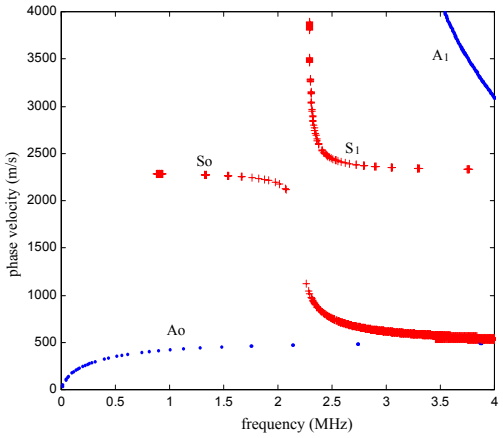

(b) Solutions for copy paper in CD

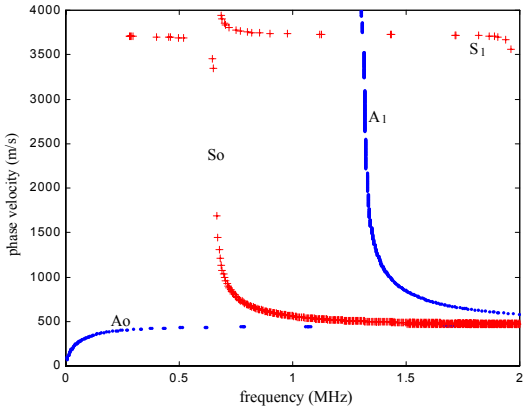

(c) Solutions for linerboard 42-lb in MD

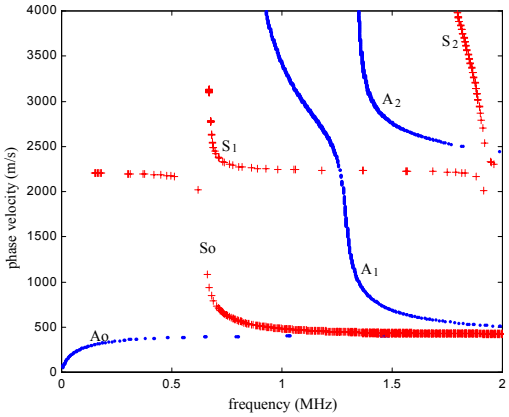

(d) Solutions for linerboard 42-lb in CD

Figure 2.6.12 Dispersion curves of copy paper and linerboard 42-lb : The grammages of copy paper and 42-lb linerboard are 80 g/m^2 and 205 g/m^2, respectively. Each wave mode is identified by a letter (S for symmetric and A for antisymmetric), followed by a number indicating the order of the mode. As the frequency increases, all modes are known to approach an asymptotic phase velocity, which is a Rayleigh surface wave.

A complete derivation of the dispersion equation is found in the study by Habeger et al. (1979), who also simplified the dispersion equation in the low frequency limit. For the two lowest modes, S_0 and A_0, the simplified relations are

$$c = \sqrt{\frac{C_{11}}{\rho}} \qquad \text{for the } S_0 \text{ mode} \qquad (2)$$

$$c = \left[2\pi \cdot f \cdot h \cdot \sqrt{\frac{C_{11}}{3\rho}} \right]^{1/2} \qquad \text{for the } A_0 \text{ mode.} \qquad (3)$$

where C_{11} is the elastic stiffness constant in MD (Pa), ρ is the apparent density of paper (kg/m^3), h is the half thickness of paper (m), f is the frequency (Hz) and c is the wave phase velocity (m/s). The error associated with using Equation 2 to approximate the value for C_{11} from the S_0 mode was found to be no more than 2% [Mann et al., 1980].

The dispersion equation was numerically solved for two paper grades: copy paper and 42-lb linerboard. The stiffness constants used to solve the equation were measured using the contact ultrasonic instruments at the Institute of Paper Science and Technology (see Section 2.3). The concept of this method is well described by Habeger et al. (1989). Figures 2.6.2 show dispersion curves for copy paper and 42-lb linerboard in MD and CD. Each wave mode is identified by a letter (S for symmetric and A for antisymmetric), followed by a number of the order. As the frequency increases, all modes are known to approach an asymptotic phase velocity [Viktorov, 1967, Mann, 1978]. This asymptotic velocity is known to be that of a Rayleigh wave, which exists on the surface of a half-space material.

Important characteristics of the dispersion curves are found by varying the values of the elastic constants. By raising or lowering the values of C_{11} or C_{22}, one can determine their effects on the S_0 and A_0 modes. The major effect of C_{11} and C_{22} is on the low frequency limit of the S_0 mode, while only a minor change is observed in the initial slope of the A_0 mode. The primary effect of C_{33} is the location shift of the cut-off frequency for the S_0 and S_1 modes. C_{13} and C_{23} have only a minor effect on the S_0 mode. The effect of C_{44} and C_{55} is on the high frequency limit of the S_0 and A_0 modes [Johnson, 1996].

During the next phase of the project, dispersion curves will be studied to analyze the inverse problem of extracting stiffness properties from measured data; that is, the elastic constants will be predicted by fitting the measured A_0 and S_0 data with the dispersion curves using non-linear regression.

2.6.2 Fabry-Pérot Interferometer Measurements

2.6.2.1 Fabry-Pérot Interferometer Methodology

Many optical techniques for measuring ultrasonic motion on surfaces have been developed for use in laser ultrasonic applications (Monchalin, 1986). Most of these methods have similar sensitivities and are based on time domain processing using homodyne, heterodyne, Fabry-Pérot, and, more recently, photorefractive interferometry (Wagner, 1990, Ing et al., 1991). Of the many optical techniques for ultrasound detection, only a few have proven capable of performing measurements in the presence of multiple speckle reflections from diffusely scattering surfaces like paper. One of these is the Confocal Fabry-Pérot self-referencing interferometry method (Monchalin and Héon, 1986) that was evaluated as a separate task on this program through the use of the facilities and expertise at the Idaho National Engineering and Environmental Laboratory (INL).

Multiple speckles are successfully demodulated due to the self-referencing nature of the Fabry-Pérot technique, i.e., the photodiode signal originates from the interference of light scattered from the paper surface and delayed portions of that light generated from multiple reflections within the Fabry-Pérot cavity. Since all of the optical wavefronts are nearly identical to that scattered from the paper surface, light from a relatively large surface area (1-4 mm^2) including many speckles is collected and interfered efficiently. This gives this detection technique the optical efficiency needed to provide sufficient sensitivity for detection on rough and/or optically

diffuse material surfaces, as exist on most types of paper. Diffuse surfaces scatter radiation into a hemisphere, resulting in only a very small amount that returns directly to the interferometer detection system. For a normal standoff distance of a few centimeters, the optical collection efficiency is typically in the 0.1% – 1% range resulting in relatively little light collection. The detection system signal to noise ratio, in the shot noise limited regime, is controlled by the amount of light entering the interferometer. There is also a limitation on how much light can be focussed onto a particular paper sample without damage. These factors place severe requirements on the optical collection efficiency and greatly affect the overall system performance and cost. These considerations have led to the choice of the Fabry-Pérot system for most industrial applications of laser ultrasonics that are actually performed in the field today.

The Fabry-Pérot interferometer system employed at the INL utilized an argon ion laser capable of focusing up to 1.5 watts of light (514 nm) onto the paper surface (Telschow, et al., 1990). A pulsed Nd:YAG laser (1064 nm) with a pulse width of about 15 ns and pulse energy up to 400 mJ was used to excite elastic waves in the paper by the thermoelastic and ablation mechanisms. Paper samples were placed at the focus of the two laser beams, similarly to that shown in Figure 2.6.3. For the moving paper measurements, the IPST web simulator was placed at the left end of the table allowing access for the laser beams to the paper surface on the revolving wheel.

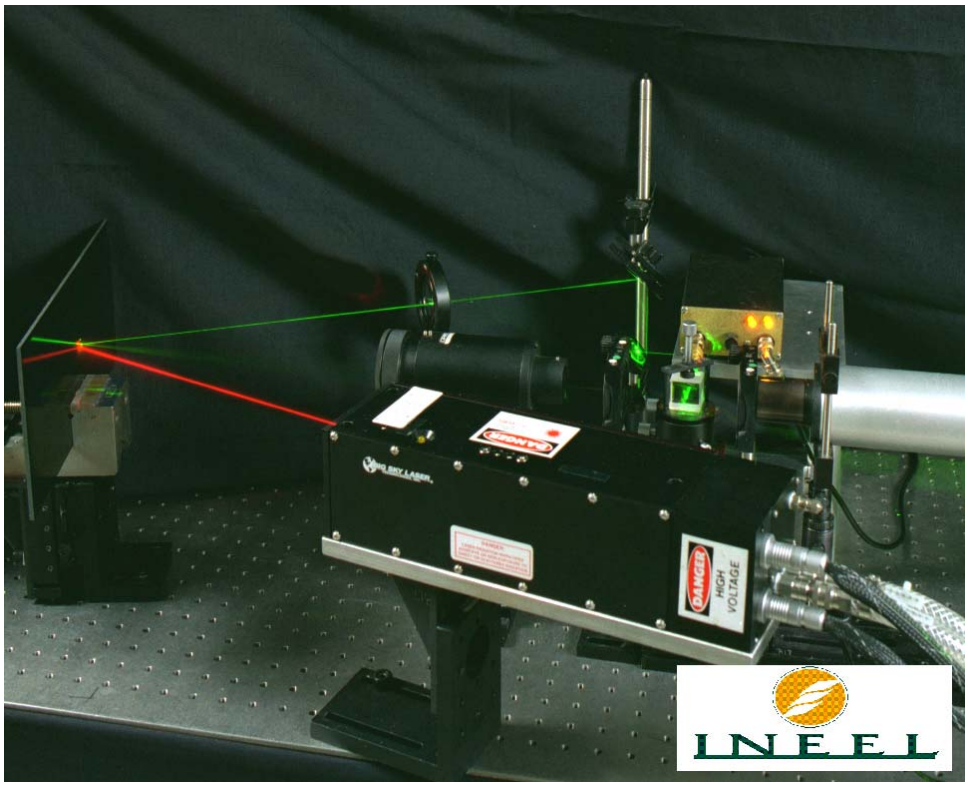

Figure 2.6.3 Picture of the INL laser ultrasonic point measurement system employing a confocal Fabry-Pérot interferometer (tube to the right), a pulsed Nd:YAG laser for excitation (black box in the foreground) and the generation and detection beams impinging onto a sample at the left.

2.6.2.2 Lamb Wave Measurements in Stationary Paper

Fabry-Pérot measurements were first conducted on stationary paper. Figures 2.6.4a,b show a comparison between the lowest order symmetric (S_0) and antisymmetric (A_0) waveforms recorded on a stationary 0.1mm thick stainless steel sheet, Figure 2.6.4a, and a piece of 0.1mm thick copy paper, Figure 2.6.4b. The laser generation was from a line source and produced clearly distinguished symmetric and anti-symmetric waves, as seen especially from the stainless steel data in Figure 2.6.4a. It is also apparent from Figure 2.6.4a that a uniform line source produces little or no signals in the interval between the S_0 and A_0 waveforms (2.5 and 3.5 μs in the picture). Figure 2.6.4b shows results under similar conditions for Lamb waves recorded from copy paper. Taking note of the longer time scales for the paper waveforms, it can be seen that the general frequency content of these waves is lower in paper than for the stainless steel. This is due to the larger attenuation that both wave modes experience in paper. In addition, complexity due to the heterogeneity of the material at the fiber level resulted in non-uniform ultrasonic generation along the line producing multiple signals arriving between the first S_0 and the A_0 wave modes. It was also observed that the paper waveforms showed considerable changes in shape with position on the paper, especially for the S_0 mode. An attempt was made to eliminate this problem by using an excitation line width of about 1mm to average over many fibers. However, it was always found that the recorded waveforms showed some dependence on location on the paper.

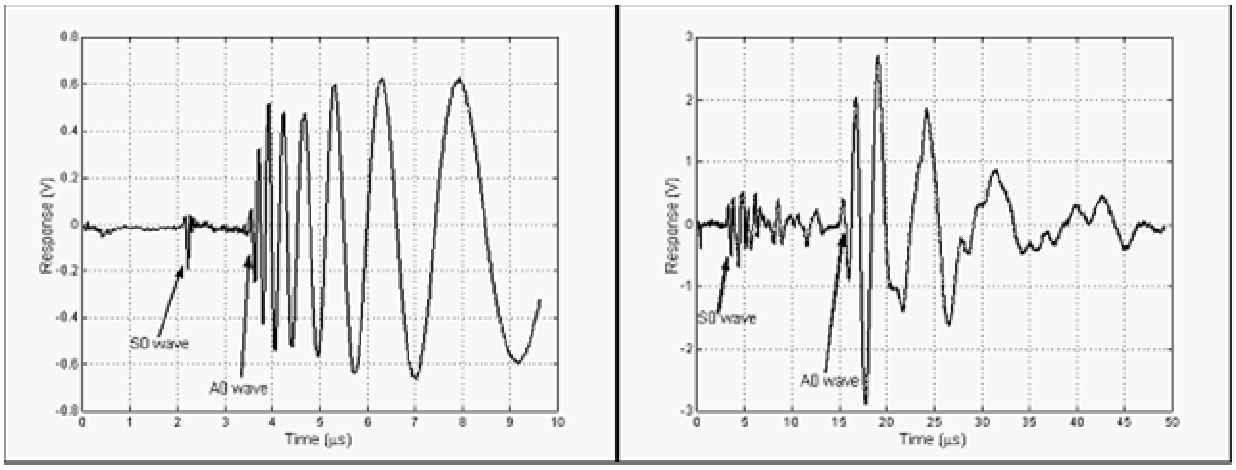

(a) (b)

Figure 2.6.4 (a) Lamb waves on thin sheets of stainless steel measured with the INEEL Fabry-Perot interferometer system, (b) Lamb waves on thin sheets of "copy" paper measured with the INEEL Fabry-Perot interferometer system.

2.6.2.2.1 Thermoelastic vs. Ablation Generation

Damage to the paper was easily accomplished at even moderate pulsed laser excitation energies. Figure 2.6.5 shows the results comparing the recorded signals both below and above the ablation threshold for 1064 nm source wavelength. The general ablation level for the papers appears to be around 20-80 MW/cm^2 for a pulse width of about 15 ns. Tests were performed to check the ablation level of copy paper using both the 1064 nm and the 532 nm radiation lines of the Nd:YAG source laser. Generally, it was observed that the first few pulses ablate something from the paper and produce a large A_0 wave. The top trace of Figure 2.6.5 shows an average of the first 16 pulses impinging on a virgin paper location. Subsequent pulses appeared to produce little or no ablation as the A_0 wave diminished. The bottom trace, taken from a different location, shows an average of 16 pulses taken after the A_0 wave diminished in amplitude. Similar results were obtained for the signals seen at 532 nm.

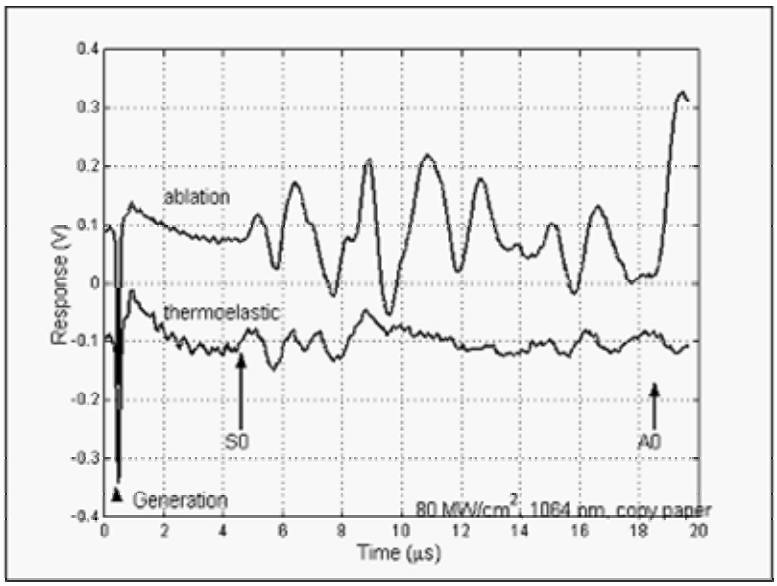

Figure 2.6.5: Thermoelastic vs. Ablation generation comparison at 1064 nm on "copy" paper.

Figure 2.6.6 compares recorded signals both below and above the ablation threshold for 532 nm source wavelength. The top of the figure shows an average of 1000 pulses at one location (40 μW detection light) at a pulse level that produced no ablation, as measured by subsequently observing no change in the paper fibers under microscopic examination. The bottom of Figure 2.6.6 shows an average of 1000 pulses at a different location (28 μW detection light) with slight ablation occurring about 30% of the time as seen from the appearance of the A_0 mode waveform on the recording oscilloscope. The ablation thresholds for copy paper were found to be approximately 80 MW/cm^2 @ 1064 nm and about 20 MW/cm^2 @ 532 nm. The difference is probably due to the lower absorption of light in this paper at the longer wavelength.

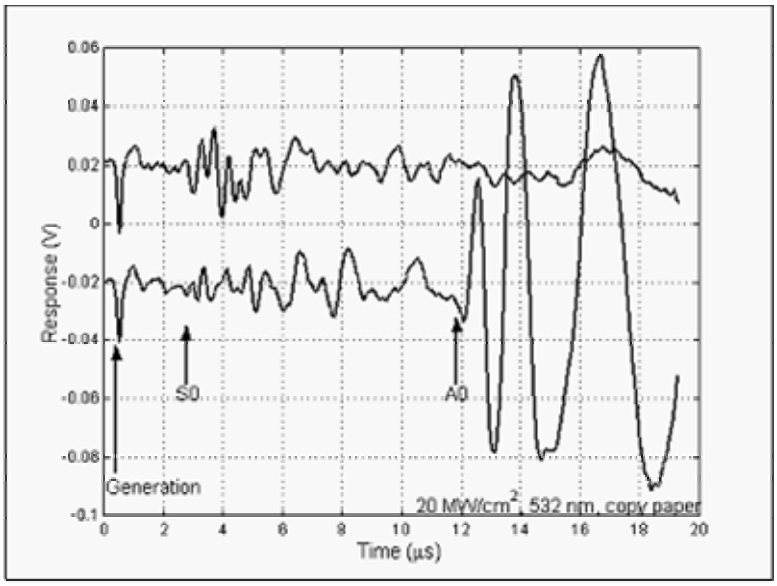

Figure 2.6.6: Comparison below and above the ablation threshold for "copy" paper at 532 nm showing the appearance of the A_0 mode waveform when ablation is present.

2.6.2.2.2 Directional S_0 & A_0 Response for paper RSK59

Measurements are shown in Figure 2.6.7 of the ultrasonic S_0 and A_0 mode wave velocities taken as a function of propagation direction on the RSK59 paper. The S_0 wave velocity in the machine direction (MD) was 3.75 (mm/□s) as determined by measurements taken over multiple distances for a signal with a bandwidth of about 1 MHz. The source to detector distance was about 6 mm and the paper was rotated keeping the source and detector geometry fixed.

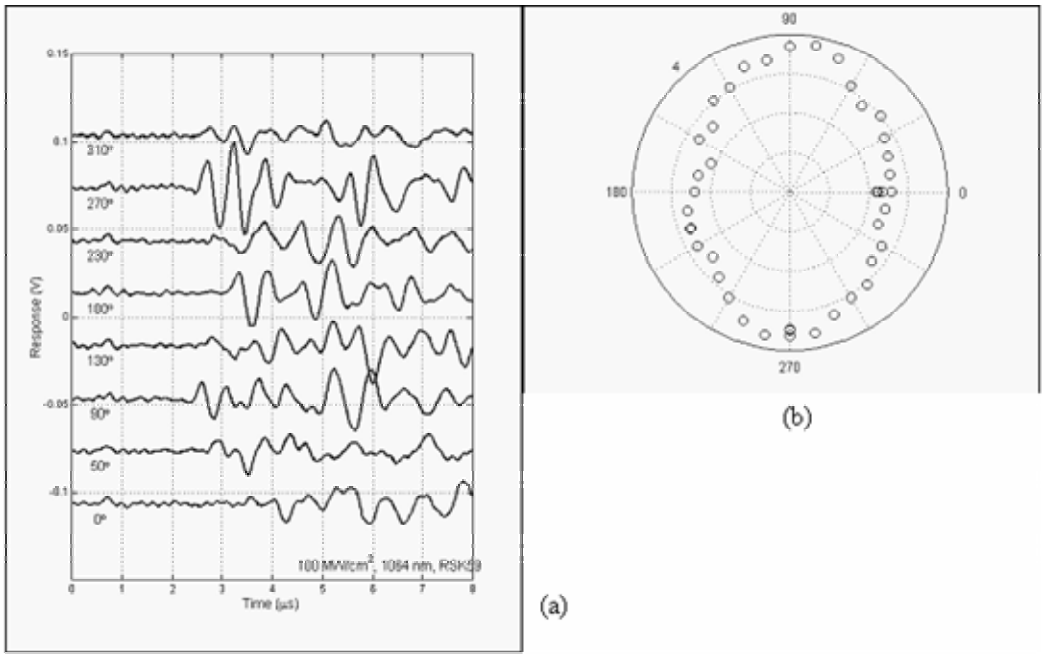

Figure 2.6.7 a: S_0 waveforms for the RSK59 paper sample taken at varying angles with respect to the CD direction (0°), 5b: S_0 wavefront velocity for the RSK59 paper sample taken at varying angles with respect to the CD direction (0°), maximum value shown is 4 mm/μs.

Significant variations in the S_0 waveforms as a function of angle were found as shown in Figure 2.6.7a, all single shot waveforms taken with slight ablation occurring on the paper. The S_0 wave speed was determined from the earliest signal arrival time. The recorded velocity ratio between the MD and the CD was CS(MD)/CS(CD) = 1.48 +/- .11 at 1 MHz which agrees well with contact measurement results for this paper. Figure 2.6.7b shows the measured velocity values taken at varying angles with respect to the CD direction. Any single measurement yields both the S_0 and A_0 waveform. The ablation mechanism yielded the larger signals and was used whenever possible as long as no significant paper damage resulted. This mechanism was particularly efficient at generating flexural motion of the paper, so the A_0 waveforms were always much larger than the S_0 waveforms. Therefore, one would prefer to measure the A_0 modes to obtain the elastic data about paper, if possible, due to this advantage.

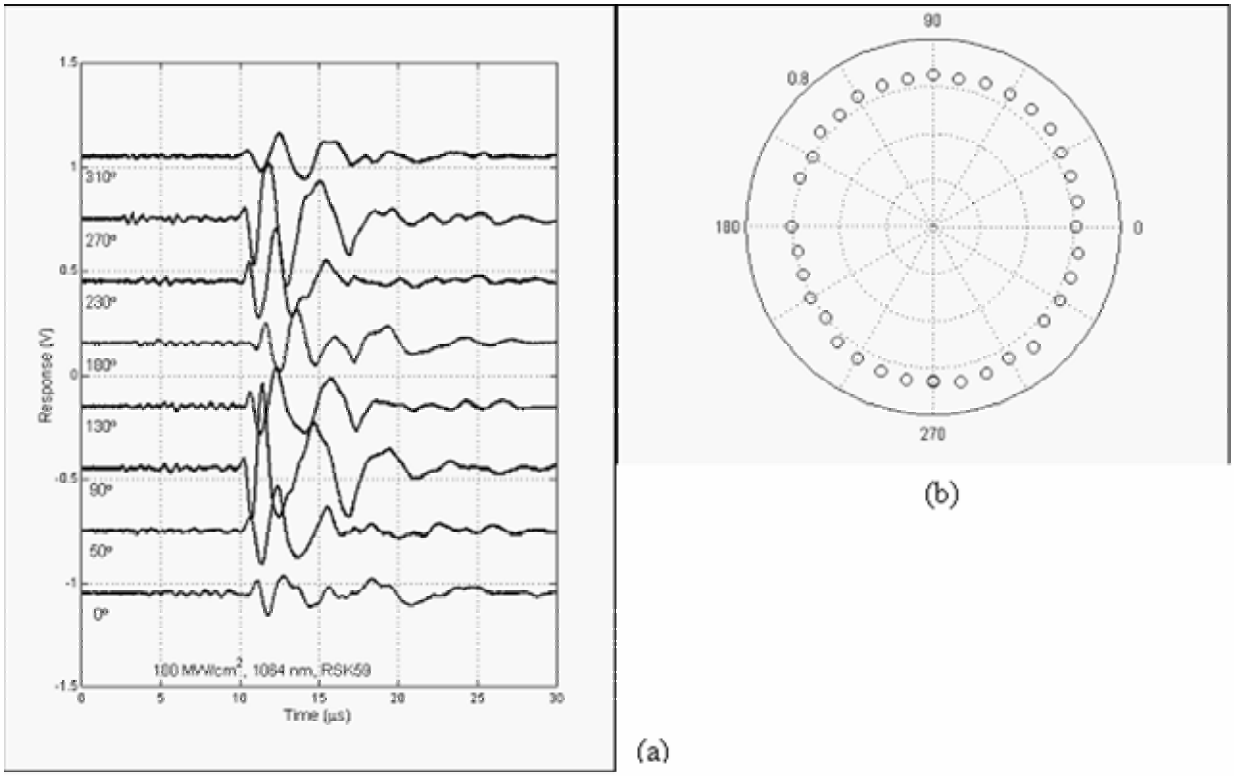

Figure 2.6.8: (a) A0 waveforms for the RSK59 paper sample taken at varying angles with respect to the CD direction (0°), (b): A0 wavefront velocity for the RSK59 paper sample taken at varying angles with respect to the CD direction (0°).

Figure 2.6.8a shows the complete waveforms recorded from the RSK59 paper including the region shown in Figure 2.6.7a. Here the time scale has been lengthened to show both the fast S_0 mode and the slower A_0 mode. Clearly the A_0 mode waveforms were the largest, but they were also dispersive. The phase velocity varied with frequency, such that it was difficult to get a unique phase velocity value from which to determine the elastic constants. However, at low frequencies, there is a well know relationship between the A_0 phase velocity and the frequency that suggests that the MD/CD ratio for the A_0 mode should be approximately the square root of that for the S_0 mode. Figure 2.6.8b shows the measured A_0 velocity values taken at varying angles with respect to the CD direction for a frequency around 1 MHz. The recorded A_0 velocity ratio between the two perpendicular directions was CA(MD)/CA(CD) = 1.07 +/- .05. Figure 2.6.9 illustrates the generally good agreement found between experimental Fabry-Pérot measurements (and photorefractive, described in Section 2.6.4) and that predicted by numerical calculation. The calculation was based on anisotropic plate wave propagation (Habeger, et al. 1979) using the elastic constants for the RSK59 paper independently determined by other means at the IPST. Some difference between experimental measurement and the theoretical calculation can be seen in the data of Figure 2.6.9 that is thought to be due to the dispersion effects present in both the S_0 and A_0 wave modes at the frequencies employed.

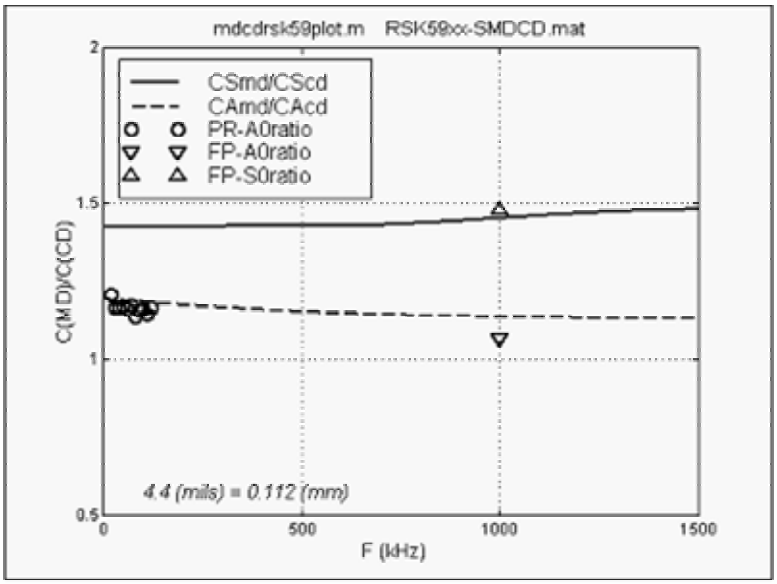

Figure 2.6.9: Comparison between the experimentally measured S_0 & A_0 MD/CD velocity ratios using the Fabry-Perot and Photorefractive methods with expectations calculated from elastic constants for this paper provided by independent IPST measurements.

2.6.2.2.3 Fabry-Pérot Laser Ultrasonic Static Paper Measurements (Summary)

The Fabry-Pérot interferometer has proven itself to be a useful device for laser ultrasonic detection on paper. It can effectively accommodate the diffusely reflecting surface of paper, readily be scanned over the paper surface to make measurements at different locations, automatically eliminates low frequency interfering signals due to vibration and laser phase noise, and has a fast response time that allows it to operate at high frequencies. This high frequency response can be detrimental. The Fabry-Pérot system at the INL is designed and optimized for operation above 1 MHz. Attenuation in the paper limited the primary wave components to occur at frequencies below 1 MHz. Dispersion in the S_0 mode occurred above 1 MHz. Both of these facts complicate the recorded waveform. Lower frequency operation would be better for recording the S_0 mode in its low frequency non-dispersive region providing simpler signal interpretation. However, the A_0 mode was always found to be the larger and its dispersion effects are well known. This opens the possibility that use of the A_0 mode would be more beneficial for determining elastic properties in paper. Additional signal processing would be required to account for the dispersion, but this is readily accomplished and performed routinely in other laser ultrasonic measurement applications.

2.6.2.2.4 Lamb Wave Measurements In Moving Paper

A machine was provided by IPST for simulation of the moving web of paper. This web simulator before modification was capable of moving the paper surface around a revolving wheel at speeds up to 400 meters/minute. Physically, the revolving paper surface allowed for contact free optical access to the moving surface that was placed approximately 1-10 cm from the optical input to the interferometer.

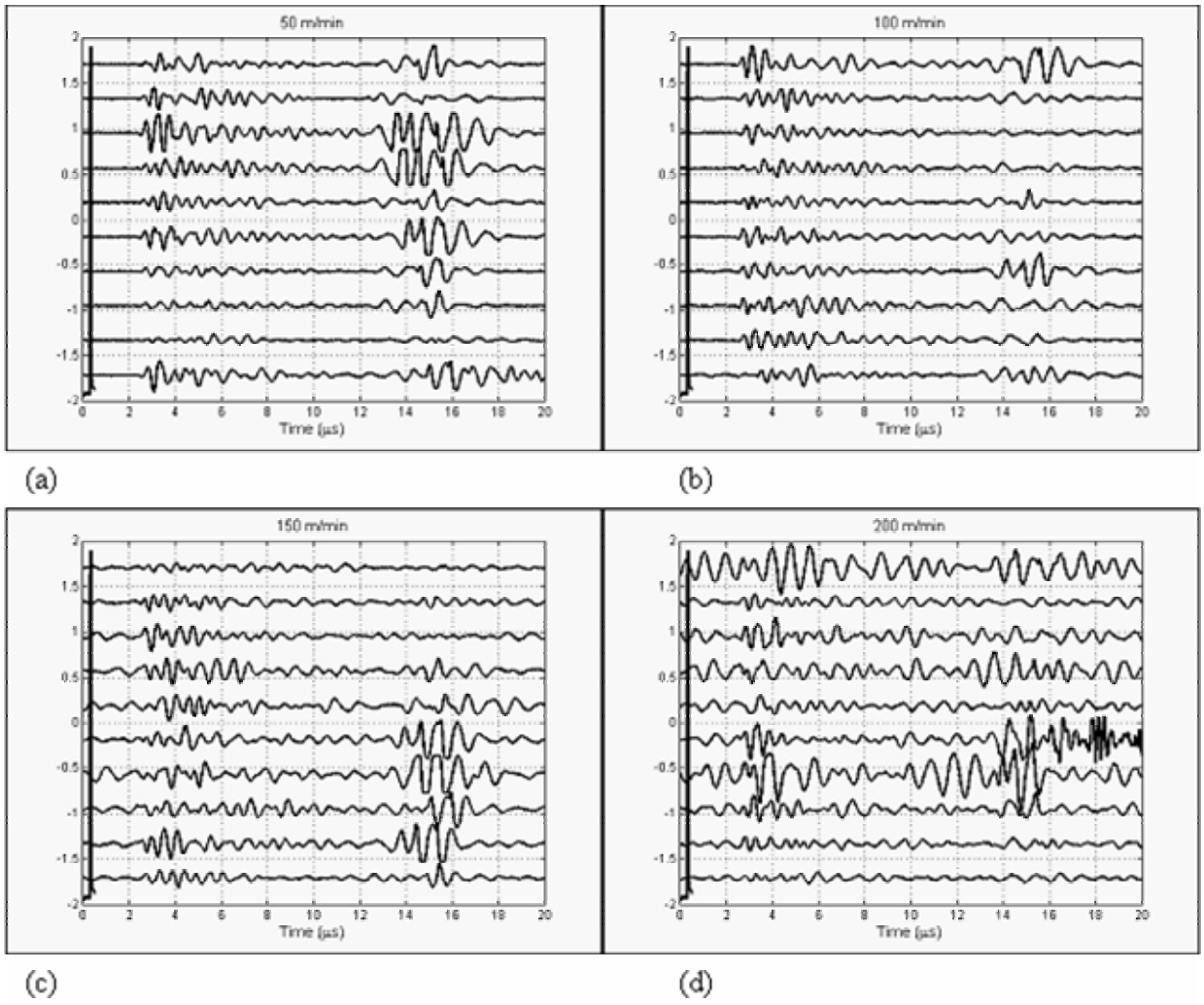

Figure 2.6.10: Repetitive single shot measurements on moving RSK59 paper showing the increase in noise due to the ambient vibration, laser, and changing speckle pattern phase noise at web speeds of (a) 50 m/min, (b): 100 m/min., (c): 150 m/min., (d): 200 m/min.

Figures 2.6.10a-d show a collection of single shot waveforms recorded successively, 1 second apart, from the moving paper surface. The first observation was that the moving paper surface added a significant source of additional noise to the detection process. This noise occurred from phase fluctuations and appeared to be due to several sources. Each waveform is from a single laser shot on a different location of the paper surface. These signals have been filtered with a 1 MHz high pass filter to remove some of the larger low frequency phase noise. Filtering was performed to optimize the S_0 mode detection and alters the waveforms leaving only the high frequency components in each waveform. The figures show that there is some variation from shot-to-shot, due to local paper properties and the generation mechanism, and

also shows significant additional noise at the higher web speeds. This is particularly apparent if one concentrates on the region before the first S_0 wave arrival with reference to the laser timing mark (bottom trace on Figures 2.6.10a-d).

Noise spectra taken at various web speeds for RSK59 are shown in Figure 2.6.11a for a detection spot size of 0.04 mm on the paper surface, Figure 2.6.12a for a 0.26 mm spot size and Figure 2.6.13a for a nearly specular plastic surface. Several observations can be made from these figures: (1) a large noise component appears at low frequencies even for stationary paper; (2) the low frequency component grows in amplitude as the web speed is increased; and (3) a plateau noise component appears that increases in frequency bandwidth but not amplitude as the web speed is increased. The overall general increase in noise with web speed is shown by the integrated noise amplitude shown in Figure 2.6.11b. These measurements were repeated for a larger detection spot size of 0.26 mm and the results are shown in Figures 2.6.12a and b. Clearly, similar behavior was seen as with the smaller spot size, but the larger spot averages over more of the paper roughness and reduces the bandwidth dependence on web speed as seen in Figure 2.6.11a. Some of the noise signals come from the moving speckle pattern recorded by the photodetector aperture. An attempt to eliminate this effect was performed by measuring the noise signals again but from a relatively smooth surface (the plastic wheel itself) that presents essentially a single speckle at the detector. The recorded noise spectrum for the plastic wheel is shown in Figure 2.6.13a and the integrated noise signal in Figure 2.6.13b. A significant reduction in the higher frequency plateau noise signal was observed.

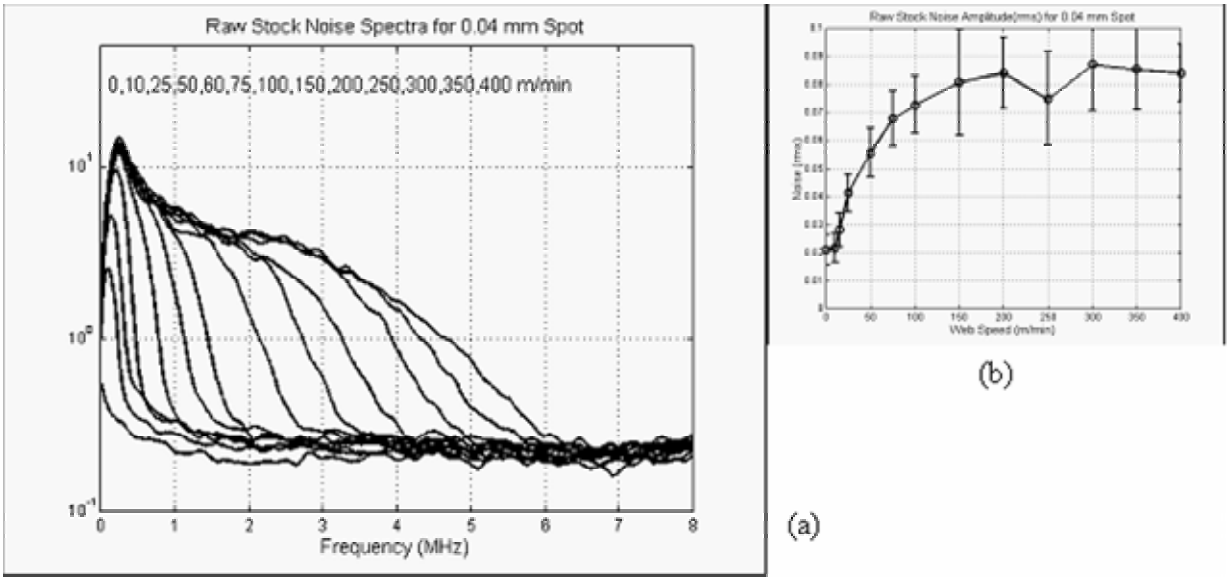

Figure 2.6.11: (a) Web simulator noise measurements from RSK59 paper for a 0.04 mm diameter detection beam spot size at various web speeds, (b) integrated noise rms amplitude measurements from RSK59 paper for a 0.04 mm diameter detection beam spot size.

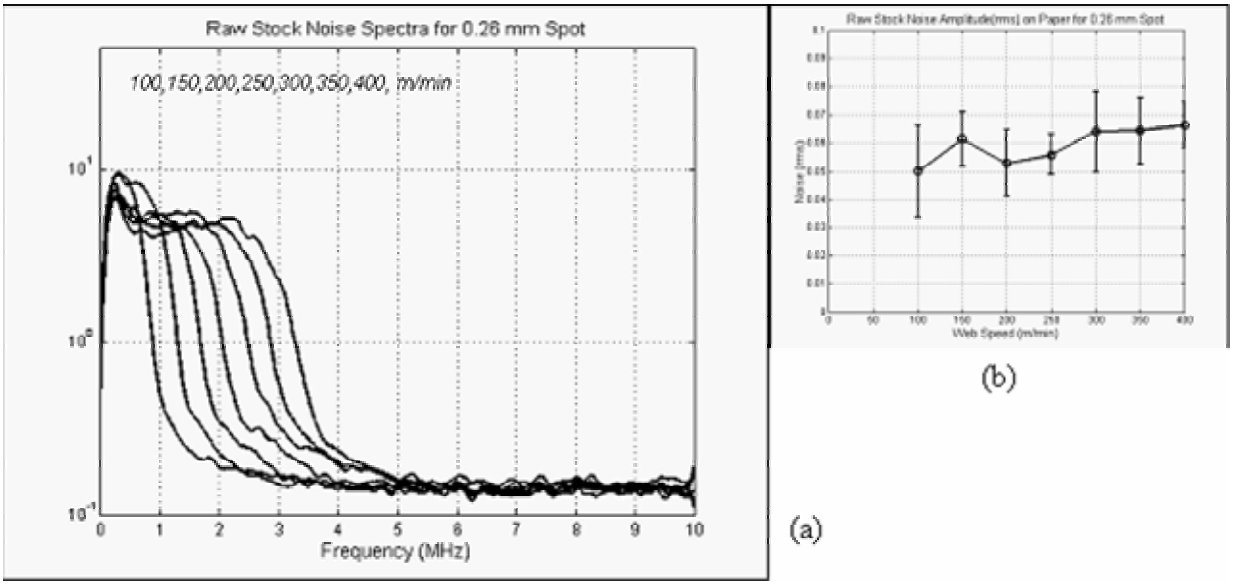

Figure 2.6.12: (a) Web simulator noise measurements from RSK59 paper for a 0.26 mm diameter detection beam spot size at various web speeds, (b) integrated noise rms amplitude measurements from RSK59 paper for a 0.26 mm diameter detection beam spot size.

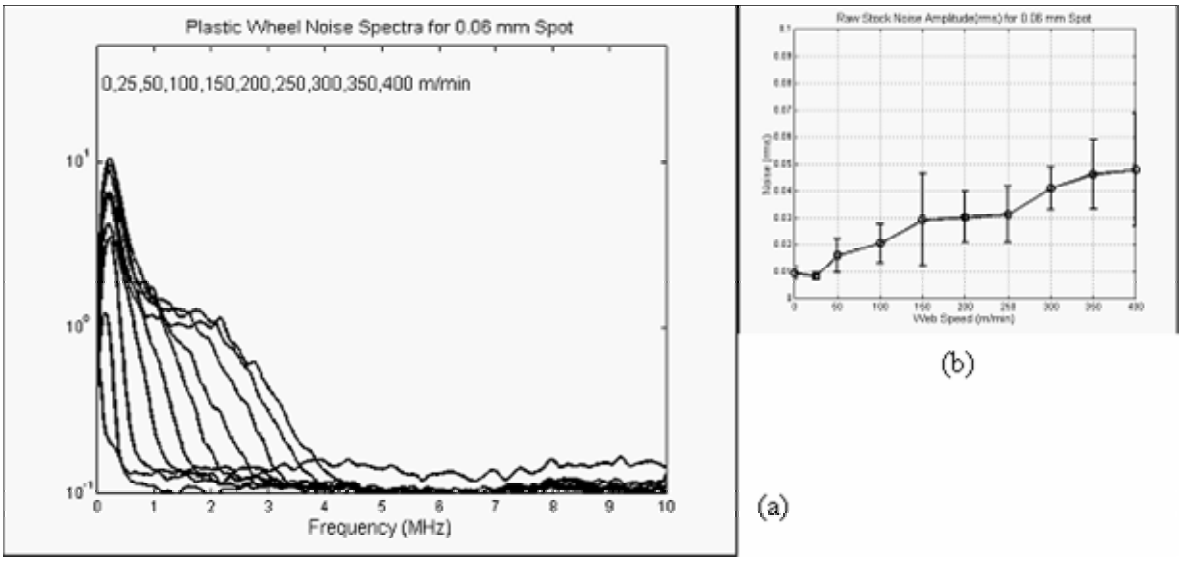

Figure 2.6.13: (a) Web simulator noise measurements from plastic wheel for a 0.08 mm diameter detection beam spot size at various web speeds, (b) integrated noise rms amplitude measurements from the plastic wheel for a 0.08 mm diameter detection beam spot.

The observed noise signal dependence on web speed can be explained by the contributions from several noise sources including

- INTRINSIC noise: inherent noise component even for stationary paper due to the phase noise from:
  - *Laboratory Vibrations* causing fluctuations in the optical path lengths between the detector and the sample surface
  - *Laser Phase Noise* in the detection laser (here an argon:ion laser)
  - *Electronic Interferometer Control Fluctuations*
  - *Electronic Signal Amplification Noise*
  - *Shot Noise* due to the detection process.

These noise components determine the maximum detectability of the Fabry-Pérot system used and are present in all the waveforms shown throughout this section. Additional noise sources due to the moving paper surface are

- FLUTTER noise: there is additional flutter and misalignment in the moving paper simulator that increases the phase noise seen as the web speed is increased. This noise source accounted for the noise component that appears to be limited to the low frequency region of the spectrum, but whose amplitude increases with web speed.
- SPECKLE noise: the moving rough paper surface produced a moving speckle pattern of light that crossed the photodetector aperture. This produced a noise component that had a fixed maximum amplitude (since the optical phase shift was limited to modulo(2π)). However, the frequency at which these speckle components move across the detector aperture increases with the web speed extending the noise bandwidth observed.

Speckle noise is seen in the spectra of Figures 2.6.11a and 2.6.12a. The plastic wheel data showed much less of this noise component, consistent with the speckle noise hypothesis.

These various noise sources combine to limit the detectability of the whole system. Figure 2.6.14 shows a comparison of the integrated noise levels described. One can conclude from these results that averaging over many speckles by using a larger detection spot size helps in that it moves the speckle noise to lower frequencies. Figure 2.6.15 shows the effect of increasing the detection spot size brought about by defocusing the instrument and normalizing for constant optical detection power. As wider spot sizes are used, the spatial resolution and frequency response of the system decreases. Other schemes are under investigation to further reduce the noise levels.

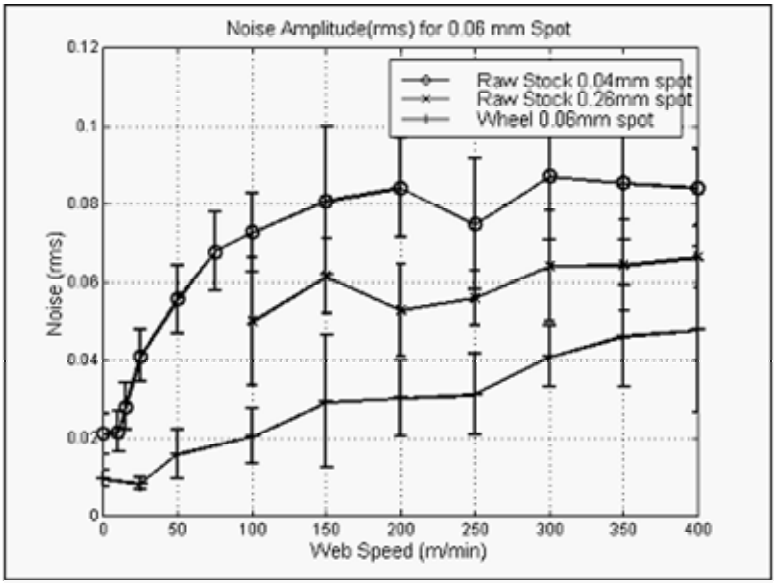

Figure 2.6.14. Comparison of the integrated noise signal amplitudes for the moving RSK59 paper with two spot sizes and for the moving plastic wheel.

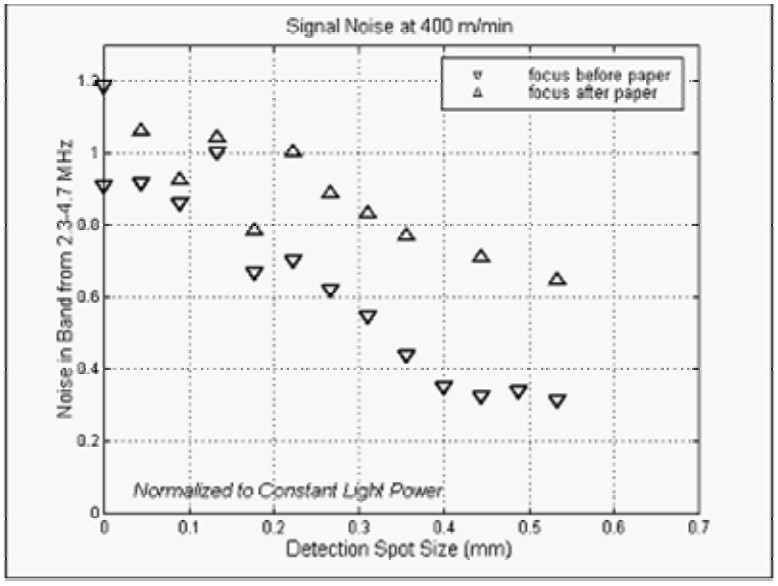

Figure 2.6.15. Integrated noise amplitude as a function of the detection spot size showing the decrease in noise level as more spatial averaging is performed on RSK59 paper.

2.6.2.2.5 Fabry-Pérot Interferometer Measurements (Summary)

To date, laser ultrasonic measurements of the S_0 and A_0 wave mode velocities in the MD & CD directions have been recorded with acceptable signal to noise ratios at web speeds up to 200 m/min using single shot detection with the INL Fabry-Pérot interferometer system. Higher speeds can be reached by using additional signal acquisition and processing techniques. Figures 2.6.16a and b show S_0 and A_0 waveforms for both the MD and CD directions on LNR42 and MED26 paper respectively. At relatively low speeds high signal to noise ratios were obtained for all the papers tested. Clearly the anisotropy between the MD and CD directions in wave speed is readily measured from either wave mode. At higher web speeds acceptable signal to noise ratios can be achieved by high pass filtering the data to eliminate the low frequency intrinsic and flutter noise. Figure 2.6.17 shows the S_0 and A_0 waveforms recorded with filtering for the RSK59 paper. Again the MD and CD anisotropy in the wave speeds is readily detectable. In order to reach an acceptable signal to noise ratio at the higher web speeds, up to 400 m/min, signals were averaged.

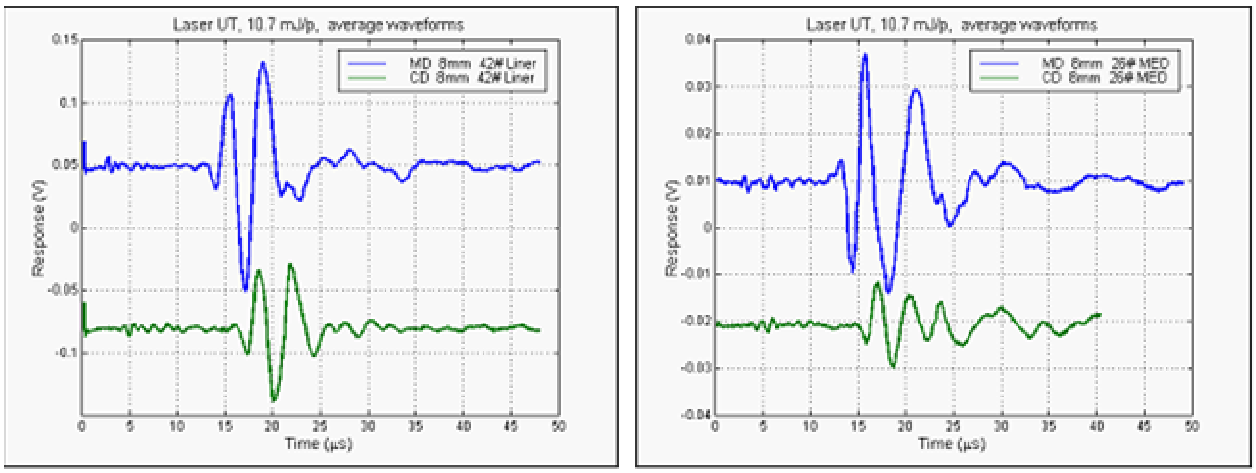

(a) (b)

Figure 2.6.16: MD/CD Fabry-Perot Laser Ultrasonic Signals –(a) LNR42, (b) MED26 paper.

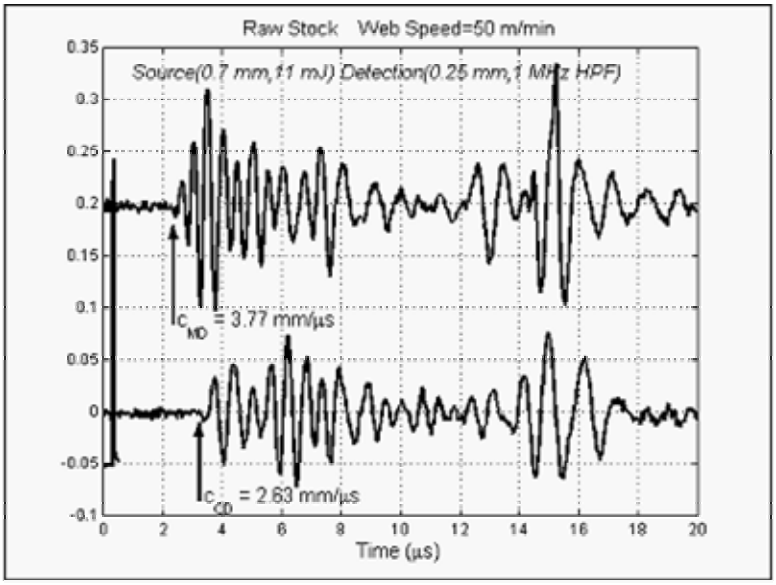

Figure 2.6.17: MD/CD Fabry-Perot Web Simulator Laser Ultrasonic Signals – RSK59 paper at 50 m/min, 1 MHz high pass filter processed.

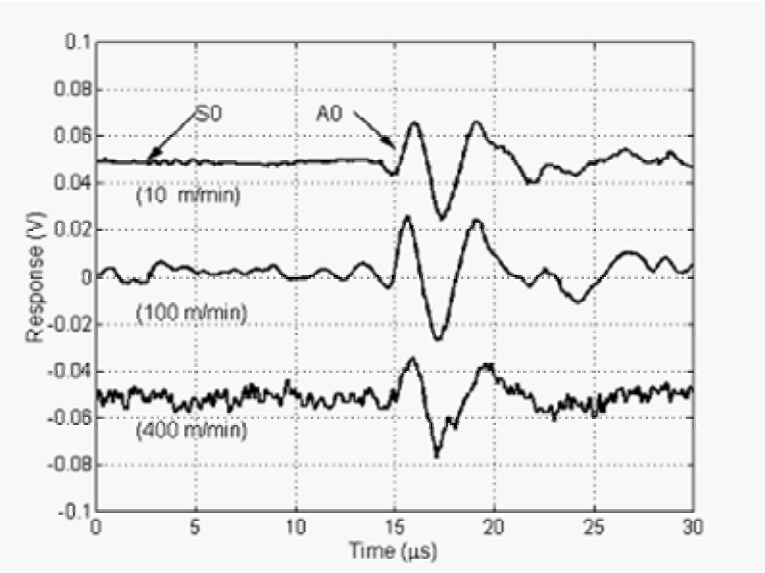

Figure 2.6.18. Comparison of the Fabry-Perot interferometer detection signals on LNR42 paper (averaged 128 times) at three different web speeds.

Figure 2.6.18 shows the waveforms recorded from LNR42 paper at speeds of 10, 100 and 400 m/min averaging 128 times. Here the S_0 wave was not discernable at higher speeds because the noise levels were too large for even averaging to filter out. However, the A_0 waveform is readily detected at all web speeds up to 400 m/min with averaging. Other mechanisms to reduce the noise level and enhance the signal detectability are under investigation. These include one described later in this report involving a reduction in the effective web speed by performing the measurements with a scanning laser detection beam as well as specialized signal processing routines for isolating signal properties from noise.

This work has shown that the Fabry-Pérot interferometer technology is a viable alternative for laser ultrasonic measurement of elastic waves in paper even under moving web conditions. All the work conducted so far has involved equipment designed for high frequency measurements not necessarily suitable for the paper measurement. Optimization of this approach would lead to improved performance over that presented here and presents a promising potential for future field implementation.

2.6.3 Time domain photorefractive measurements

2.6.3.1 Introduction (the problem of speckled light)

Of the various laser-ultrasonic methods, two wave mixing in a photorefractive crystal (PRC) offers particular appeal. First of all, the detected mechanical signal has a natural, low frequency cut-off. The large-amplitude, mechanical vibrations of the moving web will not contribute to instrument noise since the dynamic grating in the PRC progresses fast enough to eliminate low frequency motion from the mixed signal. Laser interferometry works best on a specular reflecting surface; it is not normally good at utilizing diffuse light from a rough surface. The PRC method, however, is a holographic imaging technique. A large portion of the wave front participates in the mixing and in the ultrasonic detection. The PRC approach has a reasonable chance of successfully finding tiny ultrasonic signals on rough surfaces traveling at high speed.

Because of the surface roughness of paper (many fibers) and that of fibers themselves, the light reflected from the surface is scattered almost isotropically in a half space (Lambertian source). From this arise two conclusions: 1) the power collected by a lens centered in the direction of the incoming beam will stay small, as long as the solid angle of collected light stays small; 2) the speckled nature of the reflection will make it very difficult to detect ultrasound with any interferometer which works with only one speckle, even on static surfaces.

On the other hand, the isotropic nature of light scattering on paper gives us an advantage: there is still enough power at relatively high incidence angles (40 degrees off the normal to the surface or higher) for the detection of displacements. This allows the measurements of both out-of-plane (A_0) and in-plane (S_0) displacements at the same time and thus avoids the need for two different setups.

2.6.3.2 Choice of a photorefractive interferometer

The criteria that define a photorefractive interferometer are:

- Wavelength of the detection laser
- Type of the photorefractive crystal

- Optical head of the interferometer
- Application of a high voltage to the crystal.

These criteria are described in further detail in the following sections.

2.6.3.2.1 Wavelength

The wavelength of the detection laser used with the interferometer is very important since the detection laser is usually the most expensive device in an interferometer and its wavelength cannot be changed easily. It also determines the type of photorefractive crystal to be used with the interferometer, as each crystal has a certain optimal bandwidth. The reflection coefficient of paper at this specific wavelength defines the amount of light reflected back at this wavelength. This directly affects the signal strength from the interferometer.

The wavelengths selected at IPST are 514.5 nm (Ar:ion laser) and 1064 nm (Nd:YAG laser). Some alternative choices for wavelengths could be 532 nm (doubled Nd:YVO_4 laser), or 780 nm and 852 nm (diode lasers). The selection of 514.5 nm and 1064 nm comes from the fact that relatively low cost lasers with high output powers at these wavelength are available.

Pulsed lasers (a few hundreds of μs with instantaneous powers of a few kW) can be used as the detection laser instead of a continuous one. However, the cost and complexity of such lasers did not make them suitable for the experiments during Phase I.

2.6.3.2.2 Type of photorefractive crystal

As described in section 2.5.3.5, crystals useful in our application are either the Sillenite type or the Semiconductor type. The Sillenite type crystals which work in the visible range (need to be photorefractive and transparent) are $Bi_{12}SiO_{20}$ (BSO), $Bi_{12}GeO_{20}$ (BGO), $Bi_{12}TiO_{20}$ (BTO), and are well suited for Ar:ion lasers (514.5nm) or lasers at 532 nm. The Semiconductor type crystals need to be used at infrared wavelengths because their transmission band ranges from 915nm to 1500nm. These semiconductor crystals are undoped GaAs, InP:Fe and CdTe:V. All of these can be potentially used for ultrasound detection on paper products.

In the very specific case of the photoinduced-EMF interferometer, the opposite effect is desired: total optical absorption of the beam by the crystal. For Cr:GaAs, a crystal very efficient for photoinduced-EMF detectors, the appropriate wavelength is thus in the visible (514.5 or 532nm) or in the near infrared (852 nm or lower).

For measurements on static paper, the Sillenite type crystals are appropriate since they have a high gain. Thus, the signal to noise ratio of the ultrasonic displacement is high, even with little light collected. Unfortunately, these crystals do not have a response time short enough to adapt to the constantly changing speckle pattern created by the displacement of the paper web under the beam.

Thus, for measurements on moving paper, the first choice is to use Semiconductor photorefractive crystals which have a very short response time (1 to 10 □s) but a small gain. These will, however, have smaller signal to noise ratio than Sillenite type crystals.

2.6.3.2.4 Application of high voltage to the crystal

The application of a high voltage, DC or AC, pulsed (at the moment when the ultrasonic waves need to be detected) or continuous, to a photorefractive crystal is necessary when the photorefractive gain of the crystal is small, typically in the case of semiconductor photorefractive crystals. It can also enhance the gain of Sillenite type crystals.

The high voltage across the crystal has two effects: it moves more electrons from the bright fringes to the dark fringes and thus creates a stronger electric field grating, and it shifts the phase of the electric field closer to quadrature from the interference grating.

The drawback, however, is that the application of an electric field slows down the adaptation of the crystal to the changing speckle pattern (slower response time), which is a problem in the case of Semiconductor crystals.

2.6.3.4 BSO Photorefractive Setup

2.6.3.4.1 Experimental Setup (evolution of the BSO PRC interferometer)

The first BSO photorefractive interferometers built at IPST used a mirror with a piezoelectric transducer attached to the back as a target sample. The mirror undergoes a sinusoidal displacement at 1 MHz (the resonant frequency of the transducer). Sine waves at 1 MHz were chosen at the beginning because this frequency was theoretically in the middle of the bandwidth of ultrasound generated by lasers on paper. The use of a mirror as a target sample provided a high intensity planar wavefront for the signal beam which maximized the photorefractive effect. This interferometer was labeled Version 0.1, and used an “X” shape setup for interference between the two beams. The BSO crystal thickness was 5 mm.

PRI Version 0.2 still used a mirror and a 1 MHz piezoelectric transducer, but with a “V” shape setup, crystal thickness was 5 mm.

PRI Version 0.3 continued to use the same mirror, but the optical head of the interferometer employed was a cube beam splitter plus a quarter wave plate for the first time. PRI Version 0.3 used 2.25 mm and 5 mm crystals. PRI Version 0.4 was very similar to Version 0.1 except that it used the 2.25 mm crystal which gave better results for ultrasound detection than the 5 mm one. The orientation of polarization of the incident beams and the crystal were also different.

PRI Version 0.5 was the first one to detect ultrasound on a rough surface, thus with a speckled wavefront for the signal beam. The signal beam was focused with a 20x microscope objective on an aluminum plate with the piezoelectric transducer attached on the back of the plate. The optical head used a beam splitter and a quarter wave plate in addition to the microscope objective.

PRI Version 1.0 was the first one to make measurements on paper, using a “T” (beam splitter + quarter wave) setup, as shown in Figure 2.6.38. The angle between the reference beam on the left side and the signal beam on the right side was 50°, a value theoretically and experimentally optimum for the photorefractive effect without any applied electric field.

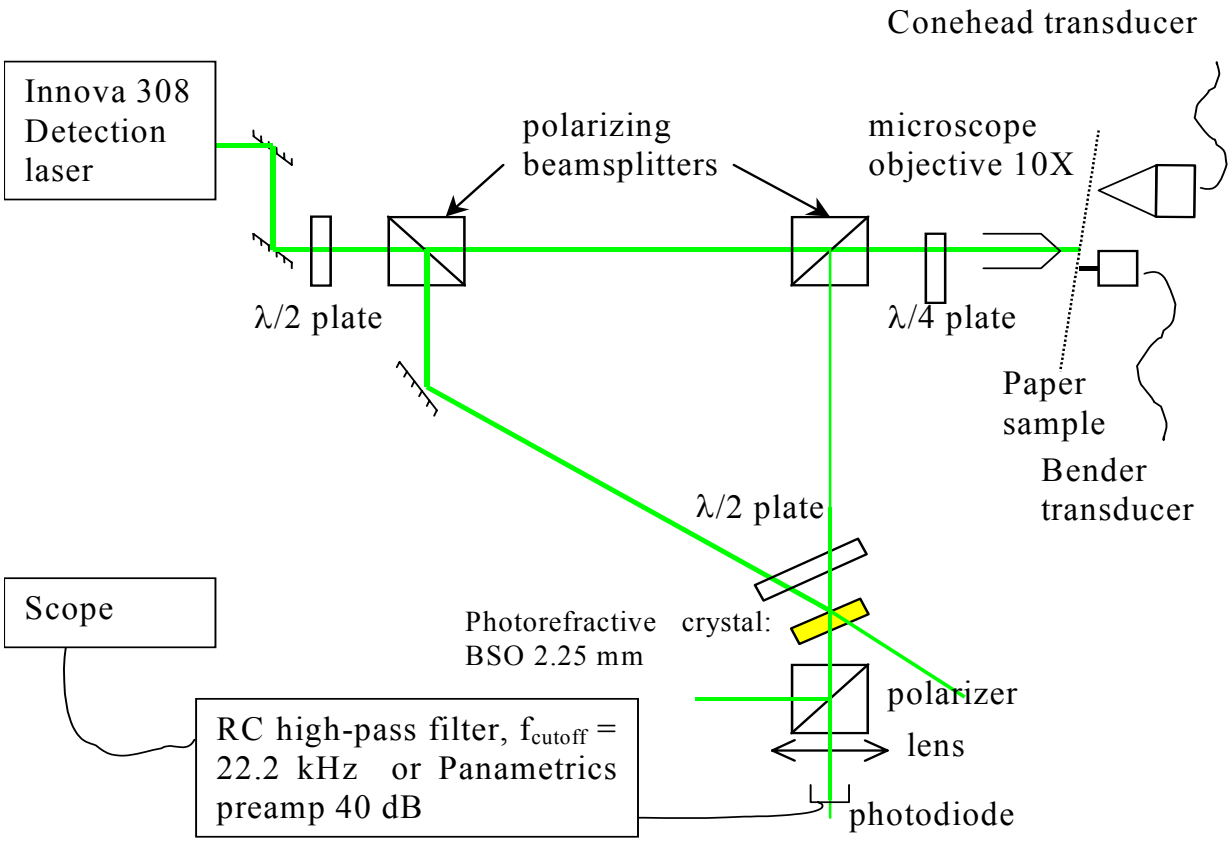

Figure 2.6.38 Schematic of Photorefractive Interferometer Version 1.0

For generating ultrasound on paper, two different contact transducers were used: a bender transducer generating mainly S_0 waves was excited at its resonance frequency of 57.8 kHz, and a "conehead" transducer generating at 57.2 kHz. The conehead transducer was in contact with paper by the tip of the cone, which had a diameter of about 1.5 mm.

Figure 2.6.39 shows a picture of the Photorefractive Interferometer Version 1.0 using the bender transducer.

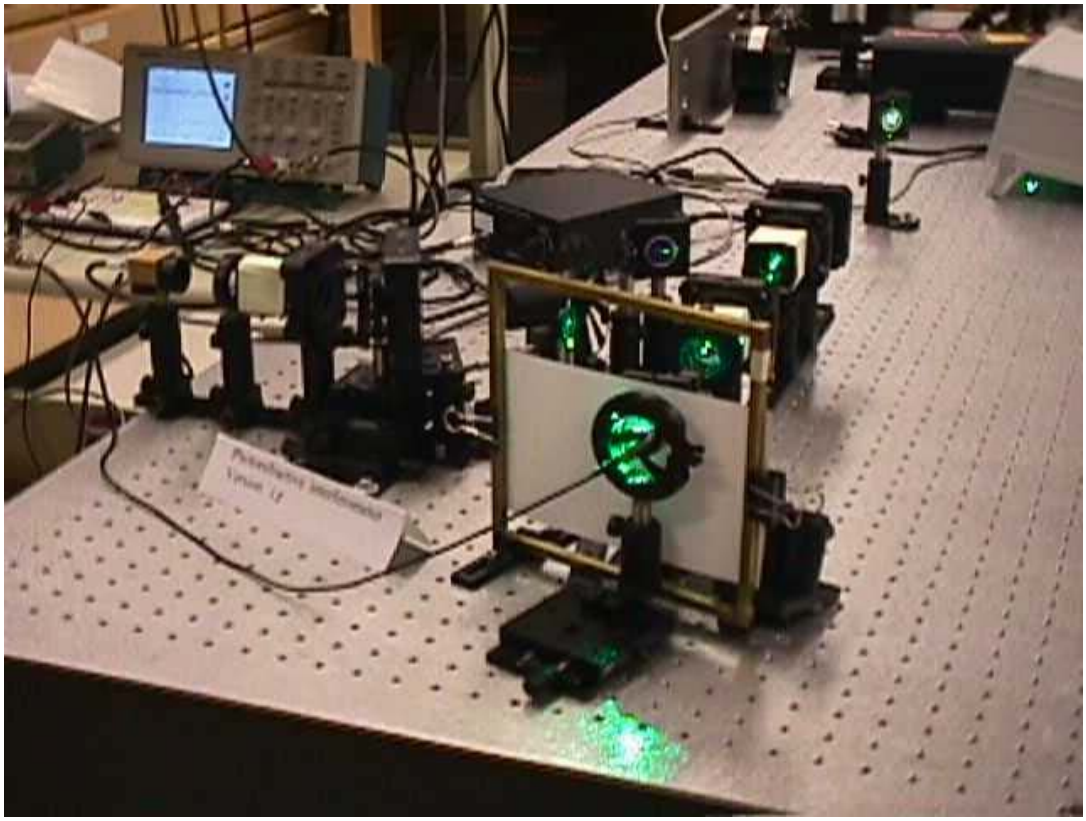

Figure 2.6.39 Photorefractive Interferometer version 1.0 detecting ultrasound on copy paper with generation made with the bender transducer.

In order to improve the signal to noise ratio, a voltage was applied across the 2.25 mm BSO crystal and a new detection setup (PRI Version 1.5) was assembled as shown in Figure 2.6.46.

For this interferometer (version 1.5) the angle between the signal beam and the pump beam was decreased from 50° to 2-5°, which is ideal when a voltage is applied to the BSO crystal. A converging lens was placed in the path of the reference beam and had a focal length of 38 mm and the focal point was just before the 45° incidence mirror.

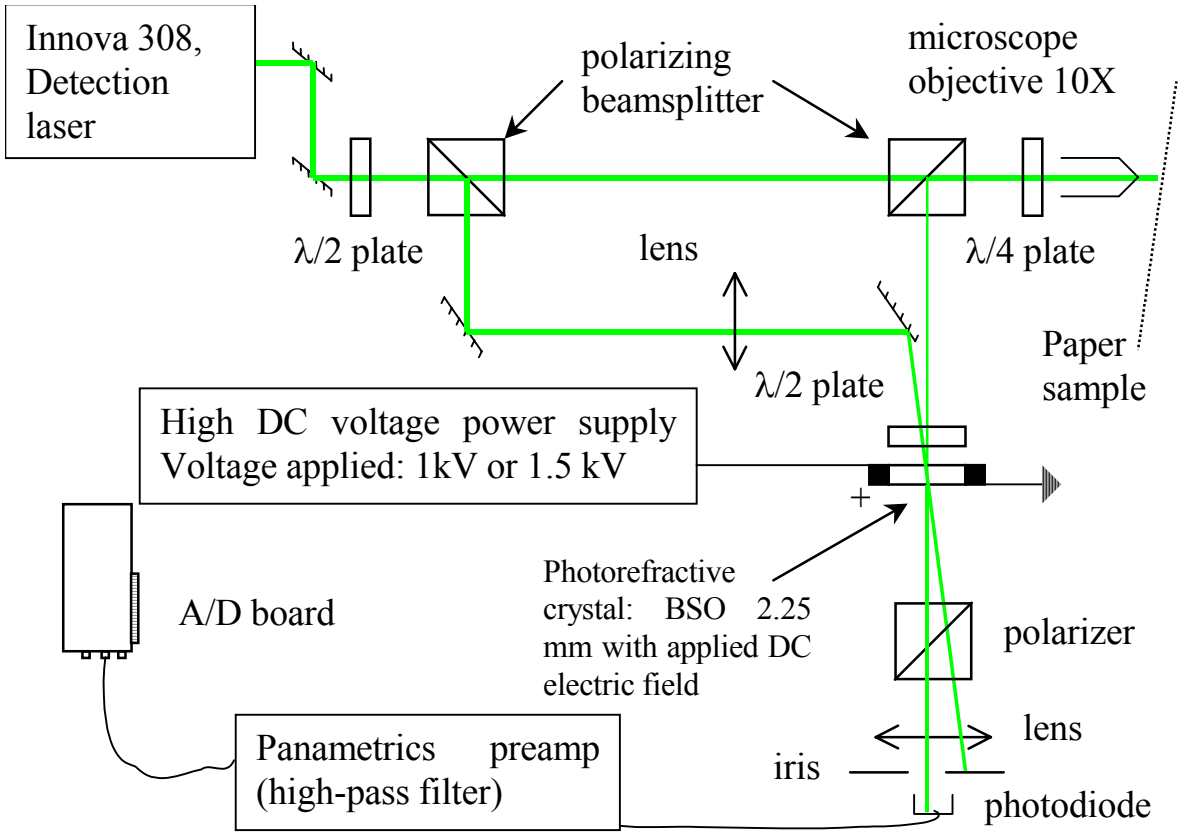

Figure 2.6.46 Schematic of Photorefractive Interferometer Version 1.5 using a BSO crystal with a DC applied voltage.

The reference beam diverges after the focal point and needs to impinge across the crystal from one electrode to another, in addition to overlapping the signal beam. This is necessary because if the electrons are not set free by this beam there will be no photoconductivity and the electric field will stay in the dark zone near the electrodes, eliminating its effect on the two-wave mixing. The iris just in front of the photodiode has been added to filter out the parasitic light of the generation pulse at 1064 nm directly scattered from the paper sample or collected by the interferometer optical head. Figures 2.4.47, 2.4.48 and 2.4.49 show several views of Version 1.5.

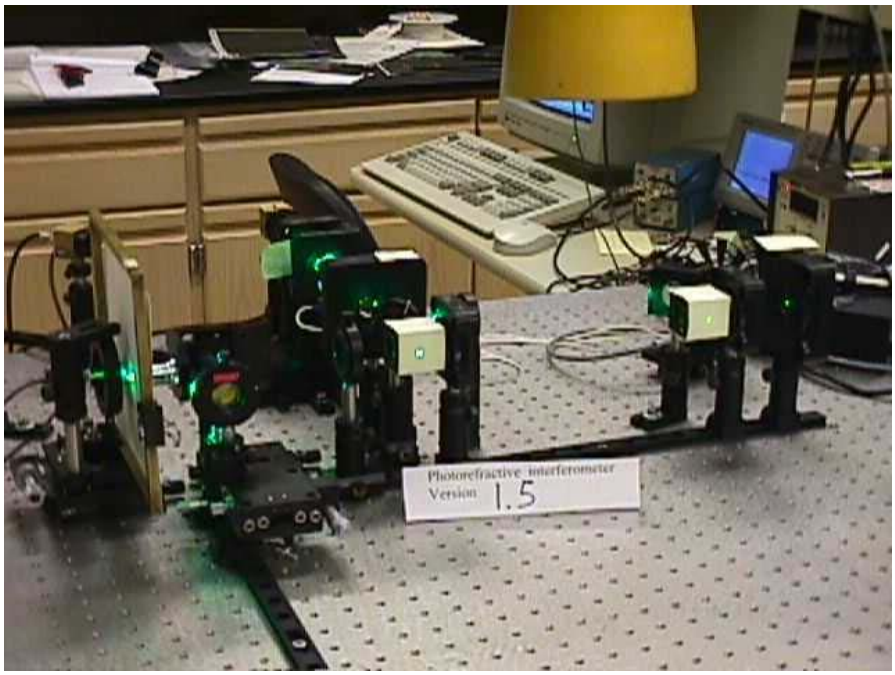

Figure 2.6.47 View of the PRI Version 1.5: Paper sample is on the left, photodiode and crystal with high voltage leads are in the center back.

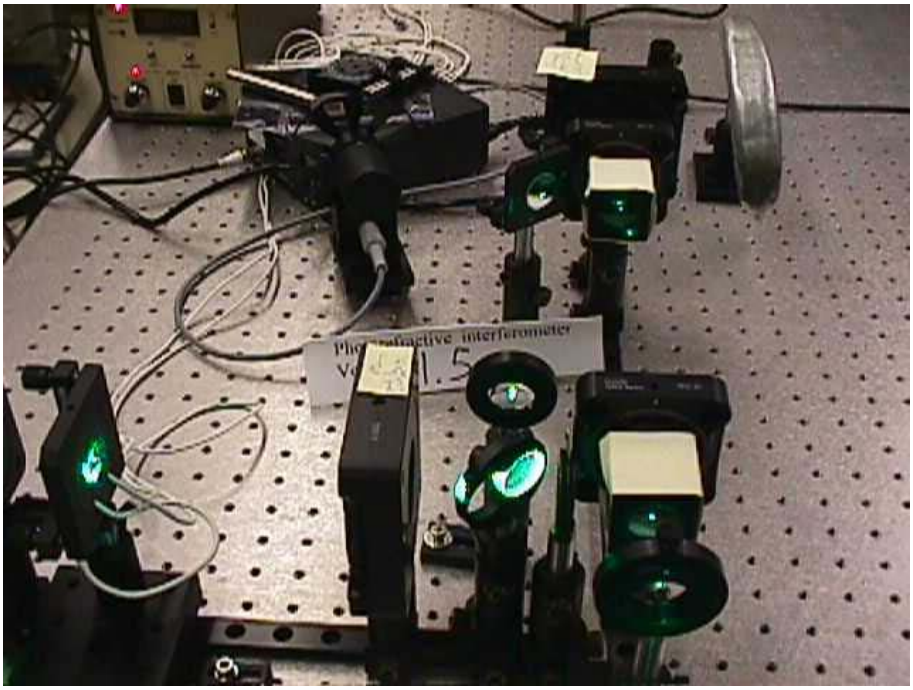

Figure 2.6.48 View of the 45° mirror (center), and of the crystal (white wires to the left).

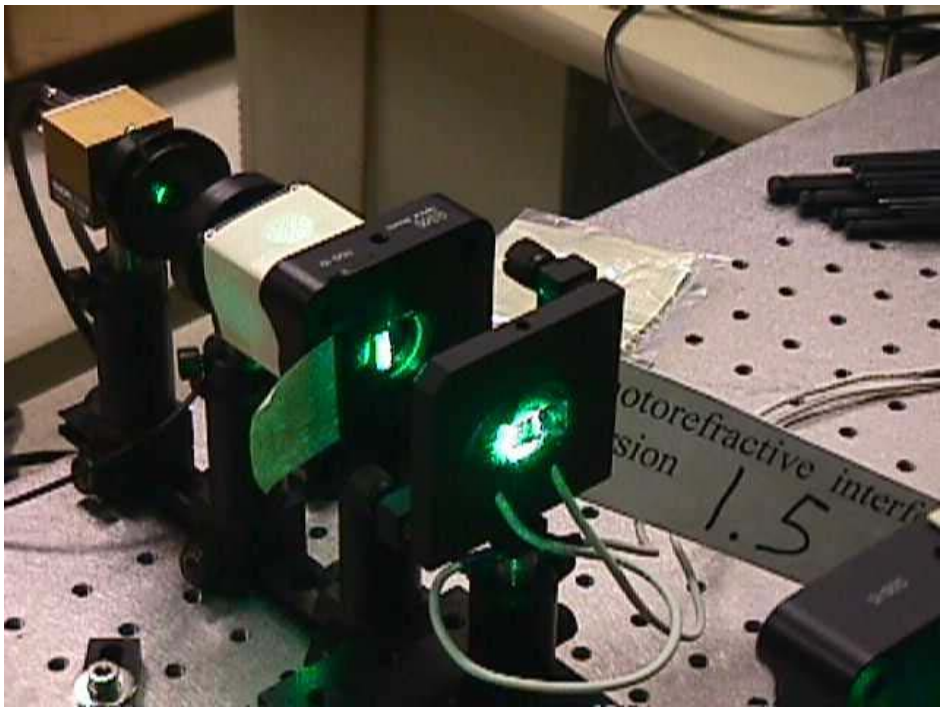

Figure 2.6.49 View of the BSO crystal with its electrodes on the sides (center).

With PRI Version 1.5, the signal to noise ratio became acceptable for laser-ultrasonics measurements. Therefore, data was recorded on static paper samples as a reference database for comparison with contact measurements.

2.6.3.4.2 Experimental setup for laser generation and laser detection on static paper grades

The experimental setup used for measurements on all paper samples was closely related to PRI Version 1.5. To detect both the A_0 and S_0 waves, the incident beam and the collected beam were placed at 40° incidence with respect to the normal to the paper surface. The detection beam was focused on the paper. The power density was kept low to avoid burning the sample.

Table 2.6.1 shows the incident power applied on the paper as a function of power measured at the output of the laser. The power of the reference beam is also shown. However, the collected power of the signal beam was below 1 mW, thus not measurable by the power meter.

Table 2.6.1 Incident power on paper and into the reference beam versus total output power.

Output power of detection laser (mW)	Incident power applied on the paper samples (mW)	type of paper grades	Power into the Reference beam (mW)
105	24.5	Medium 26-lb	67.8

120	28	33-lb linerboard, 42-lb linerboard, 69-lb linerboard, sack, tissue	77.7
140	32.5		90
150	34.8	raw stock	97
170	39.4	copy paper newsprint, art paper, bleachboard	110

On static paper samples, the spot illuminated by the laser beam is stationary so the light generates heat that must be dissipated to prevent burning. A portion of the incident beam is neither absorbed nor reflected by the paper. It just passes through the fibers through the back side of the sheet. This is especially true with low basis weight grades: copy paper, art paper, newsprint, tissue, etc.

If the incident beam is highly focused or the power is too high, it will burn a hole through the sample. The incident beam will then travel freely through the paper sample without creating any reflection and thus the signal beam will disappear.

Figure 2.6.50 shows a schematic of the BSO PRC interferometer.

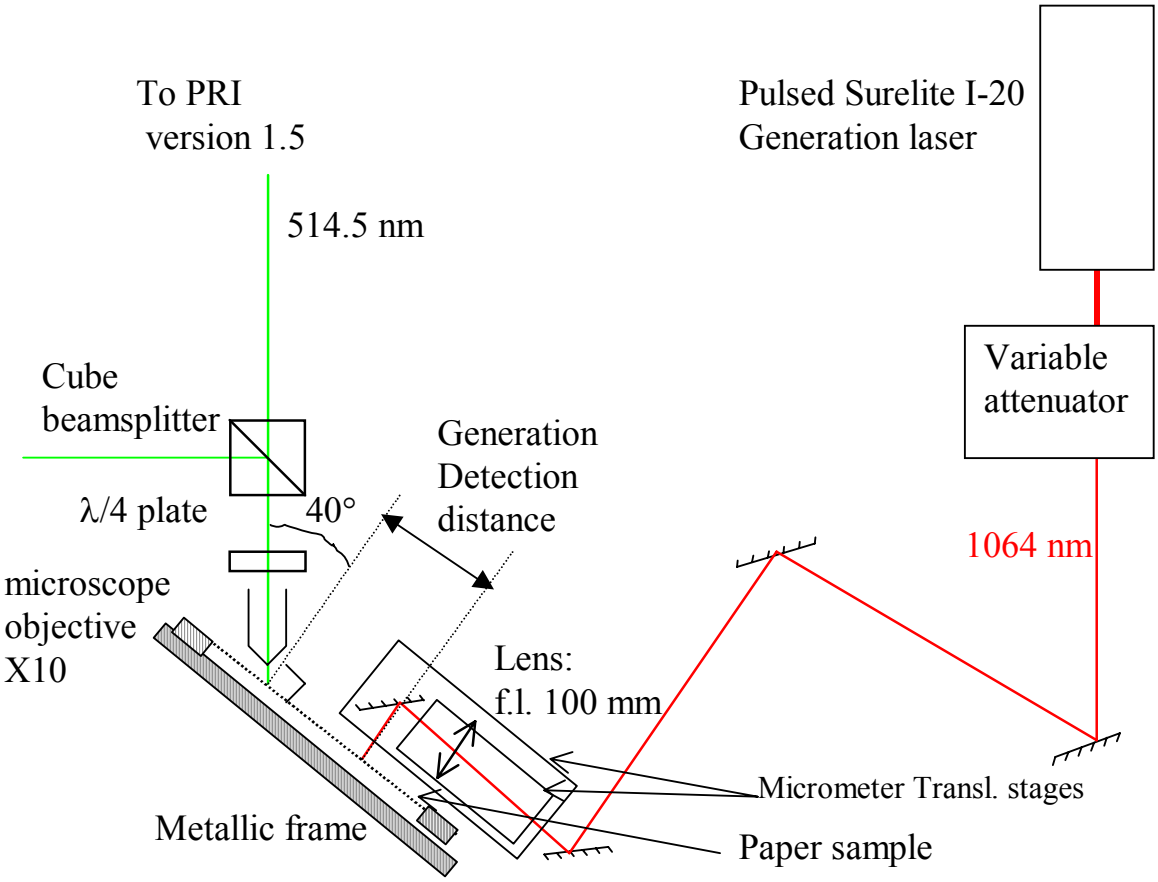

Figure 2.6.50 General schematic of the experimental setup for the tests on paper grades using BSO PRC interferometer.

2.6.3.4.3 Time Domain Photorefractive Interferometer Results

When laser ultrasonic detection is used in paper testing, signals are found to vary. This is evident in the shapes of the waveforms collected when the same configuration is used at the same detection point. The amplitude variance is obvious, however the time of wave arrival remains almost constant.

Johnson (1996) showed that, unlike in metals, some statistical variation of the waveforms in peak amplitudes and arrival time were present in paper. Using a correlation technique, he found that the relative time delay measured at the same point was within 1% difference while the delay became as large as 6% when measured at different detection points.

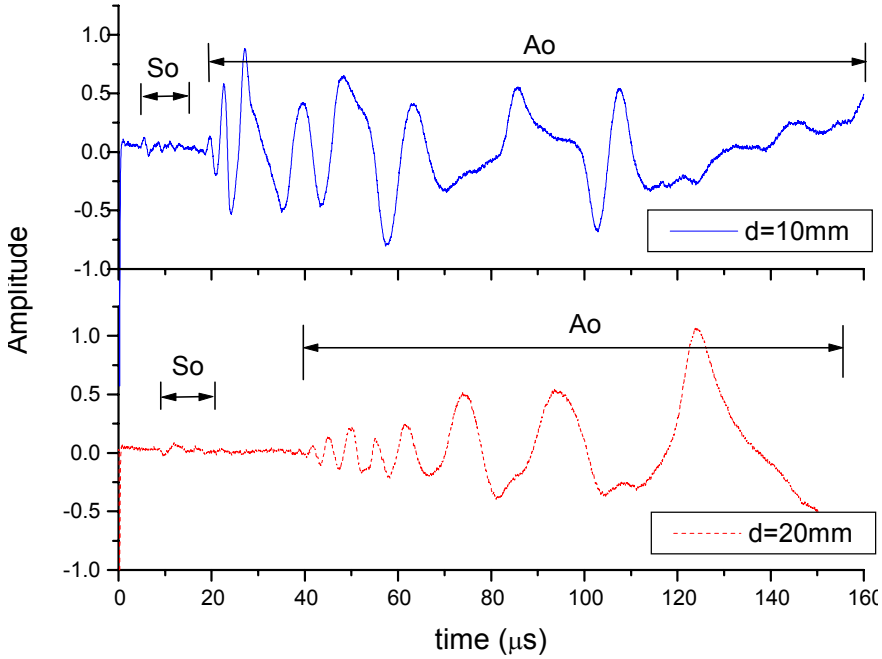

Figure 2.6.63 Signals collected with BSO PRC setup for static copy paper in CD: Sampling rate is 50MHz and energy is 6mJ. The signals were averaged 4 times.

To show the characteristics of the copy paper in CD, Figure 2.6.63 is plotted. Again, the S_0 mode is present but its shape varies noticeably. The cross-correlation function of the two S_0 signals results in the phase velocity of 1957 m/s for this case.

The S_0 mode velocity measurements in the low frequency region can be used to determine elastic stiffness constants, C_{11} or C_{22}, in MD or CD respectively. The error associated with this evaluation method is known to be less than 2% [Mann et al., 1980]. Other information that can be obtained from the S_0 mode is another elastic constant, C_{33}. Ideally, if the S_0 mode can be measured accurately around the cut-off frequency, then C_{33} can be determined independently. Yet, as Johnson (1996) found, the nature of the narrow frequency bandwidth of the CSD spectrum makes it difficult to estimate C_{33} using this method. Further work should be pursued on this matter.

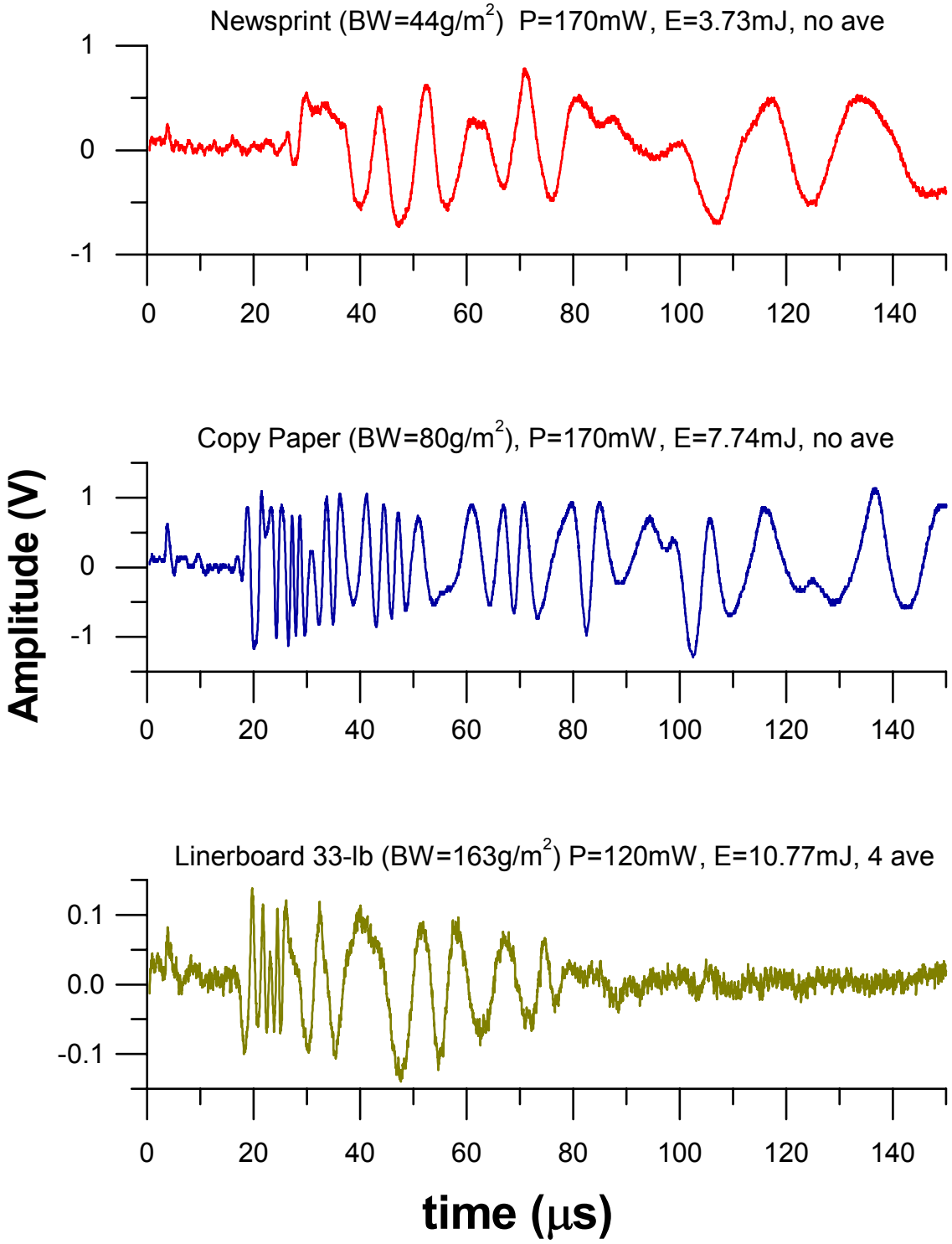

Figure 2.6.64 BSO PRC results on selected static paper samples by grammage in MD: The distance between the source and detection point was maintained at 10 mm apart and the sampling rate of 50 MHz was used throughout.

Figure 2.6.64 shows typical examples of the waveforms in MD obtained on selected static paper grades with the BSO photorefractive interferometer. The distance between the source and detection point was maintained at 10 mm apart and a sampling rate of 50 MHz was used throughout. The results from linerboard 33-lb were averaged 4 times, while the others were single shot measurements. The figure shows that each paper sample tends to respond uniquely to an ultrasonic source based on its stiffness properties. The figure also shows that the A_0 mode can easily be detected in the paper samples due to relatively large amplitudes. The amplitudes of the S_0 mode waves are small relatively. In certain samples with higher grammage, such as bleachboard and linerboard, the S_0 modes were not detected. This suggests that a technique using A_0 mode analysis should be developed rigorously so that the analysis can be based on the A_0 mode waves.

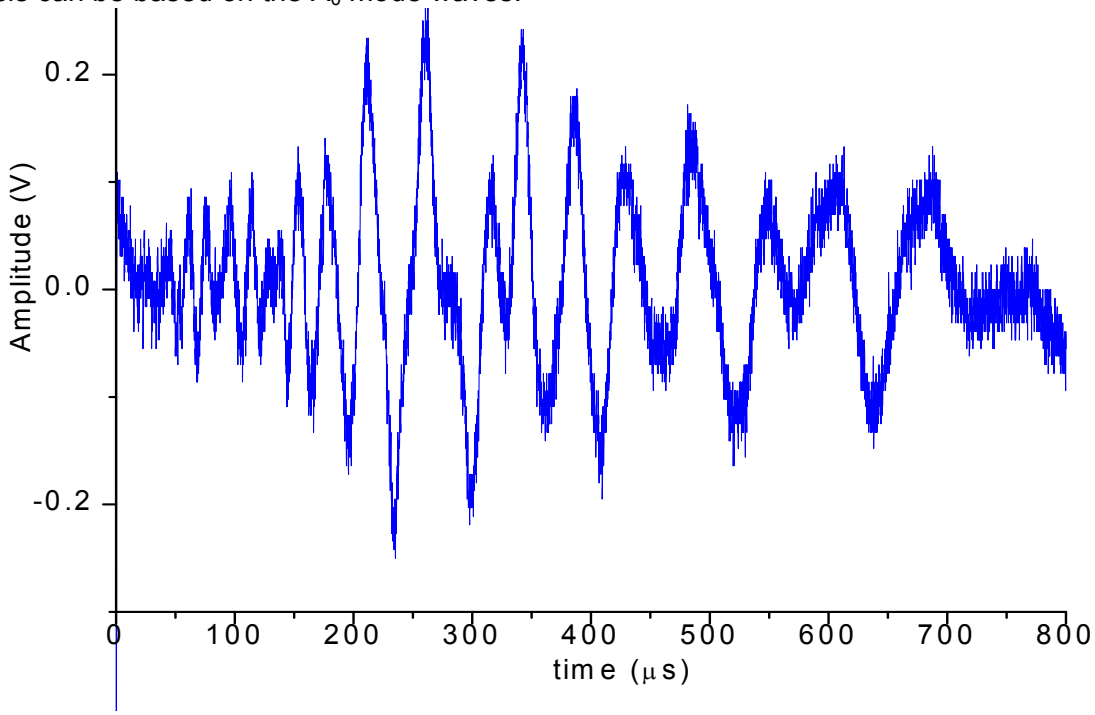

Figure 2.6.65 BSO PRC results on static 1-ply tissue paper in MD: The measurement was taken using P=120 mW and E=1.09 mJ. A single shot was used for the signal.

Figure 2.6.65 shows the BSO PRC results on a static 1-ply tissue paper in MD. Since the testing of tissue was not within the main scope of the project, only a handful of measurements were taken out of curiosity. It is noteworthy that the measurements on tissue showed encouraging results, although the response time was slower compared to other samples due to very low basis weight. So far, contact techniques have not been able to produce reliable measurements on tissue. Therefore, it shows a great potential that the current non-contact technique may be implemented on tissue as well.

The technique used here for the A_0 mode analysis is based on the one originally suggested by Sachse and Pao (1977). Later, Schumacher et al. (1993) applied it to Lamb waves. Since a time-of-flight method is not appropriate to use for the evaluation of dispersive, broadband transient waves, phase velocities are extracted from FFTs and unwrapped phase angles as a function of frequency and distance between two detection points. First, the signal generated at the same source location is recorded at two detection points along the wave path.

Second, only the region of the signal corresponding to the A_0 mode is selected and the rest is zero-padded. Then, the signal is windowed using a rectangular window. Third, each signal is processed for spectrum analysis and the FFT is plotted. Finally, the phase angle of the signal is unwrapped and the difference of the two are directly related to the phase velocity of the A_0 mode using the following relationship:

$$c = \frac{-2\pi \cdot f \cdot d}{(\Delta\phi + 2m\pi)}, \qquad (3)$$

where *c* is the phase velocity of the A_0 mode (m/s), *f* is the frequency (Hz), *d* is the distance between the two detection points (m), $\Delta\phi$ is the difference in unwrapped phase angle for a given frequency (radians), and *m* is an integer associated with a correction of the phase at lower frequency.

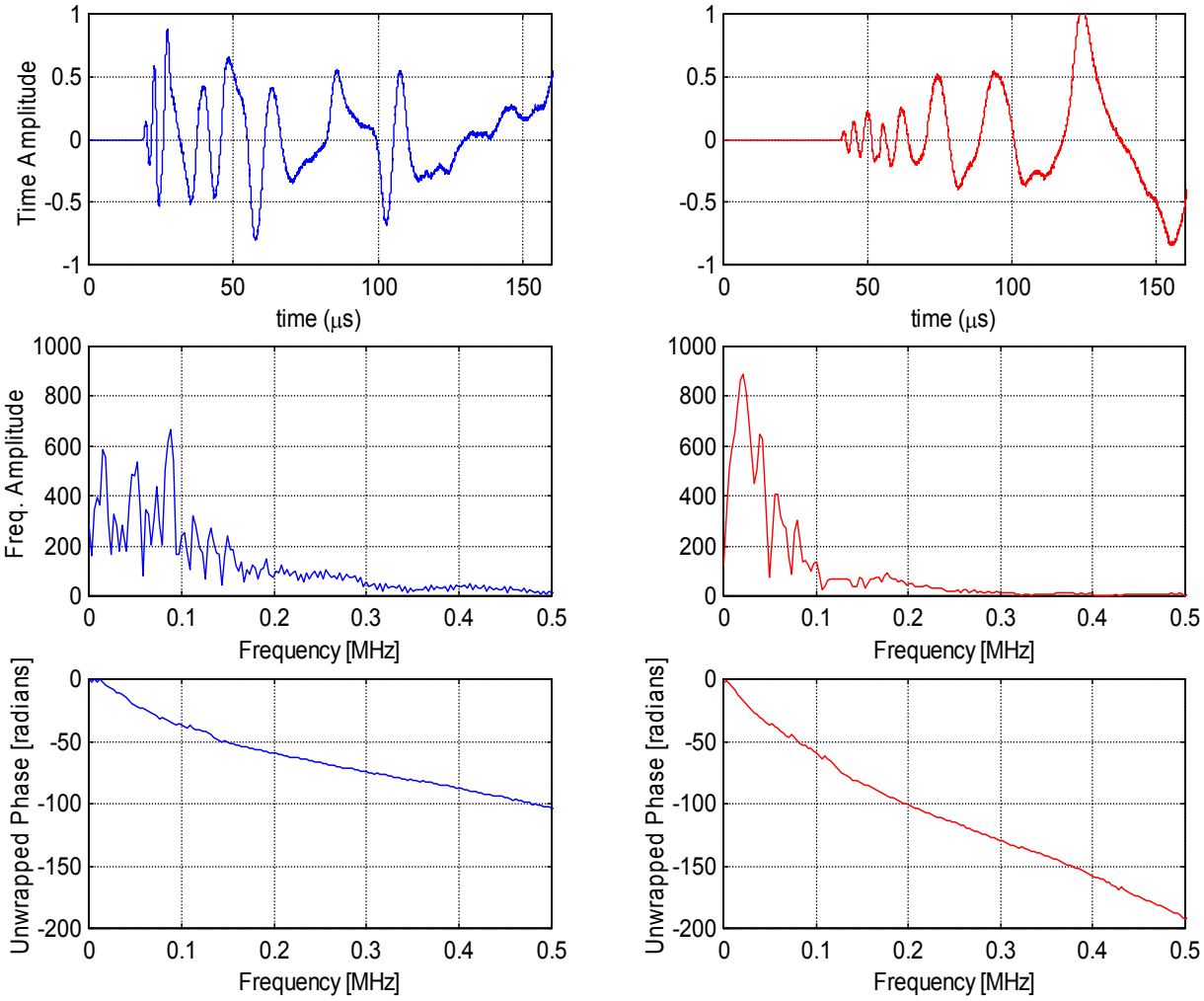

(a) d=10 mm (b) d=20 mm

Figure 2.6.66 A_0 mode analysis of the signals shown in Figure 2.6.63 on static copy paper in CD: The figure showing the portion of the wave not corresponding to the A_0 mode is zero-padded. Then, a rectangular window is superposed onto the

signal. The FFT of the signal is computed and the unwrapped phase angle is extracted.

Figure 2.6.66 shows the combination of the steps involved in the technique for evaluating the A_0 mode wave for d = 10 mm and 20 mm, respectively. For each case, the zero-padded A_0 waveform is windowed and processed to compute the FFT spectrum. The unwrapped phase angle is determined. The FFTs of the two signals indicate that the signal energy exists only in the low frequency regions below 0.3 MHz. This trend is consistent throughout the experiments. On the other hand, the results given by Johnson (1996) on static copy paper showed that the energy was still present up to 1 MHz. The reason for not being able to detect higher frequency A_0 component with the current PRC configuration was unclear. Nevertheless, it is not necessary to have the higher frequency A_0 component present to determine the paper stiffness, since the values of the stiffness constants can be evaluated using the low frequency information only.

More immediate concern comes from what value of the integer *m* should be used to correct the phase angle at the very low frequency region where the signal energy is low. As the phase unwrapping is performed from low to higher frequencies, the accuracy of the phase at a given frequency depends on that of the phase at lower frequencies, where discontinuities exist. A small error in phase angle at very low frequency may accumulate and result in a significant difference at higher frequencies.

Figure 2.6.67 shows a comparison between a theoretical A_0 dispersion curve and the results with corrected phase angles. The phase velocity determined without a correction tends to show a somewhat higher prediction in the low frequency region below 0.1 MHz, while the one corrected with -2π seems to match with the theoretical curve. Comparison with other paper samples showed that good prediction seems to come with a correction of -2π or -4π. Nevertheless, further analysis is required to determine the accuracy of the correction term *m* for the A_0 mode analysis.

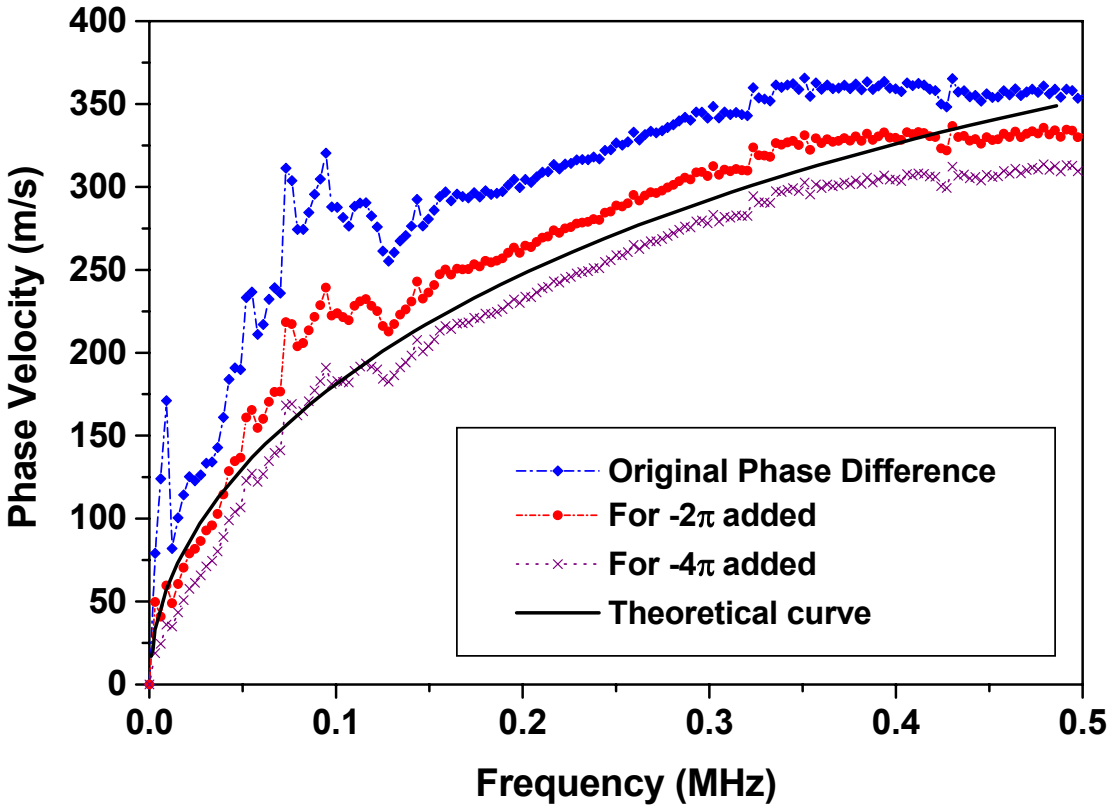

Figure 2.6.67 Comparison of the Ao mode velocities between a theoretical dispersion curve and the velocities with corrected phase angles on static copy paper.

2.6.3.4.4 Improvement of experimental setup on static paper, second round of measurements with 2 paper grades

Most of the measurements on samples were made using a strong ablation mode for generation (around 3-17 mJ/pulse over a spot of ≅ 100 μm diameter) to obtain high amplitude signals. This was not appropriate for two reasons: first, the strong ablation mode damages the paper; second, the strength of the acoustic source varies significantly with the number of shots consecutively made at the same spot. Therefore, for the new interferometer, efforts were made in two directions: reducing the damage to paper by decreasing the power density of the generation beam, and increasing the interferometer sensitivity.

The schematic of the improved version of the photorefractive interferometer (Version 1.6) is shown in Figure 2.6.68.

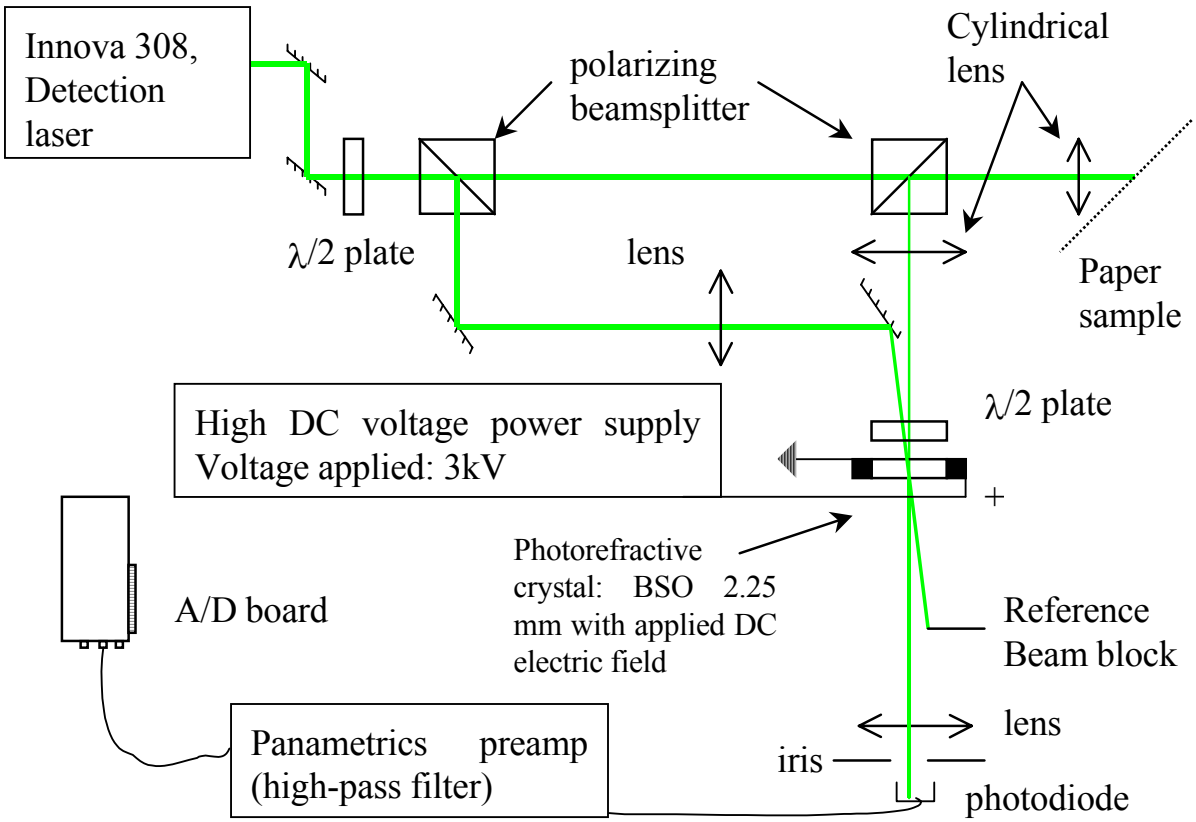

Figure 2.6.68 Schematic of photorefractive interferometer Version 1.6 (line detection).

The cylindrical lens close to the paper sample focuses the circular beam into a line along the vertical direction. The focal length is 48.9 mm at 514 nm and the diameter of the lens is 25.4 mm. It should be noted that this specific lens was intended for use with 1064 nm so was not properly anti-reflection coated for 514 nm, and thus a significant amount of the power was lost. The focused detection spot was a vertical line 2 mm long and 0.5 mm wide. Using this configuration, the interferometer was sensitive to ultrasonic waves propagating in the horizontal direction (i.e., perpendicular to the detection line). This configuration (line detection) presents a significant advantage over point detection since the total amount of power impinging on the paper can be increased without burning it.

This is especially interesting for the linerboard sample in which the damage threshold and the collected power are very low, resulting in a poor signal to noise ratio. The incoming polarization on the paper was linear horizontal as opposed to circular as in previous interferometers. It was found that the rough surface of paper was depolarizing the back-scattered light. Therefore, a quarter wave plate before the focusing lens was not necessary since the polarizing cube beamsplitter selected only the vertically polarized speckles before sending them to the crystal as a signal beam. Figure 2.6.69 shows a picture of Version 1.6.

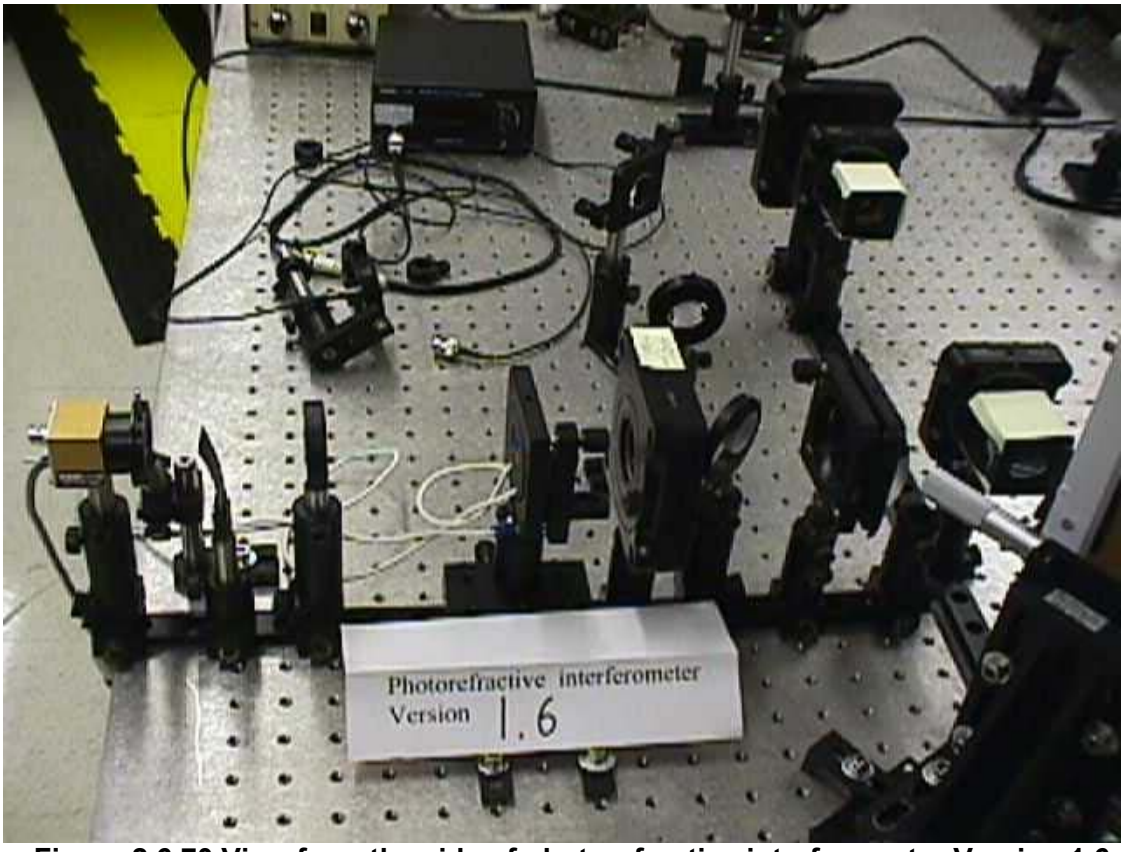

Figure 2.6.70 View from the side of photorefractive interferometer Version 1.6. PRC is the object with the white wires attached to it in the center. The photodiode is to the left, and the sample is bottom right.

As the same cylindrical lens is used to focus and collect the beam, the spot collected by the lens is a line. This line needs to be refocused to a circle by another cylindrical lens (Figure 2.6.70) onto the surface of the photorefractive BSO crystal. This enhances the interference with the reference beam.

Since the phase information (thus the ultrasonic displacements) is written by the photorefractive effect on the signal beam after it passes through the crystal, the signal beam can go directly to the photodiode without a polarizer filtering out the reference beam. Therefore, the polarizing cube beamsplitter after the crystal was removed from this setup in comparison to the PRI Version 1.5.

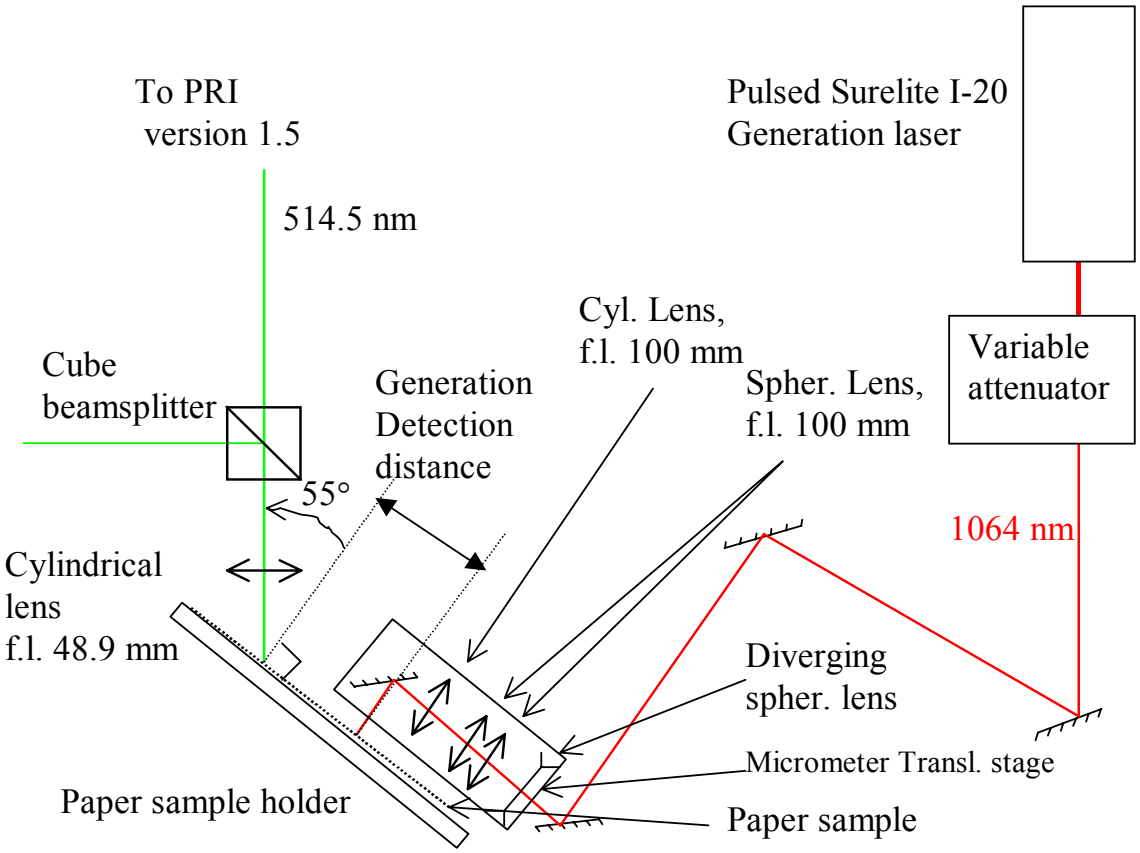

Figure 2.6.72 Schematic of the improved detection and generation systems with PRI Version 1.6.

The generation optics were also changed to generate ultrasound with a line. The advantage is that the attenuation of the amplitude occurs only due to the viscoelastic behavior of paper not due to geometrical circular spreading. This is important for the measurements taken at relatively long generation/detection distances (> 20 mm). Also, another advantage is that it is possible to generate roughly the same amplitude of displacements by putting slightly more energy per pulse without burning the sample, because the laser spot is spread out over a much larger surface (a line instead of a point).

2.6.3.4.5 Results of the improved setup

2.6.3.4.5.1 Results on 42-lb Linerboard

Further measurements were obtained for laser generated waves travelling along the cross direction (CD) of the sample. They are presented as a function of distance between the generation and the detection points. The dispersive nature of the A_0 wave is clearly visible. Because of the saturation of the photodiode by the generation laser pulse, the S_0 wave is disguised in the initial noise.

All data presented in Figure 2.6.75 are single shot measurements. Even at relatively long distance between the generation and the detection points (d = 40 mm), the A_0 waveform remains visible on 42-lb linerboard.

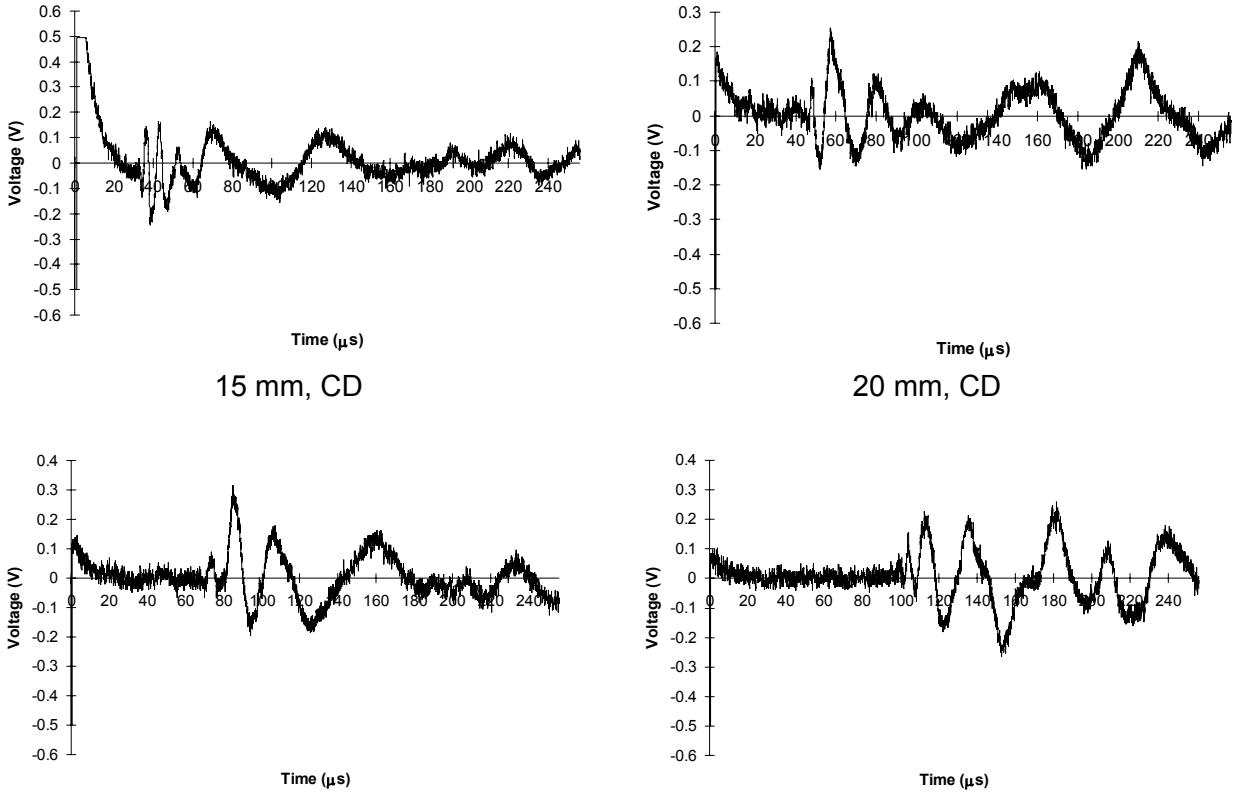

Figure 2.6.75 Laser generated ultrasound on 42lb linerboard , using improved setup. All graphs are single shot measurements.

2.6.3.4.5.2 Results on Copy Paper

Measurements were obtained for laser generated waves travelling along the cross direction (CD) and machine direction (MD) on copy paper. Again, some examples are presented as a function of distance between the generation and the detection points.

All the data presented in Figure 2.6.76 are single shot measurements along CD. The S_0 waveforms are visible but have small amplitudes compared to the A_0 waveforms. The dispersive nature of the A_0 wave is evident.

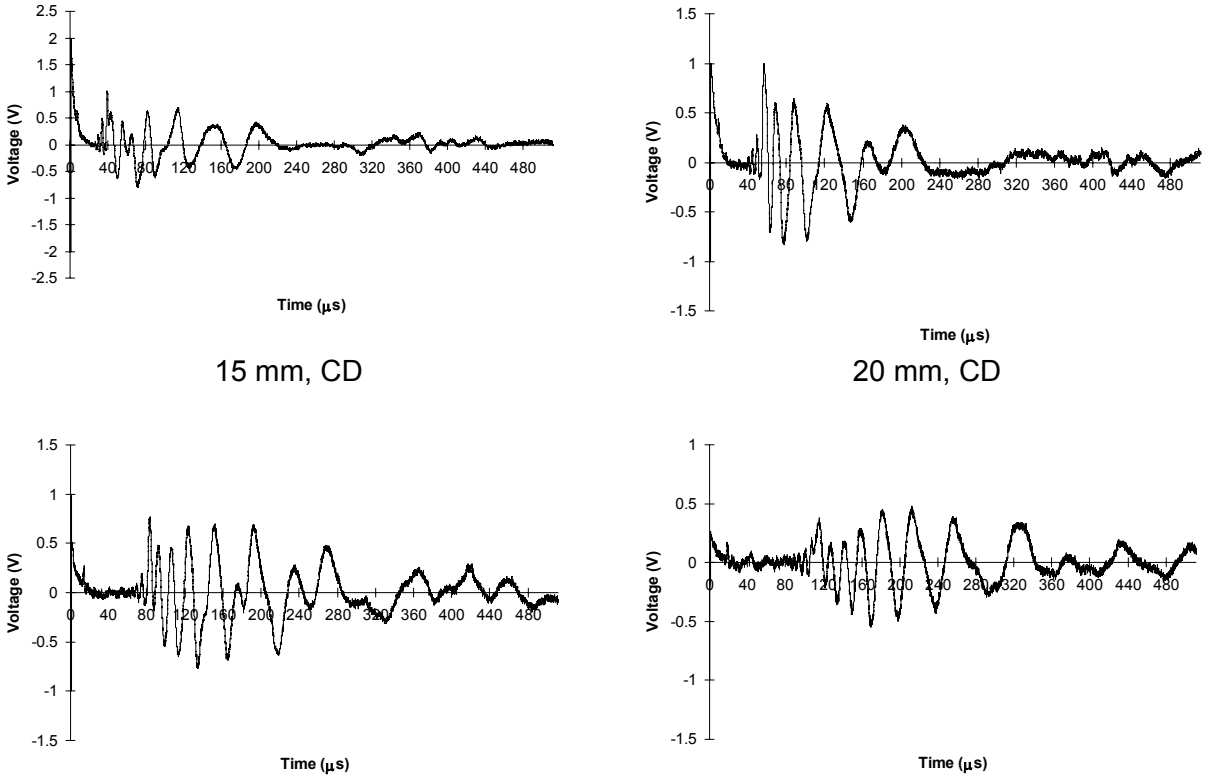

Figure 2.6.76 Laser generated ultrasound on copy paper, along CD, using improved setup. All measurements are single shot.

In Figure 2.6.76, the generation pulse had the same energy level of 40.2 mJ. The S_0 waveform is more clearly visible at longer generation-detection distances because the saturation of the photodiode by the generation pulse is not as strong. There is less 1064 nm parasitic light collected by the detection optics when the two spots are further apart and the arrival time of the S_0 wave is starting to come out of the saturation zone of the first 10 μs.

Figure 2.6.77 shows the results on copy paper along MD. The waveforms traveling along machine direction are very similar in shape to those obtained along cross direction. The time of flight is of course different because the elastic constants are different between machine direction and cross direction. Indeed, the arrival of both S_0 and A_0 waves in machine direction is earlier than in CD.

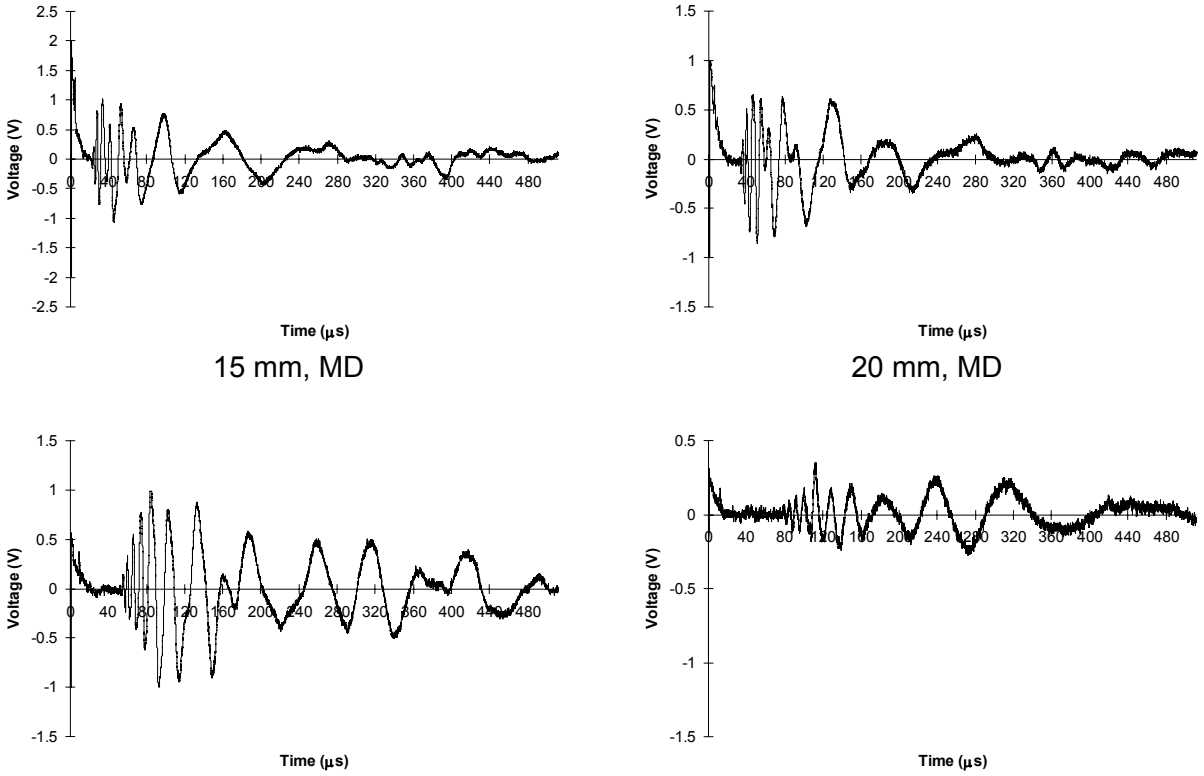

Figure 2.6.77 Single shot laser generated ultrasound on copy paper, along MD, using improved setup.

2.6.3.5 GaAs Photorefractive Setup

At the beginning of Phase II, generation and detection of ultrasound will be investigated on paper using a new photorefractive interferometer which will be developed in-house at IPST. The new interferometer will use a two-wave mixing technique with a GaAs crystal, which is known to be photorefractive in the infrared range. A continuous 600 mW Nd:YAG laser (1064 nm wavelength) will be used as a detection laser. AC or DC electric fields will be applied to the sides of the crystal to increase gain.

There are a number of reasons to investigate this type of interferometer. First, from a wavelength point of view, paper tends to have a larger reflectivity at 1064 nm than at 532 or 514 nm, as described in Sections 2.2 and 2.6.8. Second, it is interesting to implement fiber optics on the interferometer because of easy beam control. Fiber optics in the near infrared are readily available on the market and inexpensive compared to those in the visible since the fiber-optic telecommunication industry uses near-infrared diodes and this has led to a significant product development in this area. Third, under laboratory conditions, the sensitivity to displacements of two-wave mixing using crystals with an applied electric field is better than the one obtained with the photo-EMF effect. This is probably true on static or slow moving paper but remains to be shown at higher speeds

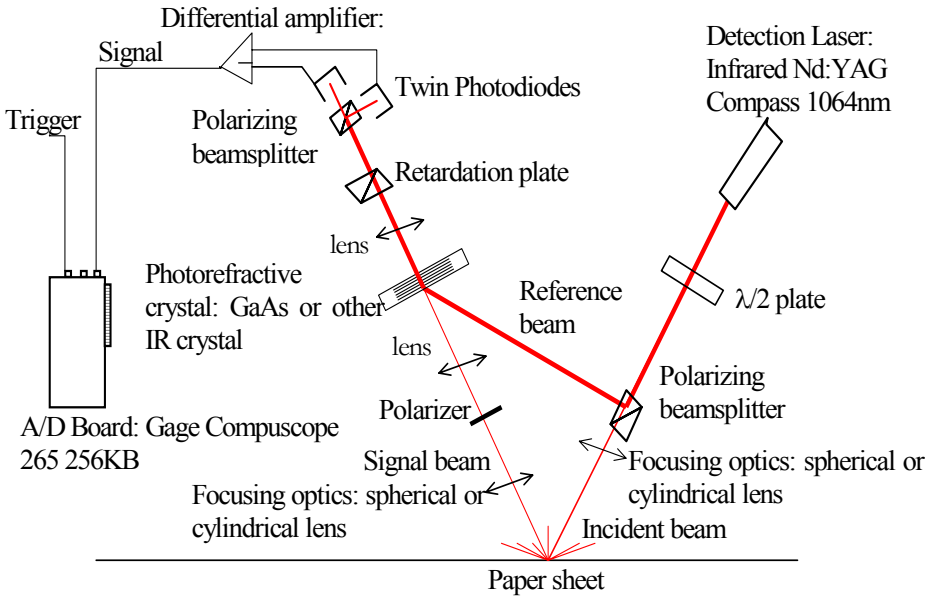

Figure 2.6.78 "V" setup for single-point Photorefractive Interferometer.

The experimental setup that we plan to use is shown schematically in Figure 2.6.78. Two photodiodes, a second polarizing beam splitter and a retardation plate are intended for quadrature detection. Since there is no optical activity (rotation of the plane of polarization with distance) in GaAs, a quadratic detection system will be more sensitive to displacements with this crystal than with a single photodiode.

2.6.4 Frequency Domain Photorefractive Imaging Interferometer Measurements

2.6.4.1 Imaging vs. Point Measurement

The paper industry has for several years utilized ultrasonic testing to evaluate the orientation and mechanical properties of paper off-line. The usual method involves measurement of sound speed between two contacting points on the paper and at numerous angles, providing data for one angular direction at a time. This information can be compiled to portray the mechanical properties in all directions.

In contrast, the INL has developed new technology that provides an image of the ultrasonic motion in the paper simultaneously in all directions over a significant area of paper. The data are optically (as opposed to computationally) processed so as to present a video image of the paper with the ultrasonic wavefronts superimposed on the image. The shape and distribution of the acoustic wavefronts provide information about sound speed and material properties in all directions along the paper simultaneously. Thus displaying in a single image such properties as anisotropy, orientation and local inhomogeneities. At the present time, the response time of the system is inadequate for on-line use in paper manufacturing, but several new developments are expected to greatly improve the response time of the system and the system's immunity to general vibration noise. During the first program year, this task has

applied this new technology to the measurement of non-moving paper elastic properties and demonstrated its imaging qualitative and quantitative capabilities.

2.6.4.2 INL Imaging Ultrasonic Camera

The INL has developed an imaging ultrasonic camera (referred to as the "INL camera" in the following discussion, patent pending)[i,ii,iii,iv,v]. The INL camera utilizes optical nonlinear processes in photorefractive materials (PRM) to record optical interferometric information about the state of vibration of the paper, and to extract from this information about the out-of-plane displacements due to vibrations of a surface. This is done in an imaging mode at high rates, so real time video images of the distribution of acoustic waves on the surface can be recorded. Unlike other types of interferometers, where the two interfering waves mix at the detector, this step occurs, in the INL camera, in the PRM where one can take advantage of the properties of photorefractivity to perform preprocessing of the data. This approach configures a type of optical analog computer to demodulate and present the ultrasonic motion in the paper.

In operation, the paper is illuminated with a laser beam that has been diverged to cover the area of interest. As the acoustic wave moves through the paper, it causes any given point on the surface to be displaced vertically by a small amount (typically on the order of nanometers or less). This displacement causes the phase of the reflected laser beam to be altered by an equivalent amount. It is this change in phase that is detected by the INL camera. The reflected light, usually called the object beam, is collected and focussed by a lens into the PRM, where it mixes with a second, mutually coherent reference beam, and interferes to create a recorded hologram of the object. The camera operates in what is usually called the non-linear two wave mixing mode (it can also operate in the alternative four wave mode), in which the reference beam reconstructs the hologram. If this were the end of the story, we would simply be slightly amplifying the object beam by adding to it the reconstructed object beam from the hologram. This is the well known non-linear amplification effect. However, in the INL camera, the reference beam has been phase modulated at a rate very close to but different from the frequency of the acoustic wave in the paper. The physical effect of this is to cause the holographic interference pattern in the PRM to move at a speed related to the frequency difference between the object and reference wave modulation rates. Since the PRM has an intrinsic response time, and holograms are both written and erased at approximately this rate, the offset frequency must be chosen so that the details of the hologram do not move so rapidly that the PRM cannot record the change. This whole process is sometimes called dynamic photorefractive holography.

The final effect is that paper vibrations at the chosen frequency contribute to the strength of the hologram and to the reconstructed wave, while others do not. Thus, the intensity (brightness) of the reconstructed holographic image of the paper is everywhere related to the amplitude of vibration of the corresponding point on the paper at the chosen frequency. This means that a video camera (or even the human eye) viewing the paper through the PRM will see a large fixed background image and a superimposed weak image that varies in intensity as the paper vibrates. These are sometimes referred to as the DC and AC components of the optical signal, respectively, in analogy to electrical signals. The frequency of the AC component is not at the original ultrasonic frequency but has been demodulated by mixing with the reference beam which has been independently modulated at a slightly different frequency. To have useful data, the DC and AC components must be separated. This is done in two wave mixing in a bismuth silicon oxide (BSO) PRM by taking advantage of the optical activity of BSO

which causes the DC and AC components to have differing polarizations. Several other methods to further improve the quality of the data are under development.

Since the hologram can't be refreshed faster than the response time of the PRM, any changes in the object wave whose frequency is significantly faster than this will not be recorded, while changes slower than the response time will be automatically compensated for. This provides one of the main advantages of the INL camera: the potential for immunity to large but slow (by ultrasonic standards) vibrations caused by other equipment or activity in the environment. Investigation is underway to incorporate this environmental adaptation capability into the camera operation.

When thin sheet materials are ultrasonically excited, there are potentially several ultrasonic modes of vibration excited. In particular, symmetric (S_0) and antisymmetric (A_0) modes will usually be generated. The velocity of the S_0 mode is faster than that of the A_0, and its amplitude is usually smaller. It has been traditional with ultrasonic methods to measure the S_0 mode because it is non-dispersive, providing simple determination of the elastic properties of the paper. However, pulsed laser excitation of ultrasound generates a broadband signal highly susceptible to dispersion effects: this can broaden the signals, and reduce the accuracy of the data. In contrast with continuous excitation as used in the INL imaging approach, the A_0 mode can be utilized because it is larger and slower, and therefore easier to detect, and also dispersion is no longer a difficulty. The usual experimental setup is shown in Figure 2.6.79.

Photorefractive Imaging of Ultrasound on Stationary Paper

The IPST team has provided the INL with a number of well characterized paper samples. The properties of these samples were determined using methods established within

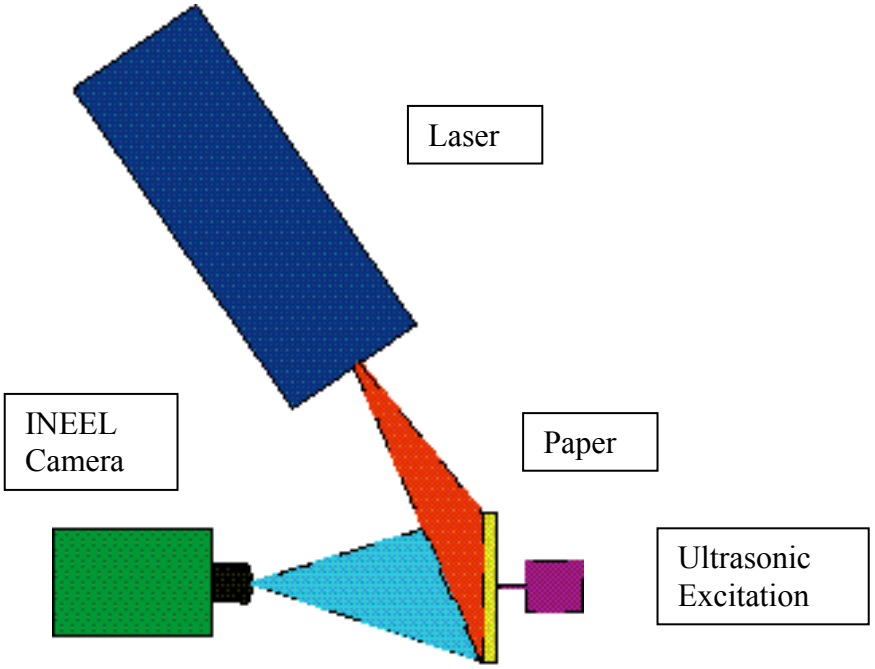

Figure 2.6.79 Schematic of the INEEL Photorefractive Ultrasonic Camera

the paper industry at the IPST. At the INL, these samples were tested using the imaging laser ultrasound system, whereby the sound speed (wavelength) in all directions of the antisymmetric (A_0) wave could be determined. The paper samples were vertically supported in an 18 cm diameter aluminum ring. Ultrasonic travelling waves were excited near the center by a point contacting piezoelectric transducer. Images of the travelling wave pattern were acquired by either an analog or digital video camera and transferred to computer disk for analysis. Analysis involved determination of the major and minor diameters of the traveling wave front and its angle relative to machine direction. Use of 2 dimensional FFT on the wavefront pattern provided an easy and useful method for analyzing the entire pattern at once. The concentric wavefront pattern of the travelling waves transforms into a single ring in the spatial frequency domain. The major and minor diameter of this ring and its orientation provide a measure of the relevant wavelength and asymmetry in the travelling wavefront.

Measurements were taken on IPST RSK59 and LNR42 samples with an analog video camera and 8 bit video digitizer. IPST provided physical properties and all but two of the anisotropic elastic constant matrix values for these paper samples. The remaining two were estimated using data for comparable materials. These values are shown in figure 2.6.80. Using these values, and appropriate plate mode theoryvi, the speed of the A_0 and S_0 modes as a function of frequency was computed for both machine and cross direction (MD and CD). The results for a 112 μm thick RSK59 paper sample in both the MD & CD is shown in Figure 2.6.81. Note the predicted dispersion of the A_0 mode due to frequency dependent sound speed. For the INL method, this is unimportant, since we operate at a single frequency. The imaging method is thus able to take advantage of the larger amplitude and lower sound speed of the A_0 mode. Alternatively, Figures 2.6.82a and 2.6.82b show the wavelengths of the A_0 and S_0 modes for the MD and CD.

RSK59 (data from IPST)	LNR42 (data from IPST)
Density = 0.818 g/cm^2	Density = 0.742 g/cm^2
Thickness = 110 μm	Thickness = 288 μm
Cmatrix (GPa)	Cmatrix (GPa)
9.85 **1.77** 0.10 *0.00* *0.00* *0.00*	**10.3** **1.82** 0.10 *0.00* *0.00* *0.00*
1.77 **4.95** 0.15 *0.00* *0.00* *0.00*	**1.82** **3.70** 0.15 *0.00* *0.00* *0.00*
0.10 0.15 **0.14** *0.00* *0.00* *0.00*	0.10 0.15 **0.10** *0.00* *0.00* *0.00*
0.00 *0.00* *0.00* **0.20** *0.00* *0.00*	*0.00* *0.00* *0.00* **0.14** *0.00* *0.00*
0.00 *0.00* *0.00* *0.00* **0.21** *0.00*	*0.00* *0.00* *0.00* *0.00* **0.16** *0.00*
0.00 *0.00* *0.00* *0.00* *0.00* **2.53**	*0.00* *0.00* *0.00* *0.00* *0.00* **2.23**

Figure 2.6.80: Elastic constants used for calculating the plate wave modes in select papers. Data and samples provided by the IPST.

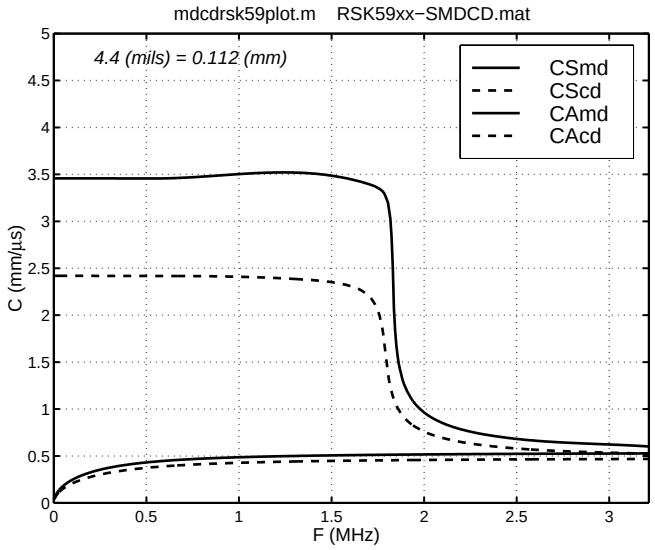

Figure 2.6.81: Calculated S_0 and A_0 mode velocities for paper sample RSK59 in the cross and machine directions.

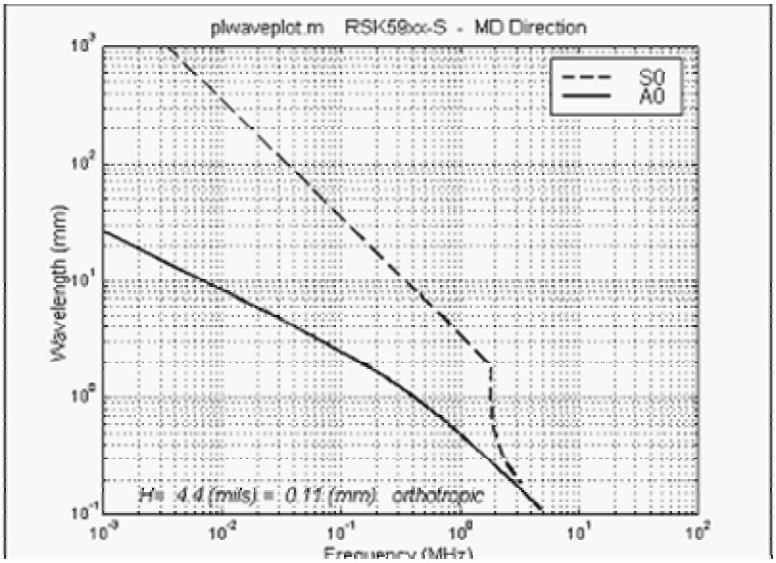

Figure 2.6.82a: Calculated S_0 and A_0 mode wavelengths for paper sample RSK59, machine direction

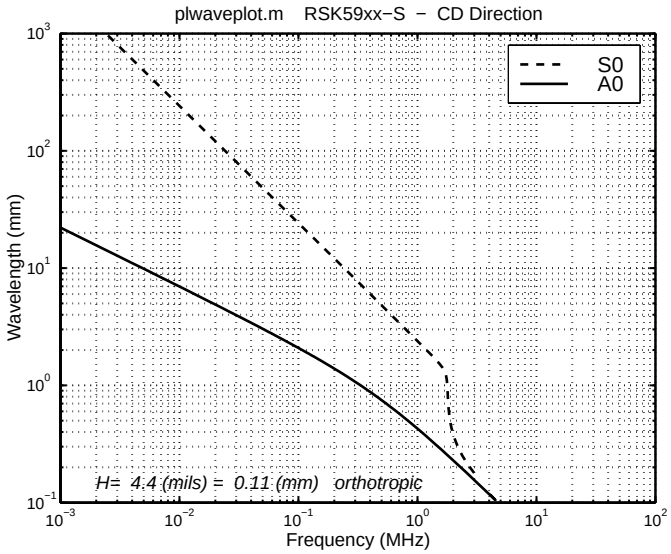

Figure 2.6.82b: Calculated S_0 and A_0 mode wavelengths for paper sample RSK59, cross direction

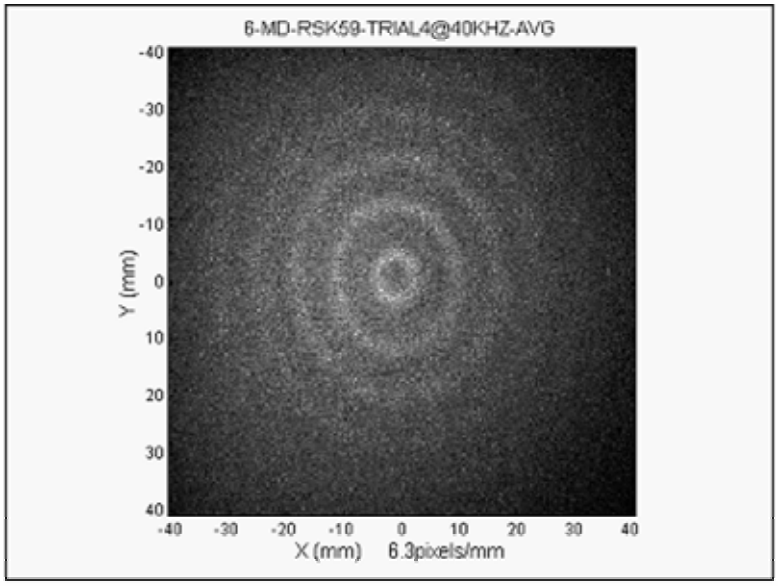

Figure 2.6.83a: INEEL Camera image of ultrasonic waves in paper sample RSK59 at 40 kHz, machine direction is vertical

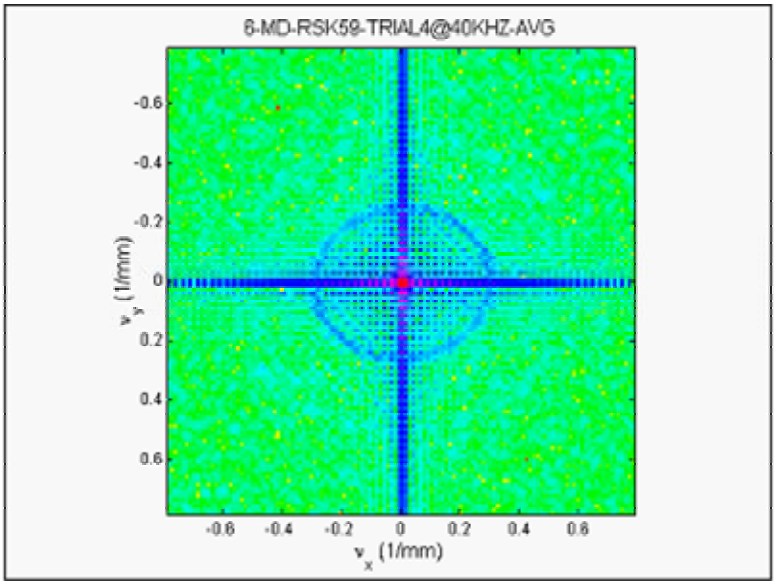

Figure 2.6.83 b: Magnitude of the Fourier transform of Figure 4a showing the MD direction to be oriented approximately +5 degrees with respect to the vertical.

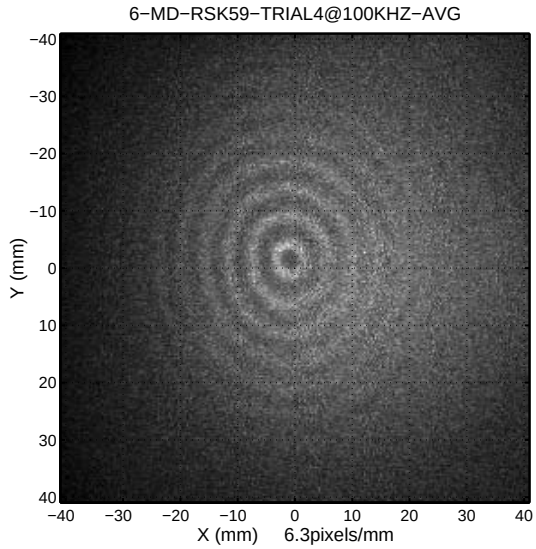

Figure 2.6.84a: INL Camera image of ultrasonic waves in paper sample RSK59 at 100 kHz

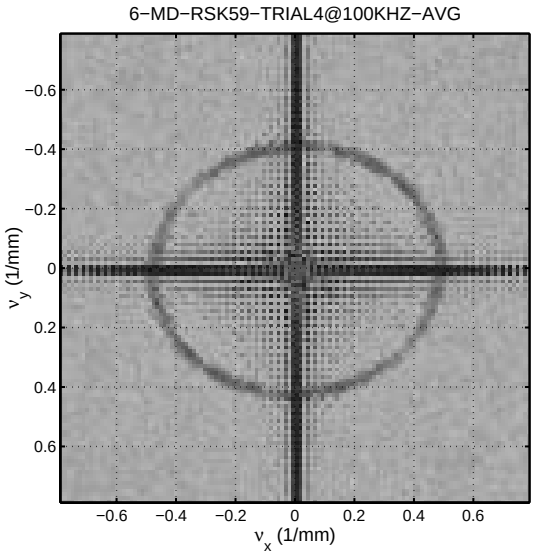

Figure 2.6.84b: Magnitude of the Fourier transform of Figure 5a showing the MD direction to be oriented approximately +5 degrees with respect to the vertical.

This FFT processing step utilizes all of the information in the image to extract wavelength data. It can be shown that the Fourier transform of a single outward traveling wave is a single ring in the transform domain that shows explicitly the wavelength anisotropy in all directions along the paper simultaneously. The somewhat elliptical form near the center of this figure shows the average wavelength in all directions, the orientation (tilt), and the MD/CD sound speed asymmetry (major and minor axis). This single figure contains all of the data normally obtained by performing multiple measurements at many angles around the paper and plotting the results in polar form.

Figures 2.6.85a and 2.6.85b show the ultrasonic A_0 mode wavelengths obtained from the FFT image data for RSK59 and LNR42 paper types respectively. Results from the calculations for these paper types using the elastic data provided independently by the IPST are shown also. Very good agreement is evident, which illustrates the quantitative capability of the imaging ultrasonic method.

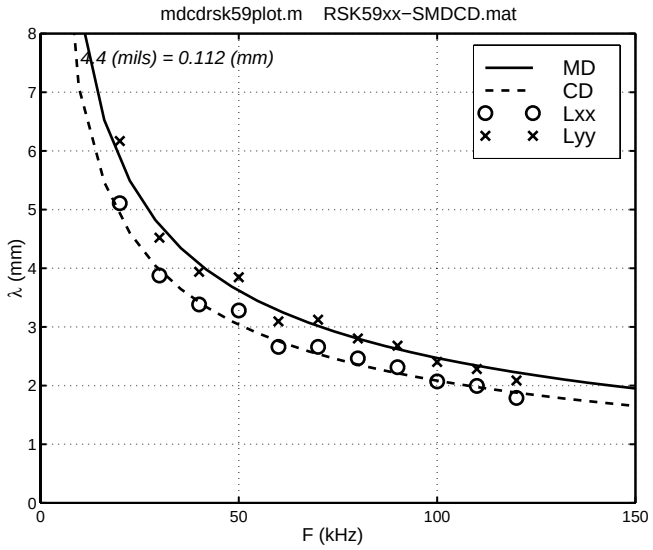

Figure 2.6.85a: Comparison of calculated and experimental wavelength data for sample RSK59 in MD and CD directions.

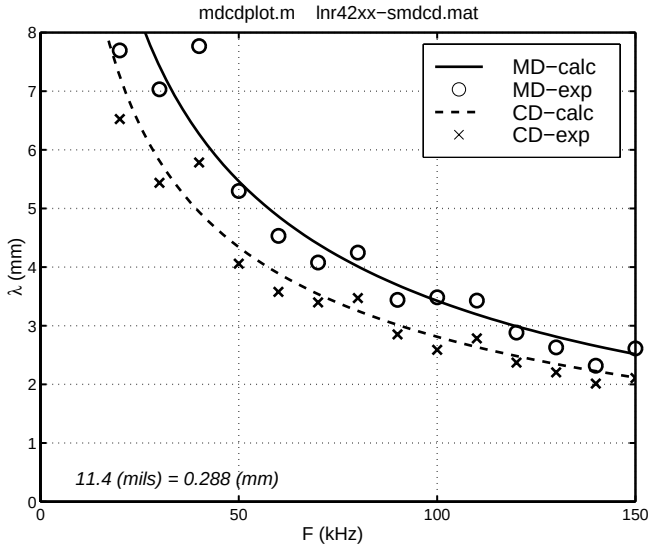

Figure 2.6.85b: Comparison of calculated and experimental wavelength data for sample LNR42 in MD and CD directions.

2.6.4.3 S_0 & A_0 MD/CD Velocity Ratio Determination

It has been traditional to use the S_0 modes for determination of certain paper properties due to the non dispersive nature of this mode. For the S_0 mode in a plate of thickness h, the wavevector is $k_{S0} = \frac{2\pi}{\lambda_{S0}}, \quad for\ k_{S0}h << 1 \quad \Rightarrow \quad h << \frac{\lambda_{S0}}{2\pi}$ the phase velocity is given by

$$C_{S0} = \frac{\omega}{k_{S0}} = f\lambda_{S0} \approx \sqrt{\left(\frac{C_{11} - C_{13}^2 / C_{33}}{\rho} \right)} \equiv C_0 \qquad \Rightarrow \qquad \left[\quad \lambda_{S0} = \frac{C_0}{f} \quad \right] \tag{1}$$

However, it can be shown that the A_0 mode can be used also. For the A_0 mode in a plate of thickness h, the wavevector is $k_{S0} = \frac{2\pi}{\lambda_{A0}}, \quad for\ k_{A0}h << 1 \quad \Rightarrow \quad h << \frac{\lambda_{A0}}{2\pi}$ the phase velocity is given by

$$C_{A0} = \frac{\omega}{k_{A0}} = f\lambda_{A0} \approx \frac{k_{A0}h}{\sqrt{3}} \sqrt{\left(\frac{C_{11} - C_{13}^2 / C_{33}}{\rho} \right)} = \frac{k_{A0}hC_0}{\sqrt{3}} = \frac{2\pi hC_0}{\lambda_{A0}\sqrt{3}} \tag{2}$$

with the consequence that the wavelength $\lambda_{A0} = \sqrt{\frac{2\pi hC_0}{f\sqrt{3}}}$ and

$$\lambda_{A0}^2 = \frac{C_0}{f}\left(\frac{2\pi h}{\sqrt{3}} \right) = \lambda_{S0}\left(\frac{2\pi h}{\sqrt{3}} \right) \qquad or \qquad C_{A0}^2 = \left(\frac{2\pi fh}{\sqrt{3}} \right) C_{S0} \tag{3}$$

Therefore, the square of the MD/CD ratio for the A_0 mode can yield the same information about $\left(\frac{C_{11} - C_{13}^2 / C_{33}}{\rho} \right)$ as the MD/CD ratio for the S_0

$$\frac{C_{S0}(MD)}{C_{S0}(CD)} = \frac{C_{A0}^2(MD)}{C_{A0}^2(CD)}, \quad for \quad h << \frac{\lambda_{A0}}{2\pi} \tag{4}$$

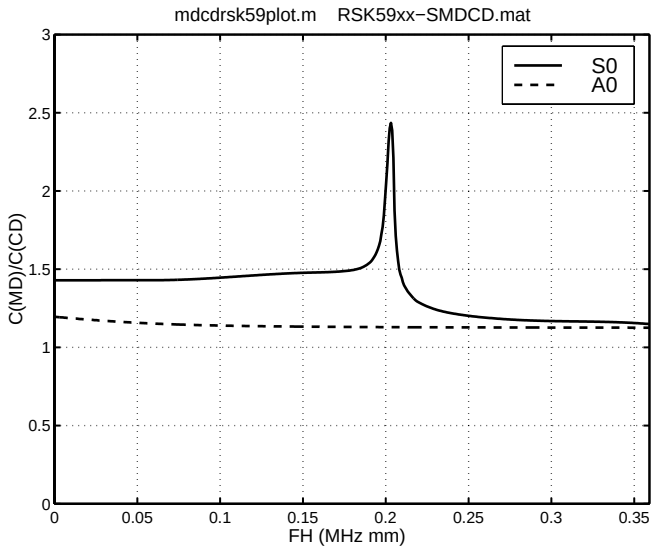

Figure 2.6.86: Calculated ratios of MD to CD velocities for A_0 and S_0 modes in sample RSK59.

Figure 2.6.86 shows the predicted S_0 mode and A_0 mode MD/CD velocity ratios as a function of frequency. The S_0 mode ratio is approximately constant at low frequencies which is why this mode is preferred for characterization of the paper stiffness. However, the A_0 mode ratio is only slightly dependent on frequency and can also be used for characterization if the frequency is well defined. Figure 2.6.87 shows the predicted and measured A_0 mode velocity ratio. Good agreement is seen for the characterization of this paper sample.

Figure 2.6.88 shows the predicted and experimentally measured values for the corresponding ratios obtained in RSK59 paper. Generally good agreement is seen for all the photorefractive imaging measurements with a deviation systematically appearing at the higher frequencies, as predicted. The calculated values show the amount of deviation between the two ratios to be expected as a function of frequency and indicate that the two ratios agree to within about 4% for frequencies up to 150 kHz.

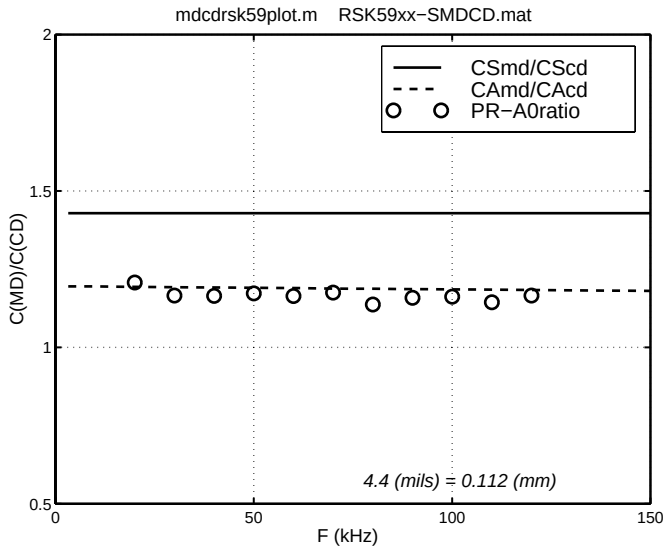

Figure 2.6.87: Comparison of calculated and experimental ratio of the MD to CD velocity of the A_0 mode at low frequency (the S_0 ratio is shown for comparison)

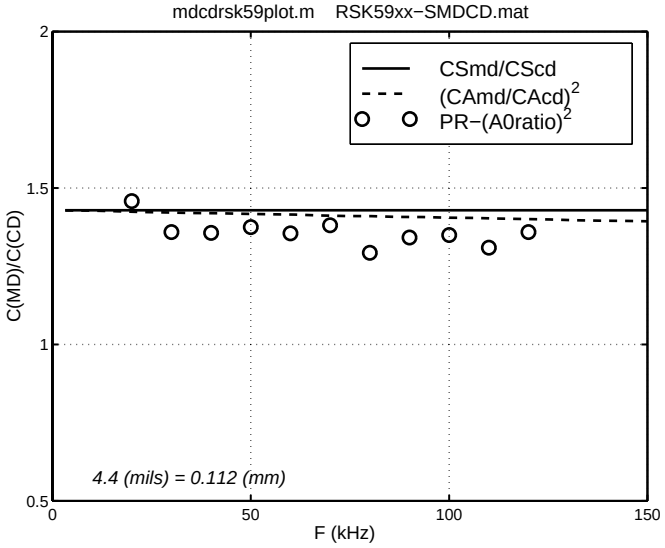

Figure 2.6.88: Calculated and experimental ratios of MD to CD velocity compared for A_0 and S_0 modes

2.6.4.4 Frequency Domain Photorefractive Imaging Interferometer Measurements (Summary)

The INL photorefractive imaging ultrasound approach offers a powerful new method for performing non-contact measurements of elastic waves in paper. The imaging approach offers an obvious improvement in measurement speed and ease over the point measurement methods. Data have been provided that show the imaging method is sensitive and quantitative, yielding the complete A_0 mode wave speed anisotropy and paper orientation in one quickly obtained image form a CCD camera. However, this technology is not yet ready for on-line implementation. Several deficiencies concerning adaptation to the moving paper web, including sensitivity, wave excitation, speed of response and adaptation to speckle noise, are yet to be resolved during future years of this research program. However, if successful, this effort will result in a unique and useful diagnostic technique for on-line process control for the paper industry.

2.6.5 Photo-induced EMF Interferometer
2.6.5.1 Experimental Setup
2.6.5.1.1 Operating principle, basics of the Photo-EMF interferometer

The photoinduced-EMF interferometer is also a photorefractive interferometer but it is quite different from the BSO photorefractive interferometer. It is designed to detect out-of-plane displacements of a surface. Under certain specific conditions, it can also detect in-plane displacements with a much smaller signal to noise ratio than for the out-of-plane configuration. In the following, the in-plane configuration is not detailed since the signal to noise ratio happened to be too poor for measurements on moving paper. Instead we will focus on the out-of-plane configuration. The core of the detection system on loan from Lasson Technologies that has been tested and improved with the IPST generation and acquisition system and IPST web simulator is the GaAs:Cr detector itself. In this system, the GaAs:Cr photorefractive crystal is used both as:

- a photoconductive beam mixer since it is a photorefractive crystal;
- a photodiode because of the current generated between the electrodes placed on its surface due to ultrasonic signals.

The amplitude of the detected signal is directly proportional to the power collected in the signal beam. So the amplitude of the signal is also proportional to the output power of the detection laser, in addition to the ultrasonic signal. The detection laser was an Ar:ion laser of which the wavelength was 514.5 nm and the maximum output power was 1.33 W.

The frequency bandwidth of the Lasson system itself was DC to 2 MHz (at -3 dB). When the current generated by the detector was too small it was amplified with a Panametrics ultrasonic preamplifier (+39.2 dB). The bandwidth of the amplifier was 13 kHz to 6 MHz (at -3 dB). The version of the Lasson detector used for the trials was not optimized for the speckles coming from paper. The bandwidth will be adapted in the future by changing the electronic filters inside the detector box (both high pass and low pass filters). Figure 2.6.89 shows the frequency response of the Panametrics preamplifier used in the setup.

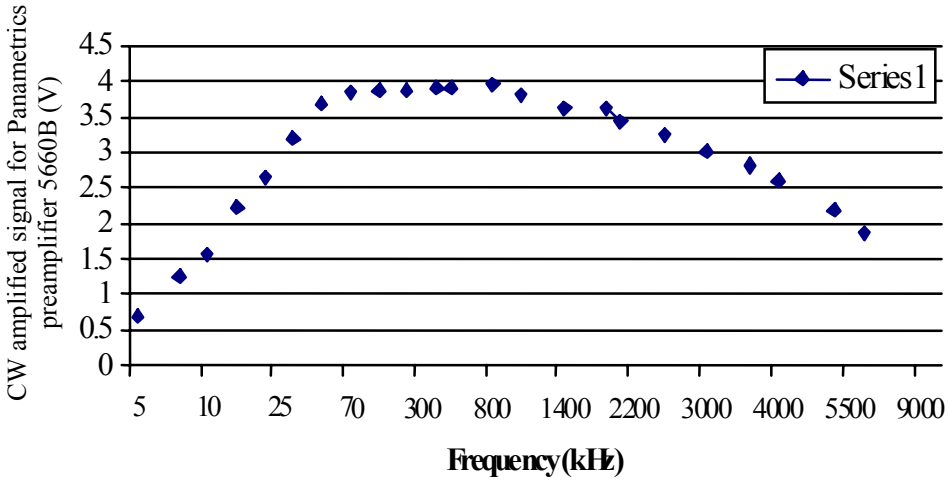

Figure 2.6.89 Frequency response of the preamplifier used for signals of small amplitude.

An improved bandwidth range would be from 20 kHz to 5 MHz. The detection system incorporating this frequency range is planned to be built and tested during Phase II.

In all experiments that were done with this interferometer, the optical system was forming an image of the spot on the paper illuminated by the detection laser onto the surface of the photorefractive crystal. The image of the spot was between the two vertical electrodes and the maximum current generated (thus the maximum signal to noise ratio) was obtained when the image covered the smallest percent of the crystal's surface (see Figure 2.6.90).

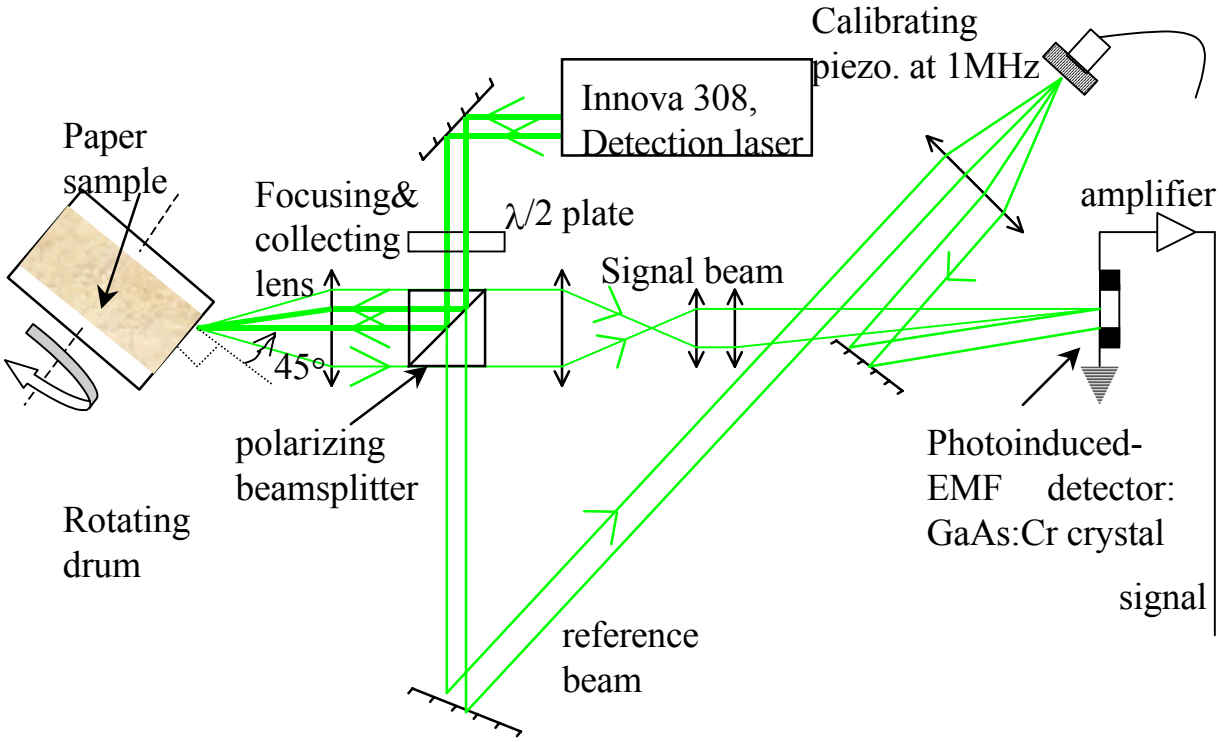

Figure 2.6.90 Photoinduced-EMF interferometer with web simulator shown at 45° incidence.

The front focusing lens for the incoming beam was used also as a collecting lens for the signal beam ("T" type measurement head) and its focal length was 100 mm. This means that when the paper surface was not in the focal plane of the focusing/collecting lens, the image on the detector was unfocused resulting in a loss of sensitivity of the interferometer. This was indeed observed at speeds over 2 m/s with the original configuration of the web simulator.

During moving paper measurements, the wobbling of the web simulator increased significantly with the rotation speed and caused the surface to shift both in the direction of the beam and perpendicularly to it for at least several mm. The original configuration of the web simulator was thus introducing some artificial fluttering whose frequencies were well above the tens of hertz encountered on a real paper web. The second configuration almost completely eliminated this artificial fluttering and the rotating drum and paper sample stayed in the same position relative to the front lens even up to 25 m/s.

The photorefractive properties of the crystal insure that the interferometer adapts to the changing speckle pattern of the paper surface. But as with any photorefractive or Fabry-Pérot interferometer, the signal decreases with the speed at which the speckle pattern changes. Thus as the web surface speed increased, the signal strength decreased.

2.6.5.1.2 Noise in the system

Fluttering caused a defocusing of the signal beam onto the GaAs:Cr detector thus resulting in a decrease of the signal (not in an increase of the noise itself in reality). The influence of fluttering can be taken care of if we use a different optical system for light collection on the signal beam.

On this setup (photoinduced-emf interferometer + web simulator + A/D board), the noise can be seen as coming from 4 different sources.

The first source is the speckle noise (or texture noise) caused by the rough surface of paper. This noise comes from the coherent nature of laser light reflected from the material's surface, interfering constructively and destructively along certain directions (speckles) in an almost random way. It is also called "pseudo signal" in the area of interferometric detection on moving parts. The higher the speed of the paper, the higher are the frequencies found in the spectrum of the pseudo signal. Above 10 m/s on paper, the highest frequencies are in the 1 MHz range. Texture noise is typically broadband.

The second source comes from the feedback of the light back-scattered by the paper surface into the cavity of the detection laser. As opposed to metallic materials, paper webs behave as depolarizing surfaces. Even with a cube beam-splitter placed just before the focusing and collecting lens, part of the light reflected off the paper comes back along the optical path into the laser cavity. Laser cavities are sensitive to speckles coming back into their amplifying medium and it results in fluctuations of the laser output power, thus in fluctuations of the amplitude of the photo-EMF signal. This noise has a spectrum that is made of narrow peaks – it is not broadband at all.

The third source is the electronic noise from the Lasson GaAs:Cr detector since the current generated by the photo-EMF effect is very small (in the nano-amp range) and has to be amplified before being converted into an output voltage. The electronic noise comes from the built-in amplifier for the detector. The electronic noise coming from the Panametrics preamplifier that is used when the signal of the detector is very small is negligible compared to other noise sources. The frequency spectrum of the electronic noise should be broadband.

The fourth (and unexpected) source of noise comes from the A/D board in the computer. By comparing the ultrasonic signals displayed on the computer (thus coming from the A/D board) and on the oscilloscope, we found that the A/D board was much more noisy that the oscilloscope. The spectrum of this noise is in the MHz range and is a problem that needs to be addressed in the future on the industrial prototype. It may come from this A/D board specifically.

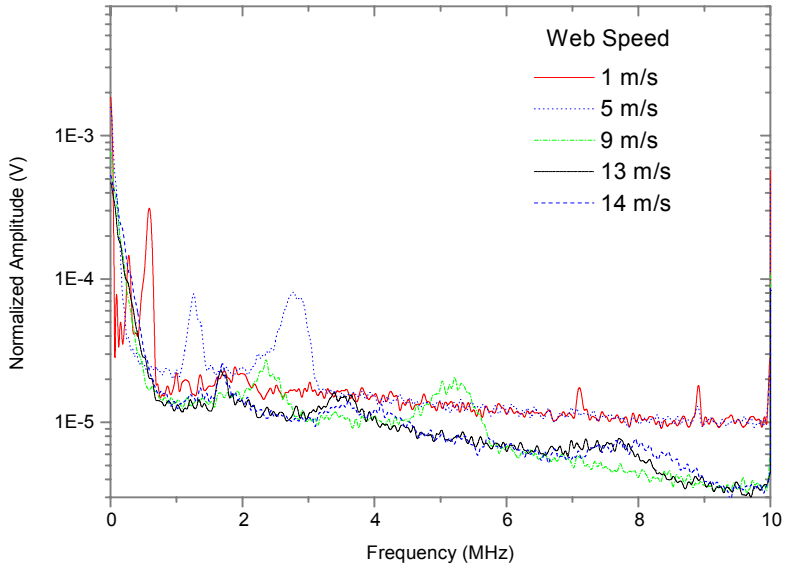

(a) Spectrum of photo-EMF detector voltage without any ultrasonic signal

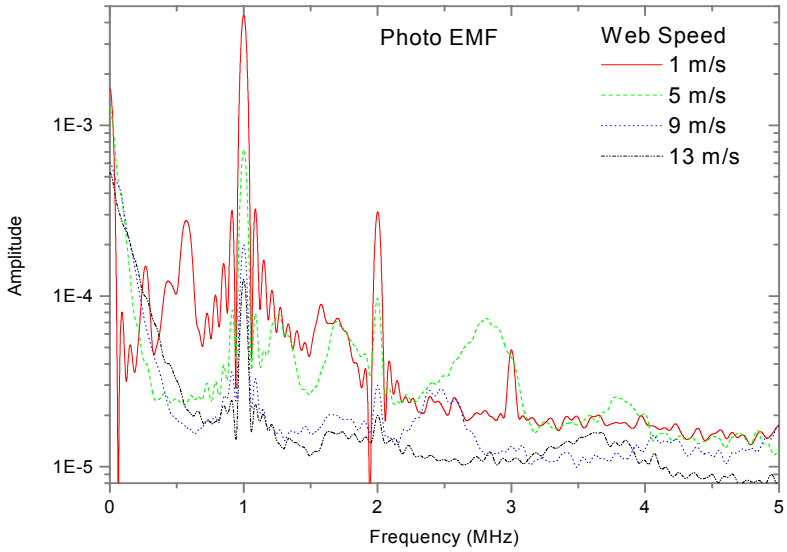

(b) Spectrum of photo-EMF detector voltage with a 1 MHz CW ultrasonic signal

Figure 2.6.91 Frequency domain noise spectra of the photoinduced–EMF on bleachboard using the Photo EMF at different web speeds.

Figure 2.6.91 shows typical noise spectra in the frequency domain obtained on a moving bleachboard using the photo-EMF detector. Figure *a* shows the amplitude and frequency of the noise without any signal present. Figure *b* was obtained with an ultrasonic signal artificially generated at 1 MHz in a CW sine wave mode using a calibrating piezoelectric transducer. Two harmonics of the 1 MHz wave can be seen in Figure *b*. It is evident from the graph that the noise peak shifts towards higher frequencies as the web speed increases from 1 m/s to 14 m/s. For each noise spectrum, there are several small peaks that exist and this indicates a number of minor sources of noise. Most likely, the big peaks at 7 and 9 MHz in the 1 m/s curve are either coming from the perturbation of the detection laser cavity by back-scattered light or from the A/D board.

The noise does not increase with the web speed. Instead the amplitude of the signal decreases thus the signal to noise ratio decreases as function of the increasing web speed, which is what is expected. This is a normal photorefractive phenomena since the faster the web goes the faster the speckle pattern changes and the less the crystal has time to adapt to the changing wavefront.

2.6.5.1.3 Configurations for the experiments

Three different configurations for detection on moving paper and one for detection on static paper were used. Static paper measurements were done first to prove the concept of a photo-EMF interferometer on paper. A circular spot was used for the generation at 1064 nm wavelength, and a circular spot for detection. On the optical head of the interferometer, a second lens was added in front of the focusing/collecting lens.

This second lens had the same diameter as the focusing/collecting lens but the resulting focal length of the two lenses was 50 mm instead of 100 mm. This increased the étendue of the interferometer but reduced the depth of focus. Thus it was in fact not really suitable for moving paper (defocusing of the image of the paper surface on the GaAs:Cr detector) and we removed it after tests on static paper were done.

After completing the proof-of-concept measurements on static paper, measurements were performed on moving paper. Because the paper was moving, the power of the detection laser was able to be increased significantly because the impinged spot was constantly moving so it could not burn the paper.

In Table 2.6.2 is presented a comparison among the different configurations we used for the trials on moving paper and figure 2.6.95 was taken of the setup used on July 9&10, 1998, with the configuration #1 of the web simulator.

Table 2.6.2 Summary of the different experimental configurations used for tests on moving paper.

Date	Generation spot and **detection incidence angle**	Paper grade investigated	Meas. along	Web simulator used for the trials
July 9 & 10, 1998	Point or 0.5 x 2 mm line, **0° (normal inc.)**	Copy paper, 42-lb linerboard Bleachboard Raw stock	CD	Configuration #1
August 13 & 14, 1998	0.5 x 11 mm line **45°**	Copy paper 42-lb linerboard Bleachboard	CD	Configuration #1
August 21, 1998	0.5 x 12 mm line **45°**	Copy paper 42-lb linerboard	CD	Configuration #2
August 24 & 25, 1998	0.5 x 14 mm line **45°**	Copy paper 42-lb linerboard Bleachboard	MD	Configuration #2

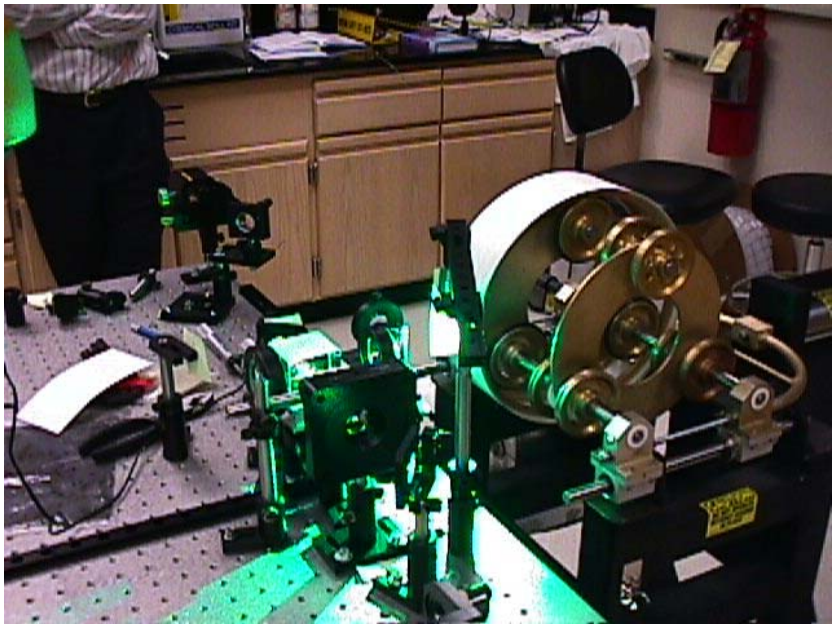

Figure 2.6.95 View of the detection system and web simulator for on-line detection of laser generated ultrasound on paper.

On August 13 & 14, 1998 it was decided to change the incidence angle for detection from 0° (normal incidence) to 45° incidence, in order to be able to detect both in-plane and out-of-plane displacements. This was done since the out-of-plane component of the S_0 wave is very small compared to the in-plane component and it had not been observed on moving paper with the 0° setup.

Another improvement consisted in using a long line for the generation spot instead of a point, in order to generate roughly the same amplitude for the ultrasonic waves but with a much smaller laser power density on paper. This change was done because the ablation damage on paper made with the circular generation spot used in the previous trials happened to be unacceptable especially on copy paper and raw stock.

One spherical diverging lens, then two spherical converging lens then one cylindrical lens were used. The paper strip was cut along the machine direction (as all paper strips used on the rotating drum) and the direction of rotation of the sheet was along machine direction like on a real paper web. The waves were traveling along cross direction (horizontal).

On the copy paper sample, signals were also recorded at 30 m/s, which is about 20% above the current production speed for copy paper (see Figure 2.6.108). This was done in order to see if the detection system was still able to detect the A_0 wave at this very high speed.

At this speed, the signal to noise ratio is very poor. Thus it is difficult to tell if the waveform that is observed is actually an A_0 wave or a shock wave traveling in the air at 30 m/s. Further analysis of the frequency content of the detected waveform should positively identify the wave.

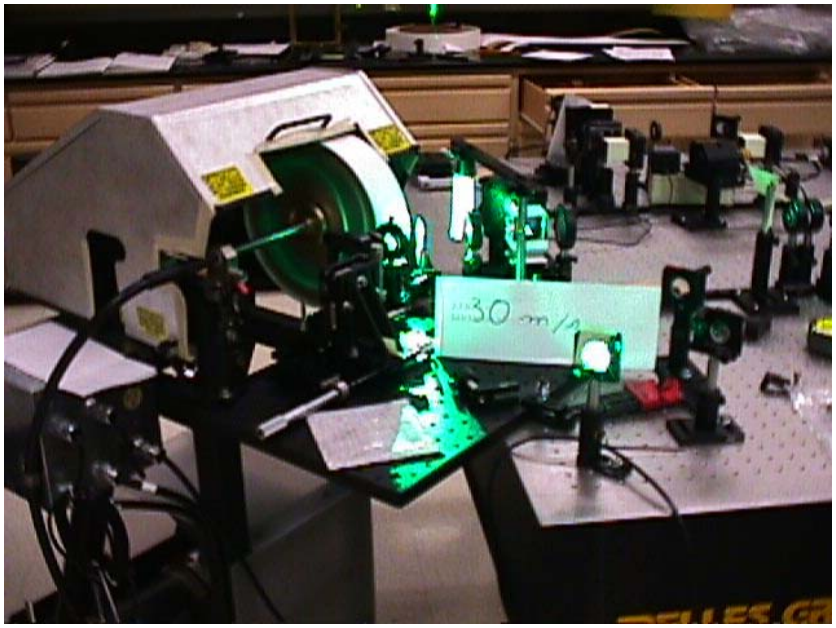

Figure 2.6.108 General view of the system running at 30 m/s on copy paper.

2.6.5.2 Results on Static Paper

The photo EMF detector was used to detect a signal generated by a source laser on static paper. Figure 2.6.110 shows typical signals recorded by the photo EMF setup at 45° incidence on a static copy paper. The top graph shows that the S_0 and A_0 mode waves are clearly detected using an out-of-plane detection configuration. On the other hand, the bottom plot shows that the signal to noise level decreases significantly using an in-plane detection configuration. The presence of the S_0 mode wave with the in-plane system is no longer obvious.

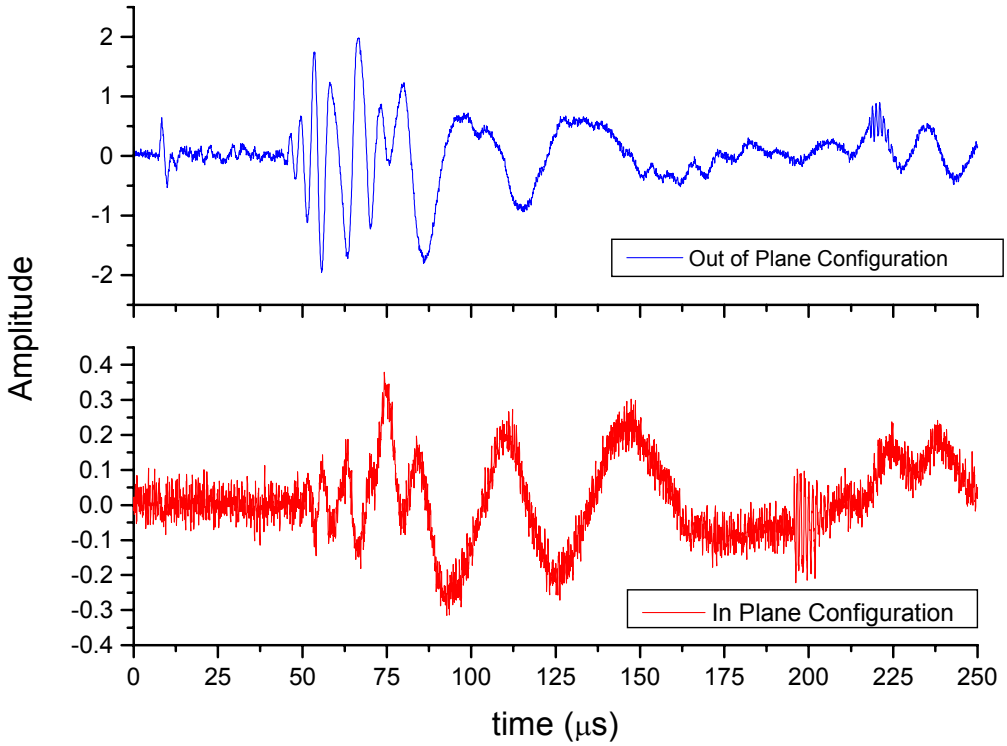

Figure 2.6.110 Photo EMF signals on static copy paper using out-of-plane (top) and in-plane (bottom) configurations: The detection laser was aimed at 45° incidence with respect to the normal to the surface.

Figure 2.6.111 shows the spectra of the signals in Figure 2.6.110 using the out-of-plane and in-plane configurations. The signal energy is mostly present in the low frequency range below 0.5 MHz. This is in agreement with the results obtained earlier by the BSO PRC setup.

Figure 2.6.112 shows ultrasonic signals on a fairly thick bleached board sample (grammage of 262 g/m^2). The S_0 mode wave is not easily detected and the A_0 mode wave tends to dampen out quickly. This behavior is in agreement with the results obtained using the BSO PRC setup earlier. The noise level is very high in the in-plane configuration.

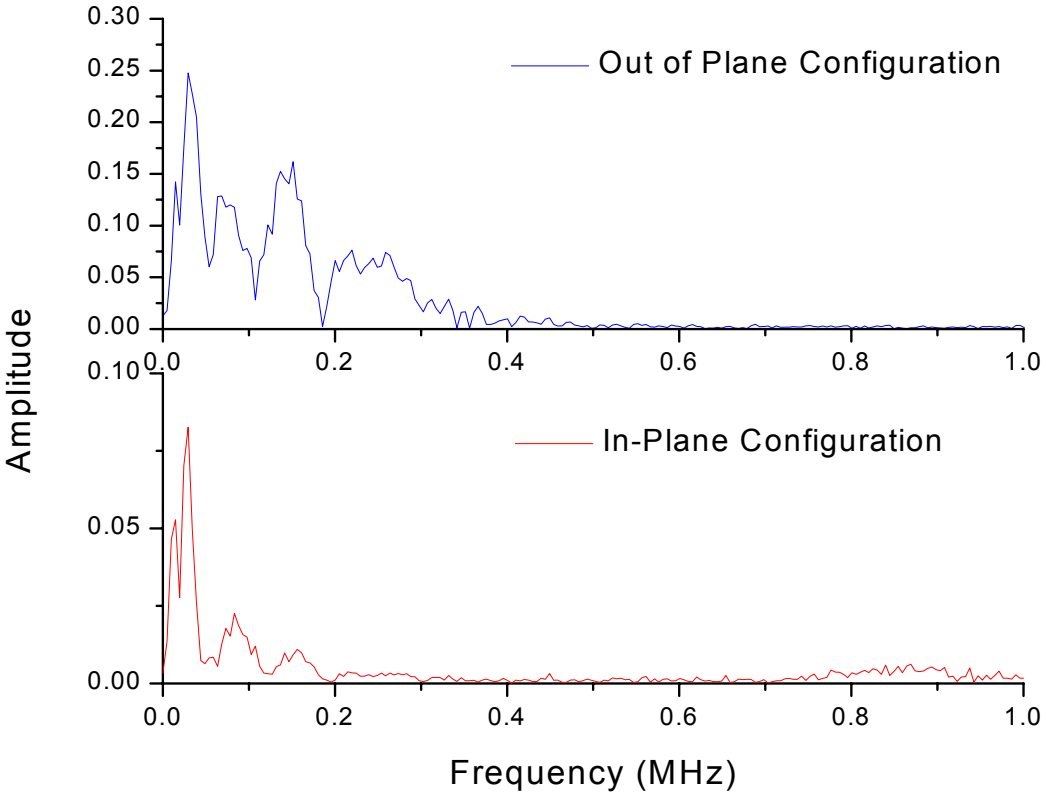

Figure 2.6.111 Frequency spectra of the signals shown in Figure 2.6.109 using the out-of-plane and in-plane configurations: The detection laser was aimed at 45° incidence with respect to normal to the surface.

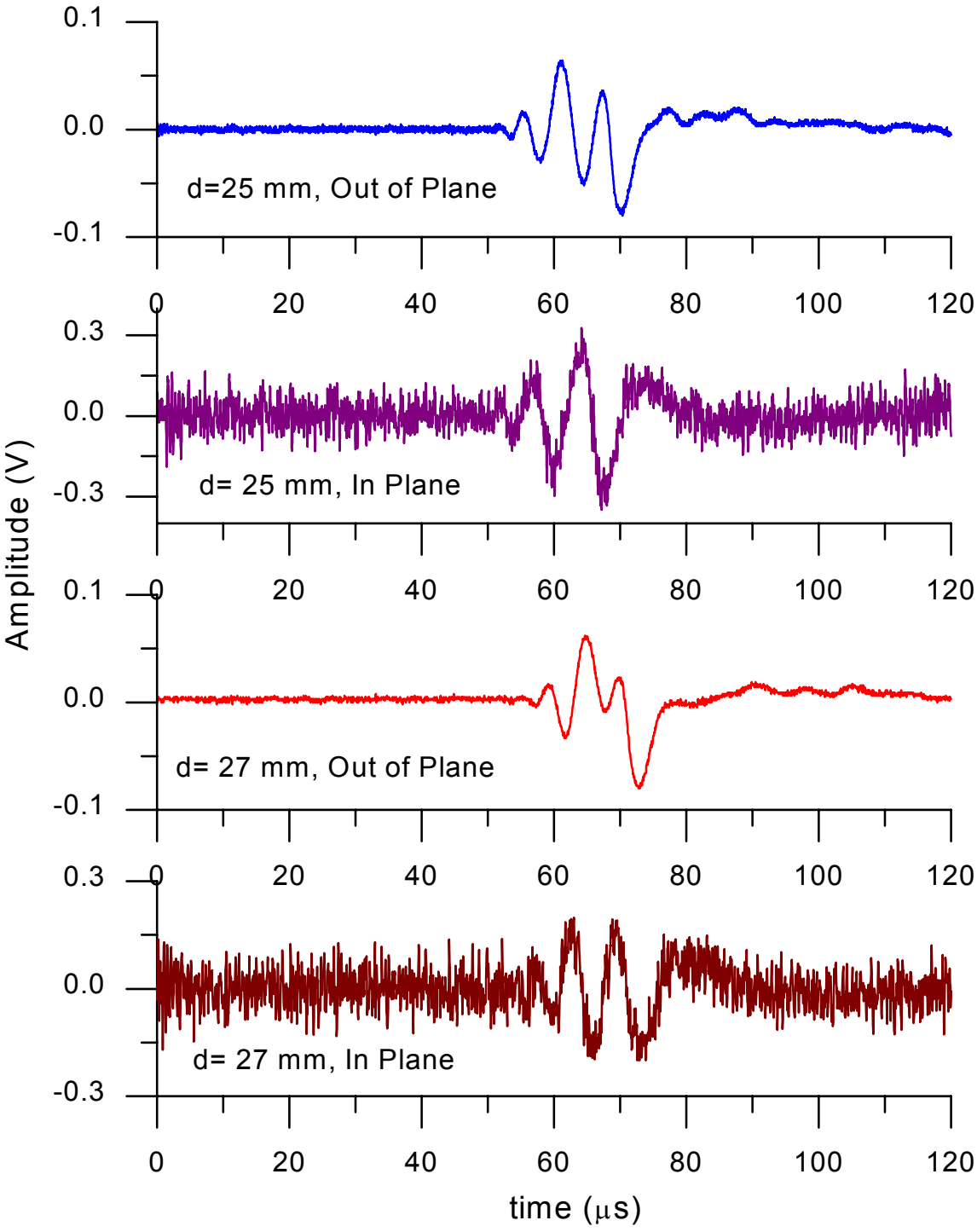

Figure 2.6.112 Signals on bleached board sample using the out-of-plane and in-plane configurations: The grammage is 262 g/m^2. A single shot was used for the signal. The S_0 mode wave is not visible and the A_0 mode wave dampens out quickly.

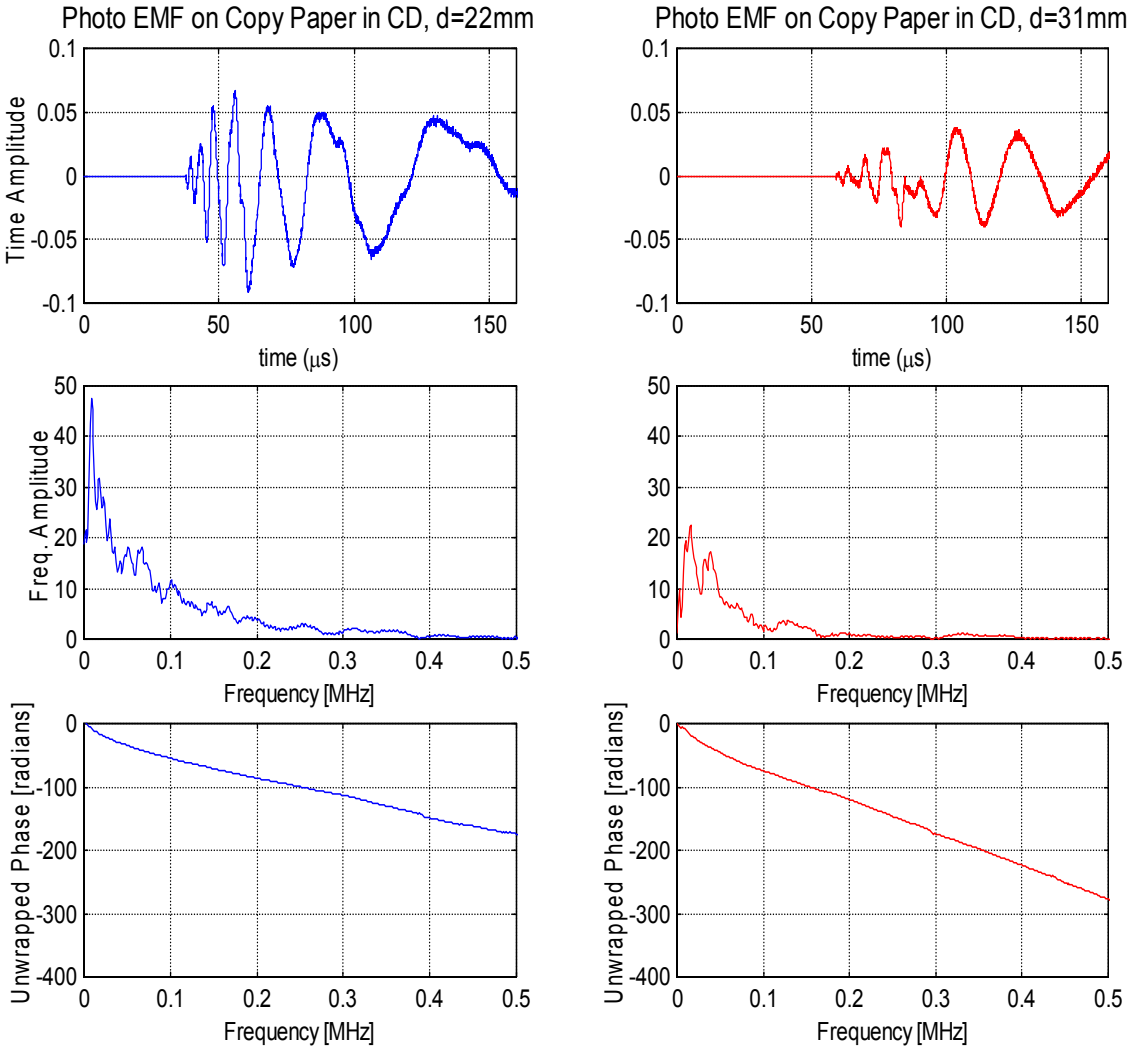

(a) d=22 mm (b) d=31 mm

Figure 2.6.113 A_0 mode analysis of the photo EMF signals on static copy paper in CD.

In Figure 2.6.113, the A_0 mode waves on static copy paper in the CD were detected at two different distances between the source and detector (d=22mm and 31mm) and were analyzed using the same technique described in Section 2.6.1.1. The FFTs of the signals are calculated and the phase angles are unwrapped. It is important to keep in mind that the phase angle information is reliable only within the frequency range where significant signal energy is present.

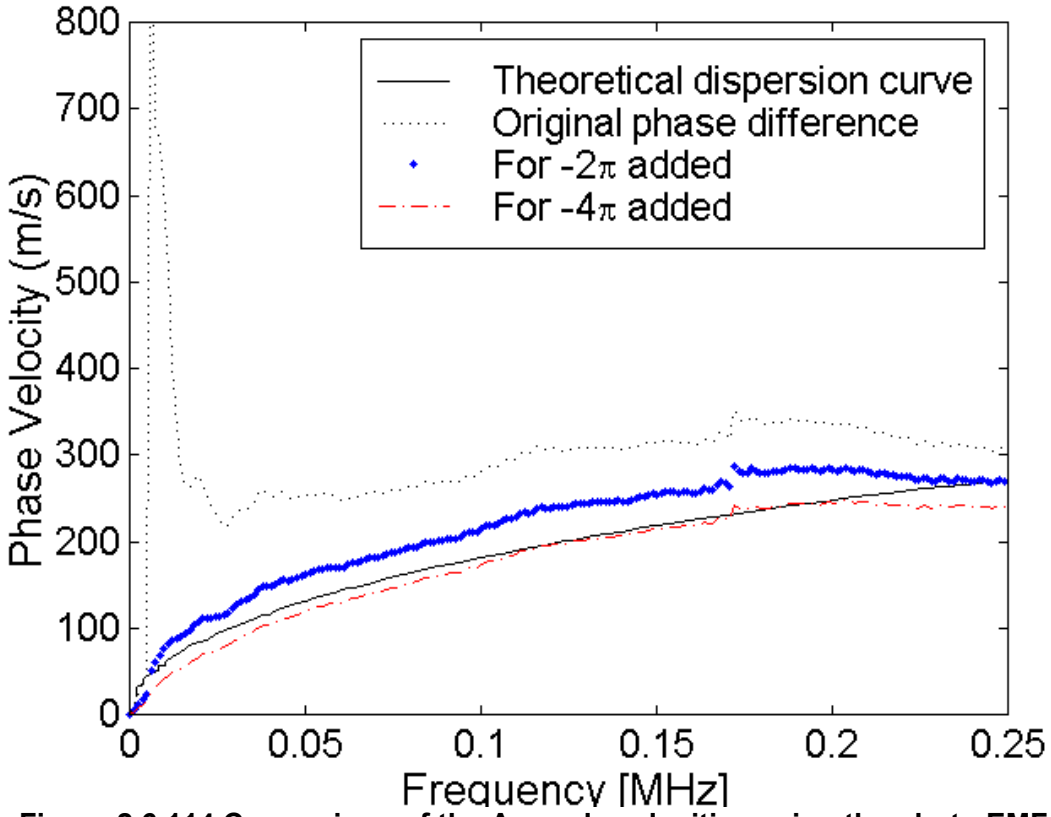

Figure 2.6.114 Comparison of the A_0 mode velocities using the photo EMF setup on static copy paper in CD.

In Figure 2.6.114, the resulting A_0 phase velocities with the corrected phase angles are plotted against the theoretical dispersion curve corresponding to the A_0 mode for static copy paper in the CD. The phase velocity with the -4π correction shows good agreement with the theoretical curve up to 0.2 MHz in frequency. This range also corresponds to the region where signal energy exists. Therefore, we can only be confident of the accuracy of the phase velocity in this region. In the frequency region over 0.2 MHz, the phase velocities deviate from the theoretical curve due to the lack of energy present. Hence, the results in this region are not reliable. Also, when the phase angle is not corrected, the result plotted in Figure 2.6.114 shows that significant error may occur at very low frequency. In order to circumvent this error, Johnson (1996) suggested using a simplified low frequency approximation for the A_0 mode. Nevertheless, this method is not feasible in the current analysis since it requires the information of the S_0 mode wave, which may or may not be available.

2.6.5.3 Moving Paper Results

Figure 2.6.115 shows an assortment of typical results obtained by the photo EMF interferometer on moving bleached board in the CD at increasing speeds. The distance between the source and detection spot was maintained at 15 mm. The power of the detection laser was kept at 1.33 W and the energy level of the source laser was 25.1 mJ. The detection beam was at 45° incidence. At speeds up to 6 m/s, the shapes of the A_0 mode waveforms are clearly noticeable. As the web speed increases further, the magnitude of the A_0 signal decreases; that is, the A_0 signal becomes harder to distinguish from the noise. At 14 m/s, the A_0

signal becomes almost indistinguishable from the texture noise present. For the S_0 mode, the signal is detectable at 1 m/s, although it disappears quickly as the speed increases.

Figure 2.6.116 shows the corresponding FFT spectra of the signals shown in Figure 2.6.115. Most of the A_0 signal energy is present below 0.5 MHz. The broadband noise, as discussed in the previous noise analysis, appears to shift to higher frequency as the web speed increases up to a certain speed. That is, at 2 m/s, the broadband noise peak is approximately at 0.7 MHz. At 4 m/s, it is at 1.2 MHz. At speeds higher than 6 m/s, it exists at 1.6 MHz. Also noticeable is the sharp peak at approximately 1.75 MHz for higher web speeds. It results from the burst of energy that exists within the first 10 μs and is related to the saturation of the photodetector by the generation laser.

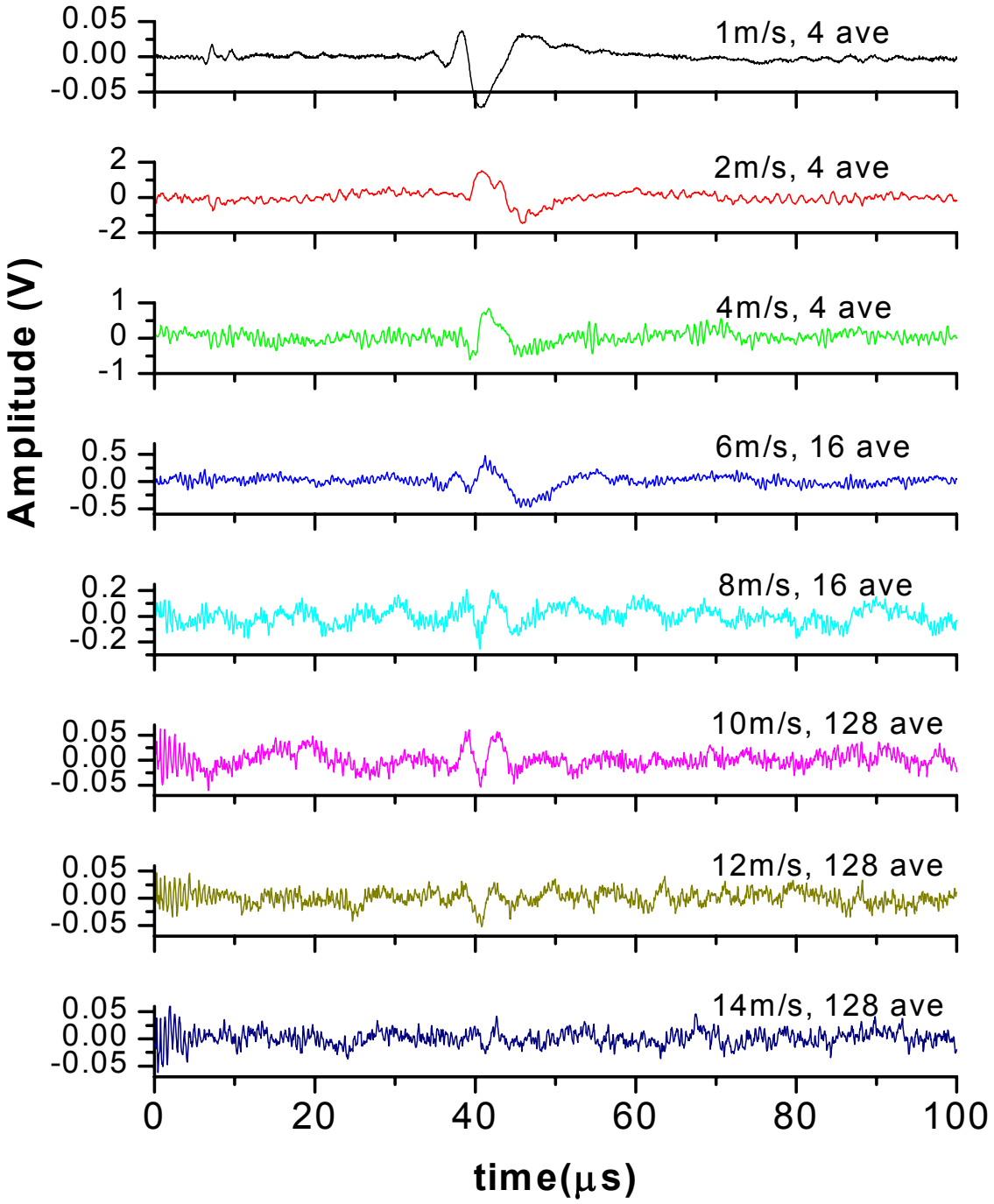

Figure 2.6.115 Comparison of the Photo EMF signals on bleachboard in CD at different web speeds: d=15mm, P=1.33W, E=25.1mJ using a line generation in ablation mode. The incidence of the detection beam is at 45° with respect to normal to the surface. The amplifier was not used for the signal at 1 m/s. Then, the signals were amplified at 39.7 dB. Data taken August 14th.

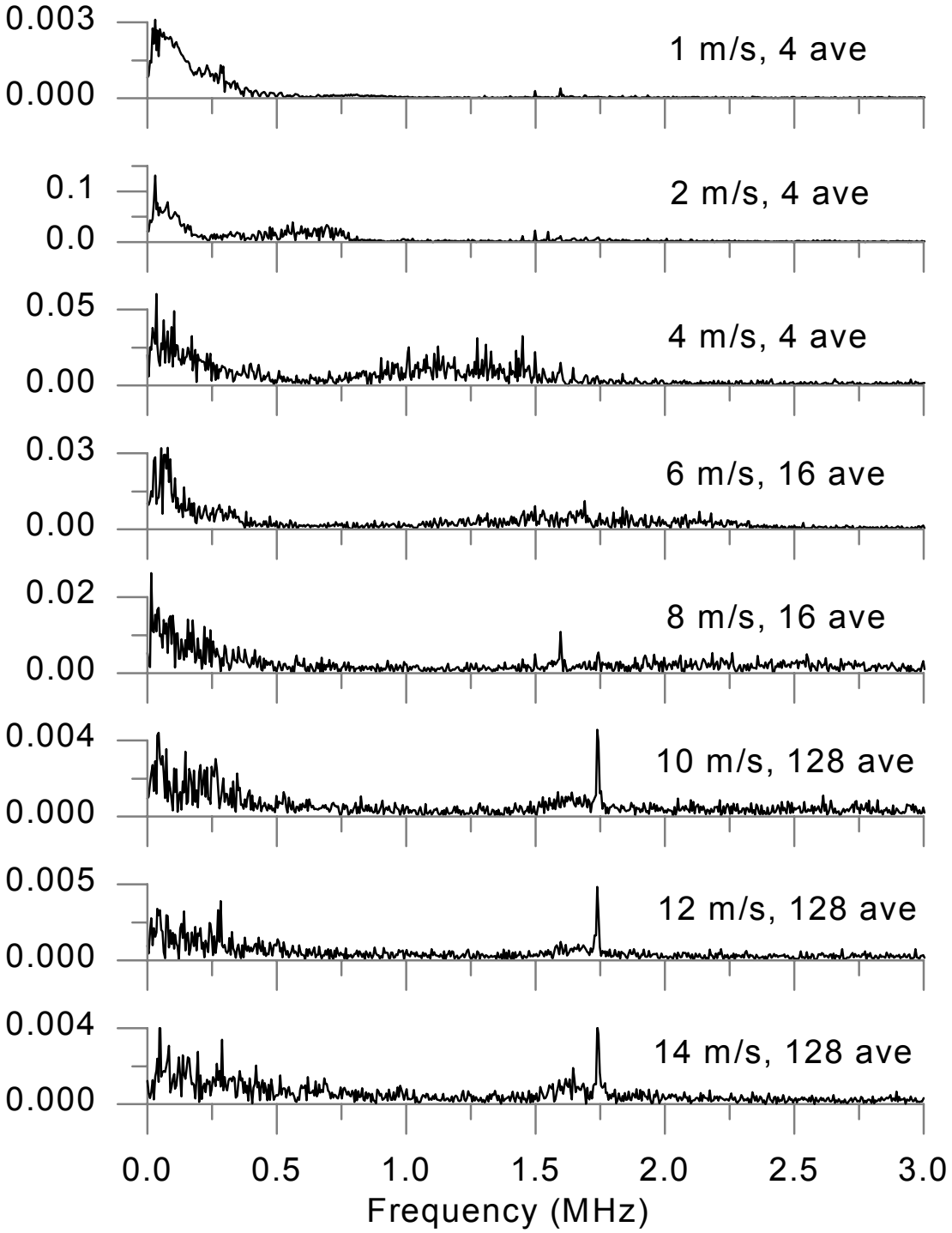

Figure 2.6.116 FFT spectra of the Photo EMF signals shown in Figure 2.6.112 on bleachboard in CD at different web speeds: d=15mm, P=1.33W, E=25.1mJ using a line generation in ablation mode. The incidence of the detection beam is at 45° with respect to normal to the surface.

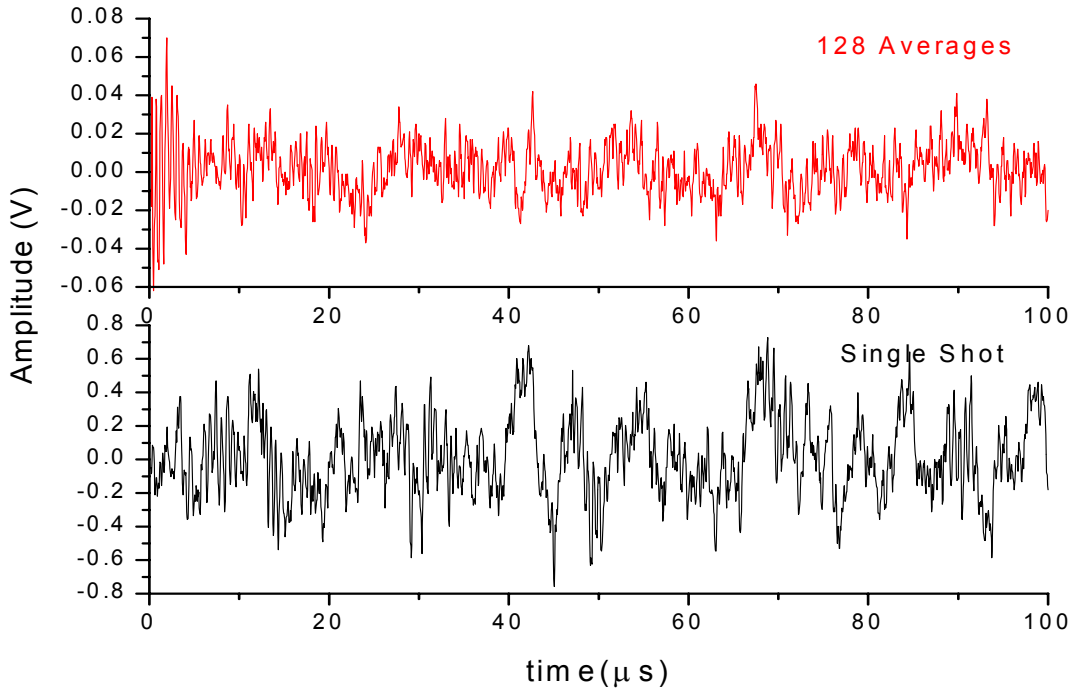

Figure 2.6.117 (a) Comparison of signals at 14 m/s using 128 averages and a single shot on bleachboard: The figure indicates that the amplitude becomes one order of magnitude smaller when signal is averaged at 128 times.

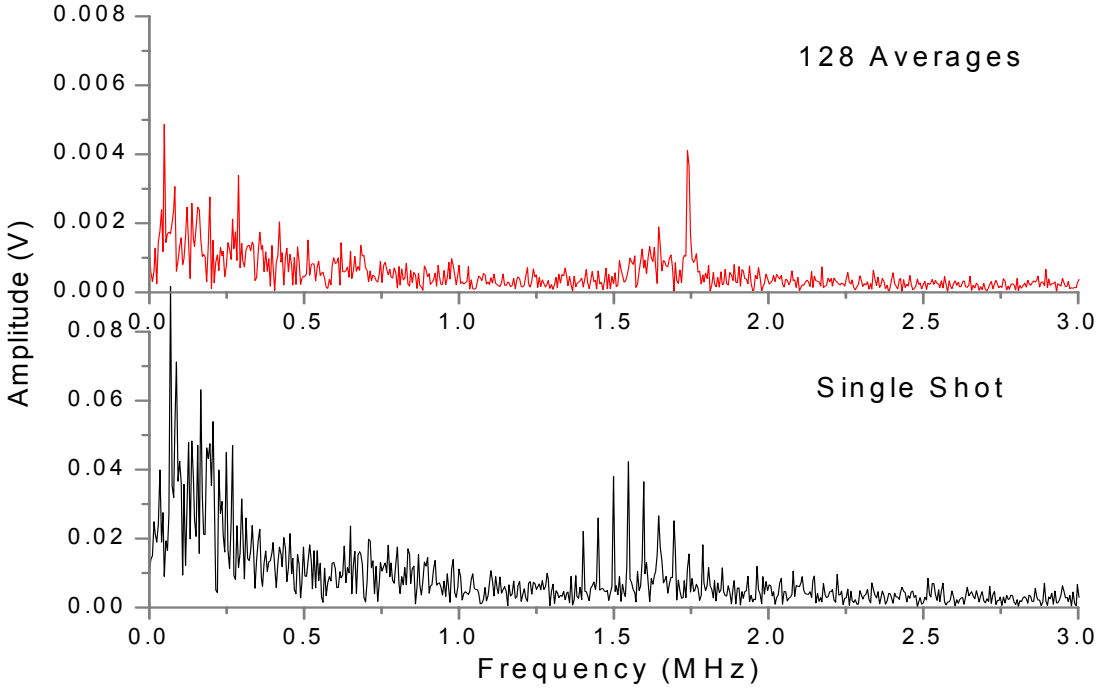

Figure 2.6.117 (b) FFT Spectra for Figure 2.6.117 (a).

The characteristics of bleached board are very different from those of copy paper. The grammage is very high at 262 g/m^2. Signals are not expected to be well formed. Nevertheless, the results at high speeds are very promising.

The plots in Figure 2.6.117a and b compare two signals obtained on bleached board at 14 m/s with the setup as of August 14th. For *a* and *b*, the top signal is averaged at 128 times while the bottom one is obtained by a single shot. The signal with the 128 times average has an amplitude magnitude that is one order smaller than that of the single shot. This is caused by extreme variability in the sample and hence variability in the signal (therefore averaging causes the signal to disappear). The A_0 in contained in the frequency range below 0.5 MHz. The frequency analysis shows that there appears to be a noise peak existing at 1.6 MHz. Most likely, the set of peaks around 1.5 MHz in the single shot data is laser noise (feedback into the laser cavity).

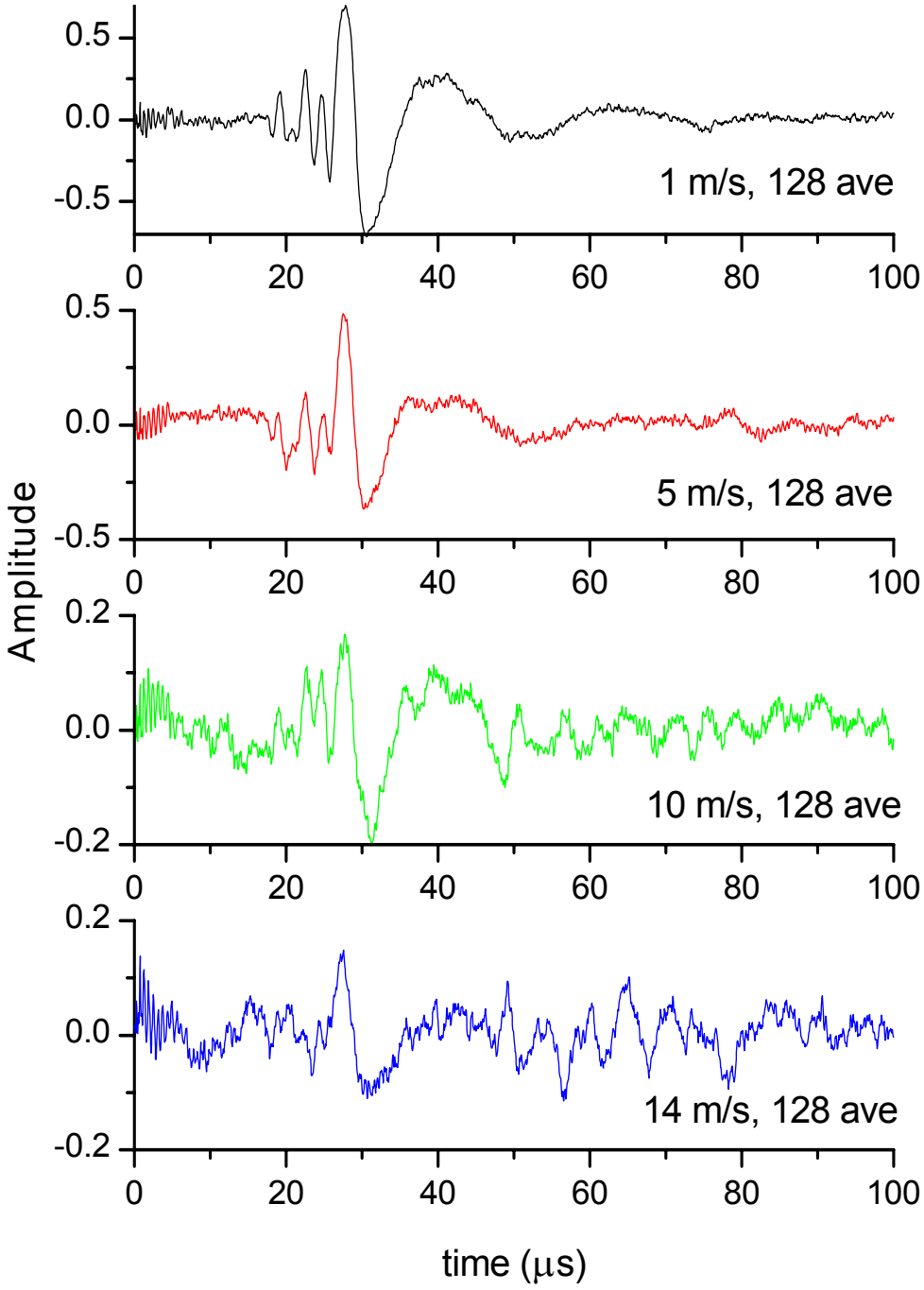

Figure 2.6.118 Change of signal amplitudes against web speeds on copy paper in CD: d=10mm, E=25.1mJ, and P=1.33W using a line generation in ablation mode. All signals are averaged 128 times. The incidence of the detection beam is at 45°. Data taken on August 14.

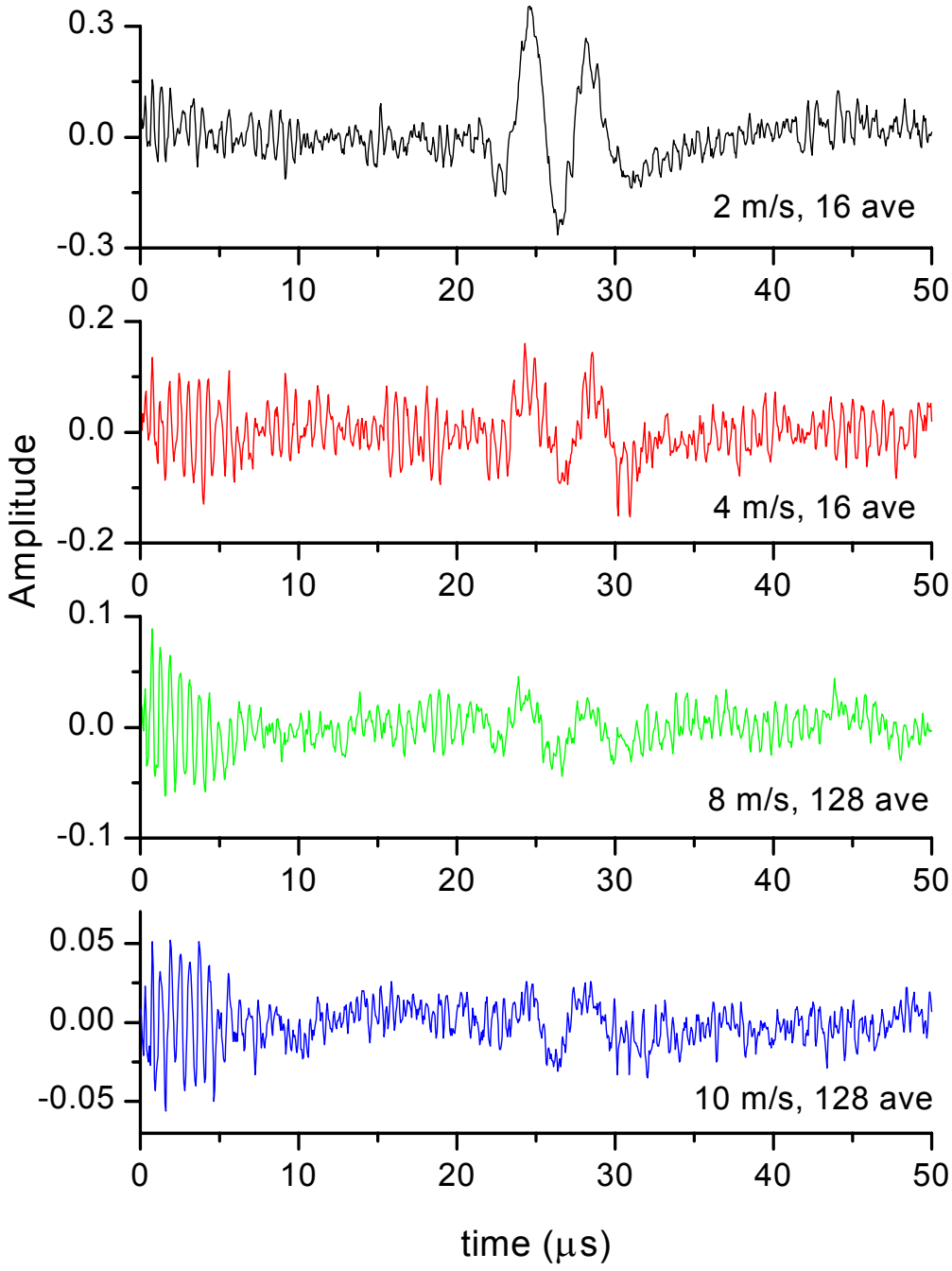

Figure 2.6.119 Change of signal amplitudes vs. web speeds on linerboard 42-lb in CD: d=10mm, E=25.1mJ, P=0.72W using a line generation in ablation mode. The incidence of the detection beam is at 45°. Data taken on August 14.

Typical waveforms obtained with copy paper and 42-lb linerboard are plotted in Figures 2.6.118 and 2.6.119, respectively. The distance *d* between the source and the detection spot was maintained at 10 mm for both figures. The energy level of the source laser was 25.1 mJ using a line generation in ablation mode. The incident angle of the detection beam was at 45° with respect to the normal to the surface. The power of the detection laser was at 1.33 W for copy paper and 0.72 W for 42-lb linerboard.

As previously described with the bleached board sample, the signal amplitude decreases as the web speed increases. The overall signals on the copy paper are fairly clean without much noise present up to 14 m/s. On the other hand, the signals on the 42-lb linerboard tend to contain more texture noise and dampen out quickly. At web speeds higher than 8 m/s, the S/N ratio becomes very low. Notice that the results shown in Figures 2.6.115, 2.6.118 and 2.6.119 so far were obtained with the web simulator in the original configuration limited to the maximum speed of 14 m/s.

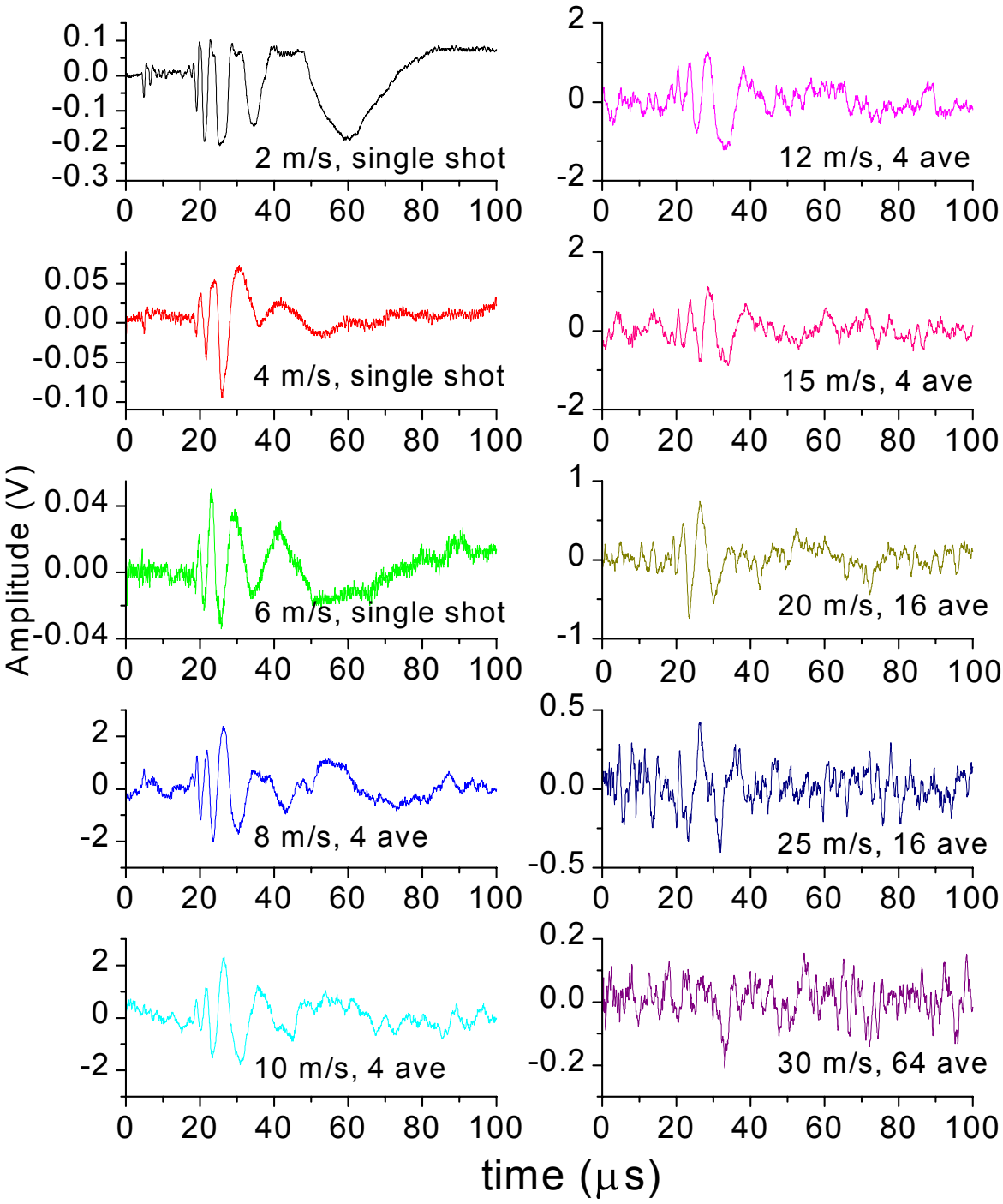

Figure 2.6.120 Comparison of the signals on copy paper in CD at different web speeds after modification of the web simulator: d=10mm, P=1.33W, E=25.6mJ using a line generation in the intermediate regime. Data taken on August 21.

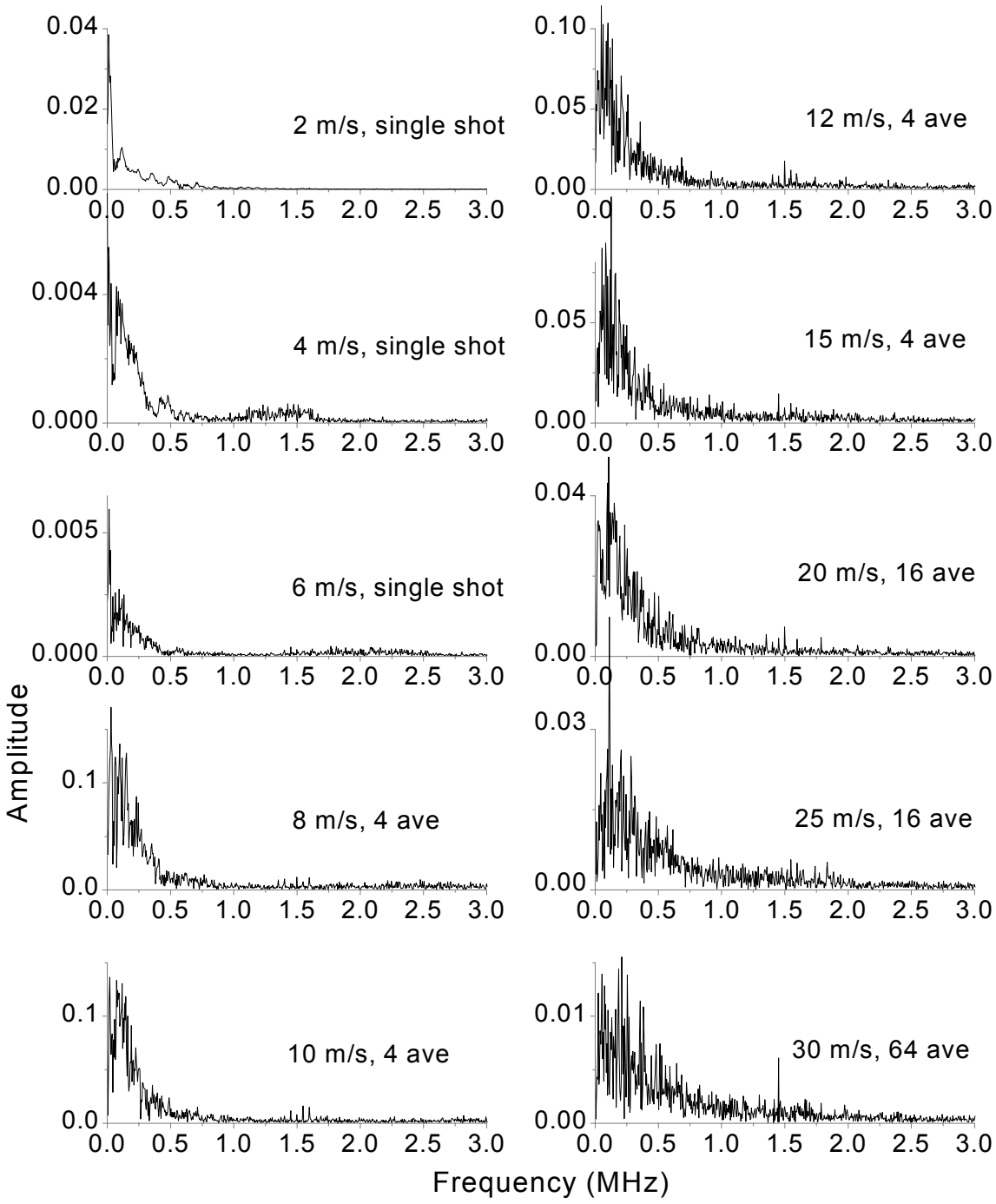

Figure 2.6.121 FFT spectra of the signals shown in Figure 2.6.120 on copy paper in CD at different web speeds after modification of the web simulator: d=10mm, P=1.33W, E=25.6mJ using a line generation in the intermediate regime. Data taken August 21st.

Figure 2.6.120 shows the combination of signals obtained on copy paper in the CD after the web simulator was modified to increase the maximum speed to 30 m/s. The distance, the power and the energy per pulse were maintained at 10 mm, 1.33 W and 25.6 mJ, respectively. The source laser was operated in intermediate regime using a line generation.

Since a typical papermaking machine can run as fast as 30 m/s, Figure 2.6.120 shows the remarkable possibility of implementing the current non-contact laser ultrasonic technique on a real papermaking machine. For typical copy paper, machine speed runs at 18.5 m/s (3650 ft/min) (Biermann, 1993). At that speed, the waveform can be detected clearly using the current setup as shown in Figure 2.6.120. By improving the current configuration and optimizing the laser optics, the S/N ratio can be further improved.

Figure 2.6.121 shows the corresponding FFT spectra of the signals on copy paper in CD shown in Figure 2.6.120. Again, the signal energy is mostly present in the low frequency region. The noise level appears to be relatively low after the web simulator was modified. There still seems to be noise present at approximately 1.5 MHz for high speeds.

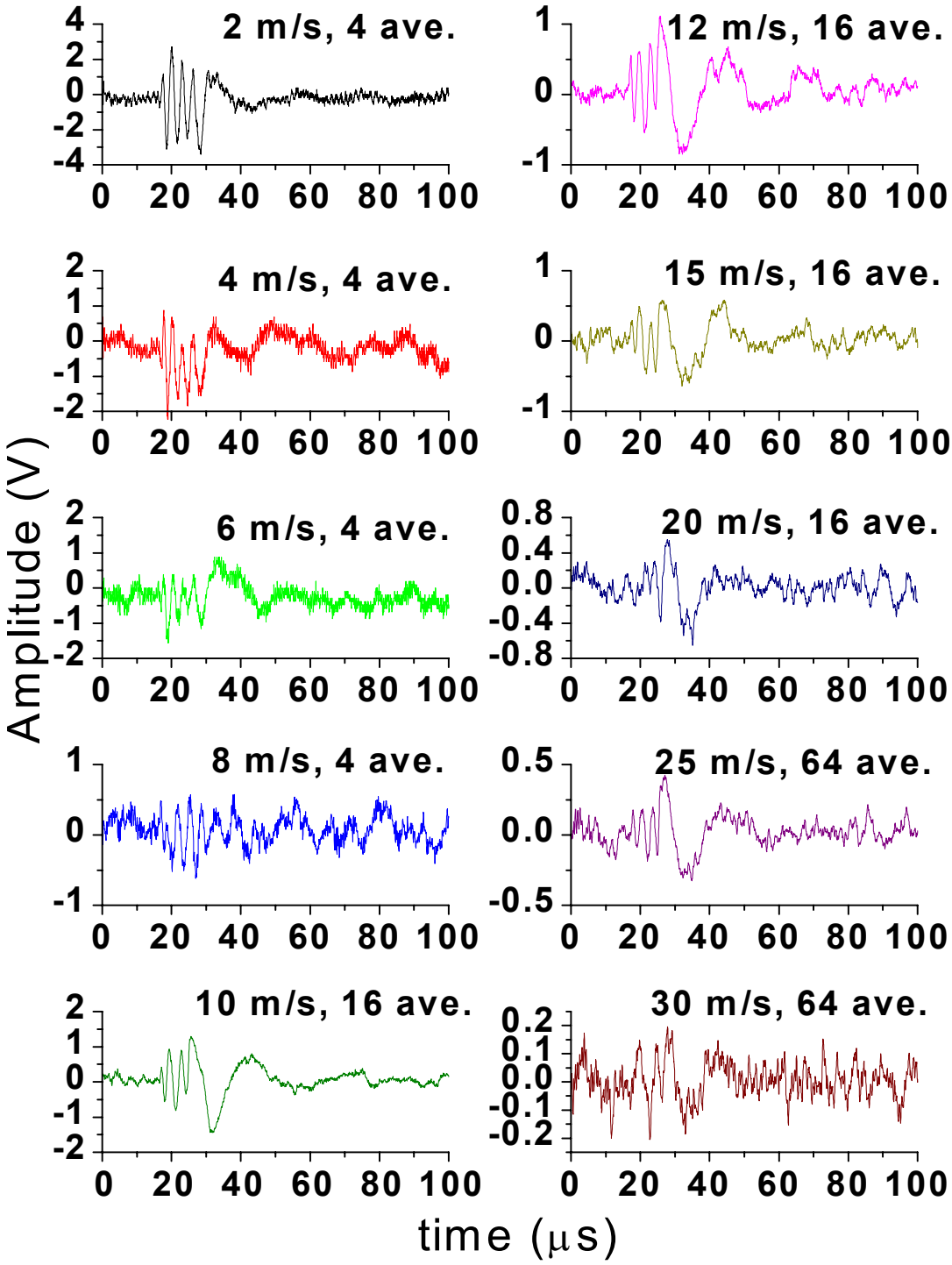

Figure 2.6.127 Comparison of the signals on copy paper in MD at different web speeds: d = 10 mm, P = 1.33 W, E =26.7mJ using a line generation in the intermediate regime up to 8 m/s and in the ablation mode from 10 m/s. Maximum power density was used at 30 m/s by decreasing the generation spot diameter. Data taken August 24th and 25th.

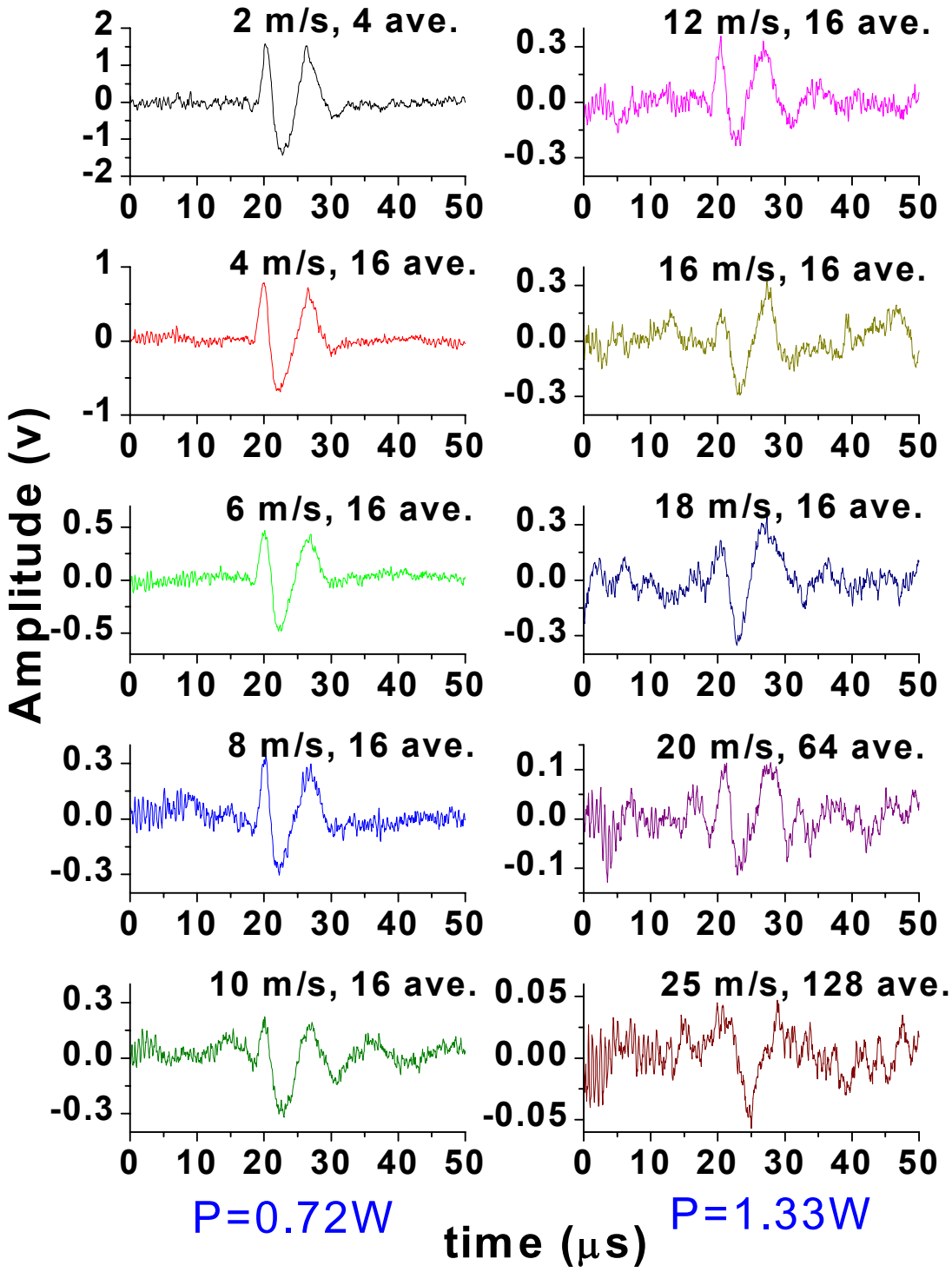

Figure 2.6.128 Comparison of the signals on linerboard 42-lb in MD at different web speeds: d = 10 mm and E =26.7mJ using a line generation in the intermediate regime. Power was increased from 0.72 W to 1.33 W at speeds from 12 m/s. Data taken on August 24 and 25.

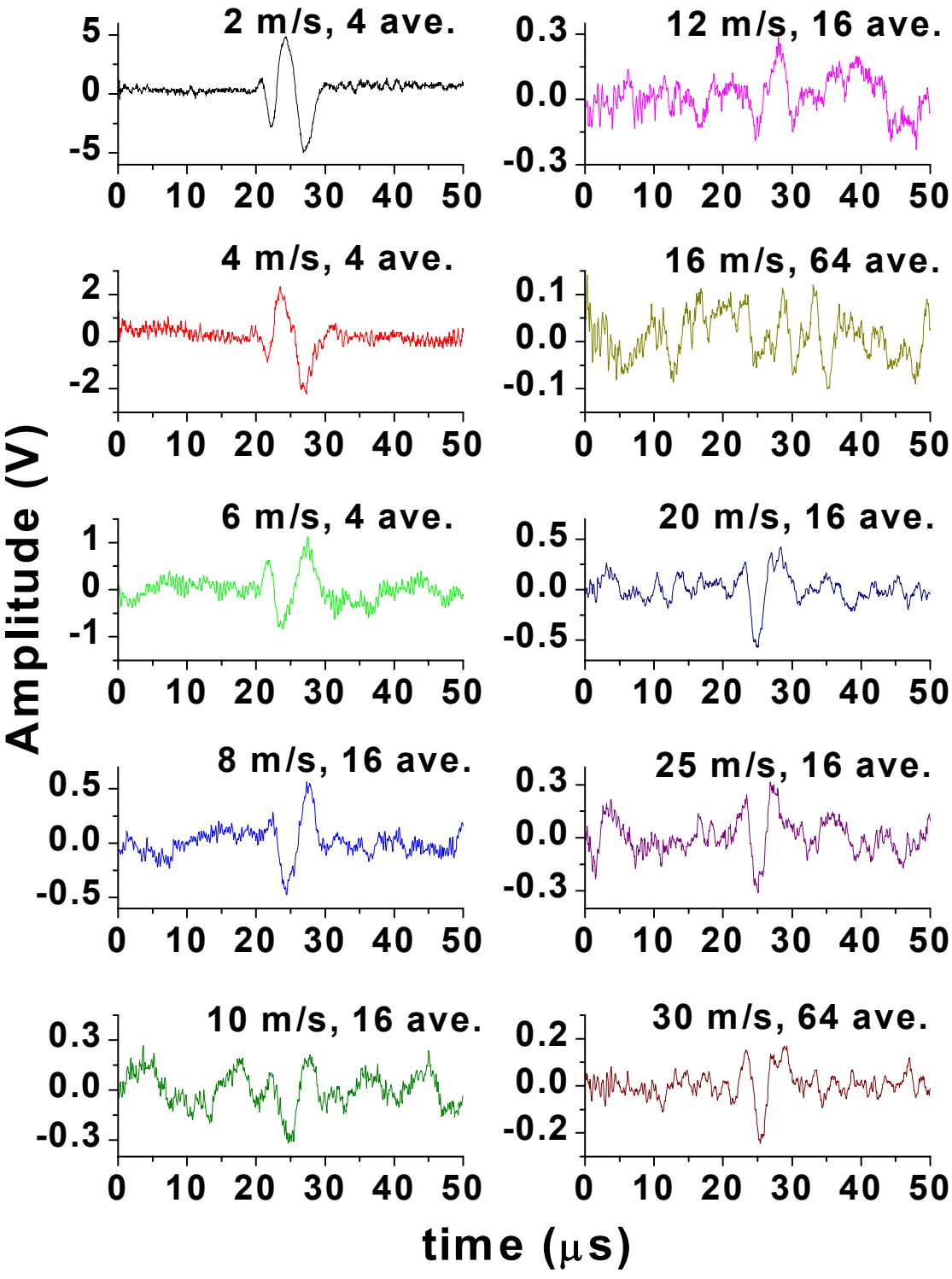

Figure 2.6.129 Comparison of the signals on bleachboard in MD at different web speeds: d = 10 mm, P = 1.33 W, E =26.7mJ using a line generation in the intermediate regime up to 16 m/s and in the ablation mode from 20 m/s. Data taken on August 24 and 25.

4 CONCLUSIONS

At the end of this first year, we are proud to announce that all goals for the first year have been met or exceeded, and the ultimate goal of the control of a paper machine appears reachable. These goals included:

1. *Laboratory demonstration of laser ultrasonic characterization of moving paper.*
- Two web simulators capable of web speeds over 25 m/s plus flutter were built.
- Five different laser ultrasonic detectors were evaluated, including demonstrations on moving paper at production speeds with three (Fabry-Pérot, photoinduced-EMF, self-mixing).

2. *Development of image analysis and light scattering methods for fiber orientation distribution (FOD) measurements.*
- Design and building of a direct fiber orientation measurement instrument using dyed fibers in paper.
- Investigation of a light scattering/transmission method to measure fiber orientation, including comparison of different analysis methods.

In addition to these goals, other tasks (some from Phases II & III) were begun as well:

- Characterization of a wide range of samples as reference samples.
- Investigation into using an optical scanner to reduce texture noise levels on moving paper.
- Investigation of different laser wavelengths for efficient generation of ultrasound, including a literature survey and experimental work.
- Beginning of evaluation of the effect of temperature and moisture on ultrasonic properties.

These technologies are the basis to better understand the papermaking process. During Phase II (years II and III), these technologies will be optimized and integrated together to make an attempt at monitoring the papermaking process in a laboratory environment. Phase II will involve extensive testing of the above technologies on moving paper, as well as beginning to understand how they interact with the various papermaking variables. Phase II will culminate in the demonstration of an on-line, integrated instrument demonstration in the laboratory.

This on-line laboratory instrument will be taken in Phase III to two mill demonstrations, where single-point on machine measurements will be made during the fourth year of the project. Phase III will focus on making the necessary modifications to the instrument to make it a robust performer in the mill. The tradeoffs between economics and technical capabilities will be evaluated, with the ideal of a capable yet cost effective instrument package as the final goal.

LITERATURE CITED

Baum, G.A. "Elastic properties, paper quality, and process control," Appita, 40(4), 288-294 (1987).

Baum, G.A., Pers, K., Shepard, D.R. and Ave'Lallemant, T.R., "Wet Straining of Paper", TAPPI J. 67(5): 100-104 (1984).

Biermann, C., "Handbook of Pulping and Papermaking", Academic Press, 492-495 (1996).

Brodeur, P.H., Johnson, M.A., Berthelot, Y.H., and Gerhardstein, J.P., "Noncontact Laser Generation and Detection of Lamb Waves in Paper", J. Pulp and Paper Sc. 23(5) J238-J243 (1997).

Castagnede, B., Berthelot, Y.H. "Photoacoustic interactions by modulation and laser impact: Applications in mechanics and physics of anisotropic solids", J. Acoustique, 5, 417-453 (1992).

Cheng, J.C. and Berthelot, Y.H., "Theory of Laser-generated Transient Lamb Waves in Orthotropic Plates", J. Phys. D: Appl. Phys., 29: 1857-1867 (1996).

Delaye, P., Blouin, A., Drolet, D., de Montmorillon, L.A., Roosen, G., Monchalin, J.P., "Detection of ultrasonic motion of a scattering surface by photorefractive InP:Fe under an applied DC field", J. Opt. Soc. Am. B, 14(7), 1723-1734 (1997).

Edwards, C., Taylor, G.S., Palmer, S.B., "Ultrasonic generation with a pulsed TEA-CO2 laser", J.Phys. D: Applied Physics, 22(9), 1266-1270 (1989).

Gould, J.M., "Characterization of Lignin *in Situ* by Photoacoustic Spectroscopy", Plant Physiology 70, 1521-1525 (1982).

Habeger C. C., Mann R. W., and Baum, G. A., "Ultrasonic Plate Waves in Paper", Ultrasonics 17 , 57 (1979).

Habeger, C.C. and Wink, W.A., "Ultrasonic Velocity Measurements in the Thickness Direction of Paper", Journal of Applied Polymer Science, 32, 4503-4540 (1986).

Habeger, C.C., Van Zummeren, M.L., Wink, W.A., Pankonin, B.M. and Goodlin, R.S., "Using a Robot-based Instrument to Measure the In-plane Ultrasonic Velocities of Paper", Tappi J. 72(7): 171-175 (1989).

Hale, T.C., Telschow, K. "Optical Lock-in Vibration Detection using Photorefractive Frequency Domain Processing," Appl. Phys. Lett. 69, 2632 (1996).

Hale, T.C., Telschow, K.L., Deason, V.A., "Photorefractive optical lock-in vibration spectral measurement," Applied Optics, 111, 8248 – 8258, (1997).

Hess, T.R. and Brodeur, P.H., "Effects of Wet Straining and Drying on Fibre Orientation and Elastic Stiffness Orientation", J. of Pulp & Paper Sc. 22(5) J160-J164 (1996).

Ing, R.K., Monchalin, J.P., "Broadband optical detection of ultrasound by two-wave mixing in a photorefractive crystal", Appl. Phys. Lett. 59(25), 3233-3235 (1991)

Ishisaki, M., "Comparative Study of Fiber and Stiffness Orientation Distribution", *A190 Independent Research Report*, Institute of Paper Science and Technology (1997).

Johnson, M., "Investigation of the Mechanical Properties of Copy Paper using Laser Generated and Detected Lamb Waves", *Ph.D. Thesis*, Georgia Institute of Technology (May 1996).

Jordan, B.D., O'Neill, M., "Round Robin Study of Paper Colorimetry", J Pulp and Paper Sc. 14(5) J113-J120 (September 1988).

Kohl, A. and Hartig, W., "Optical Determination of Fiber Orientation", Das Papier 39(10A): V172-V177 (1985).

O'Shea, D., *Elements of Modern Optical Design*, John Wiley and Sons, Inc. (1985).

Mann, R.W., "Elastic Wave Propagation in Paper", *Ph.D. Thesis*, Institute of Paper Chemistry (1978).

Mann, R.W., Baum, G.A., and Habeger, C.C., Determination of All Nine Orthotropic Elastic Constants for Machine-made Paper, Tappi, 63(2), 163-166 (1980).

Monchalin, J.-P., “Optical Detection of Ultrasound”, IEEE Trans. UFFC 33, 485 (1986).
Monchalin, J.-P., and Héon, R., “Laser Ultrasonic generation and Optical detection with a Confocal Fabry-Perot Interferometer”, Mater. Eval. 44, 1231 (1986).
Niskanen, K.J. and Sadowski, J.W., “Critical Evaluation of Some Methods used to Determine Fibre Orientation in Paper”, Proc. Paper Phys. Conf., 107-111 (1987).
Pope, J.M., “Near-Infrared Spectroscopy of Wood Products”, from *Surface Analysis of Paper*, ed. by Conners, T., Banerjee, S., CRC Press, 142-151 (1995).
Pourdeyhimi, B., “Assessing Fiber Orientation in Nonwoven Fabrics”, INDA Journal of Nonwovens Research, 5(4), 29-36, (1993).
Sachse, W. and Pao, Y.H., “On the Determination of Phase and Group Velocities of Dispersive Waves”, J. Appl. Phys., 49(8): 4320-4327 (1978).
Schulgasser, K, “Fiber Orientation in Machine-made Paper”, J. Mater. Sci., 20: 859-866 (1985).
Schumacher, N.A., Burger, C.P. and Gien, P.H., “A Laser-based Investigation of High-order Modes in Transient Lamb Waves”, J. Acoust. Soc. Am. 93(5): 2981-2984 (1993).
Scott, W.E., Dearth, L.R., “Optical Properties of Paper”, from *Pulp and Paper Manufacture, Volume 9, Mill Control & Control Systems: Quality & Testing, Environmental, Corrosion, Electrical*, ed. by Kouris, M., Kocurek, M., Joint Textbook Committee, 152-191 (1992).
Scruby C. and Drain, L. *Laser Ultrasonics*, Adams Hilger, New York (1990).
Silvy, J. “Structural Study of Fiber Networks: The Cellulosic Fiber Case”, *Doctoral Thesis*, L’Institut National Polytechnique, Grenoble, France (1982).
Syre, H.R. and Hagen, W., “Improving paper Quality through On-line Measurement and Control of Fiber Orientation”, conference proceedings On Papermaking and Paper Machine Technology, Helsinki, Finland, 51-60 (1995).
Tappi Test Methods, TAPPI Press (1998).
Telschow, K.L., Walter, J.B. and Garcia, G.V., "Laser Ultrasonic Monitoring of Ceramic Sintering", J. Appl. Phys. 68 (12), 6077 (1990).
Telschow, K.L., Deason, V. A., Ricks, K.L. and Schley, R. S., "Photorefractive laser ultrasound spectroscopy for materials characterization," accepted for publication in the Proceedings of the Eighth International Symposium on Nondestructive Characterization of Materials, Boulder, CO, June 15-20, (1997).
Telschow, K.L., Deason, V. A., “Structural Vibration Mode Imaging Using Photorefractive Holography,” Proceedings of the 16th International Congress on Acoustics / 135th Acoustical Society of America Meeting Seattle, WA, pp 1873-1874, June 20-26, 1998.
Telschow, K.L., Deason, V. A., Schley, R. S., and Watson, S. M., “Imaging of Lamb Waves in Plates for Quantitative Determination of Anisotropy using Photorefractive Dynamic Holography,” submitted to the Reviews of Progress in Quantitative NDE, Vol. 19, edited by D. O. Thompson and D. E. Chimenti, Plenum Press, New York (1998).
Van Zummeren, M., Young, D., Habeger, C., Baum, G., and Treleven, R., “Automatic Determination of Ultrasound Velocities in Planar Materials”, Ultrasonics, 25, 288-294 (1987).
Viktorov, I.A., “Rayleigh and Lamb Waves”, *Plenum Press*, New York (1967).

Wagner, J. W., "Optical Detection of Ultrasound," *Physical Acoustics*, Vol.XIX, Eds. Thurston, R.N., and Pierce, A.D., Academic Press, New York, Ch. 5 (1990).
Webb, D.J, Kiebling, A., Sturman, B. I., Shamonina, E., and Ringhofer, K. H. “Verification of the standard model of the photorefractive nonlinearity in BSO crystals”, Optics Comm. 108 31-36 (1994).
Yeh, P., “Introduction to Photorefractive Nonlinear Optics” John Wiley and sons, New York (1993).

GT Mechanical Engineering Dept. work – Effects of moisture and temperature on the bending stiffness and the shear rigidity of paper

Yves H. Berthelot and David A. Griggs, Georgia Institute of Technology

I: Overview:

A laboratory system has been designed, built, and calibrated to measure the effects of moisture and temperature on the bending stiffness and shear rigidity of paper. The methodology consists in generating and detecting optically the first antisymmetric (A0) Lamb mode in a paper sample placed inside a controlled environmental chamber. The ultrasonic waveform depends on the bending stiffness and shear rigidity of the sample. The objective is to extract these mechanical properties from the measured waveforms. A clear advantage of the experimental method is its noncontact (optical) nature. In addition, laser ultrasonics is inherently a very broadband technique that is particularly well adapted to this problem.

II: Experimental Arrangement:

The laser generation is a short pulse Nd:YAG laser and the detection system is a Mach-Zehnder fiber optic interferometer using a CW Argon-ion laser. It was found that the signal-to-noise ratio was much improved by using two separate miniature lenses to send and receive the laser light to and from the sample. The paper sample is placed on a holder inside an environmental chamber where the temperature and relative humidity can be accurately controlled. The temperature range is 23 to 85^{o}C, while the RH range is 25% to 85% (with some temperature restrictions). The moisture content is determined in accordance with TAPPI standard, by measuring the weight of the paper with a precision scale. The signal recorded on the digital oscilloscope is proportional to the instantaneous normal velocity of the sample at the detection point.

Non-contact, broadband Optical bench for laser generation and Mach-Zehnder interferometric detection using optical fibers

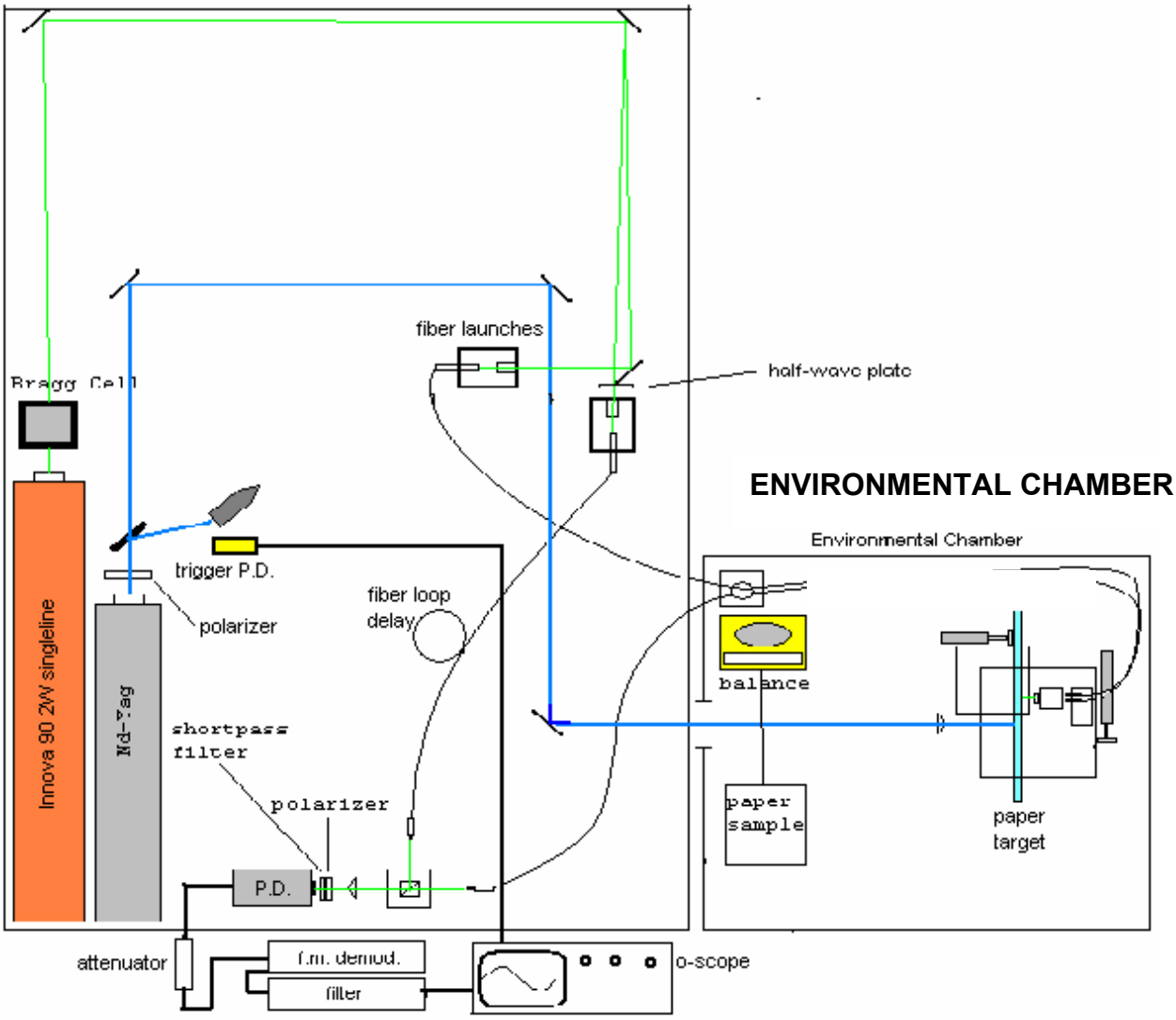

III: Signal Analysis:

The signal (time waveform) is transferred to a computer. Several steps are necessary to extract the bending stiffness and the shear rigidity. First the signal is truncated to analyze only the A0 part of the waveform. Then the Continuous Wavelet Transform (CWT) of the signal is taken using the MATLAB wavelet toolbox function CWT. The output of the CWT routine is a three-dimensional array representing the energy at various arrival times and various "scales". The scale of the CWT is inversely proportional to frequency, so that the CWT is a time-frequency representation of the signal, much like in the standard spectrograms. The CWT plot is a two-dimensional color plot, where the color represents the energy. Clearly, the CWT shows a ridge representing the time of arrival of wave packets of a given frequency. The projection of the ridge in the time-frequency plane can be directly converted as a group velocity dispersion curve, Cgr(f), since the time of arrival, t(f) , of a wavepacket of frequency f is by definition the source receiver distance divided by the group velocity at that frequency. It is interesting to note that using the complex Morlet wavelet (instead of the real valued Morlet wavelet used in the MATLAB routine CWT) significantly improved the estimates of the group velocity dispersion curve. The last step in the analysis of the signal is to extract the bending stiffness and the shear rigidity from the group velocity dispersion curve. This is done by using a MATLAB nonlinear optimization routine ("fmins") that minimizes the objective function

$$\Delta^2 = \sum_{j=1}^{N} [Cgr(f) - \hat{C}gr(f, D, SR)]^2$$

where N is the number of data points on the experimental dispersion curve Cgr(f), and where $\hat{C}gr(f, D, SR)$ denotes the predicted dispersion curve which depends on the bending stiffness, D, and the shear rigidity, SR, as well as the basis weight BW (known) of the paper. It can be shown that for the A0 mode, an excellent approximation of the group velocity is

$$C_{gr}(\omega) = \frac{\sqrt{2(b\omega^2 + \sqrt{b^2\omega^4 + 4a\omega^2})}}{b\omega + \frac{b^2\omega^3 + 2a\omega}{\sqrt{b^2\omega^4 + 4a\omega^2}}}$$

where $\omega = 2\pi f$, b=BW/SR , and a =BW/D.

Methodology: Analyze the (A0-mode) group velocity dependence on frequency (dispersion) using the wavelet transform.

For various temperatures, moistures

Time-domain Waveform

↓

Wavelet Transform (Complex Morlet)

↓

Ridge finder And dispersion curve Of the group velocity

$C_{gr}(f)=dist/[t(f)]_{ridge}$

↓

Best Fit with Expected dispersion

↓

Bending stiffness Shear Rigidity

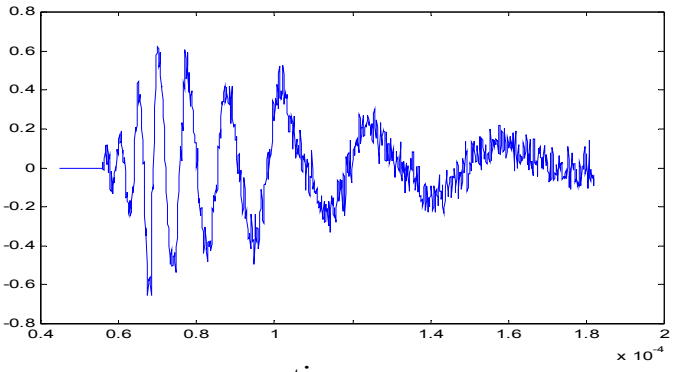

time

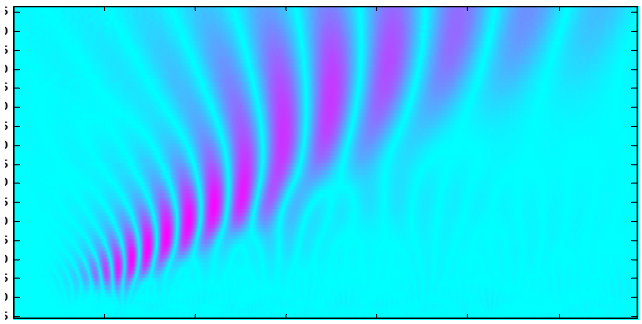

Arrival time

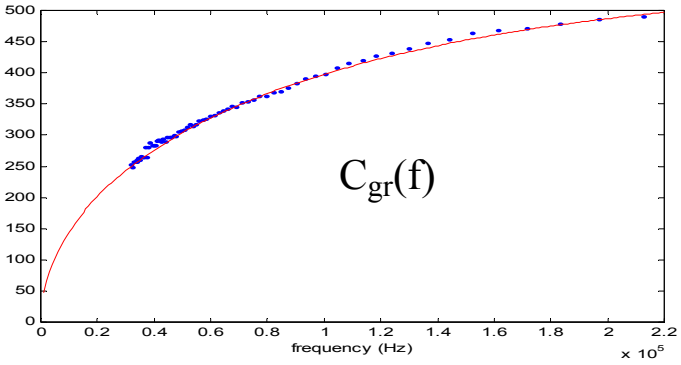

frequency

DISPERSION CUVE FOR THE A0 MODE

PHASE VELOCITY:

$$C_{ph}^4 + \omega^2\left(\frac{D}{SR}\right)C_{ph}^2 - \omega^2\left(\frac{D}{BW}\right) = 0 \quad (1)$$

$C_{ph}(\omega)$= phase speed (m/s) SR = Shear rigidity (N/m)

D = Bending stiffness (N.m) BW = basis weight (kg/m^2)

Or $$k^4 = a\omega^2\,(1 + k^2 d) \quad (2)$$

$k(\omega) = \omega/ C_{ph}(\omega)$ = wavenumber (1/m); a = BW/D b=BW/SR

d=D/SR

GROUP VELOCITY: $$\frac{\partial k}{\partial \omega} \equiv \frac{1}{C_{gr}(\omega)}$$ **So that,**

$$C_{gr}(\omega) = \frac{\sqrt{2(b\omega^2 + \sqrt{b^2\omega^4 + 4a\omega^2})}}{b\omega + \dfrac{b^2\omega^3 + 2a\omega}{\sqrt{b^2\omega^4 + 4a\omega^2}}}$$

Find (a,b) i.e.,(D, SR) for best fit with data; i.e., minimize:

$$\Delta^2 = \sum_{j=1}^{N}[Cgr(f) - \hat{C}gr(f, D, SR)]^2$$

IV: Results and Conclusions:

A laser ultrasonic system has been designed, built, calibrated, and used to measure the A_0 Lamb mode propagating in copy paper under well controlled environmental conditions (temperature and moisture). The objective of the experiment was to determine the dependence of the bending stiffness and shear rigidity on moisture and temperature, so that one could normalize measurements taken at various environmental conditions with an on-line monitoring system in a paper mill.

The excellent sensitivity of the detection interferometer resulted in part from the use of separate send-receive optical fibers and illuminations of a spot size on the paper that was very close to the diffraction limit (a few microns). Ultrasonic waveforms with relatively high signal-to-noise were recorded even at larger source receiver separation distances (up to 29 mm). These waveforms show clearly a large number of oscillations and therefore significant dispersion, typically in the 50 kHz to 300 kHz range. These waveforms were obtained with a laser source that was a small line-source (about 6 mm), perpendicular to the propagation path. In this study the usual propagation path was in the cross-direction, CD, which is perpendicular to the fibers' direction. Even with a line source, the laser power at the generation spot ablated the sample. Ablation was not a major concern since the system is not designed to be used on-line, but rather it is designed to provide information on the dependence of the bending stiffness and shear rigidity on temperature and moisture content.

An important contribution was to develop a signal processing method capable of extracting bending stiffness and shear rigidity from a single A_0 ultrasonic Lamb wave. This was achieved by matching the dispersion curves (group velocity versus frequency) of the data to those predicted from the orthotropic plate model. Dispersion was obtained from a single waveform by evaluating the analytic wavelet transform of the signal.

The technique was tested on a known sample, a silicon wafer. The dispersion curve measured by the wavelet transform was in complete agreement with the theoretical dispersion curve calculated for the silicon wafer.

Some calculations and experiments were also done to estimate the errors associated with the transient heating of the paper sample near the excitation line-source and the continuous heating of the paper sample near the detection point. It was found that these errors were small compared to the other sources of error in the experiment. The largest source of error in the determination of the material properties was the sample variability. Paper is

heterogeneous and anisotropic. The local variations in density, thickness, fiber clusters, etc., have a significant effect on the variability of the ultrasonic waveforms in the paper. It was found that the error due to sample variability (for a single sample) and measurement technique was about 14 % for bending stiffness and 42 % for shear rigidity.

Data was taken in the cross direction, CD, for copy paper (grammage = 80 g/m^2) at 25, 50, 75°C, at moisture contents ranging from 3.5 to about 9 % moisture content (PMC), depending on the temperature (corresponding to relative humidities of about 15 to 80 %).

As expected, it was found that bending stiffness decreased when temperature or moisture content increased.

The bending stiffness changed with temperature by -1.1×10^{-6} N.m / °C and with moisture content by -2.5×10^{-5} N.m / 1 PMC. The dependence of shear rigidity on temperature and moisture was inconclusive because of the large error associated with its determination.

Off-line Laboratory instrument technical report: IPST's internal PAC report from July 2002 to June 2003

Significant improvements made between July 2002 and June 2003:

- Fiber optic delivery of both generation and detection beams
- Smaller and less expensive generation laser available for lab instrument
- Considerably smaller and much less expensive detection laser implemented
- Automatic acquisition of waveforms and run of lasers
- Automatic MD-CD and polar plot testing
- Signal analysis method mostly automated

To summarize, an automated laser ultrasonics instrument has been assembled, that uses fiber optics for both the generation and detection. Grade testing has been started. To be fully automated and save operators' time, the signal analysis requires the completion of a more robust 2π offset determination routine than the one existing currently. This is part of the continuation of this project for FY04 as this will also benefit the on-line Laser ultrasonic system.

We would like to welcome requests for testing from paper mills having problems with formation on the web of the paper machine that affect the bending stiffness or shear rigidity of their paper or boards. The laboratory instrument provides information on the bending stiffness of paper or boards with a very precise spatial resolution (down to 1 mm) exceeding the capabilities of the Tabor stiffness test. Therefore, it is possible to detect features caused by small scale variations of the stiffness in the paper that conventional stiffness tests cannot measure.

DISCUSSION:

Hardware Development

We have tested then purchased a generation laser to be dedicated and integrated to the laboratory instrument. Its advantages are a much smaller footprint for the laser head than the current laser, a much longer time interval between maintenance operations, for a smaller price. It will be integrated to the laboratory instrument after the full-scale mill demonstration of the on-line sensor (DOE project DE-FC07-97ID13578) because we will use that laser for the demonstration.

IPST tested then purchased a detection laser for integration to the laboratory instrument. One of its advantages is a significantly smaller footprint than the current laser, but mostly, a much smaller price tag compared to the current laser which is an older model. However free lunches don't exist in the technical world. Hence we had to purchase and add an optical isolator to this new laser because it was too sensitive to the light back-scattered from the fiber optic tip, compared to the previous laser, if it were to be used as is. We calculated that the cost reduction achieved was well worth adding a little complexity to the instrument. Using this new detection laser and the new generation laser we purchased last quarter decreases considerably the cost of a potential LUS lab instrument measuring Flexural and Shear Rigidities. A more accurate near/far translation stage for the generation probe was also implemented to the instrument as we found out the previous stage was not reliable enough.

We have hardened the link between the interferometer and the robot that carries the fiber optics with a stainless steel flexible hose.

Software Development

We have continued the testing and software writing of the probe manipulation of the lab instrument with the existing generation laser. The robot has been programmed to do polar plots determination and standard MD-CD testing. We have automated a process to optimize the elevation of the laser optics above the paper sample for each measurement.

We have done several studies for optimizing the displacement of the probe on two grades: white raw stock (87 g/m^2) and 42-Lb brown linerboard (205 g/m^2). They concluded that for both papers grades (and any grade) at least 10 signals should be averaged before any analysis, and that the sample should be translated 0.1 mm between laser firing to avoid signal washout from the generation beam repeatedly impinging the paper.

We have automated further the signal processing and it can now determine automatically the best frequency range over which the mechanical constants are calculated. Moreover, both the previous and newer generation lasers (interlock open, laser firing, etc…) are now controlled by the software through the computer.

The automated signals analysis software routine is giving good results on lightweight paper and light linerboard. We still have some difficulties with the quality of the A0 waves obtained on heavy linerboard and are working to improve the signal to noise ratio.

Our last remaining major software challenge is creating a robust and reliable 2π offset determination routine. The Ao plate wave presents no clear indication of the moment of arrival of energy under the detector in terms of out-of-plane displacement of the paper.

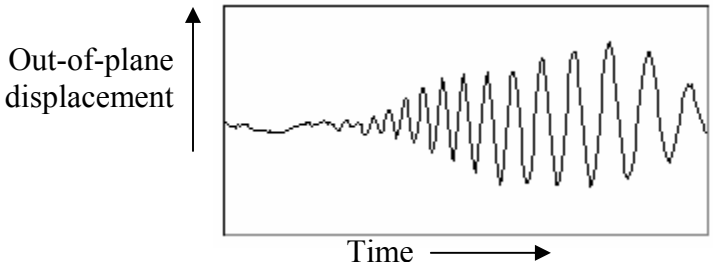

Also, the Fourier transform produces phase data that is ambiguous in the sense of absolute phase, providing only relative measures of phase at any given frequency between +/- π. If it were possible to reference any given phase back to the phase at very low frequencies where wavelengths are very long, then it would be a fairly straightforward matter to determine absolute phase at higher frequencies (shorter wavelengths). But, the Ao wave mode in paper contains very little energy at very low frequencies and/or is complicated by lower frequency vibrations set up in the sheet following the emission, rendering the lowest frequency phase data indeterminate, and complicating such referencing, though it may still be possible to reference moderately low frequencies/long wavelengths.

Efforts to provide a robust algorithm based on low frequency referencing have shown promise, but no algorithm yet implemented has worked reliably all the time. Part of that has to do with

the quality of the ultrasonic signals, which have been improved as our knowledge of the physical situation has increased. Also, the equally important ability to identify and reject bad signals has improved as well, occasional bad signals being a practical and unavoidable fact due to emissions laser inconsistencies and other factors.

One fail-safe alternative method relies on knowing a ball-park estimate of the FR for a given paper before-hand and then choosing the integral multiple of 2pi that results in a flexural rigidity closest to that ball-park estimate. This is a reasonable technique in that a single 2pi offset from the correct multiple of 2pi leads to fairly drastic changes in calculated FR, which are fairly easy to identify as inaccurate. Obviously, such a technique always works, assuming that source ultrasonic signals are of reasonable quality, the initial ball-park estimate is reasonable good, and the variation of FR from location to location is considerably less than the difference in FR from one 2pi multiple offset to the next. However, our intention is to avoid having to assume a typical value of FR at all and we continue to work on doing so.

Comparison to other stiffness tests

We have compared both the Laboratory Instrument Two-Wave Mixing and Mach-Zehnder LUS results (on-line sensor) to measurements more commonly used by the industry (Tabor test, resonance method, and contact ultrasonic testing) so as to establish a correlation. We expect that once confidence in the laser ultrasonic measurement has been established, this correlation will reveal the inherent uncertainty that plagues the conventional mechanical measurements. Results are presented in Table 1 hereafter.

Whereas Tabor and resonance tests measure bending stiffness directly, contact ultrasonics estimates bending stiffness from a measured planar Young's modulus and a measured thickness (a more thorough discussion of contact ultrasonic bending and thin material bending stiffness in general is included in the Bending Stiffness Tutorial attached to the end of this document). Contact ultrasonic predictions are inherently less accurate than direct bending measures, due primarily to the ambiguity of measuring the thickness of rough and compressible media and of the assumption that paper is homogeneous along the thickness direction.

Tension

It was expected that the tension that paper is subjected to has some influence upon the measured flexural stiffness and shear rigidity. Also, lower basis weight grades (copy, magazine and newsprint grades) were expected to vary more under the range of tensions expected during manufacture and printing operations than heavier basis weights. To study the influence of tension, a test fixture was designed and constructed that would allow paper samples to be subjected to known tensions while being measured. It was confirmed that tension did play a part and that the effect was significant for the lower basis weights within the low frequency regime of the phase velocity curve. A tension term was then added to the phase velocity calculations as follows:

The dispersion equation for Ao plate waves in paper (excluding tension):

$c^4 + \omega^2 (6D/5SR)\, c^2 - \omega^2 (D/BW) = 0$

The dispersion equation with a tension term added:

$c^4 + [\omega^2 (6D/5SR) - T/BW]\, c^2 - \omega^2 (D/BW)\, [1+6T/5SR] = 0$

where c = phase velocity (m/sec)
ω = angular frequency (radians/sec)
D = flexural stiffness (N*m)
SR = shear rigidity (N/m)
BW = basis weight (kg/m^2)
T = tension (force per width)

The following charts illustrate the influence of tension on the phase velocity dispersion curve for a typical liner and a typical copy paper.

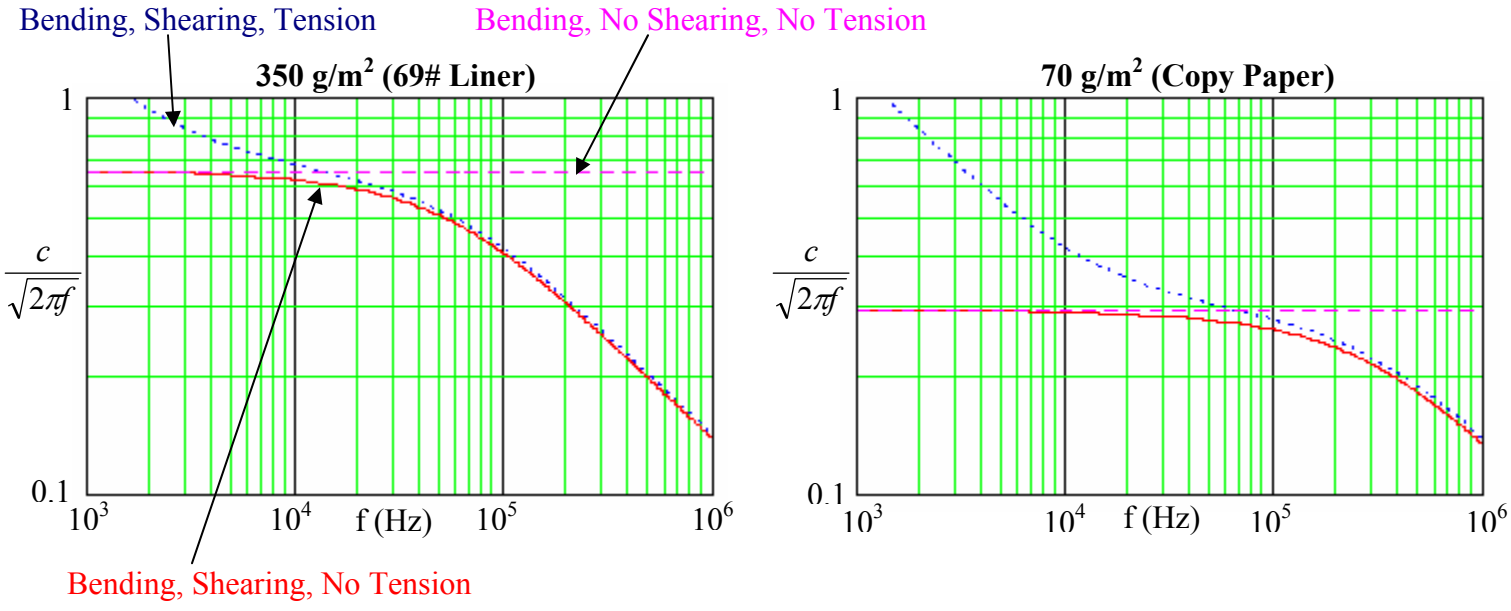

The question remained as to how the tension term should be treated. Either it would be possible to derive tension from the phase velocity curve and enhance the value of the instrumentation by adding tension as a third measured value. Or it would be necessary to supply the tension term from some external measure of tension to keep flexural stiffness and shear rigidity calculations accurate. For higher basis weights, the supplied tension term may be left at zero without detrimental effects. After careful study of low basis weight papers subjected to varying tensions, it was decided that predicting tension was not reliable and that tension should be determined externally and applied as an input to improve the calculations of flexural stiffness and shear rigidity for low basis weight papers subjected to moderate to high tensional forces.

For completeness, the phase calculation software driving the determination of elastic constants from ultrasonic signals was updated to accommodate both a mode where tension is supplied as an input and where tension is calculated as an output at the touch of a button.

Automated MD/CD and Polar Testing

Paper is a material that generally varies a great deal from position to position, having to do with basis weight formation and other factors. Thus, multiple measurements and statistics that are representative of the entirety of the width and breadth of a specimen and represent statistically reliable average values are virtually always an important component of paper testing. Planar orientation profiles and other secondary calculations (geometric means, max/min ratios, etc.) are also helpful additional indicators of certain aspects of product performance just as they have been with IPST's traditional planar ultrasonic modulus of elasticity and shear modulus testing. In support of this, integrated/automated MD/CD and polar profiling interfaces and algorithms have been included into the laser ultrasonics laboratory unit. These interfaces will enable the use of the technology for routine operators/technicians who need have no great expertise in the LUS technology, handling most of the details involved. They will also help leverage the unique ability of the LUS technology to make measurements at multiple angles (i.e. MD bending, CD bending and intervening angles) on the same specimen sample area, which traditional cut sample testing cannot do, since specimens must be cut specifically for a given measurement orientation and cannot be used again.

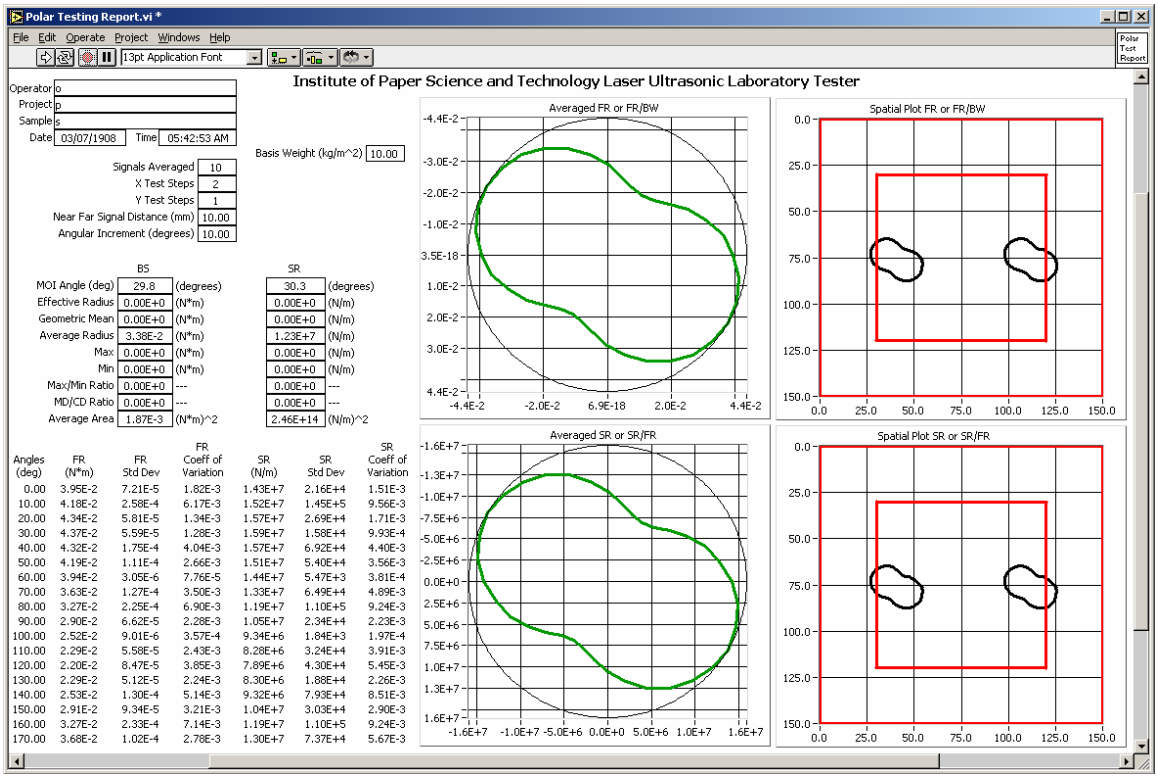

Focal Distance and Table Levelness

It was known that the optical focal distance from the paper surface to the objective lens fronting the interferometer that transduces tiny out-of-plane displacements into electrical signals is critical to obtaining reliable measures of out-of-plane displacement due to the passage of the Ao waveform through the plane of the paper. But it was not known with precision over what range the interferometer would produce an adequate response. Therefore, a study was undertaken to determine what that effective range was by incrementally changing the optic to paper surface distance and measuring signal amplitudes. It was found that if the optic is as much as a half millimeter too high or too low, the interferometer will lose most of it's sensitivity A nominal working range for reliable operation was determined to be approximately ±0.2 mm.

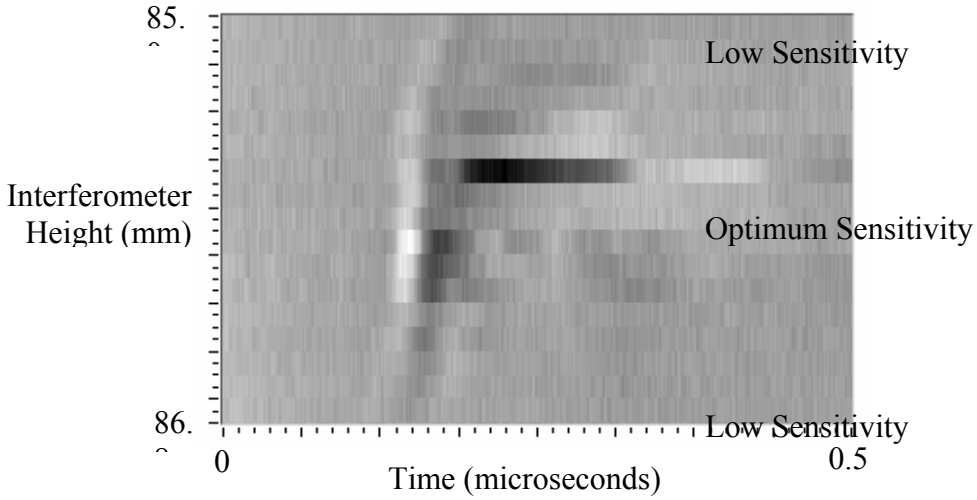

Even the thickness of the specimen itself can vary the distance from the optic to the paper surface significantly. Since that and other mechanical stability issues caused some lack of confidence in the assumption that a constant and precise distance from optic to sample surface could be expected at all times and because setting an optimal optic to surface distance manually is time consuming and difficult, it was decided to automate the determination of that optimal distance. Software and signal acquisition components were added to the laboratory unit to quickly sweep the optic through a range of height above the specimen and determine automatically the most optimal distance within approximately two seconds at the touch of a button. The mechanical system for holding the specimen under moderate tension and driving planar and rotational displacements of the specimen beneath the static interferometer optic is fairly complex and includes several components. It was decided to study the levelness of a typical specimen within the specimen holder. The levelness was found to vary by slightly more than a millimeter over a planar span of 6 inches X 6 inches (See Fig below). In view of this, it was decided that the efficient automated height optimization could reasonably be undertaken automatically prior to each individual laser shot/acquisition/measurement. Thus, an optional mode for doing so was included in the system software. This feature will guarantee that all measurements are taken with optimal interferometer characteristics.

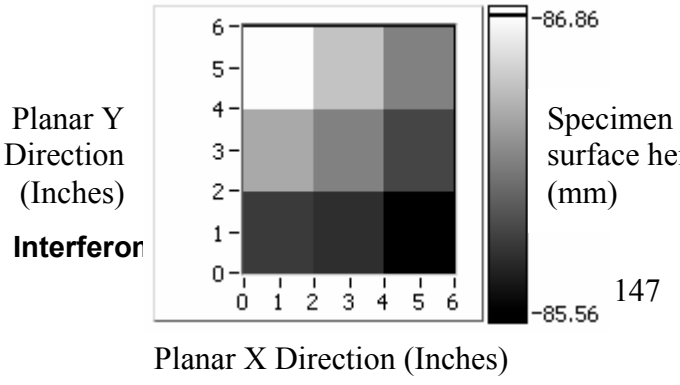

Interferon

In the course of working to understand some unexpected results from ultrasonic signals during phase velocity analysis, it became apparent that some signal distortions existed. Further examination revealed that the anomalies corresponded with signals generated by large emissions energies, which ironically were expected to produce good signal to noise ratios and good elastic constant determinations. A study of ultrasonic waveforms with incrementally increasing emissions energies was conducted to better understand the phenomenon. Examination of those signals clearly revealed the reasons for the anomalies. The two-wave mixing interferometer imposes a limit on the range of out-of-plane displacements that are measurable without distortion, the range being a function of the wavelength of the interferometer laser. Exceeding this range results in signal inversions (i.e. apparent decreasing amplitude with increasing out-of-plane displacement). This inversion effect appears as a leveling off of amplitude (saturation) when displacement barely exceeds the interferometer's range. For cases where displacement exceeds the range by a factor of two or more, signal inversion occurs and the result is an apparent frequency multiplication as illustrated below:

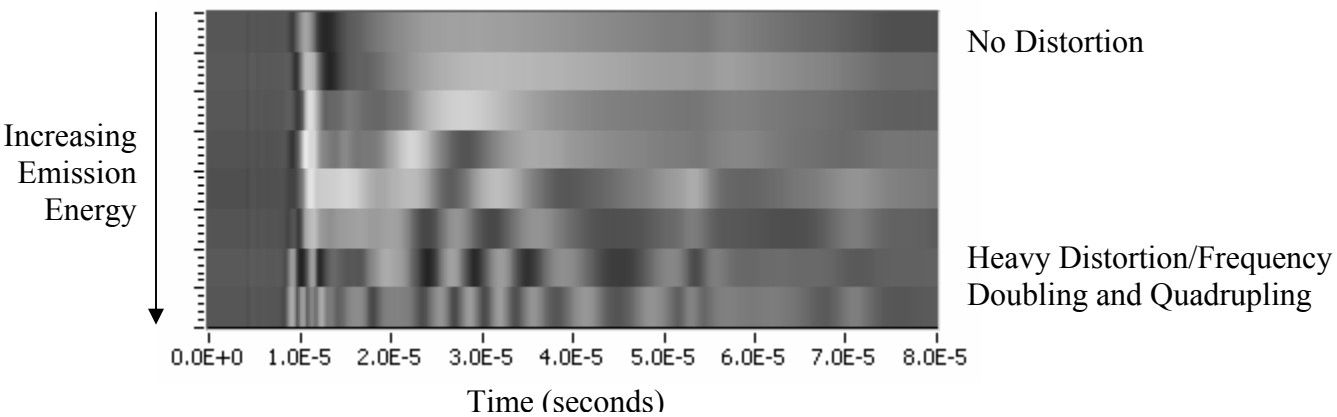

After pinning down the theory behind the distortions and in order to understand to what degree these inversions were affecting the accuracy of the flexural stiffness and shear rigidity measurements from the phase velocity curves, the inversion effect was modeled mathematically. It was found that, theoretically at least, the influence of the inversion effect on the phase velocity curve (derived from the raw phase component of the Fourier transform of the ultrasonic signals) is relatively modest for intermediate levels of saturation and only becomes pronounced with heavy saturation (A). The effect on the magnitude of the Fourier transform, however, is significant (B). Even moderate distortions can lead to regions of low magnitude, and those regions render the corresponding regions of the phase velocity curve indeterminate. When dealing with actual laser ultrasonic signals, the practical situation is even worse. Since a smooth phase velocity curve is necessary for a successful determination of elastic constants, even modest levels of distortion must be identified and avoided.

Currently, it is a cumbersome task to check for signal inversions and interferometer displacement range limitations and determine optimal energy output levels. Naturally, it is preferable to increase the emissions energy as much as possible to improve the signal to noise ratio while avoiding both ablation damage to the paper and interferometer distortions. The newly acquired emissions laser, having an automated control of emissions energy levels, will allow an automated means of setting optimal emissions levels quickly, further enhancing the

value and robustness of the laboratory unit. Automated control of emissions energy levels will be included shortly after the new emissions laser is integrated into the laboratory unit.

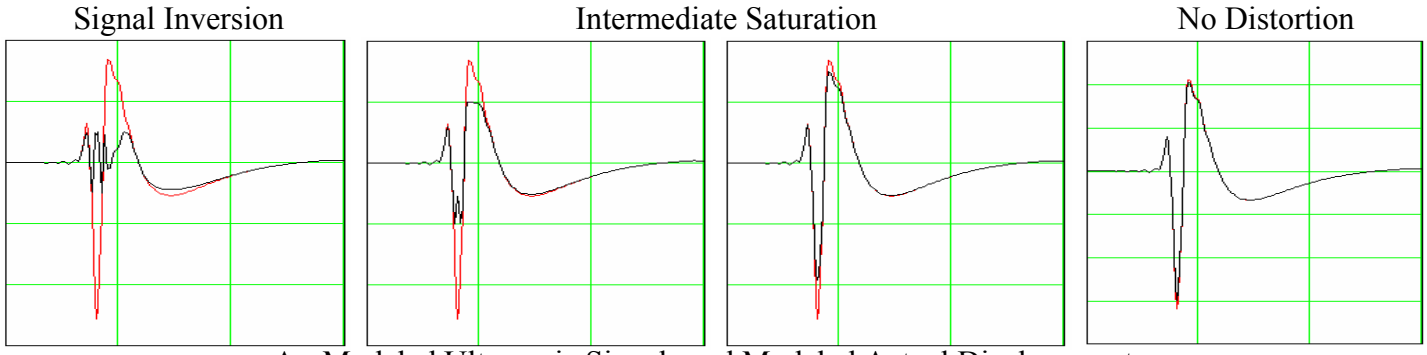

A - Modeled Ultrasonic Signals and Modeled Actual Displacements

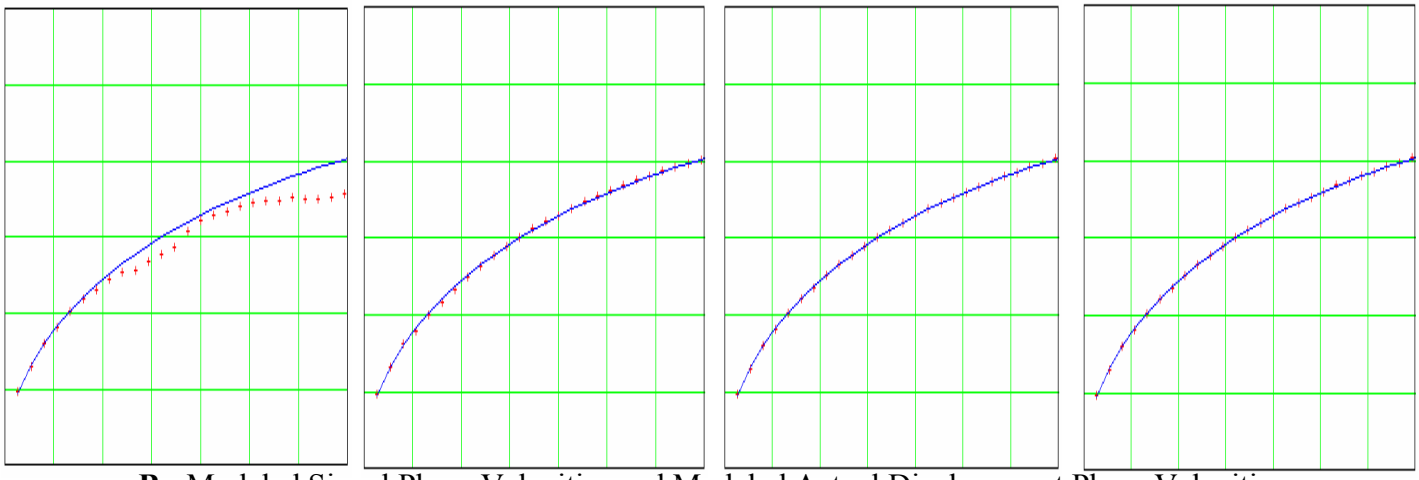

B - Modeled Signal Phase Velocities and Modeled Actual Displacement Phase Velocities

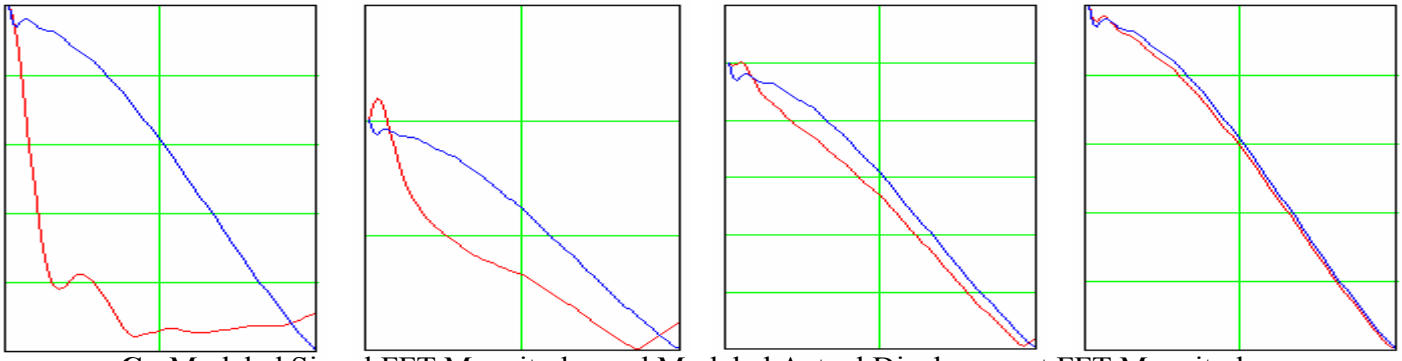

C - Modeled Signal FFT Magnitudes and Modeled Actual Displacement FFT Magnitudes

Frequency range limitations

The determination of flexural rigidity and shear stiffness is performed by fitting a modeled phase velocity curve that includes FR, SR, basis weight and tension coefficients to the phase velocity generated from the phase difference between the near and far distance ultrasonic signals. In general, the greater the frequency range of the phase velocity dispersion curve included in the fit, the better the results. In practice, however, the range is limited by the frequency band for which there is a significant amount of ultrasonic energy. That band is a function of excitation laser energy, distance traveled by the ultrasonic waves due to attenuation while in transit through the paper, thickness, density, interferometer sensitivity and other complicating factors. For those frequencies where the amount of energy drops to insufficient levels, the phase curve becomes indeterminant, which can lead to discontinuities and errors in fitting the modeled phase velocity curve. The interferometer distortions mentioned previously can also inject those narrow zones of low energy (and phase discontinuity) throughout the nominal frequency range used for making the elastic coefficients measurements, so steps to identify and avoid those distortions/inversions will become an automated part of the instrumentation. Increasing the amount of emissions energy injected into the paper with minimal visible marking and optimal interferometer sensitivity and immunity from noise have also been a primary goal over the last year's work.

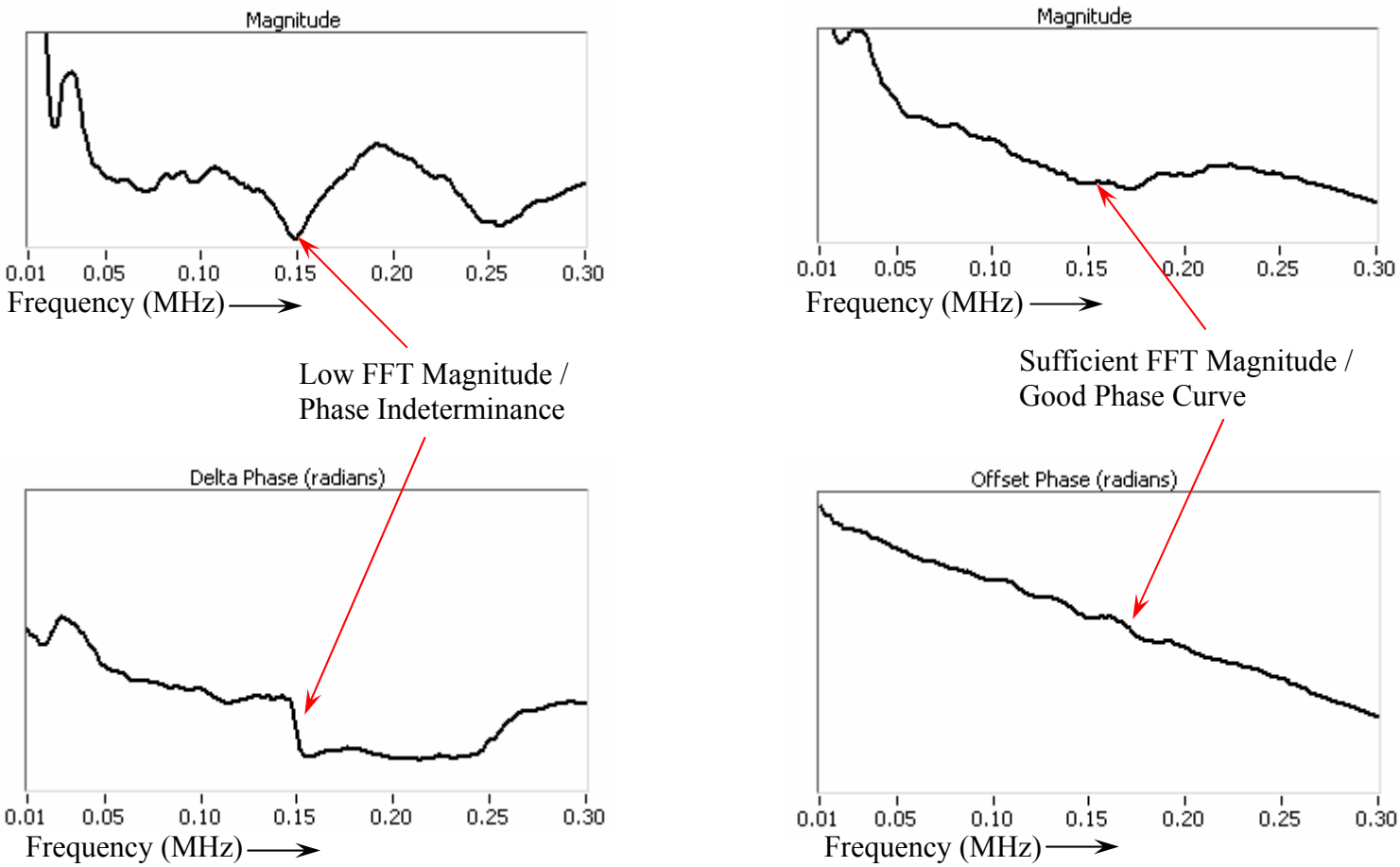

Frequency Range Auto Detection

The nominal band of frequencies having sufficient energy to include in the determination of elastic constants from the phase velocity curve varies with the paper grade being measured and with other factors. In order to keep the use of the instrumentation simple, such that anyone could apply it with relative ease, it was decided to automate the determination of the appropriate frequency range as a routine component of sample testing.

The determination proceeds as follows. The low and high frequency limits are set to defaults which are considered to be a minimum range through which all nominal bands will pass through. The low frequency limit is swept in fractional steps through ever lower frequencies until a default low frequency limit is reached with the error between modeled phase velocity and actual phase velocity calculated at each step. The low frequency limit is then set to the frequency at which the lowest error occurred. The same series of steps is then performed for the high frequency limit which is swept through increasingly higher frequencies until a default high frequency limit is reached. In short, the frequency range is set to produce a minimum error between modeled and actual phase velocities.

The error is expressed as a percentage and is calculated as:

$$\frac{\sqrt{\sum\left(1-\frac{C_{actual}}{C_{\mathrm{mod}eled}}\right)^2}}{\sqrt{n}*\ln(f_h-f_l)}*100$$

Where:
c = phase velocity
f_h = high frequency Limit
f_l = low frequency limit
n = number of points between f_h and f_l

Modeled and Actual Phase Velocity Curves

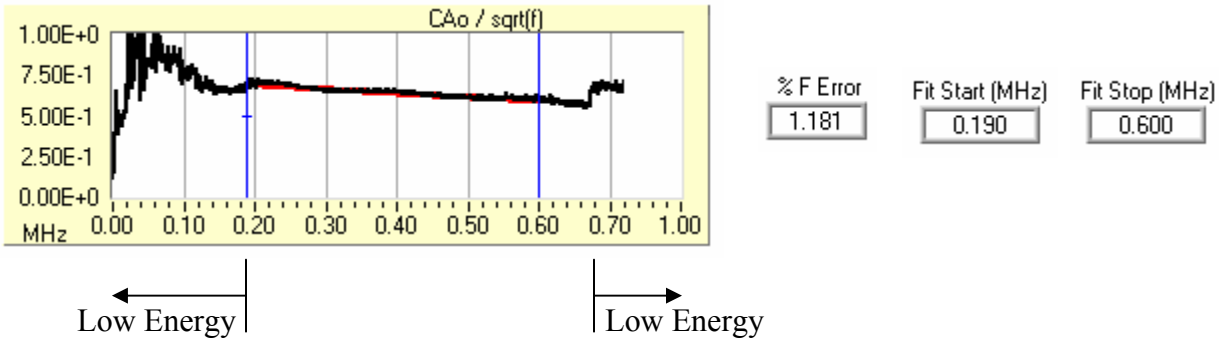

Emissions Laser Artifacts

Early in the design stage, it was decided to build the apparatus with both emissions and interferometry optics placed on the same side of the paper, for ease of design and construction, as a two sided design would have been considerably more cumbersome and expensive. However, one consequence of the single sided design is that some light from the emission laser couples directly into the interferometer optic, adding a transient impulse to the displacement signal. That impulse saturates the interferometer amplifier and appears as an early-arriving exponential decay prior to the arrival of the actual ultrasonic signal. The transient can complicate the phase spectra of the displacement signal, and subsequently complicate the determination of elastic constants. The first solution was to use a different interferometer signal amplifier with a wider passband that reduced the time of decay considerably. However, the increased passband reduced the signal to noise ratio at the high frequency end as well, causing more problems than it solved. Instead, a combination of two complimentary solutions were chosen instead, the first being to employ as large a separation distance between interferometry and emissions optics as possible to resolve the transient from the early arriving, high frequency component of the Ao signals in time as much as possible. The second involved placing a conical cap over the interferometry optic such that only the portion of the paper whose displacement is actually measured is unobstructed from the interferometer optics. The amplitude of the transient is reduced and the time for the transient to decay to insignificant levels is also reduced. With the transient isolated, it then becomes a simple matter to remove the artifact altogether from the signal mathematically.

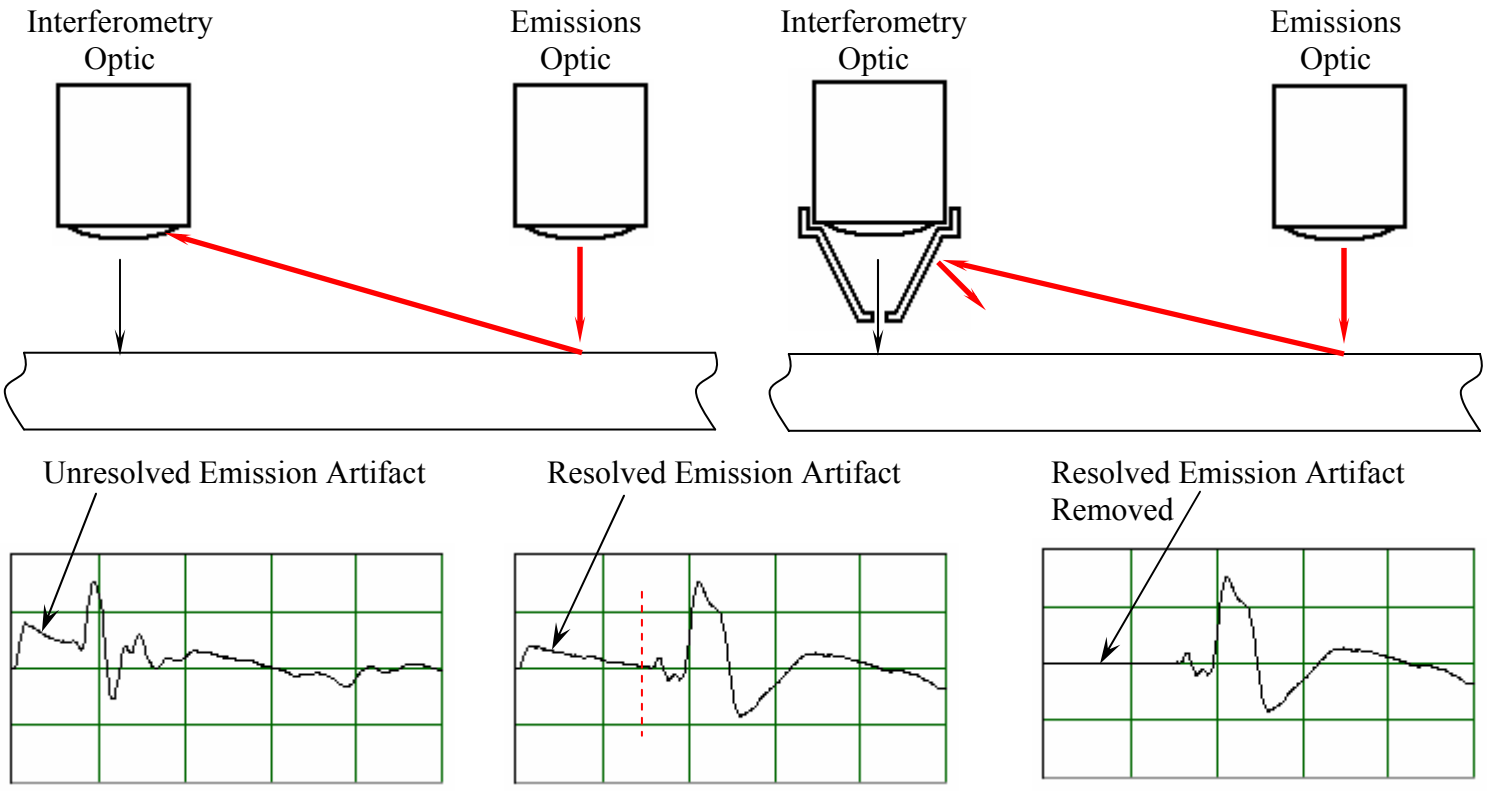

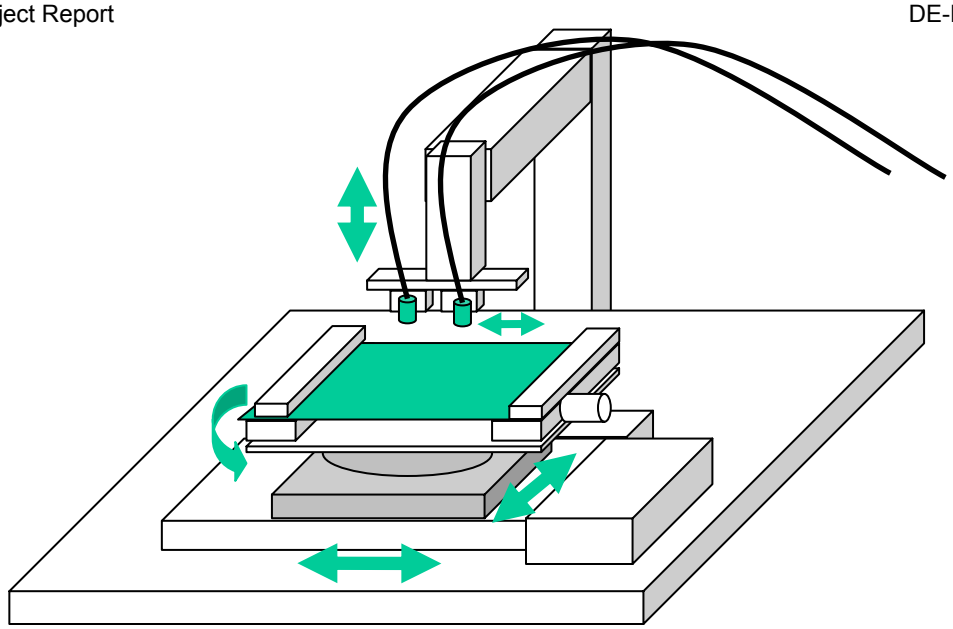

Axes of Robotic Mechanical Translation/Rotation ↑, and Fiber Optic Delivery ↓

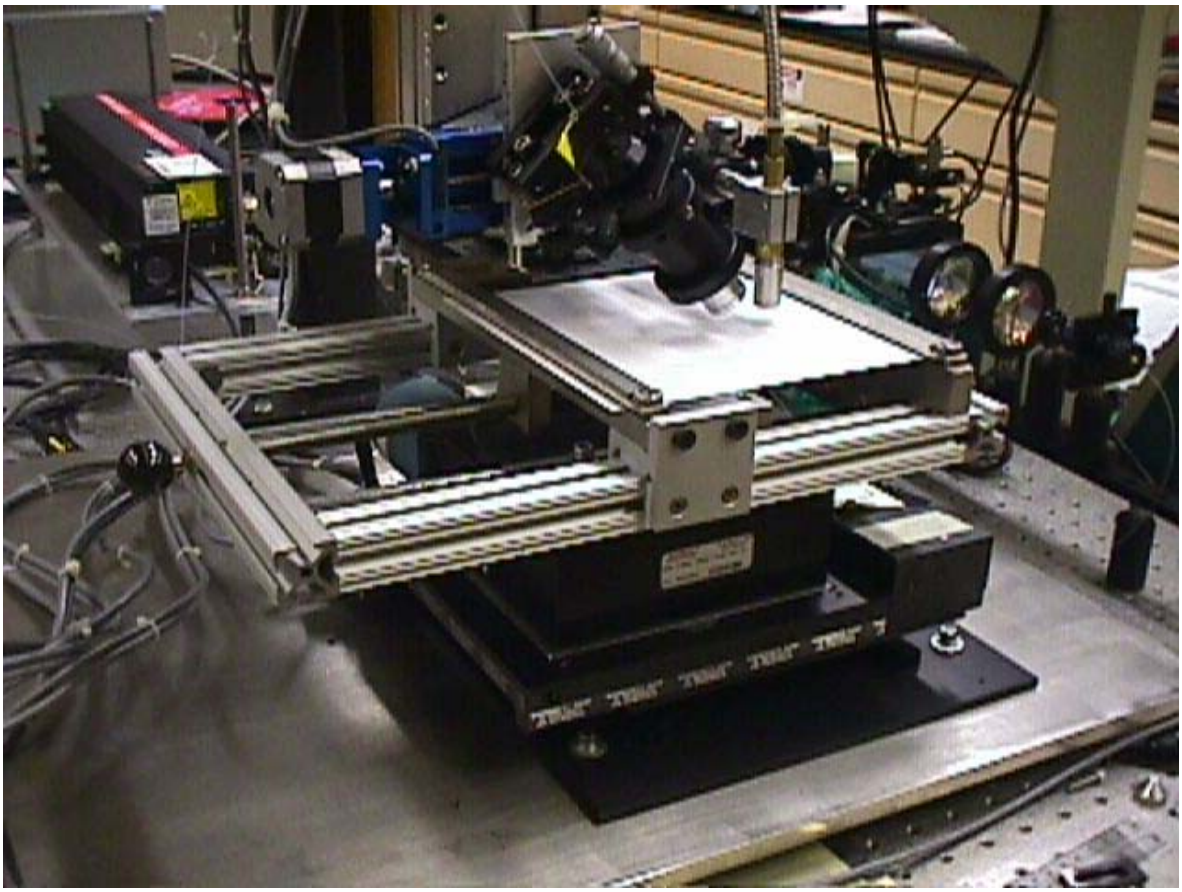

Preliminary Taber and Laser Ultrasonic Bending Comparison

An initial look at the ability of the laser ultrasonic technique to predict mechanical bending stiffness shows promising results. The LUS technique actually measures flexural rigidity, which is approximately equal to bending stiffness. The two differ only by the inclusion of a Poisson's ratio term that accounts for lateral dimensional change in response to strain in the direction of the induced stress. In general, flexural rigidity is higher than bending stiffness by approximately ten percent. Encouragingly, the LUS technique is effective over a broad range of basis weights and grades.

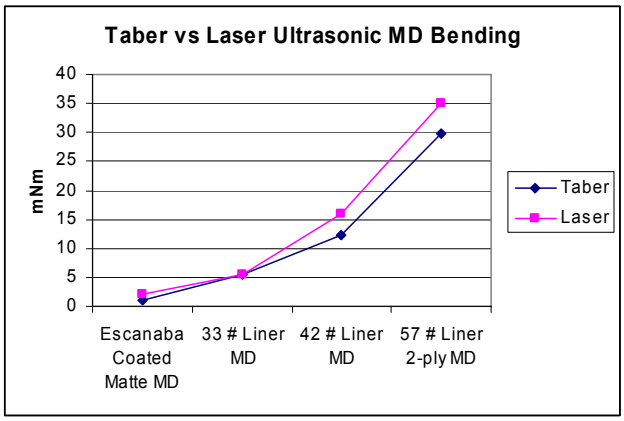

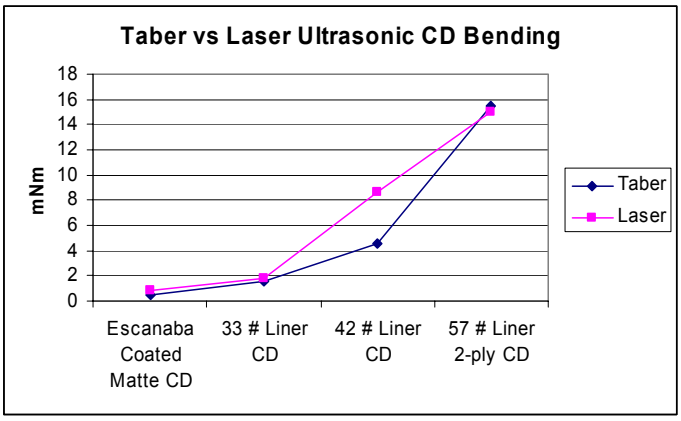

Sample Name	BW (g/m^2)	MD/ CD		Taber	Contact	Laboratory instrument
Escanaba Coated Matte	111	MD	D(mNm	1.05±0.03		2.02±0.04[19]
			SR(kN/	N/A		38±1
		CD	D(mNm	0.487±0.006		0.86±0.02[19]
			SR(kN/	N/A		38±2
26 lb lnr	126	MD	D(mNm	4.07±0.06	4.48	
			SR(kN/	N/A	24	
		CD	D(mNm	1.22±0.02	1.94	
			SR(kN/	N/A	21	
Escanaba Coated Glossy	153	MD	D(mNm	0.786±0.009		
			SR(kN/	N/A		
		CD	D(mNm	0.509±0.007		
			SR(kN/	N/A		
33 lb lnr	165	MD	D(mNm	5.6±0.2	7±2	5.4±0.3
			SR(kN/	N/A	21±4	33±1
		CD	D(mNm	1.51±0.04	2.8±0.8	1.85±0.08[17]
			SR(kN/	N/A	16±2	20±2
42 lb lnr	210	MD	D(mNm	12.2±0.3	18.1	15.9±0.8
			SR(kN/	N/A	45	49±4
		CD	D(mNm	4.6±0.1	5.8	8.6
			SR(kN/	N/A	28	30.8
57 lb lnr 2-ply	280	MD	D(mNm	29.7±0.2	36.7±0.7	35±2
			SR(kN/	N/A	34±5	35.8±0.7
		CD	D(mNm	15.5±0.1	17.9±0.4	15±1
			SR(kN/	N/A	28±3	34.8±0.4
69 lb lnr	337	MD	D(mNm	60±1	69.7	
			SR(kN/	N/A	36±2	
		CD	D(mNm	22.3±0.2	27.2	
			SR(kN/	N/A	26±3	

Table 1: Comprehensive table of Flexural Rigidity and Shear Rigidity

Off-line Laboratory instrument technical report: IPST's internal PAC report from July 2003 to June 2004

A) Executive Summary for Laser Ultrasonics Laboratory Instrument:

Main Characteristics of Completed Laser Ultrasonic Laboratory Instrument (June 2004):

- All optical
- Non contact
- can be non-destructive
- testing and evaluation of mechanical properties
- Broad band, acoustic waves frequency: 5 kHz to 8 MHz (can be upgraded to 200 MHz)
- Wavelength of the probed acoustic waves : a few tens micrometer to several mm
- Samples: paper, paperboard, plates, foils, films/substrates comprising papers, wood, plastic foils, metal foils

Laser Ultrasonic Laboratory Instrument Sub-components:

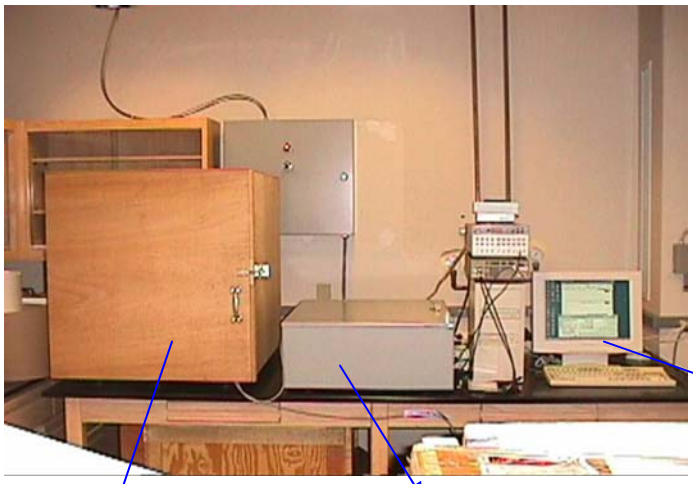

Software and automation

End-effectors with fiber optics

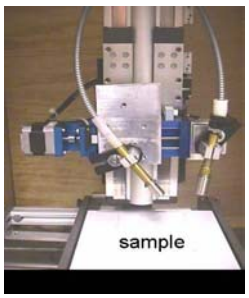

Two-Wave mixing interferometer

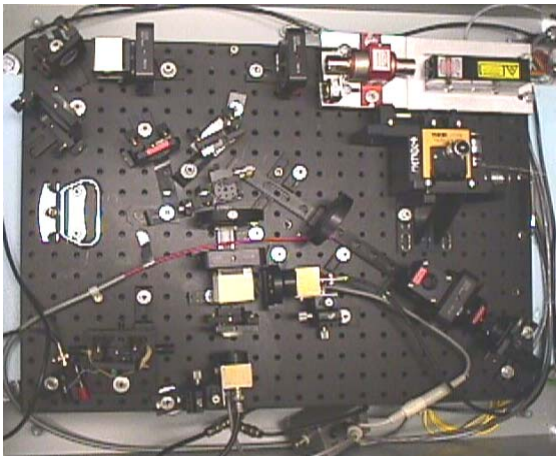

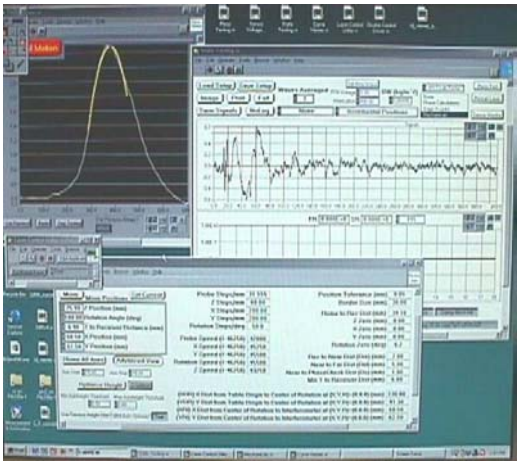

Measurements performed by laser ultrasonics instrument:

Samples and thickness (d)	Waves measured	Properties of materials obtained
Thin Plates, foils thickness d < ultrasonic wavelength	Plate (Lamb) waves	→Flexural Rigidity (≅ bending stiffness) →Shear Rigidity →Thickness if Young's or shear modulus is known
Thick plates thickness d > wavelength	Longitudinal wave Surface (Rayleigh) wave	→Young's modulus of elasticity → Shear modulus
Films on substrates d ~ wavelength	Modified Surface Rayleigh Pseudo surface modes	→ Shear modulus → Elastic moduli to which the waves are sensitive to.

B) Improvements, studies, results about laboratory instrument from July 2003 to June 2004

B-1) **Optical reconfiguration of interferometer.**

Original two wave mixing (TWM) interferometer (left graphs), and Improved two wave mixing interferometer (right graph). The small graph on the left is a part of signal optics that sits out of the original TWM interferometer and a long sliding rail is not shown in the graph.

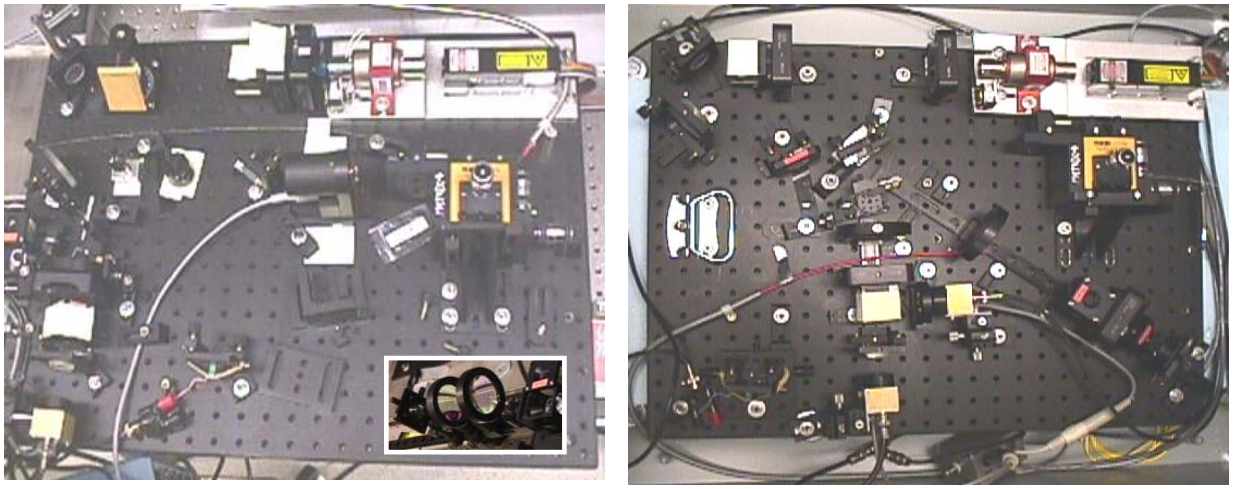

Improvements: two balanced detectors, increasing S/N ratio twice.
New optical layout , the signal beam optics (small photos in original TWM) was arranged on the plate. The new set-up is more compact and can be enclosed inside a box.

B-2) **Enclosing the system.**

Closure of TWM, and measurement robot system in metal and wooden enclosures

B-3) **Solving vibration problem that affected measurements.**

A wooden enclosure was previously built to house the instrumentation as a means of containing the potentially dangerous high intensity laser light and enabling the placement of the instrumentation within laboratories having no interlocks or other laser safety precautions. The instrument was placed in the enclosure. However, mechanical vibrations from the building and from personnel activities nearby the instrument (including speech of a conversational volume!) affected the ability to measure, those vibrations competing with the very small out-of-plane displacements with the passage of A0 waves. Therefore, rubber feet and soft, thick foam sheets were placed below the instrument at strategic locations to block vibrations from the building and solid table on which the unit is mounted and to dampen vibrations induced into the enclosure from the air surrounding it. The additions brought the vibrations to within manageable levels.

B-4) **Sinusoid Generator Circuit.**

Occasionally, it is necessary to vibrate a component of the interferometry optics within the laboratory tester using a consistent 50 KHz excitation sinusoid in order to check the integrity of the optical system and to check for problems with mechanical vibrations. Traditionally that excitation was provided by a function generator, and a scope was used to examine the quality of the interferometry signal. An inexpensive (<$50) circuit was built, which could generate such a nearly pure sinusoid with just an existing power supply, a sinusoid generator chip and a few miscellaneous electronic components. A software interface was also developed to replace the scope and to provide other assistance in checking the integrity of the system. The integrated circuit and interface could be put to use with the touch of a button, increasing the convenience and speed of the integrity test considerably.

After power-on, the circuit worked as expected. However after ten to twenty minutes of continuous operation, the sinusoid generator chip would flat-line for reasons not understood. Believing the chip to be faulty, it was replaced by an identical chip which suffered the same flat-line problem. The miscellaneous electronic components supporting the operation of the chip were replaced, though their replacement did not alleviate the problem. Further examination of the flat-lining problem will be undertaken as soon as possible.

B-5) **Faster Averaging of ultrasonic waves.**

Previously, a 365 micrometer diameter fiber optic was used to couple emissions laser energy to the focusing optics and sheet in support of the laboratory unit. It was possible to inject up to 10 mJ into the optic with up to about 60% transfer efficiency without damaging the fiber optic. Unfortunately, without defocusing the beam spot at the specimen surface, the energy density within the finite spot diameter proved to be great enough to permanently damage that localized point on the specimen such that attempting to generate waves repeatedly on the same point resulted in diminishing wave amplitudes. Thus, in order to build low noise multi wave averages for analysis, it was necessary to emit a burst and acquire the wave, move the focusing optics a small amount, wait a couple of seconds for mechanical vibrations resulting from the motorized mechanical movement to die out, and then acquire the next component wave. Unfortunately, this process was slow and made for long duration tests per paper sample.

The 365 micrometer diameter fiber optic was replaced with a 550 micrometer fiber optic. Though limited to the same 10 mJ laser energy injection into the optic without damage, it was possible to get improved transfer efficiency (as much as 80%) through the optic without damage and, therefore, more energy focused onto the sheet with each burst. Also, the larger spot diameter, being proportional to the fiber optic diameter, resulted in a lower energy density at the burst spot without defocusing the beam. The lower energy density turned out to be below the specimen damage threshold, enabling in-place averaging without mechanical movements (and subsequent delays) for the first time.

Thus, it became possible to make use of the laser's free-running capability (20 Hz max burst rate) and produce low noise wave averages for analysis in seconds rather than minutes. Additionally, the larger diameter fiber optic proved to be easier to couple to the source laser.

B-6) **Original and unambiguous method for the measurement of mechanical characteristics of samples: 2D FFT Density of State method.**

In developing methods for laser generation and detection of A0 plate waves in paper and other thin materials, the ultrasonic signals observed have tended to deviate from the ideal, containing multiple wave modes and other artifacts, complicating analyses that make use of them. However, the nature and causes of those deviations are very difficult to determine simply by observing the raw signals, themselves. A better means of analyzing those signals was needed.

To fill that need, a means of generating dispersion curves was developed. This method entails incrementally increasing the separation distance between the emissions and interferometer spots and recording a series of waves, one for each separation (**A**) (see hereafter). The wave series is then stacked to form a two-dimensional array (**B**). A 2D Fourier transform of the array is then calculated, which produces a dispersion curve (wave number versus frequency). As shown in (**C**), two primary wave modes are evident – an A0 mode and a constant velocity mode (the straight line), which turns out to be a compression wave, which propagates through the air and changes the refractive index of the air as it passes through the interferometer beam. The much improved understanding of the signal derived from the dispersion curve then lead to effective means of controlling the unwanted refractive index wave with the use of an appropriate barrier. Such an understanding and subsequent solution could not have been found simply by observing a single raw signal. As pictured in (**D**), even highly complex signals containing numerous wave modes can be analyzed and understood with the use of such a dispersion curve.

The incremental displacements, wave acquisitions and calculations were automated to provide minimum difficulty in generating those curves and were implemented in both the laboratory and on-line versions of the flexural and shear rigidity measurement instrumentation being developed. A paper describing the technique “Noncontact Determination of Elastic Moduli by Two Dimensional Fourier Transformation and Laser Ultrasonic Technique” will shortly be published in the journal “Review of Scientific Instruments” early in 2005.

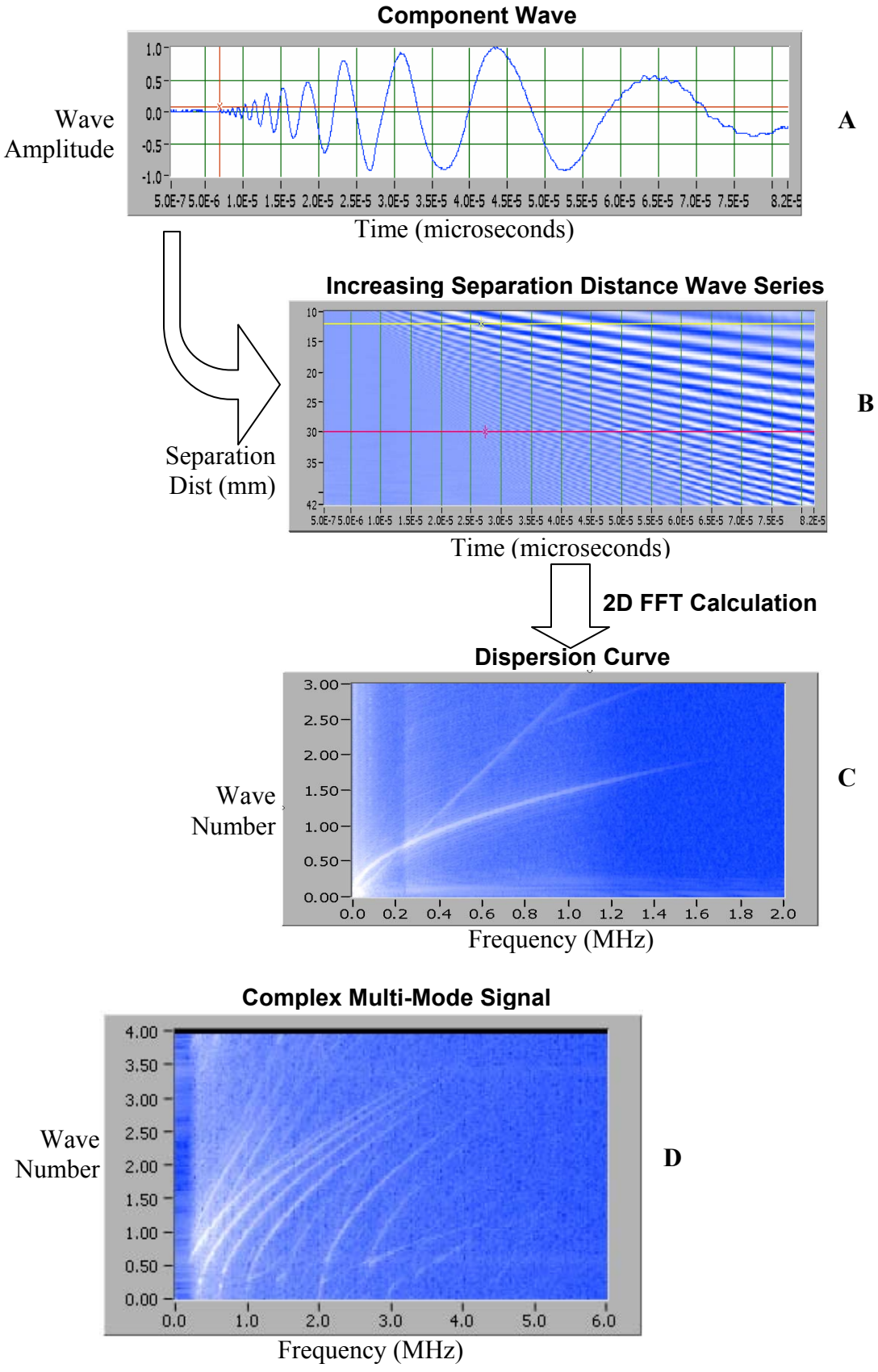
Component Wave
Wave Amplitude
Time (microseconds)
A
Increasing Separation Distance Wave Series
Separation Dist (mm)
Time (microseconds)
B
2D FFT Calculation
Dispersion Curve
Wave Number
Frequency (MHz)
C
Complex Multi-Mode Signal
Wave Number
Frequency (MHz)
D

B-7) **Sample stage: Hard Surface Specimen Mount.**

Initially, a suspended sheet holder was designed and built for the laboratory tester to hold paper specimens under moderate tensions below the laser emission and interferometry optics. However, this design proved to be cumbersome and impractical when mounting and dismounting specimens. Additionally, it was not easy to mount the specimens while assuring that the stress distribution through the sheet was uniform and light enough throughout the entire specimen area to prevent tensional effects from influencing the measured flexural and shear rigidities. Also, it was difficult to fix the holder in place such that the paper surface within the holder would be exactly normal to the direction of the measurement beam. A sloped specimen surface necessitates a slow optimal height determination of the specimen below the laser optics at all locations throughout the specimen area in order to place the location under test within the narrow depth of focus of the emission beam. Lastly, since the laser optics are placed very close to the specimen surface, collisions between the laser optics and screws holding the specimens in place via compression bars at opposite ends of the specimen area represented a danger.

The suspended sheet holder was developed partly in the belief that sheet contact with a surface would detrimentally affect the ability to measure the flexural and shear rigidities of the sheet. However, in searching for a more practical means of specimen mounting, a study was undertaken to determine if contact with a hard surface would affect the measured FR/SR values. No detrimental effects were observed. A further concern that a portion of the emissions laser energy passing through the specimen and reflecting back from the support surface could induce a secondary excitation and resultant artifacts into the measurement turned out not to represent a problem.

Therefore, it was decided to replace the suspended sheet holder with a simpler steel plate support surface and then hold specimens against the plate with thin refrigerator magnet strips. Tension was no longer a consideration. Collisions between the optics and sheet holder were avoided owing to the thinness of the magnets. Specimen contact with the support surface was not a problem, probably owing to the miniscule size of the out-of-plane displacements associated with the passage of the A0 waves through the sheet (on the order of microns). The plate could be fixed to be level with relatively high precision relative to the optics making it possible to conduct a single height optimization for a given specimen and keep that height constant while testing the entire area of the specimen, resulting in an increase in testing throughput.

B-8) **Some results of the laser ultrasonics laboratory instrument:**

Polar testing on 42 Lb linerboard (205g / m^2), FR in MD is more than twice of those in CD, where SR is about one quarter more than in CD.

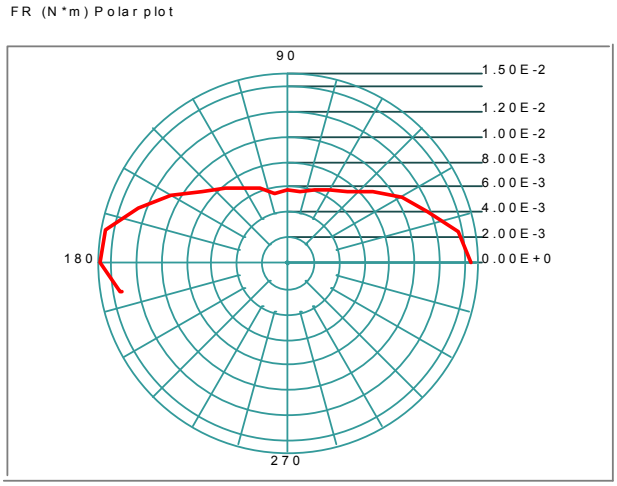

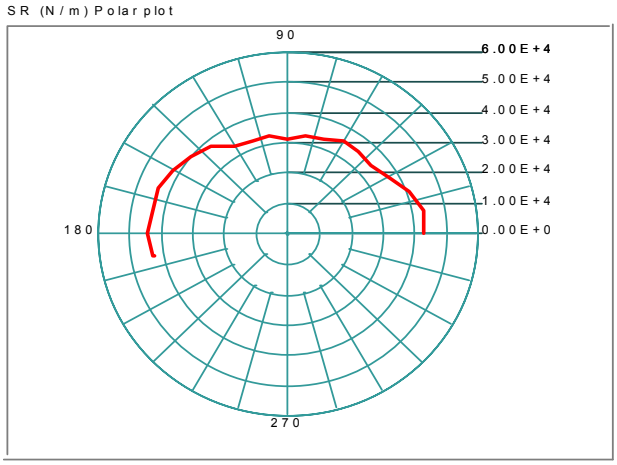

Polar testing of FR on copy paper and Escanaba publication paper. The maximum of FR is slight off (~ 10 degree)

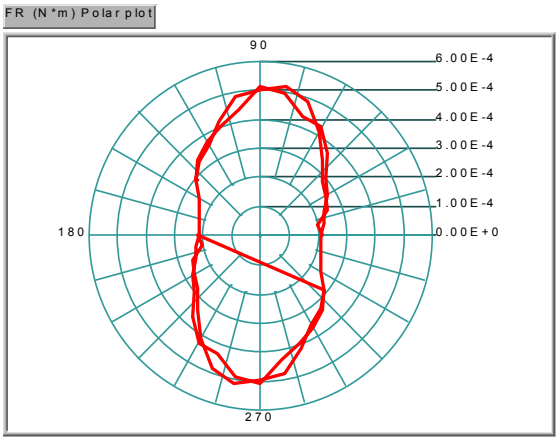

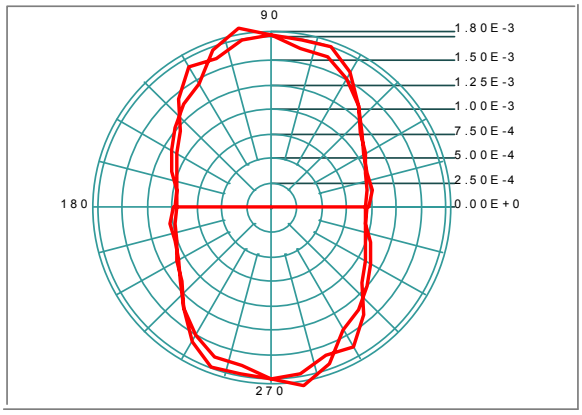

On Brass foil (50 µm thick), Out-of-plane displacements in the time-domain for a separation distance of 12 mm (top) and 30 mm (bottom).

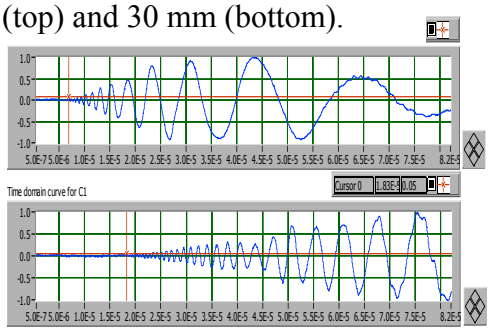

A typical displacement waveform image in the time and space domain. The horizontal axis is time in second, the vertical axis is the separation distance Dgd in mm from the generation laser spot to the detection laser spot.

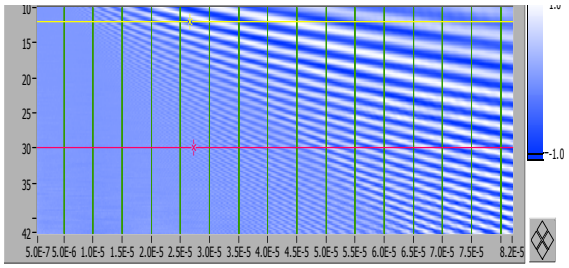

Dispersion of Ao waves on 50 µm thick brass, stainless steel:

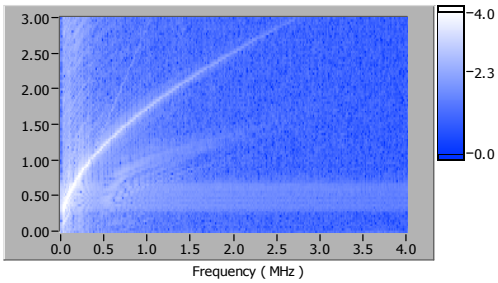

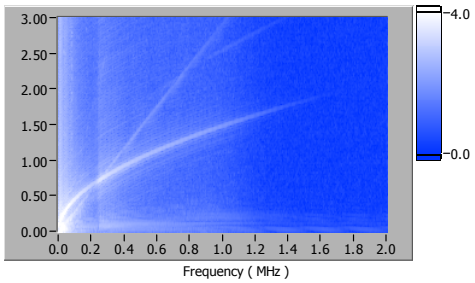

High order Lamb waves in 1.27mm Al plate:

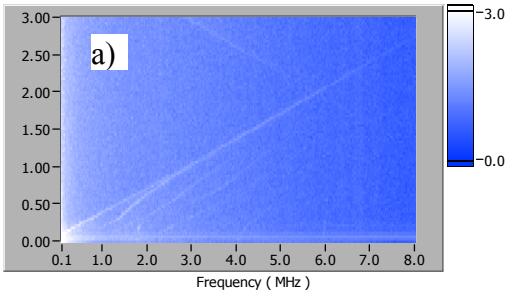

Band gaps on a phononic crystal:

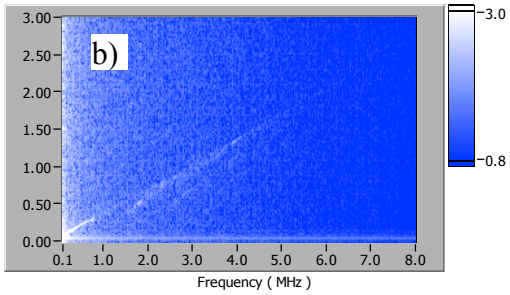

Time Domain displacement image and discrete A0 and S0 waves on 50 µm thick, 1mm wide brass stripe:

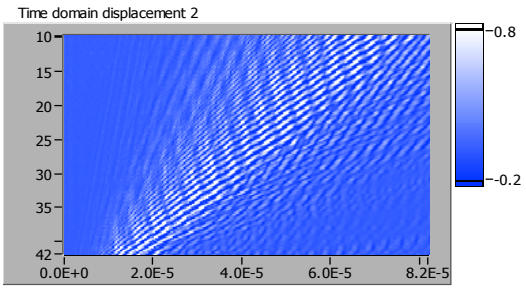

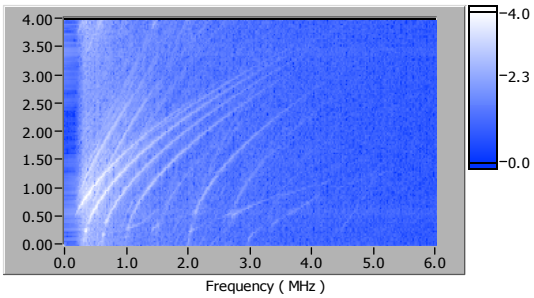

Trial of laser ultrasonics prototype system on Mead Paper's pilot coater in Chillicothe, OH, August 2001

*Note: this part of the report comes from a published article dedicated to the results of the prototype trial. The reference of the article is: "P. Ridgway, R. Russo, E. Lafond, C. Habeger, T. Jackson, "**Laser Ultrasonic System for On-Line Measurement of Elastic properties of Paper**", Journal of Pulp and Paper Science, **29**(9), pp. 289-293, September 2003"*

Abstract: A laser-based ultrasonic system for non-contact measurement of the elastic properties of paper was evaluated on a pilot paper coating machine operating at paper web speeds of up to 25.4 m/s (5,000 ft /min). Flexural rigidity and out-of-plane shear rigidity were calculated from the frequency dependence of the phase velocity of Ao mode Lamb waves. These ultrasonic waves were generated in the paper with a pulsed Nd:YAG laser. Fiber optic delivery of the generation pulse was demonstrated. Lamb waves were detected with a Mach-Zehnder interferometer coupled with a scanning mirror/timing system to compensate for paper motion. Six paper grades ranging in basis weight from 39 to 100g/m^2, and a 280g/m^2 paperboard were tested. For the six paper grades, the on-line laser-ultrasonic measurements of flexural rigidity agreed within experimental error with conventional laboratory contact ultrasonic measurements on stationary samples. The effects of web tension and moisture content on flexural rigidity measurements were quantified. The low frequency signal amplitude from the paperboard was insufficient for accurate measurements.

Introduction:
In laser ultrasonics (LUS), also known as laser-based ultrasonics, acoustic waves are generated with a pulsed laser in a material to determine one or more of its physical properties. These acoustic waves are monitored with a laser-based detector, usually a form of interferometer, without physical contact to the sample (vii). In this work, plate (Lamb) waves (viii) are detected several millimeters from the generation point as they propagate along the sheet. A diagram of this system is shown in Figure 1.

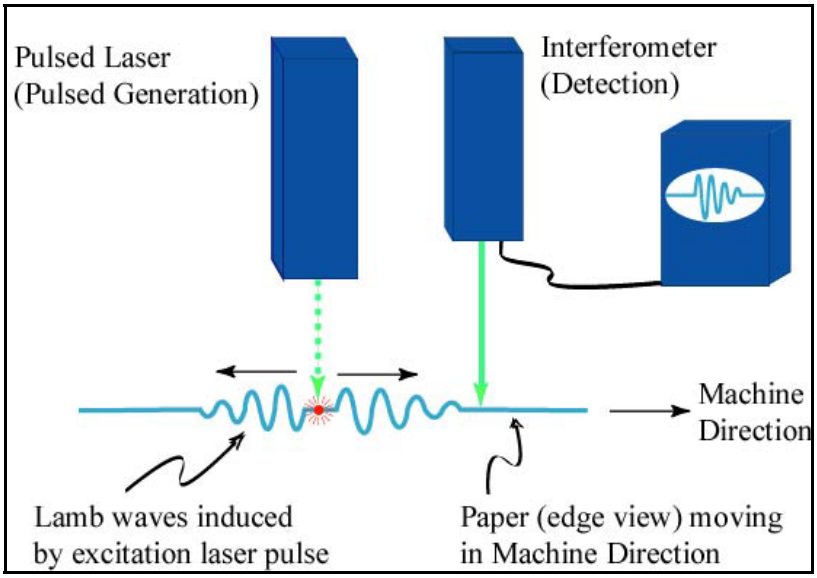

Figure 1. System for LUS analysis of paper.

Laser ultrasonics has been applied in recent years to measurement of mechanical properties of paper in the laboratory (ix,x). Further laboratory demonstrations of LUS on moving paper demonstrated the opportunity for routine measurement of these properties during manufacture, and for feedback control of the papermaking process based on these measurements (xi,xii). Further developments in signal processing and the results of the first (to our knowledge) demonstration of LUS on moving paper in an industrial setting are discussed in this paper.

LUS signal energy in paper goes predominantly into the zero order anti-symmetric (Ao) mode plate wave (ix). The Ao mode is characterized by relatively large (hundreds of nanometers) out-of plane displacements, which are easily detected with commercially available laser vibrometers. In this work, a Fourier transform, 'phase unwrapping' computational method was used to calculate two elastic properties from a phase velocity versus frequency dispersion curve that was constructed from two Ao wave signals (xiii). The properties are flexural rigidity (D) and out-of-plane shear rigidity, SR (for a homogeneous material shear rigidity is equal to shear modulus times caliper). Flexural rigidity differs slightly (it is about 9% larger) from bending stiffness (BS) through a term the depends on the in-plane Poisson's ratios (ν_{xy} and ν_{yx}):

$$D = BS/(1-\nu_{xy}\nu_{yx})$$

The flexural rigidity measurement comes primarily from the low frequency portions of the dispersion curve, whereas shear rigidity comes from the high frequency components. As basis weight decreases, the division between the high and low frequency regimes of the dispersion curve moves to higher frequencies. For low basis weight papers, there is little range for SR determination in our LUS frequency range (about 10 KHz to 600 KHz). In practice, this means that LUS methods provide good estimates of D and SR for paperboard products, but only good D values for conventional papers.

Bending stiffness is routinely measured in paper mill laboratories. Bending stiffness is of interest because it is closely related to flexural rigidity, which is the determining factor in the rigidity of paper sheets and structures. Of all the elastic parameters that could conceivably be measured on-line, flexural rigidity is the one most directly related to important end use performance and the one of most practical value. Out of plane shear rigidity is a sensitive indicator of fiber bonding and is an important contributor to in-plane compressive strength (xiv). In addition to monitoring end-use properties, on-line measurements of D and SR are potentially useful as inputs for feedback process control.

LUS measurements are complementary to contact ultrasonic techniques. Contact methods are applicable to the detection of low frequency zero order symmetric (S_0) plate waves (viii), in-plane shear horizontal plate waves, and out-of-plane bulk waves (xv,xvi,xvii,xviii,xix,xx). Rather than flexural and shear rigidity, contact methods provide determinations of planar stiffness, in-plane shear rigidity, and effective out-of-plane bulk stiffness. The contact transducer coefficients find application through correlation with strength properties, whereas flexural rigidity is of practical importance in its own right. Another advantage of LUS is that it does not require physical contact with the sheet, eliminating that potential cause of paper damage.

Experimental

The experimental system consisted of a pulsed Nd:YAG laser (New Wave Minilase III) which delivers a 5 nanosecond pulse at 1.06 μm for ultrasound generation, a Mach-Zehnder interferometer (Polytec-PI OFV303/OVD02) which includes a continuous, low-power (eye-safe) helium-neon laser source for detection, a scanning mirror to move the detection laser beam and track paper motion, and a timing system to fire the generation laser when the detection beam is in the proper position on the paper surface. The scanning mirror optics innovation was crucial. Without it, textural noise from the moving, rough paper surface under the detection laser would saturate the LUS signal. Details of the apparatus have been described previously (xi). The system has since been modified to rotate the scanning mirror with a feedback-controlled DC servomotor and to collect data with a personal computer equipped with an oscilloscope card (Gage Compuscope 1250) operated with LabView-based software.

An alternative fiber optic delivery system for the excitation beam was incorporated, as shown in Figure 2. Fiber optic delivery demonstrates the potential to position excitation laser at an arbitrary distance from the primary apparatus, thus reducing the size of the sensor-head and number of components mounted near the paper surface.

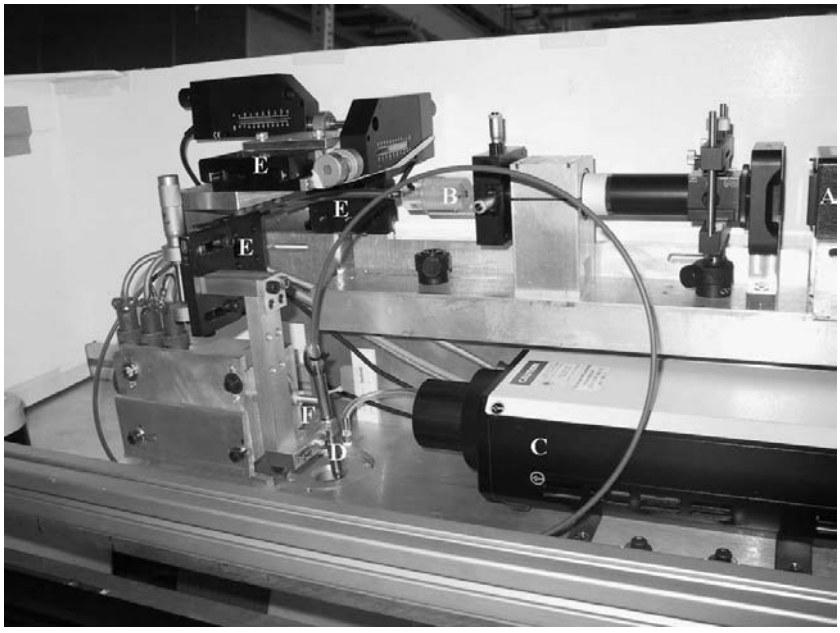

Figure 2. Optical fiber delivery system for excitation pulse. A: excitation laser; B: optical fiber insertion; C: Mach-Zehnder interferometer (detector); D: tube aligning optical fiber output and focusing lens; E: translation stages and motorized actuators for positioning the excitation spot in the MD and CD; F: spinning shaft holding the detector's scanning mirror (hidden)

The LUS system was installed on a pilot coating machine at the Mead (now MeadWestvaco) research facility in Chillicothe, Ohio (Figure 3). This machine drives a 76 cm (30") wide paper web at up to 25.4 m/s (5,000 ft/min) from a supply reel to a take-up reel. The LUS system was used to measure D and SR in the machine (MD) and cross (CD) directions at paper speeds up

to 25.4 m/s (5,000 ft/min). Moisture, MD web tension, basis weight and paper speed were independently varied to explore their effects on the measurements.

Figure 3. LUS system installed on pilot coating machine.

To generate the ultrasonic signal, the generation laser beam was focused on the sheet with a 150 mm focal length spherical lens. When the laser beam was delivered by the optical fiber, it was focused with a 10mm focal length aspheric lens. The laser pulse energies were as high as possible without causing visible damage to the paper, and ranged from 2 to 8 mJ. The detection interferometer beam was focused onto the paper at a position separated by either 5 or 10 mm from the position where the generation beam was focused.

Paper samples in 76 cm (30 inch) wide rolls 0.6 to 1.5 m (2 to 5 feet) in diameter were used in the tests. They included three uncoated white papers with basis weights of 39, 67, and 72 g/m^2, two coated white paper samples with basis weights of 93 and 99 g/m^2, and two uncoated papers with basis weights of 93 and 94 g/m^2 that were coated “upstream” from the LUS test stand. Data were also collected on an uncoated brown paperboard of basis weight 280 g/m^2. All the paper samples tested at MeadWestvaco Research were later analyzed by contact ultrasonics to obtain independent estimates of D and SR (xxi).

Test sheets were subjected, off-line, to laser shots at multiple locations under the same conditions used to generate the on-line ultrasound data. These paper samples were then printed with solid blocks of color in order to evaluate the damage from the laser shots. Laser marking of the sheets was very slight. MeadWestvaco print quality inspectors were able to locate some of the laser shots, but they considered the level of damage to be insignificant and well within product specifications.

LUS Signal Analysis

The Fourier transforms of two ultrasonic signals, recorded at different excitation-to-reception separations (d) (usually 5 or 10 mm), were used to calculate the phase velocity C as a function of angular frequency, ω. At each frequency, the phase velocity was calculated from the difference in separation, Δd, and difference in Fourier phase-$\Delta\varphi$,

$$C(\omega) = -\omega\Delta d/\Delta\varphi \quad .$$

A plot of the phase velocity versus frequency is known as a dispersion curve. In order to calculate values of D/(basis weight, BW) and SR/BW, an approximate relationship of c(to D/BWand D/SR,

$$c(\omega) = c^4+(D/SR)\omega^2c^2-(D/BW)\omega^2 = 0 \quad ,$$

was fitted to a selected region of the curve by an iterated, least square method. A proper determination of the dispersion equation requires the solution of a complex transcendental equation involving in-plane and out-of-plane elastic properties (viii,xx). For the Ao mode at low frequencies, wave motion can be modeled with beam equations. The above, simplified dispersion equation is easily derived if deformation is taken as the sum of shear and bending deformations, plane sections of the beam are assumed to remain planar during wave motion, and rotational inertia is ignored. We made mathematical comparisons between the full and approximate dispersion equation for typical papers in the frequency range of our measurements and found very small differences (xxii).

A partially automated Lab View program was used for data acquisition, signal averaging and curve fitting. Ten to twenty signals at each separation were averaged. The resulting pair of signals and the web basis weight were used to calculate D and SR. For a single data collection run on a given paper sample, multiple measurements are reported as an average value with a standard deviation.

Results

Effect of Web Speed

LUS measurements were made on three uncoated papers as the web speed was increased incrementally to the upper limit of the machine. Tables 1 and 2 document the results. The data show that the measured D and SR are not affected by web speed, within experimental error.

Web Speed/ Basis Wt.	5.1 m/s (1kfpm)	10.2 m/s (2kfpm)	20.3 m/s (4kfpm)	25.4 m/s (5kfpm)
72 (g/m^2)		3.9 ± 0.7	4.1 ± 0.3	3.9 ± 0.2
67 (g/m^2)		4.7 ± 0.5		5.3 ± 0.2
39 (g/m^2)	1.8 ± 0.2	1.8 ± 0.2		

Table 1. Effect of web speed on LUS measurement of flexural rigidity (*10^{-4} N*m)

Web Speed/ Basis Wt.	5.1 m/s (1kfpm)	10.2 m/s (2kfpm)	20.3 m/s (4kfpm)	25.4 m/s (5kfpm)
72 (g/m^2)		3.0 ± 0.2	2.88 ± 0.02	3.1 ± 0.2
67 (g/m^2)		2.3 ± 0.6		2.1 ± 0.2
39 (g/m^2)	0.63 ± 0.09	0.590± 0.001		

Table 2. Effect of web speed on LUS measurement of shear rigidity (*10^4 N/m)

Correlation with Contact Measurements

The online LUS values at the running moisture content were compared to contact ultrasonics measurements made in a laboratory at 50% relative humidity. If one assumes that paper is homogeneous and of known thickness, contact ultrasonic analyses of So waves can be used to estimate D (xxiii). Specifically, for contact ultrasonics the flexural rigidity (D) is computed as

$$D = V_{S0}^2 BWt^2/12$$

from the velocity of the low-frequency (70 kHz) portion of the S_0 Lamb wave (V_{S0}), the basis weight (BW), and the caliper (t). The validity of this computation rests on the dubious assumption that paper is a homogeneous plate of well-defined and uniform thickness. However, paper stiffness values vary through the thickness, its surface is very irregular, and thickness determinations are notoriously dependent on the surface conformability of the caliper platens and on the mechanical load under which thickness is measured. The wave properties monitored in the LUS technique provide a more direct and therefore more reliable measure of flexural rigidity, because no assumptions are made about sheet thickness. Nevertheless, D calculated from the contact ultrasonic measurement should be within 20-40% of the true value of the flexural rigidity, and a comparison provides a sanity check.

The out-of-plane shear rigidity (shear modulus times caliper, SR) can be calculated from the contact out-of-plane shear velocity (V_{ZS}), the basis weight (BW) and the caliper (t)(xxiii):

$$SR = V_{ZS}^2 BWt$$

However, paper thickness and time-of-flight measurements are both required to determine V_{ZS}. Once again, the LUS measurement of SR is a more direct and reliable measurement than the contact ultrasonic technique because the latter relies on (the cube of) an estimate of sheet thickness (caliper).

Laser-ultrasonic flexural rigidity measurements in the MD and CD on all paper types except 280g/m^2 paperboard were compared to the contact transducer–based results (Figure). A linear fit to the data and a line representing 1:1 correspondence between contact and LUS measurements show the overall close correspondence between the two techniques.

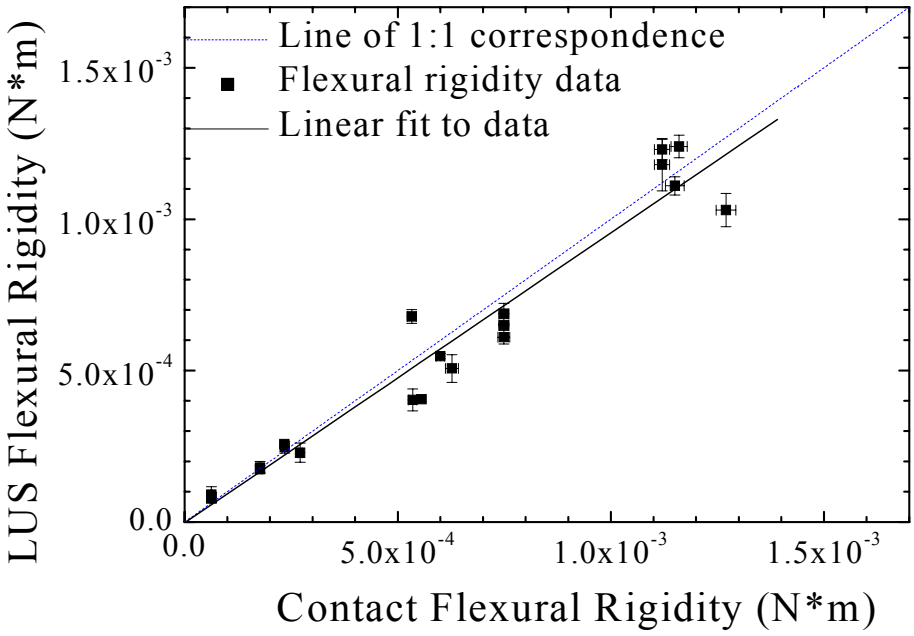

Figure 4. Correlation of flexural rigidity values derived from LUS with contact transducer measurements.

The vertical error bars on the data points in Figure 4 indicate a variance of approximately 10% for LUS determined flexural rigidity. From laboratory experience, this reflects the real variability in paper properties rather than uncertainties in measurement. Over the short span (5mm) of the LUS measurements, variations of this magnitude are expected in paper. Due to these local variations in D, timely, meaningful measurements of average paper mechanical properties can be realized only by averaging a large number of on-line measurements.

Laser-ultrasonic measurements of SR, in the MD and CD, were compared to contact transducer–based results (Figure 5). As indicated by the large error bars, this measurement is much less reliable than the measurement of D, whether by laser or contact ultrasonics. Also, the correlation between contact and LUS measurements of SR is much weaker. This discrepancy may be due to the lack of sufficient high frequency content in the LUS signals. The high frequency components of the signal strongly affect the SR measurement; and high frequency components of the acoustic wave tend to damp out more rapidly in paper.

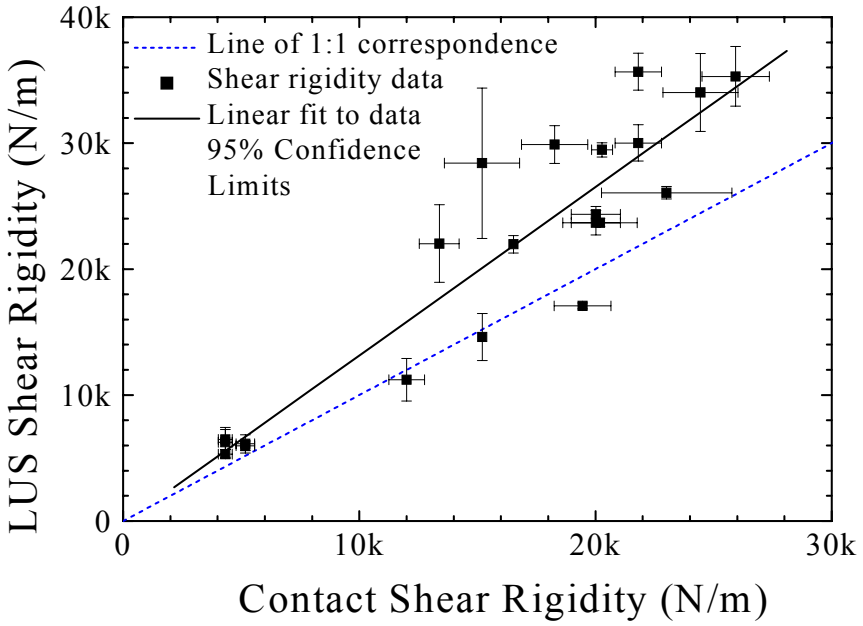

Figure 5. Correlation of shear rigidity values derived from LUS with contact transducer measurements.

Effect of moisture

A 95 g/m^2 pre-coated, white paper was first tested “dry” (moisture content: 3.0 wt-%), and then re-measured with moisture applied at one of the coater stations to allow a “wet” (moisture content: 6.8 wt-%) test. A Comparison (Table 3) of the results of these two runs provides an on-line demonstration of the influence of moisture on D and SR. The mean flexural rigidity in the MD was 16 ±3% lower and in the CD was 9 ±4% lower for the moistened paper. For each weight-percent increase in moisture, the MD flexural rigidity decreased 4.2% and the CD flexural rigidity decreased 2.4%. The moisture effect on SR was less than the experimental variability (6%).

Measurement Axis	MD		CD	
Moisture Content (wt-% water)	2.96 ± 0.04 (Dry)	6.8 ± 0.6 (Wet)	2.96 ± 0.04 (Dry)	6.8 ± 0.6 (Wet)
D ± std. dev. of mean (x10^{-4}N*m)	11.8 ± 0.05 (3x avg)	9.9 ± 0.3 (4x avg)	6.50 ± 0.03 (3x avg)	5.9 ± 0.2 (3x avg)
SR± std. dev. of mean (x10^{4}N/m)	3.36 ±0.09 (3x avg)	3.0 ± 0.07 (4x avg)	2.4 ± 0.1 (3x avg)	2.43 ± 0.04 (3x avg)

Table 3. Effect of Moisture on LUS measurements on pre-coated white 95 g/m^2 paper

Laboratory experiments on "copy paper" (approximately 80 g/m^2) over a different moisture content range (5-10%), resulted in a three percent decrease in MD flexural rigidity *per* percentage increase in moisture content (xxiv). The experimental methods, the conditions and the paper sample in the laboratory study were different. However, the results of those studies agree, and both studies show that flexural rigidity is sensitive to increasing moisture. Moisture content must be taken into account when evaluating flexural rigidity measurements.

Effect of Tension

From a theoretical point-of-view (xxiii), web tension on very lightweight papers should cause a detectable increase in phase velocity at the low frequency end of the A_0 dispersion curve. If (as was the case) tension is not taken in account in the elastic constant determination, tension should lead to an apparent increase in flexural rigidity (which is predominantly calculated from the low frequency portion of the dispersion curve) and to no change in shear rigidity (which comes from the high frequency portion). An experiment was conducted on the lowest basis weight grade to see if the flexural rigidity effect manifests itself in the on-line testing measurement. Machine direction tension was set at 2.6 and 4.4 N/cm (1.5 and 2.5 lb/in) during measurements on a 39 g/m^2 uncoated white paper. The average MD flexural rigidity rose about 6% from 1.75 10^{-4} Nm to 1.86 10^{-4} Nm as tension was increased (Table 4). At the 2.6 N/cm (1.5 lb/in) setting, seven on-line measurements were made, and the standard deviation was 0.11 10^{-4} Nm. Thus, the standard deviation in the mean was 0.04 10^{-4} Nm. Four measurements were made at 4.4 N/cm (2.5 lb/in), the standard deviation was 0.08 10^{-4} Nm and the standard deviation in the mean was 0.04 10^{-4} Nm. Consistent with theoretical expectations tension experiments in the laboratory produced an apparent 10% change in MD flexural rigidity on this paper grade over this tension range (xxiii). This value compares well with the on-line measurement. The on-line tension effect on lightweight papers was statistically significant and of the expected magnitude.

Measurement Axis	MD		CD	
MD Tension N/cm (lb_f/in)	2.6 (1.5)	4.4 (2.5)	2.6 (1.5)	4.4 (2.5)
D $\pm$ std. dev. of mean (x10^{-4}N*m)	1.75 $\pm$ 0.04 (3x avg)	1.86 $\pm$ 0.04 (3x avg)	0.9 $\pm$ 0.1 (3x avg)	0.8 $\pm$ 0.05 (3x avg)
SR$\pm$ std. dev. of mean (x10^4N/m)	0.60 $\pm$ 0.02 (3x avg)	0.585 $\pm$ 0.006 (3x avg)	0.53 $\pm$ 0.02 (3x avg)	0.65 $\pm$ 0.03 (3x avg)

Table 4. Effect of tension on LUS measurements on uncoated white 39g/m^2 paper

Paperboard Results

Laser ultrasonic analysis of the brown paperboard (basis weight of 280 g/m^2) was much less reproducible and had a poor correspondence with contact measurements. These results reflect those obtained with the Mach-Zehnder interferometer in the laboratory, where accurate flexural rigidity can be extracted from data collected from paper samples of basis weights up to 165 g/m^2. LUS and contact transducer-based measurements on this sample are given in Table 5. Flexural rigidity measured by LUS was much lower than that obtained by contact ultrasonics, especially in the cross direction.

Measurement Axis		MD		CD	
Measurement Type		LUS	Contact	LUS	Contact
D ± std. dev. of mean ($x10^{-2}$N*m)	Trial 1	1.14 ± 0.04 (4x avg)	3.67 ± .02 (8x avg)	0.31 ± 0.08 (7x avg)	1.79 ± 0.01 (8x avg)
	Trial 2	2.8 ± 0.3 (10x avg)		0.47 ± 0.07 (5x avg)	
SR ± std. dev. of mean ($x10^{4}$N/m)	Trial 1	4.7 ± 0.2 (4x avg)	5.1 ± 0.2 (10x avg)	3.3 ± 0.2 (7x avg)	4.8 ± 0.1 (10x avg)
	Trial 2	4.0 ± 0.2 (10x avg)		4.2 ± 0.7 (5x avg)	

Table 5. Comparison of LUS and contact measurements of flexural rigidity and shear rigidity on 280g/m^2 paperboard

Generally, as basis weight increases, there is a decrease in the upper limit of the frequency range over which Ao phase velocity depends almost exclusively on D. The inaccurate results on the 280 g/m^2 paperboard indicate a necessity to monitor lower frequencies than could be detected with the sensor as configured.

There is a lower limit to the frequencies that can be detected with the online sensor (at a given web speed) due to the changing optical path length associated with the detection system's spinning mirror. The low-frequency sensitivity of the Mach-Zehnder detector is well matched to the rest of the sensor system in that the aforementioned changing optical path length does not saturate the detector. Methods for increasing the amplitude of the low-frequency components of signals on heavy grades are under investigation, with the goal of enhanced detection of lower frequencies in the online sensor.

In the meantime, for laboratory laser ultrasonic measurements on stationary paper, we use a Two Wave Mixing (TWM) interferometer which is much more sensitive to lower frequencies, resulting in accurate flexural rigidity measurements on grades with basis weights up to 210g/m^2.

Figures 6 and 7 are re-plots of the data in Figures 4 and 5 with the paperboard data added to show that the paperboard is significantly stiffer than the other paper grades, and to show that there is much less agreement between the contact and laser ultrasonic measurements for the paperboard than for the other samples.

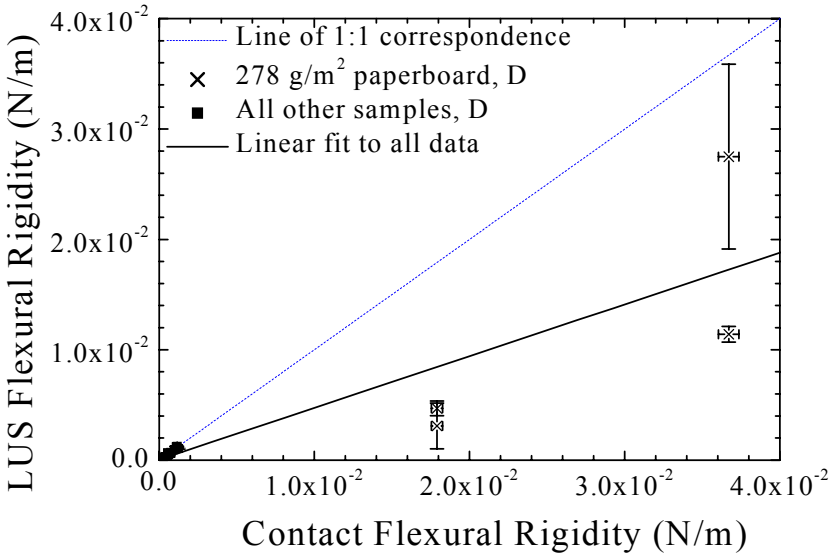

Figure 6. Correlation of flexural rigidity values derived from LUS versus contact transducer measurements, including paperboard data.

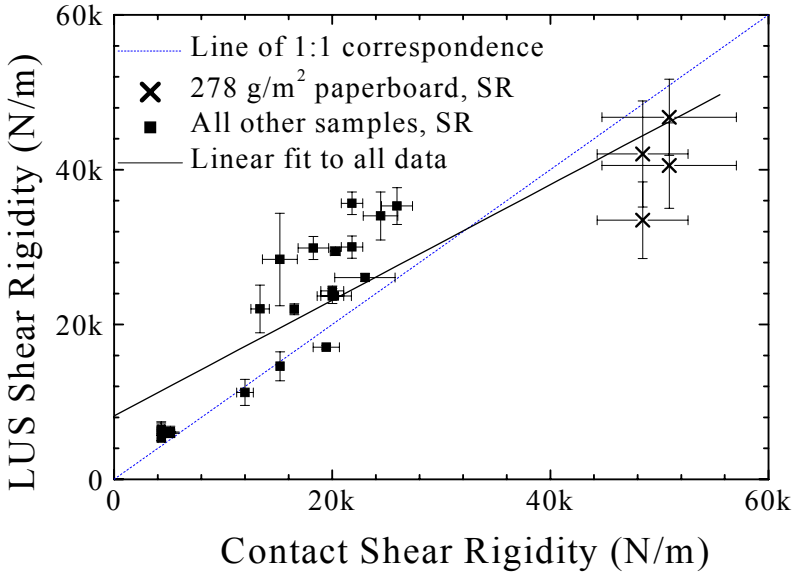

Figure 7. Correlation of shear rigidity values derived from LUS versus contact transducer measurements, including paperboard data.

Summary

Laser ultrasonic measurement of paper flexural rigidity has been demonstrated in an industrial environment on paper webs moving at speeds up to 25.4 m/s (5,000 ft/min). To our knowledge, this is the first time that elastic parameters measurements have been reported at such high web speeds on paper. The flexural rigidity measurements for papers with basis weights up to 100 g/m^2 agree well with contact transducer-based measurements in the lab.

The data confirm that flexural rigidity is strongly affected by moisture. To allow comparison of flexural rigidity and shear rigidity properties of different paper samples, and to permit specifications for flexural rigidity and shear rigidity to be established, specifications must include a moisture content, and the measurements must be corrected to the value at that moisture content.

The influence of MD tension on the online flexural rigidity measurements compares well with theoretical predictions and laboratory experience.

Acknowledgment:

We thank Rick Goodlin of MeadWestvaco Corp. and Brad Pankonin of ABB Corp. for consultation and appreciation to Mead (MeadWestvaco) Corp. for providing equipment, facilities and support personnel for the Research Facility trial. The research was supported by the Department of Energy, Office of Industrial Technologies, Agenda 2020, American Forest Products and Paper Industry Sensors and Controls Task Group, through Gideon Varga under Contracts No. DE-AC03-76SF00098 and DE-FC07-97ID13587.

References

(1) Scruby, C. B. and Drain, L. E. “Laser Ultrasonics, Techniques and Applications”, Adam Hilger, NY 1990.
(2) Graff, K. F., “Wave Motion in Elastic Solids”, Dover, New York, (1975)
(3) Johnson, M. A, PhD Thesis, Georgia Institute of Technology (1996)
(4) Berthelot, Y.H. and Johnson, M. A. “Laser Ultrasonics in Copy Paper” Opt.Eng. 36(2):408-416 (1997)
(5) Ridgway, P.L.,Hunt, A.J., Quinby-Hunt, M., and Russo, R.E., “Laser Ultrasonics on Moving Paper”, Ultrasonics 37:395-403 (1999)
(6) B. Pouet, E. Lafond, B. Pufahl, D. Bacher, P. Brodeur, and M. Klein, “On-Machine Characterization of Moving Paper Using a Photo-Emf Laser Ultrasonics Method”, SPIE Conference on Nondestructive Evaluation Techniques for Aging Infrastructure & Manufacturing/Process Control and Sensors for Manufacturing, Newport, CA, SPIE **3589**:160 (1999)
(7) Jong, J.H., Brodeur, P.H,Lafond E.F., Gerhardstein J.P., and Pufahl B.M. “Laser Ultrasonics for Noncontact Measurement of Lamb Waves in Static and Moving Paper”, J Pulp Paper Sci 26(10):358-366 (2000)
(8) Habeger, C.C. and Whitsitt, W.J.,”A Mathematical Model of Compressive Strength in Paperboard” Fiber Sci. and Tech. 19:215 (1983)
(9) Baum, G. A., and Habeger, C. C., “On-line Measurement of Paper Mechanical Properties”, Tappi 63(6):63-66 (1980)
(10) Habeger, C. C., and Baum, G. A., “On-line Measurement of Paper Mechanical Properties”, Tappi 69(6):106-111 (1986)

(11) Vahey, D. W., “Ultrasonic-Based Strength Sensor for On-Line Measurements”, Tappi 70(3): 79-82 (1987)
(12) Pankonin, B., and Jimmerson, D., “Mill Experiences with On-Line Ultrasound-Based Stiffness Measurement”s, 1999 Engineering/Process and product quality conference and trade fair, Anaheim, CA, USA, 12-16 Sept. 1999, vol. 2:919-928
(13) Hall, M. S., “On-Line Ultrasonic Measurement of Strength in Paper”, Sensors 7(7):13-20 (1990)
(14) Habeger, C. C., Mann, R. W., and Baum, G. A., “Ultrasonic Plate Waves in Paper”, Ultrasonics, 17:57-62 (1979)
(15) Contact measurements and the corresponding calculations of flexural rigidity and shear rigidity were made at the Institute of Paper Science and Technology (IPST), Atlanta, GA, USA
(16) Unpublished work of Chuck Habeger and Ted Jackson, Institute of Paper Science and Technology (IPST), Atlanta, GA, USA
(17) Habeger, C. C., “Ultrasonic Determinations of Paper Stiffness Parameters”, p257-312 in “Handbook of Physical Testing of Paper”, Vol 1, Mark, R.; Habeger, C.; Borch, J.; and Lyne, M. eds., Marcel Dekker, New York (2001)
(18) Cornwell, M, and Berthelot, Y.H. **“**Noncontact Determination of the Bending Stiffness of Paper Using Laser Ultrasonics and Wavelet Analysis: Effects of Moisture and Temperature”, IEEE ultrasonics conference in Atlanta, Oct 7-10, 2001
(19) Lafond, E.F., Brodeur, P.H., Gerhardstein, J.P., Habeger, C.C., Telschow, K.L., “Photorefractive interferometers for ultrasonic measurements on paper”, Ultrasonics 40: 1019-1023 (2002)

On-line sensor for full scale mill trial (preparation for Escanaba) - Jan. 2003 - June 2004

We are already preparing for the full scale mill demonstration trials and plan to visit our potential host mill this month (April 2003).

Using experience from the August 2001 pilot machine trial, we need to harden, automate, and repackage the laser ultrasonic instrumentation. We need to show the Dept. of Energy that the sensor will work as well on a real paper machine as on a pilot coater. Elastic constants will be reported in real time.

LBNL is leading the hardware development of the on-line sensor at Berkeley, CA using their miniaturized interferometer. IPST provides some hardware (such as web stabilizer; fiber optic launch and fiber optic for generation laser) and almost all the software that is necessary to acquire the raw data, to process it so as to extract the flexural rigidity and shear rigidity on real time, and store it for later retrieval.

We plan to do the full scale mill trial this coming summer or fall and install the sensor during a scheduled mill shutdown. We will then observe the evolution of the flexural rigidity in real time, record it, and also record the other physical properties of the web.

During the mill trial we intend to collect paper samples and compare the on-line stiffness data with the off-line post-production test routinely made by the mill's testing laboratory. After the mill trial, we will compare the results of on-line flexural rigidity with the off-line results (Tabor bending stiffness) and we expect to find a good correlation of the trend.

We anticipate the testing to occur on a light-weight uncoated grade. In the continuation of the project there is a need for extending the instrument's capability above 165 g/m^2, towards linerboards.

Next fiscal year we plan to start a long-term installation (6 months to 1 year) of the sensor in a mill, to devise process control strategies with the mill's process control engineers.

SUMMARY OF RESULTS AND KEY CONCLUSIONS ABOUT ON-LINE SENSOR:

Sensor hardware development in preparation for a full scale mill trial at Escanaba, MI, MeadWestvaco mill:

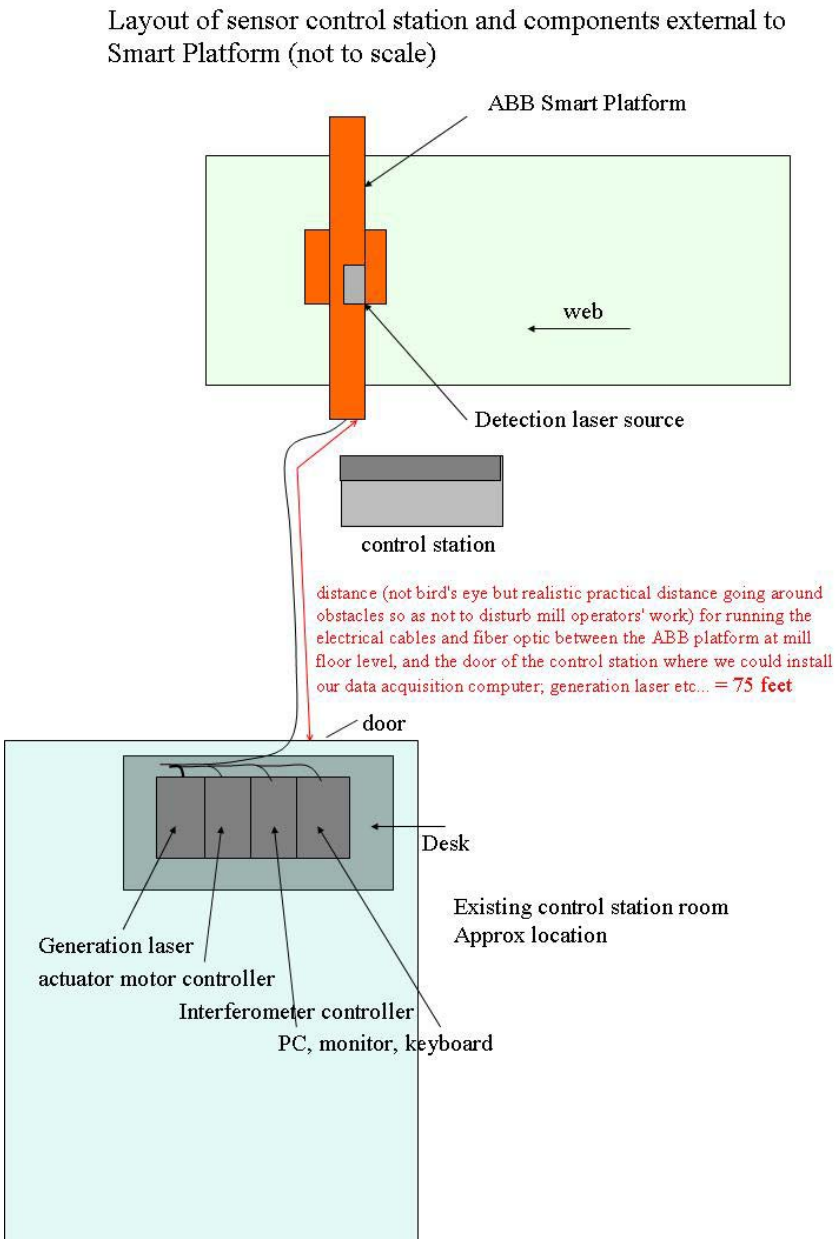

General layout of sensor system for installation planned at Escanaba, MI mill.

Hereafter we show some of the CAD drawings used to produce a miniaturized version of the on-line stiffness sensor.

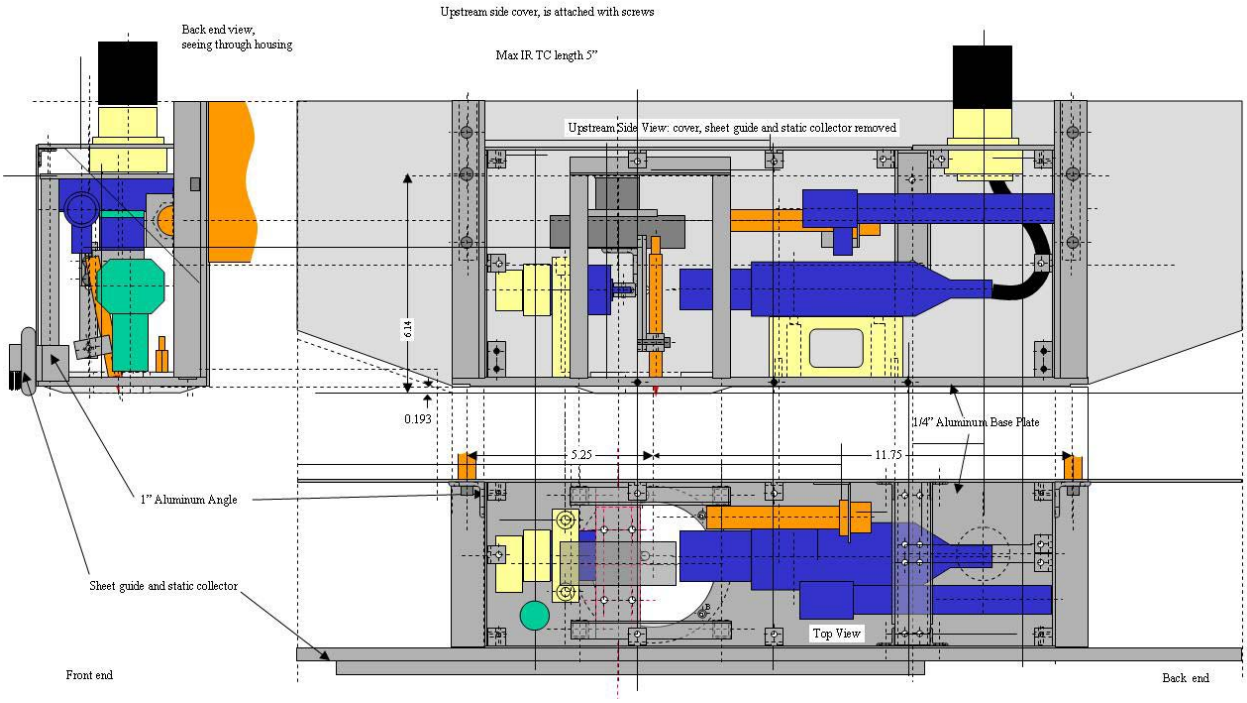

Back side of sensor housing

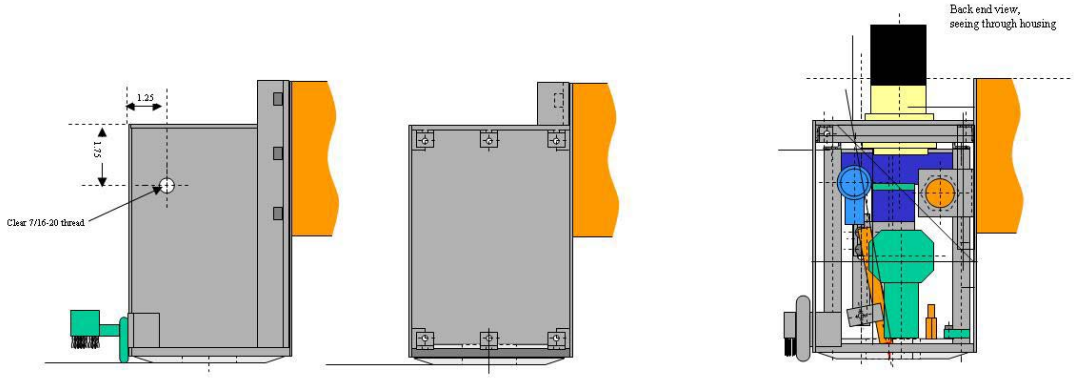

Some CAD drawings for the sensor module to be attached to the ABB scanning head on the ABB platform across the web (task done mostly by LBNL).

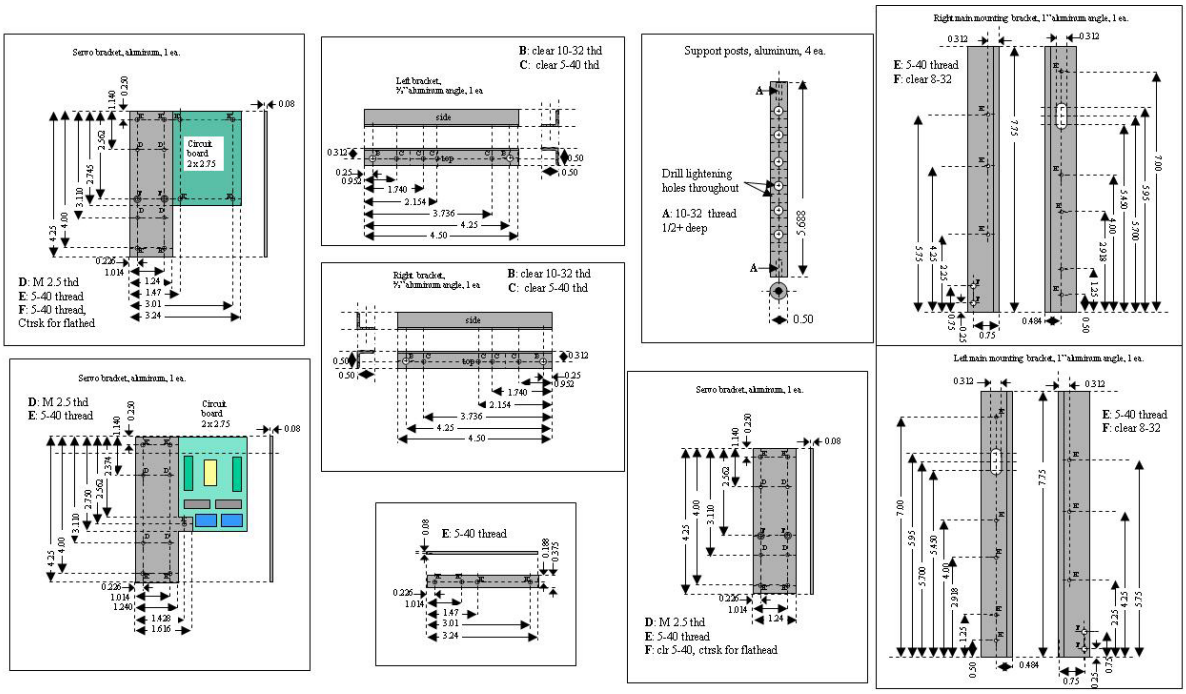

Some CAD drawings for the sensor module to be attached to the ABB scanning head on the ABB platform across the web (task done mostly by LBNL).

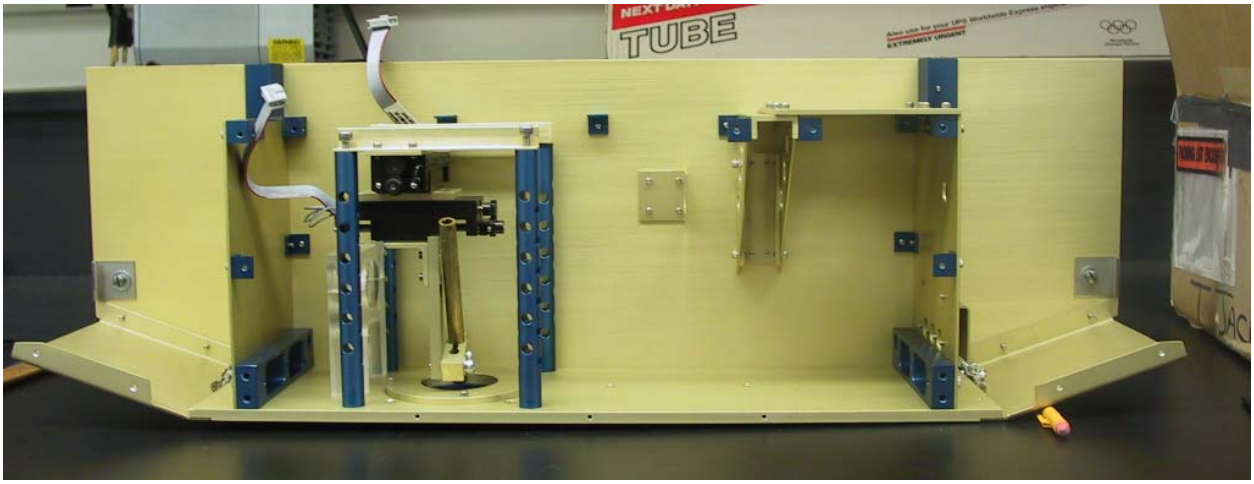

Stiffness sensor module partly assembled

Miniaturized interferometer before its integration inside the module

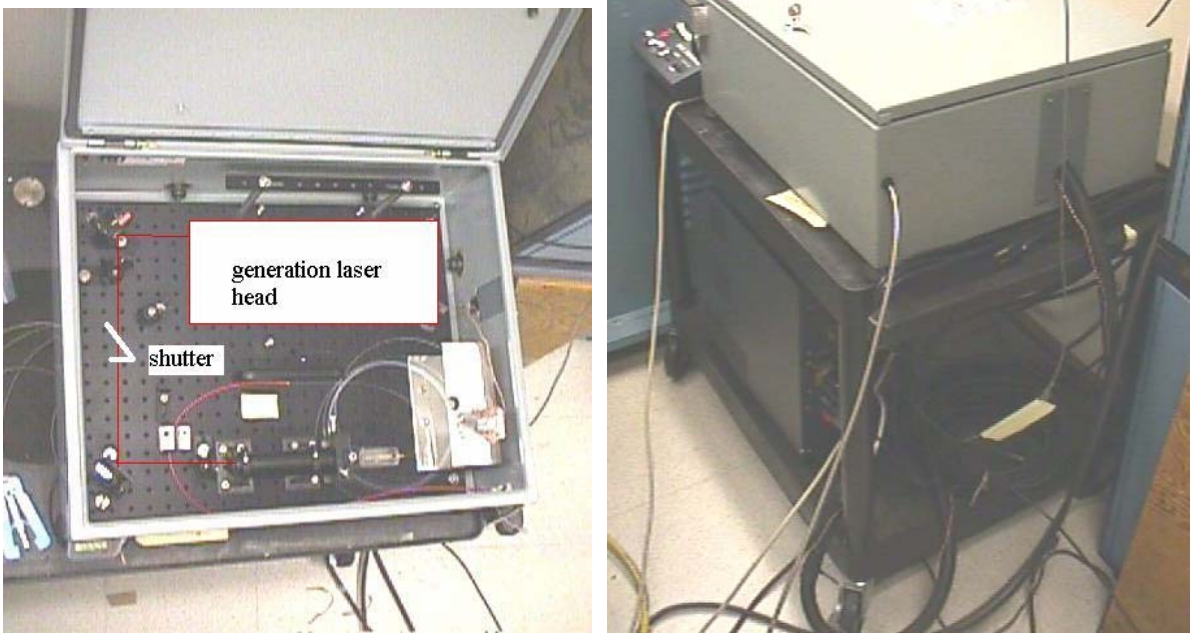

Pictures of generation laser subsystem

Auxiliary subsystem supplying power to motors and spinning mirror, purge air and cooling to sensor module, and air to the Bernoulli plate (web stabilizer)

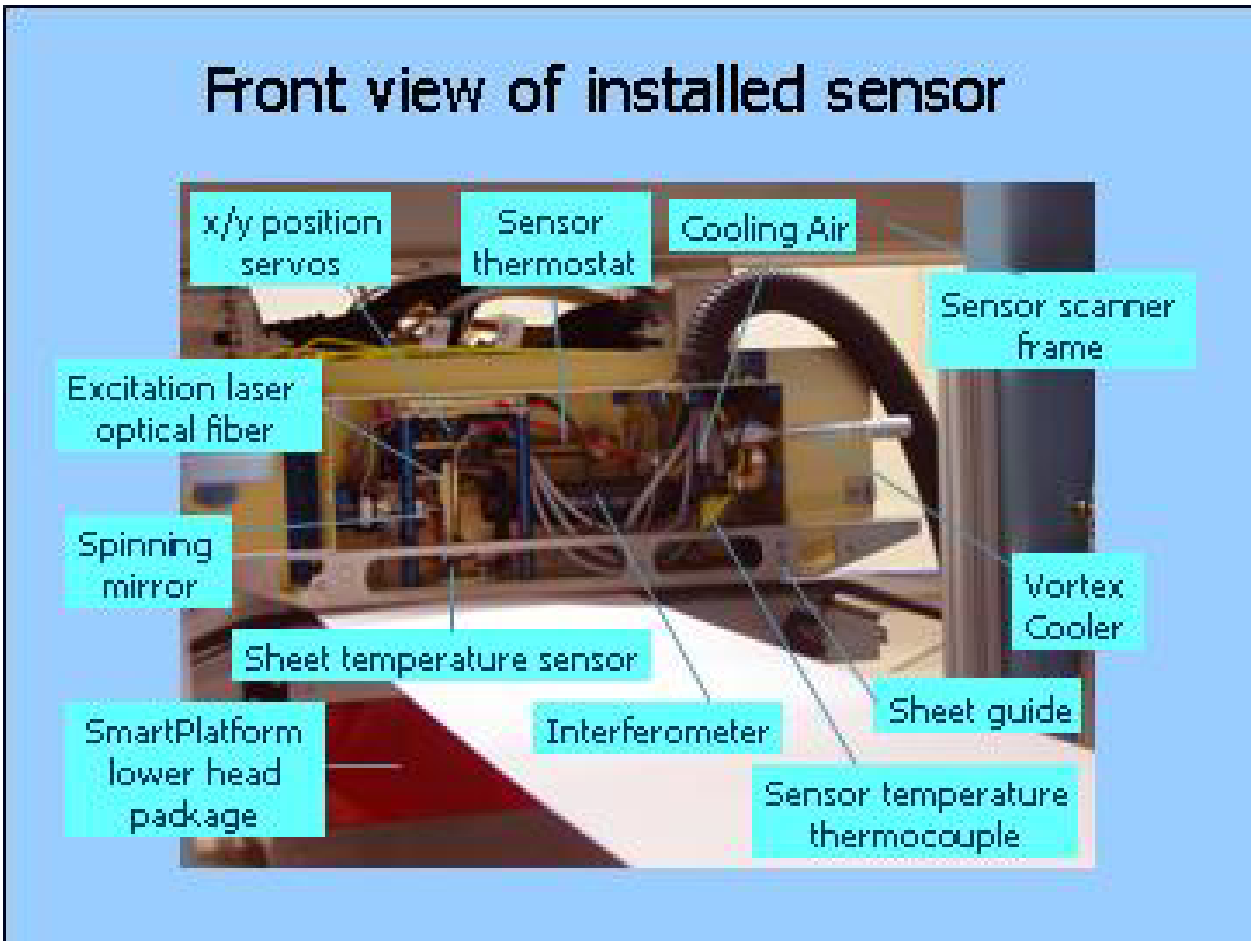

Sensor in action during shake down trials on IPST web handler in winter-spring 2004. The web speed was from 5 m/s to 10 m/s.

Side view of sensor during shake down trial on IPST web handler in winter-spring 2004. Note the sensor is attached to the ABB scanner head and scans the web thanks to the ABB scanner head like the other sensors do.

Sensor software development:

Calculation Efficiency

For static specimens (i.e. static interferometer beam direction mirror), the maximum rate at which individual stiffness measurements can be made with the on-line instrumentation is limited by the maximum firing rate of the excitation laser (approximately 10 shots/sec). For moving paper, the maximum theoretical rate would be a function of the distance between the moving paper and the interferometer beam steering mirror and of the speed of the paper under the steered beam, so long as that theoretical rate is less than or equal to the 10 shots/sec maximum rate. When the theoretical rate exceeds the emission laser's maximum rate, the theoretical rate must be integrally subdivided (i.e. every other mirror rotation) to bring the theoretical rate below the max.

Since, the theoretical limit of the effective rate (with or without subdivision) can reach that max rate in some cases, it was decided that the 10 Hz rate should serve as the natural measurement rate bottleneck of the instrument and that supporting software and electronics should be designed so as to be fast/efficient enough to support that rate.

Achieving that goal represented a considerable computational challenge. In support of it, the acquisition and analysis software (originally borrowed from the software developed for the laboratory LUS instrument) was streamlined for greater speed. Additionally, fast, multi-processor pc hardware was integrated. Also, other necessary supporting functions (mirror spin rate monitoring and control, web speed monitoring, cross direction scanning head position monitoring, basis weight, moisture, temperature data collection) were designed so as to make fullest use of available hardware in such as way as to be transparent to the pc's processor and thereby free it from most of the burden of supporting those tasks (i.e. using transparent hardware counters for timing functions, buffered analog input functions, etc). Additionally, other design choices were made so as to perform necessary computational tasks (i.e. data waterfall

display) at the momentarily motionless ends of CD scans so as to leave the processor relatively unburdened during the scans themselves so as to devote itself fully and uninterruptedly to the considerable task of performing the signals analysis itself (i.e. Fourier transforms, non-linear fitting, etc).

Those goals were achieved, and the sensor can achieve the maximum 10 measurements per second rate of the emissions laser. That strategy will provide the best quantity of data, statistics and measurement resolution possible with the current excitation laser embodiment.

Signal Duration Limiting

The later arriving portions of the A0 signal always contain some unwanted artifacts due to late arriving reflections from the walls of the Bernoulli plate and other surfaces through which the emission and interferometer optics emit and transducer signals. Previously, we did not have an effective method for dividing the near-ideal, early-arriving portions of the signal from the latter portions. That deficiency was remedied by progressively attenuating a portion of the signal of arbitrary and selectable width falling beyond the early-arriving near-ideal portion of the signal (the region marked by the right-most two cursors as shown below). At the middle cursor, the signal is passed without attenuation. To the right of the right-most cursor, the signal is entirely attenuated. In between those two cursors, the signal is progressively attenuated according to a half Hanning window. The attenuated and unattenuated signals are shown in black and green respectively. The progressive attenuation helps to keep the Fourier phase (from which the flexural and shear stiffnesses are derived) smoother and closer to that of an ideal A0 signal, resulting in a further improvement in the quality and consistency of the signal analysis.

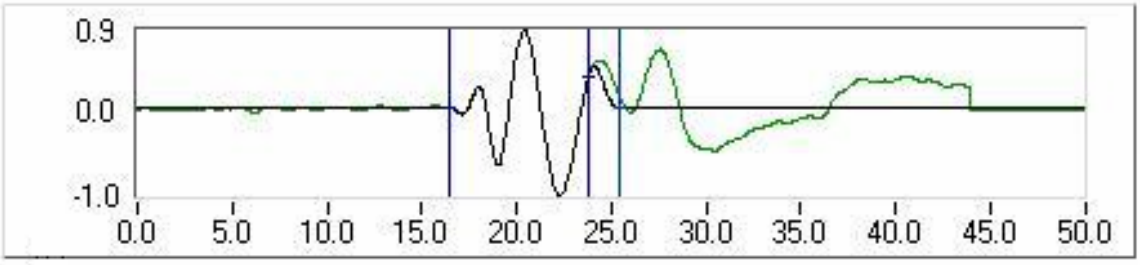

Supporting On-line Electronics and ABB Smart Platform Interfacing

A number of supporting electronics have been designed and built to interface with the ABB scanner to acquire variables necessary to the stiffness measurements and sensor operation (i.e. basis weight signal and shutter interlock state, moisture and CD position) were constructed with the assistance and advice of ABB. Some of these are illustrated in the figures below:

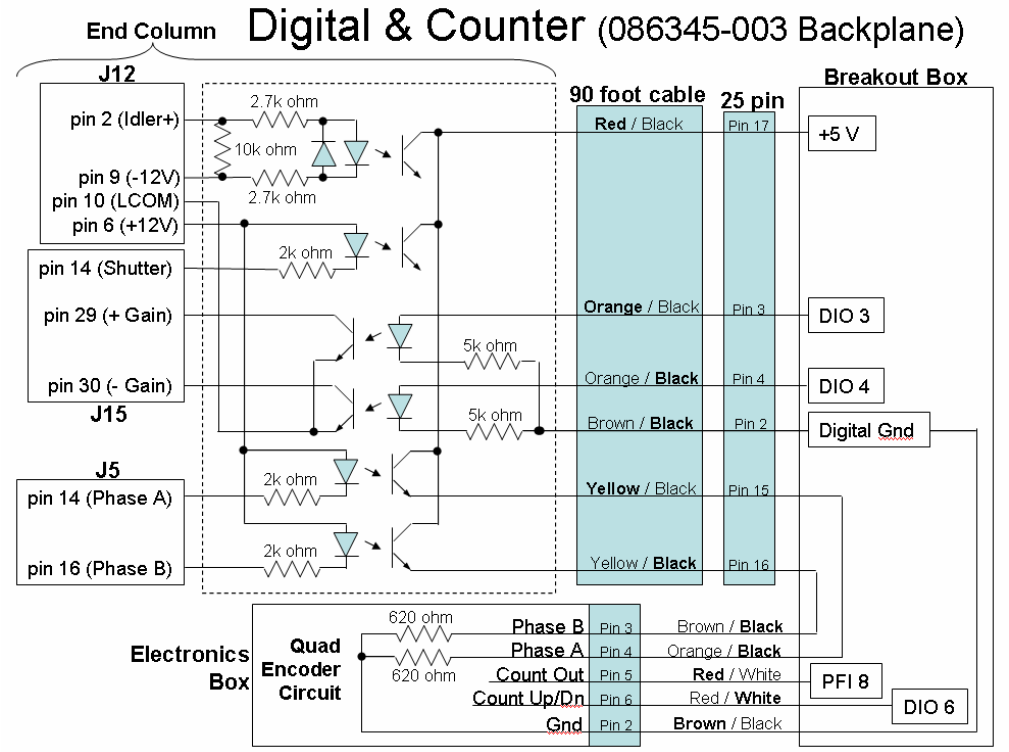
End Column
Digital & Counter (086345-003 Backplane)
J12
pin 2 (Idler+)
pin 9 (-12V)
pin 10 (LCOM)
pin 6 (+12V)
pin 14 (Shutter)
pin 29 (+ Gain)
pin 30 (- Gain)
J15
J5
pin 14 (Phase A)
pin 16 (Phase B)
2.7k ohm
10k ohm
2.7k ohm
2k ohm
5k ohm
5k ohm
2k ohm
2k ohm
90 foot cable
25 pin
Breakout Box
Red / Black
Pin 17
+5 V
Orange / Black
Pin 3
DIO 3
Orange / Black
Pin 4
DIO 4
Brown / Black
Pin 2
Digital Gnd
Yellow / Black
Pin 15
Yellow / Black
Pin 16
Electronics Box
Quad Encoder Circuit
620 ohm
620 ohm
Phase B
Phase A
Count Out
Count Up/Dn
Gnd
Pin 3
Pin 4
Pin 5
Pin 6
Pin 2
Brown / Black
Orange / Black
Red / White
Red / White
Brown / Black
PFI 8
DIO 6

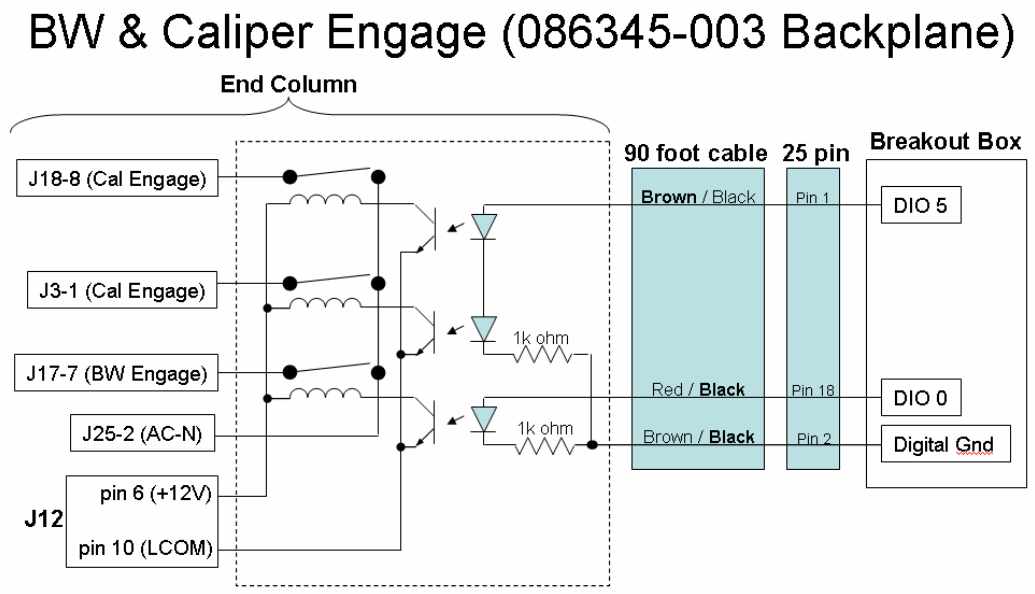
BW & Caliper Engage (086345-003 Backplane)
End Column
J18-8 (Cal Engage)
J3-1 (Cal Engage)
J17-7 (BW Engage)
J25-2 (AC-N)
J12
pin 6 (+12V)
pin 10 (LCOM)
1k ohm
1k ohm
90 foot cable
25 pin
Breakout Box
Brown / Black
Pin 1
DIO 5
Red / Black
Pin 18
DIO 0
Brown / Black
Pin 2
Digital Gnd

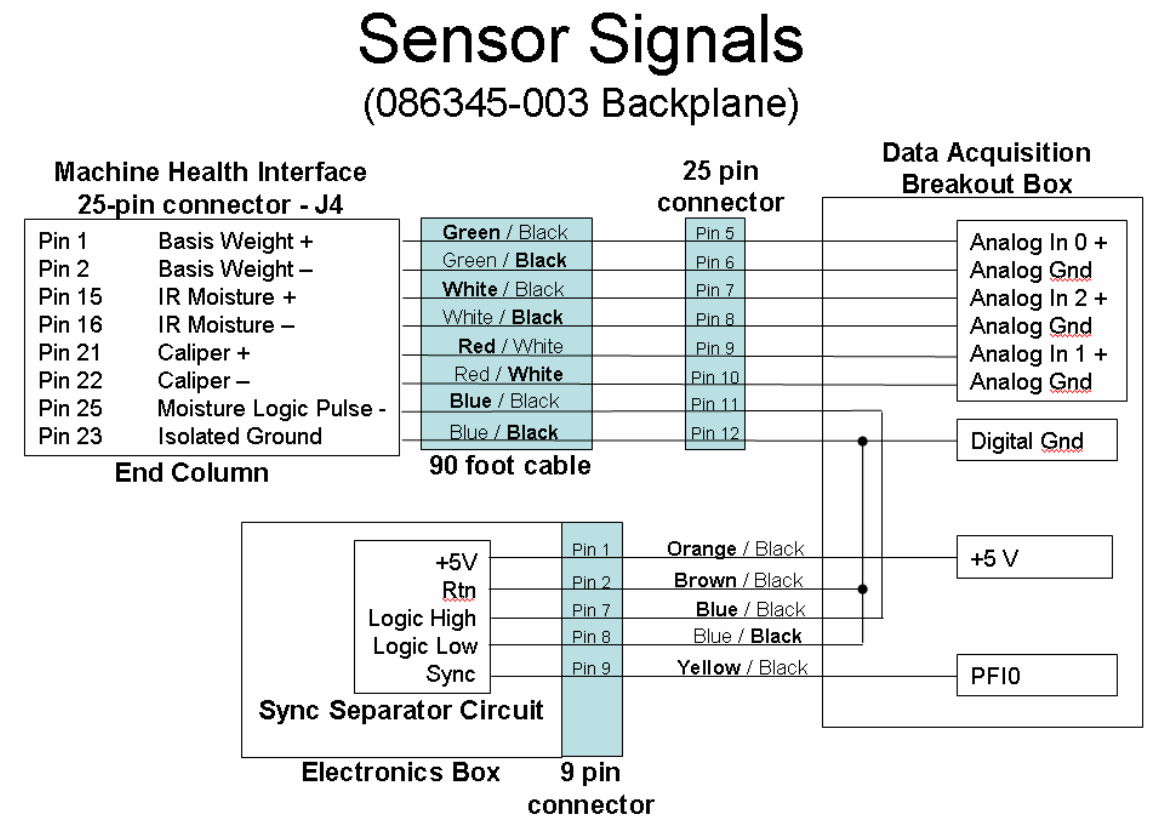
Sensor Signals
(086345-003 Backplane)
Machine Health Interface
25-pin connector - J4
Pin 1 Basis Weight +
Pin 2 Basis Weight –
Pin 15 IR Moisture +
Pin 16 IR Moisture –
Pin 21 Caliper +
Pin 22 Caliper –
Pin 25 Moisture Logic Pulse -
Pin 23 Isolated Ground
End Column
Green / Black
Green / Black
White / Black
White / Black
Red / White
Red / White
Blue / Black
Blue / Black
90 foot cable
25 pin connector
Pin 5
Pin 6
Pin 7
Pin 8
Pin 9
Pin 10
Pin 11
Pin 12
Data Acquisition Breakout Box
Analog In 0 +
Analog Gnd
Analog In 2 +
Analog Gnd
Analog In 1 +
Analog Gnd
Digital Gnd
+5V
Rtn
Logic High
Logic Low
Sync
Sync Separator Circuit
Pin 1
Pin 2
Pin 7
Pin 8
Pin 9
Orange / Black
Brown / Black
Blue / Black
Blue / Black
Yellow / Black
+5 V
PFI0
Electronics Box
9 pin connector

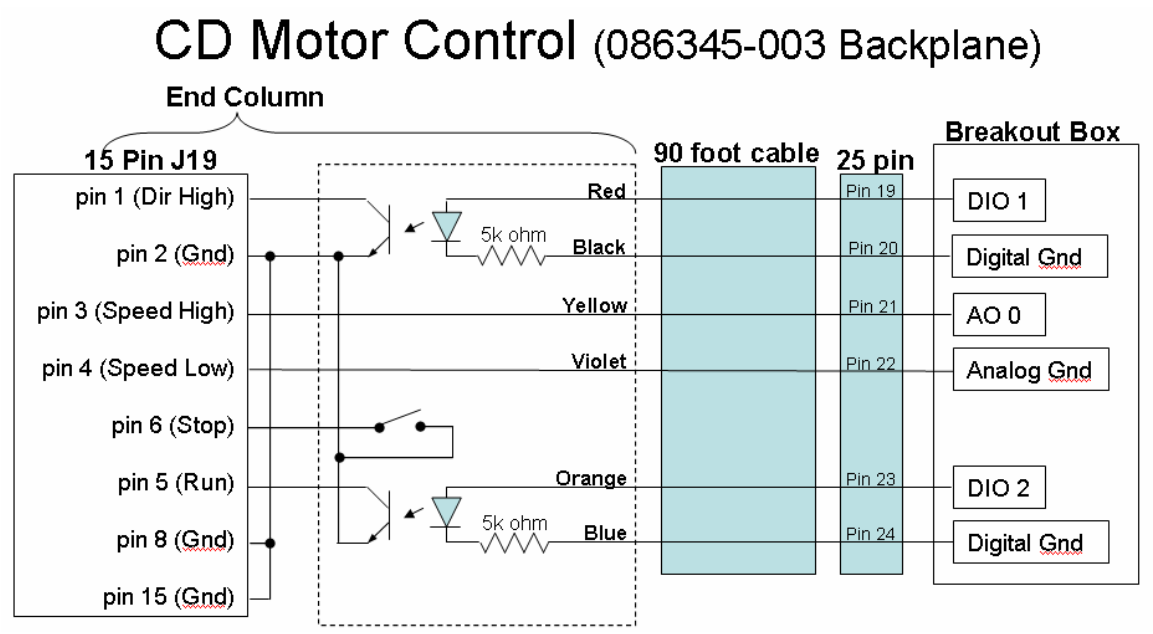
CD Motor Control (086345-003 Backplane)
End Column
15 Pin J19
pin 1 (Dir High)
pin 2 (Gnd)
pin 3 (Speed High)
pin 4 (Speed Low)
pin 6 (Stop)
pin 5 (Run)
pin 8 (Gnd)
pin 15 (Gnd)
5k ohm
5k ohm
Red
Black
Yellow
Violet
Orange
Blue
90 foot cable
25 pin
Pin 19
Pin 20
Pin 21
Pin 22
Pin 23
Pin 24
Breakout Box
DIO 1
Digital Gnd
AO 0
Analog Gnd
DIO 2
Digital Gnd

Studies on the sensor

All the studies that were done to ensure that the sensor was working properly are not displayed here as it would take too much space in this report. We limited ourselves to only present this one as an example.

Barrier study

With the help of studies performed with IPST's laboratory instrumentation and the use of its new automated dispersion curve generation technique (see the section titled **2D FFT Dispersion Curve Generation**), it was found that some artifacts are present within the signals, which can influence on the quality of the signals analysis. Among these artifacts are a compression wave, which travels through the air from the point of excitation and causes a momentary change in the index of refraction of the air below the interferometer beam, visible as the straight line within the dispersion curve (A) and which interferes with the pure A0 wave (B).

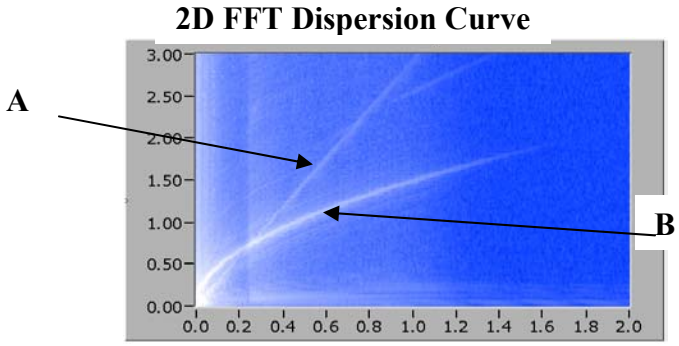

Further study appeared to indicate the presence of another artifact. This one most likely has to do with the undesirable injection of energy by the emission laser into a specimen area surrounding the emission spot with a diameter of approximately a few millimeters. In an effort to minimize the influence of both kinds of artifacts, the inclusion of a barrier between the emission and interferometer spots was studied. Although placing a simple wall between the emission and interferometer spots appeared to help in the elimination of the refractive index wave artifact, the fix was only partial. So, a more sophisticated circular barrier, entirely surrounding the emission spot, was fashioned and attached to the emitter optic. The circular barrier, in addition to stopping the refraction index artifact, was also intended to limit the injection of energy into the specimen within approximately 1 mm of the emission spot itself. As can be seen in the graphs below, the results were fairly dramatic. The barrier signal corresponds to an ideal A0 waveform for a longer time interval relative to the initial arrival of the higher frequency components of the signal than does the signal without a barrier. A longer near-ideal waveform free of artifacts results in a better and more consistent signal analysis in support of the stiffness calculation. Barrier studies will continue as time allows up to the commencement of the upcoming mill trial.

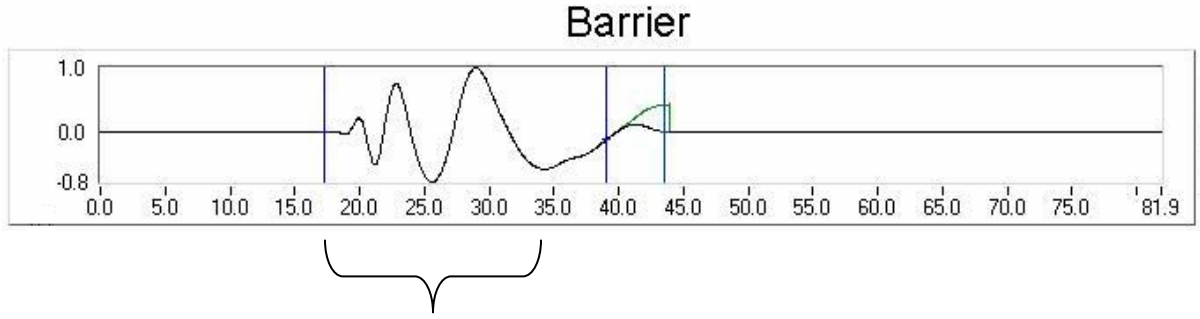

Regions without artifacts

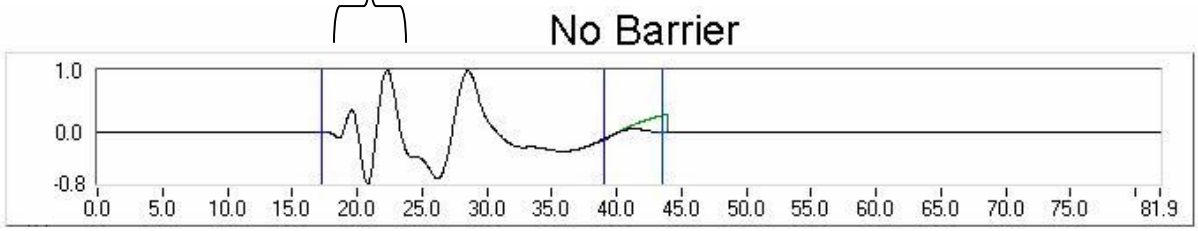

No Barrier – less ideal magnitude spectrum

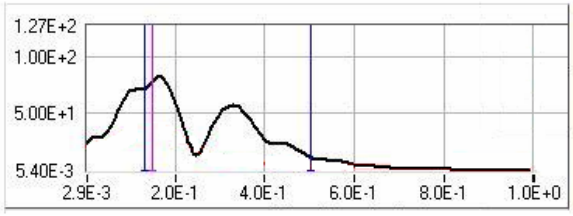

Barrier – more ideal magnitude spectrum

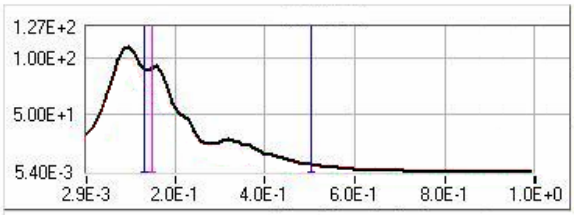

General Conclusion of this Report:

This report detailed the work accomplished on the U.S. Dept. of Energy project named "Contactless Real-Time Monitoring of Paper Mechanical Behavior During Papermaking" by five organizations. These organizations are the Institute of Paper Science and Technology at Georgia Tech (IPST), the Lawrence Berkeley National Laboratory (LBNL), the Idaho National Laboratory (INL), the department of Mechanical Engineering at Georgia Tech (Georgia Tech/ME), and Asea Brown Boveri company (ABB). The report covers the period from October 1, 1997 to March 31, 2004.

The project is mainly geared towards creating an on-line sensor able to measure the stiffness of paper on paper machines, on-line and without any contact, which will ultimately allow paper makers to adjust stiffness by process control.
Over the course of this project, the team found several interferometric methods suitable for on-line and real-time measurements of ultrasonic waves on paper, which are correlated to paper stiffness. After comparisons between methods, one of them was chosen and a first prototype was developed that was tested on a pilot coater machine in Chillicothe, Ohio in 2001. The prototype worked well even on paper moving at 5000 feet/min (25.4 m/s) but was at a fixed position across the web. Following the success of this prototype, a scanning, miniaturized, and hardened sensor was developed to be attached to an ABB scanning platform across the web of a commercial paper machine. This was a much complex endeavor as in that case the moving parts are numerous and access to the sensor is extremely restricted due to the uninterrupted production of paper.

The on-line sensor measures two out-of-plane mechanical properties of paper that are important to paper manufacturers for the post-processing of their products, and these properties are flexural rigidity (related to bending stiffness, important for copier and publication papers), and shear rigidity (important for paperboards and bleached boards). Currently these properties are measured off-line using destructive tests and results are known with a large delay which prevents the process control of stiffness on paper machines. As a result, to stay within stiffness specifications, paper makers are usually obliged to over-engineer the web using more fibers, energy and chemicals that necessary, which results in significant waste of raw materials and energy.

An off-line laboratory instrument using the same method and similar software as the one built for the one-line sensor has also been developed by IPST to validate the results of the on-line sensor. Like the on-line sensor it uses a laser to generate acoustic waves in the web, and an optical interferometer to detect them, plus a complex signal processing algorithm to extract the flexural rigidity and shear rigidity information from the web. It is fully automated and uses fiber optics for laser spot delivery to the sample. This instrument has also demonstrated it can measure the mechanical properties of metal foils and mm-thick wood plates successfully.

Acknowledgments:

We thank Rick Goodlin of MeadWestvaco Corp., Brad Pankonin and Ake Hellstrom of ABB Corp. for consultation and guidance and want to express our appreciation to Mead (MeadWestvaco) Corp. for providing equipment, facilities and support personnel for the pilot coater trial.
We are grateful of Mark Ryan from MeadWestvaco Escanaba mill (Now NewPage Corp.) for his support regarding installation on paper machine #1.

We are aso thankfull to Gideon Varga, Valri Robinson, Dickson Ozokwelu, Joe Springer, and the members of the Agenda 2020 committee for their support on this project.

The research was supported by the Department of Energy, Office of Industrial Technologies, Agenda 2020, American Forest Products and Paper Industry Sensors and Controls Task Group, under Contracts No. DE-AC03-76SF00098 and DE-FC07-97ID13587, and internally by the Institute of Paper Science and Technology at Georgia Tech under the Project Advisory Committee fund.

Annex:

Annex I: List of awards

1. 2004 Van Den Akker Prize for Paper Physics. International prize awarded by TAPPI Paper Physics Committee

2. Outstanding Research Paper for 2003, awarded by TAPPI (Technical Association of Pulp & Paper Industries) for:

   "Laser Ultrasonic System for On-Line Measurement of Elastic Properties of Paper" , Journal of Pulp and Paper Science, Vol. 29, No. 9, pp. 289-293, September 2003.

Annex II: List of publications and conference proceedings issued from this research

1. P. Ridgway, R. Russo, E. Lafond, C. Habeger, T. Jackson, “Laser ultrasonic system for on-line measurement of elastic properties of paper”, *World Congress on Ultrasonics 2003 Proceedings*, Paris, France, September 2003, pp. 1427-1430, 2004
2. E. Lafond, T. Jackson, P. Ridgway, C. Habeger, R. Russo, X. Zhang, “A fully fiberized laser-ultrasonic instrument for measuring the stiffness properties of paper”, *World Congress on Ultrasonics 2003 Proceedings*, Paris, France, September 2003, pp. 1431-1434, 2004
3. P. Ridgway, R. Russo, E. Lafond, C. Habeger, T. Jackson, “Laser Ultrasonic System for Online Measurement of Elastic Properties of Paper”, *Tappi Fall Technical conference Proceedings*, Chicago, IL, 2003
4. P. Ridgway, R. Russo, E. Lafond, C. Habeger, T. Jackson, “Laser Ultrasonic System for On-Line Measurement of Elastic properties of Paper”, *Journal of Pulp and Paper Science*, **29**(9), pp. 289-293, September 2003
5. E. Lafond, P. Ridgway, T. Jackson, C. Habeger, R. Russo, “A laboratory laser-ultrasonic instrument for measuring the mechanical properties of paper webs”, *Review of Progress in Quantitative Non-Destructive Evaluation*, Bellingham, WA, July 2002, **22**(B), pp. 1665-1672, 2003
6. E. Lafond, P. Brodeur, J. Gerhardstein, C. Habeger, K. Telschow, “Photorefractive interferometers for ultrasonics measurements on paper”, *Ultrasonics*, **40** (2002), pp. 1019-1023, December 2002
7. D. Griggs, Y. Berthelot, and M. Cornwell, and C. Habeger, "Noncontact determination of the bending stiffness of paper using laser ultrasonics and wavelet analysis: effects of temperature and moisture content", *Proceedings of the 2001 Ultrasonics Symposium,* 2002
8. E. Lafond, C. Habeger, T. Jackson, “Caracterisation mecanique sans contact de produits papetiers par generation laser et interferometer photorefractif” (in French), *Instrumentation Mesure Metrologie*, **1**(1-2), pp. 143-153, October 2001
9. J. Jong, P. Brodeur, E. Lafond, J. Gerhardstein, B. Pufahl, “Laser Ultrasonics for Non-Contact Measurement of Lamb Waves in Static and Moving Paper”, *Journal of Pulp and Paper Science*, **26**(10), pp. 358-366, October 2000
10. J. Walter, K. Telschow, J. Gerhardstein, B. Pufahl, C. Habeger, E. Lafond, P. Brodeur, “Fabry-Perot Laser Ultrasonic Elastic Anisotropy Measurements on a Moving Paper Web”, *Review of Progress in Quantitative Non-Destructive Evaluation*, Montreal, Canada, July 1999, **19**(A), pp. 247-254, 2000
11. P. Ridgway, A. Hunt, M. Quinby-Hunt, R. Russo, “Laser Ultrasonics on Moving Paper”, *Ultrasonics*, **37**(6), pp. 395-403, 1999
12. P. Brodeur, J. Gerhardstein, E. Lafond, et al., “Monitoring the Mechanical Behavior of Paper during Papermaking”, *International Paper Physics Conference proceedings,* San Diego, CA, pp 437-445, September 1999
13. Jong, J.H., Brodeur, P.H. and Gerhardstein, J.P., "Measurement and Analysis of Stiffness Properties in Moving Paper using Non-Contact Laser Ultrasonics", *Proceedings of*

the TAPPI International Paper Physics Conference, San Diego, CA, pp. 19-27, September 1999

14. Gerhardstein, J.P., Lafond, E.F., Jong, J.H., Pufahl, B.M. and Brodeur, P.H., "Noncontact Laser Ultrasonics Measurement of Texture Noise Using a Moving Web Simulator", *Proc. Engineering/Process and Product Quality Conference*, Anaheim, CA, pp.929-935, September 1999

15. E. Lafond, J. Gerhardstein, P. Brodeur, “Non-contact Characterization of Static Paper Materials Using a Photorefractive Interferometer”, *SPIE Conference on Nondestructive Evaluation Techniques for Aging Infrastructure & Manufacturing / Process Control and Sensors for Manufacturing,* Newport, CA, SPIE **3589**, pp. 30-41, 1999

16. B. Pouet, E. Lafond, B. Pufahl, D. Bacher, P. Brodeur, M. Klein, “On-Machine Characterization of Moving Paper Using a Photo-emf Laser Ultrasonics method”, *SPIE Conference on Nondestructive Evaluation Techniques for Aging Infrastructure & Manufacturing / Process Control and Sensors for Manufacturing,* Newport, CA, SPIE **3589**, pp. 160-169, 1999

17. J. Jong, E. Lafond, P. Brodeur, J. Gerhardstein, B. Pufahl, “Dispersion of Lamb Waves Propagating in Static and Moving Paper to Measure Stiffness Using Non-contact Laser Ultrasonics”, *85th annual meeting of Canadian Pulp and Paper Association*, Montreal, Canada, January 1999

18. P. Brodeur, J. Gerhardstein, “Overview of Applications of Ultrasonics in the Pulp and Paper Industry”, *Proceedings of 1998 IEEE International Ultrasonics Symposium,* Sendai, Japan, October 1998

Annex III: List of patents, patents applications, and invention disclosures

Patents

Name of patent; (inventors):	Patent No.	Issued	Status
Non-Contact Measurements of Ultrasonic Waves on Paper Webs (Co-Inventors – Brodeur, Lafond)	6,115,127	9/5/00	Active
System & Method of Reducing Motion-Induced Noise in the Optical Detection Of an Ultrasound Signal in a Moving Body of Material (Co-Inventors – Habeger, Lafond, Brodeur, Gerhardstein)	6,356,846	3/12/02	Active

Invention Disclosures

Name of invention; (inventors):	Date Filed	Status
Peanut-Shell Laser Ultrasonic Excitation (Co-Inventors -Habeger, Lafond, Spicer (JHU, Johns Hopkins University))	6/21/99	DOE should be the owner
Process to Reduce Laser-Induced Damage in a Fiber Web (Inventor: Lafond)	2/17/00	NA
Separation of Elastic Waves Generated Simultaneously in a Web Using a Diffractive Lens (Reported to DOE) (Co-Inventors – Lafond, Ridgway (LBNL))	8/11/00	NA
Applications of Micro Electro Mechanical Systems for Ultrasonic Testing of Web-Like Materials (Co-Inventors – Berthelot (GTRC, Georgia Tech), Lafond (IPST)	11/11/02	NA